

**FORMATION OF REPLACEMENT DOLOMITE BY INFILTRATION OF
DIFFUSE EFFLUENT: LATEMAR CARBONATE BUILDUP, DOLOMITES,
NORTHERN ITALY**

by
Sarah Katherine Carmichael

A dissertation submitted to Johns Hopkins University in conformity with the
requirements for the degree of Doctor of Philosophy

Baltimore, Maryland
July, 2006

© 2006 Sarah Carmichael
All rights reserved

Abstract

Massive dolomite typically forms at depth and elevated temperature through replacement of limestone by its reaction with flowing dolomitizing fluid. Analysis of the spatial distribution of elements, isotopes, and heat with transport theory leads to insights into the flow system that produced dolomite in the Latemar carbonate buildup.

Dolomitization was arrested, and both dolomite and unreacted limestone well-exposed in three dimensions. Boundaries between the dolomitized and undolomitized regions were mapped on meter to kilometer-scales. The distribution of dolomite directly images an orthogonal lattice of interconnected vertical tube-like and bedding-parallel sheet-like fluid flow channels.

The $^{87}\text{Sr}/^{86}\text{Sr}$ of Latemar dolomite and the salinity of fluid inclusions in dolomite, previously measured by others, imply that a seawater-derived fluid was the dolomitizing fluid. Dolomite has $\delta^{18}\text{O} = 21.5\text{-}27.4\text{‰}$ (VSMOW), corresponding to temperatures of 50-90°C (assuming equilibration with fluid of $\delta^{18}\text{O} = 0$). Electron microprobe and LA-ICPMS data for the dolomite show enrichment in Fe (1,600-19,000 ppm), Mn (66-430 ppm), and Zn (1.7-16 ppm) relative to unreacted limestone. The concentrations of Fe and Zn in dolomite display a positive linear correlation with that of Mn; concentrations of other transition metals show no correlation with Mn. These data suggest that the dolomitizing fluid is analogous to modern diffuse effluent at mid-ocean ridges, and was a mixture of seawater and hydrothermal fluid produced by reaction between seawater and rocks of the adjacent Predazzo igneous complex that was the driving mechanism for

dolomitization. The distribution of dolomite and its variability in $\delta^{18}\text{O}$ at the outcrop scale (23-28‰) indicate that fluid flow occurred in multiple, spatially restricted pulses.

The time-integrated fluid flux, q , can be estimated from mass balance using the spatial extent of dolomitization in the field and the Ca/Mg of the dolomitizing fluid.

Assuming diffuse effluent as the dolomitizing fluid, and temperatures of 50-90°C, and \approx 1 km of dolomite along the flow path, $q = 1.9 \cdot 10^7 - 1.6 \cdot 10^8 \text{ cm}^3 \text{ fluid/cm}^2 \text{ rock}$.

Quantitative analysis of outcrop-scale temperature gradients ($T \approx 10\text{-}25^\circ\text{C/m}$) with heat transport theory suggests that dolomitization occurred in a minimum of ~ 400 fluid pulses over a total duration of flow and reaction possibly as short as ~ 30 years.

First Reader: Prof. John M. Ferry

Morton K. Blaustein Department of Earth and Planetary Sciences
Johns Hopkins University

Second Reader: Prof. Dimitri Sverjensky

Morton K. Blaustein Department of Earth and Planetary Sciences
Johns Hopkins University

ACKNOWLEDGMENTS

This thesis would not have been possible without the input and guidance of many people. In particular, I am indebted to my advisor, Dr. John Ferry, for his guidance both in the field and in the classroom. His attention to detail, encouragement, patience, and willingness to humor me when I insisted on carrying enough ingredients for two three-course meals to a remote Swiss rifugio is most sincerely appreciated.

Dr. Dimitri Sverjensky, my second reader, provided invaluable assistance with SUPCRT, EQ3, and EQ6 both inside and outside the classroom. My work has greatly benefited from discussions with Dr. Linda Hinnov, Dr. Sakiko Olsen, and Dr. Lawrie Hardie. Dr. Nereo Preto and Dr. Alberto Riva at the University of Ferrara, Italy, provided invaluable help in the course of my fieldwork in the Latemar.

Stable isotope analyses were carried out with the help of Dr. J. Alan Kaufmann at the University of Maryland. LA-ICPMS analyses were carried out with the help of Dr. William McDonough and Dr. Richard Ash at the University of Maryland. Cathodoluminescence images were taken with the help of Dr. Sorena Sorenson at the Smithsonian Insitute. Dr. Karen Von Damm at the University of New Hampshire was very generous with her time and expertise on the chemistry of diffuse effluent.

Three summers of fieldwork in the Italian Alps were made even more rewarding with the hospitality of Nicola and Antonio Gabrielli of Predazzo, at the Rifugio Torre di Pisa. Likewise, I have to thank my truly excellent field assistants, Dr. Sarah Penniston-Dorland and Laurel Mutti, for their willingness to help me survey thousands of data points and collect and carry out over a hundred kilos of rocks in their backpacks.

I am greatly appreciative of my fellow graduate students in the department. In particular, Dr. Beatriz Funatsu and Dr. Hagay Amit, and postdoctoral fellow Dr. Jennifer McIntosh, who have been absolutely wonderful friends during these challenging years. To my roommate, Claire Jarvis, and my friends, Mary McDonough, Elliot Laster, James Kuzner, Gary Desjardins, and last but not least Holly Hinson, I owe a sincere thank you for your friendship, love, patience, and ability to make me laugh at the end of the day. I also want to thank the Tobin family for their support and encouragement throughout my academic career.

I owe my parents, John and Kristin Carmichael, and my sister, Elicia Carmichael, a thousand thank yous. I could not have done this without their constant love, support, encouragement, sense of humor, and care packages filled with peculiar clippings from the local newspaper.

Acknowledgment is made to the Donors of the American Chemical Society Petroleum Research Fund (award 42246-AC8) and the National Science Foundation (award EAR-0229267) for support of this research. Additional field work support was provided by the Stuart Mossum Fund and the Robert Balk Fund.

TABLE OF CONTENTS

Abstract	ii
Acknowledgements	iv
Table of Contents	vi
List of Tables	vii
List of Figures	viii
Chapter 1: Introduction	1
Chapter 2: Geology	7
Regional Geology	7
The Latemar Carbonate Buildup.....	10
Chapter 3: Methods of Investigation	16
Chapter 4: Dolomite Distribution	21
Limestone-dolomite contacts	22
Outcrop scale field relations	28
Regional scale field relations	39
Summary	42
Chapter 5: Mineralogy, Texture, and Mineral Chemistry of Dolomites and Limestones	47
Mineralogy and Textures	47
Major Element Chemistry.....	63
Trace Element Chemistry	68
Chapter 6: Stable Isotopes	90
Chapter 7: Source of Dolomitizing Fluid	99
⁸⁷ Sr/ ⁸⁶ Sr.....	99
Fluid inclusions.....	99
Ca/Mg ratio	100
Trace elements	102
Chapter 8: Temperature of Dolomitization	109
Fluid inclusions.....	109
Oxygen isotopes.....	110
Chapter 9 - Time-integrated Fluid Flux: Estimation and Applications	117
Reaction mechanism	117
Amount of fluid as a time-integrated fluid flux:	
Replacement at constant C and O	118
Replacement at constant volume	126
Isotope reaction fronts.....	128
Trace element requirements of dolomitization	132
Chapter 10: Mechanism and Duration of Reactive Flow	135
Appendix I: Sample Locations	143
Appendix II: Major Element data	156
Appendix III: Trace Element data	176
Appendix IV: Stable Isotope data	184
References	196
Vita	217

LIST OF TABLES

Table 5.1. Modal distribution of minerals in limestone, orange (Fe-rich) dolomite, and tan (Fe-poor) dolomite	48
Table 5.2. Average major element chemistry (Ca, Mg, Fe) of limestone and dolomite according to protolith, in cations per CO ₃	67
Table 5.3. Average LA-ICPMS and microprobe data for Latemar calcites and dolomites, in cations per CO ₃	79
Table 7.1. Ca/Mg of fluid coexisting with calcite and dolomite.	101
Table 7.2. Potential dolomitizing fluids.	103
Table 8.1. Temperatures calculated from δ ¹⁸ O in calcite and dolomite using Equations 8.1-8.8.	113
Table 9.1a. Compositions of calcite and dolomite used to calculate the time-integrated fluid flux.	120
Table 9.1b. Compositions of fluids used to calculate the time-integrated fluid flux.	120
Table 9.2. Calculation of time-integrated fluid flux using diffuse effluent (DE2) at 70°C, (ρ _{DE2} =1.0265 g/cm ³) as a dolomitizing fluid.	123
Table 9.3. Calculated time-integrated fluid flux of dolomitization, using three diffuse effluent chemistries (DE1-DE3) and Triassic seawater at a range of T = 50-150°C.	124
Table 9.4. Calculated time-integrated fluid flux of dolomitization, using Triassic seawater and three diffuse effluent chemistries based on variable Fe content as a dolomitizing fluid, at variable input temperatures and a temperature gradient of -50°C/km along the flow path.....	125
Table 9.5. Location of isotope reaction fronts calculated following Dipple and Ferry (1992) and Ferry and Gerdes (1998) using DE2 diffuse effluent chemistry at 70°C along an isothermal flow path for 1 km of dolomitization.	129
Table 9.6. Budget of trace elements.	134
Table 10.1. Symbols in Equations 10.1-10.4.	139
Table 10.2. Input values and calculated results from Equations 10.1-10.4.	140

LIST OF FIGURES

Figure 2.1. Regional geological setting of the Dolomites.	8
Figure 2.2. Stratigraphic column of the Trento Plateau, southern Alps.	11
Figure 2.3. Geologic map of Latemar and adjacent buildups.	12
Figure 2.4. Reef structure of Latemar.	13
Figure 3.1. Orthographic aerial photograph with sample locations.	17
Figure 4.1a. Panoramic photo of platform interior, facing west.	23
Figure 4.1b. Panoramic map of the platform interior facing west (tracing of digital photo in Figure 4.1a).	24
Figure 4.2. Normalized modes of dolomites and limestones.	25
Figure 4.3. Distribution of limestone and dolomite at the meter scale at two limestone-dolomite contacts (Location 8).	26
Figure 4.4. Digital photograph of polished surface of sample L-8P (Figure 4.2), stained for calcite (red) and dolomite (blue), showing dolomite veins in limestone.	27
Figure 4.5. Sheet-like bodies of dolomite parallel to bedding planes in limestone Location 7.	29
Figure 4.6. Sheet-like bodies of dolomite parallel to bedding planes in limestone (Location 8).	30
Figure 4.7. Sheet-like bodies of dolomite parallel to bedding planes in limestone (Location 10).	31
Figure 4.8. Map of Location 2 showing bedding-parallel sheets of dolomite.	32
Figure 4.9. Photograph of dolomite breccia showing limestone and dolomite blocks (base of Traverse B).	33
Figure 4.10. Dolomite breccia (Location 11).	34
Figure 4.11. Dolomite breccia exposed on hill (Location 12).	35
Figure 4.12. Photograph looking south to base of Traverse A.	37
Figure 4.13. Map view of Location 1.	38
Figure 4.14. Irregularly shaped dolomite bodies with sub-vertical and sub- horizontal contacts developed in limestone approximately horizontal layers at Location 13.	40
Figure 4.15. Panoramic view of irregularly shaped dolomite bodies in Location 6 traced from a digital photograph.	41
Figure 4.16. Cumulative fraction of dolomite (black) and limestone (gray) as a function of elevation in the Latemar buildup.	43
Figure 4.17. Cumulative fraction of horizontal or nearly horizontal (black) and vertical or nearly vertical (gray) dolomite-limestone contacts as a function of elevation in the Latemar buildup.	44
Figure 4.18. Schematic diagram of trellis-like structure of replacement dolomite illustrated in cross section.	45
Figure 5.1. BSE image of representative dolomite-free limestone with trace euhedral K-feldspar (sample LAS-17).	50
Figure 5.2. Representative BSE image of dolomite grains in dolomite-poor limestone (sample L-11F).	51

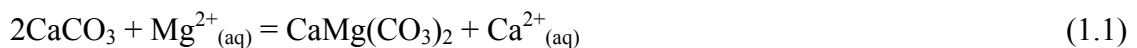
Figure 5.3. BSE image of dolomite developed along fracture in limestone (sample L-12F).....	52
Figure 5.4. Digital photograph of polished surface of sample LAS-7, stained for calcite (red) and dolomite (blue), showing preferential dolomitization of aragonitic dasycladacean algae fossils (arrows).....	53
Figure 5.5. BSE image of preferential dolomitization of aragonitic dasycladacean algae and possibly aragonitic carbonate clasts (sample L-12D).....	54
Figure 5.6. BSE image of strings of dolomite and K-feldspar developed along stylolite in limestone (sample LES-8).....	55
Figure 5.7. BSE image of K-feldspar and Fe-oxide developed with dolomite along stylolite in limestone (sample L-8H).	56
Figure 5.8. BSE image of dolomite associated with Fe-oxide and K-feldspar (sample LAS-31).....	57
Figure 5.9. BSE image of dolomite associated with Fe-oxide in limestone (sample L-1H).....	58
Figure 5.10. Representative BSE image of zoned dolomite grains, that have calcite inclusion-rich cores and concentrically zoned, inclusion-free rims (sample L-1C).....	59
Figure 5.11. BSE image of example of concentric compositionally zoned, tan, Fe-poor dolomite, with calcite inclusions scattered throughout the dolomite (sample 8T-4).....	60
Figure 5.12. Representative BSE image of unzoned, tan, Fe-poor dolomite (sample LAS-5).....	61
Figure 5.13. BSE image of example of orange, Fe-poor dolomite exhibiting patchy rather than concentric compositional zoning (sample L-13B).....	62
Figure 5.14. BSE image of inclusion-free quartz in unzoned, Fe-rich, inclusion-free dolomite (sample L-6B).....	64
Figure 5.15. BSE image of quartz with calcite inclusions in tan, Fe-poor, unzoned dolomite (sample LES-14).	65
Figure 5.16. CL image of compositional zoning in tan, Fe-poor dolomite (sample L-12B).	66
Figure 5.17. Major element composition of calcite in isotopically unaltered limestone (whole rock $\delta^{18}\text{O} > 26\text{‰}$).....	69
Figure 5.18. Major element composition of calcite in dolomite-free limestone.....	70
Figure 5.19. Major element composition of calcite from outcrops that contain both limestone and dolomite.	71
Figure 5.20. Major element composition of calcite from limestone outcrops in Traverses A-F.....	72
Figure 5.21. Major element composition of dolomite from outcrops that contain both limestone and dolomite.	73
Figure 5.22. Major element composition of dolomite from dolomite outcrops in Traverses A-F.	74
Figure 5.23. Major element composition of dolomite in outcrops of dolomite breccia.	75
Figure 5.24. Major element composition of orange dolomite.	76

Figure 5.25. BSE image and X-ray maps of dolomite zoning in sample 7T-3, (a) BSE image, (b) Fe X-ray map, (c) Mg X-ray map, and (d) Ca X-ray map.....	77
Figure 5.26. Concentrations of Fe and Mn in calcite and dolomite, measured by LA-ICPMS.....	81
Figure 5.27. Concentrations of Zn and Mn in calcite and dolomite, measured by LA-ICPMS.....	82
Figure 5.28. Concentrations of Sr and Mn in calcite and dolomite, measured by LA-ICPMS.....	83
Figure 5.29. Concentrations of Cr and Mn in calcite and dolomite, measured by LA-ICPMS.....	84
Figure 5.30. Concentrations of Co and Mn in calcite and dolomite, measured by LA-ICPMS.....	85
Figure 5.31. Concentrations of Cu and Mn in calcite and dolomite, measured by LA-ICPMS.....	86
Figure 5.32. Concentrations of Ni and Mn in calcite and dolomite, measured by LA-ICPMS.....	87
Figure 5.33. Concentrations of Ba and Mn in calcite and dolomite, measured by LA-ICPMS.....	88
Figure 5.34. Concentrations of Pb and Mn in calcite and dolomite, measured by LA-ICPMS.....	89
Figure 6.1. Measured $\delta^{13}\text{C}$ vs. $\delta^{18}\text{O}_{\text{Cal}}$ for calcite samples.....	91
Figure 6.2. $\delta^{13}\text{C}$ vs. $\delta^{18}\text{O}_{\text{Dol}}$ or $\delta^{18}\text{O}_{\text{Cal}} + \Delta_{\text{Dol-Cal}}$ for calcite and dolomite samples, grouped according to rock type.....	93
Figure 6.3. $\delta^{13}\text{C}$ vs. $\delta^{18}\text{O}_{\text{Dol}}$ or $\delta^{18}\text{O}_{\text{Cal}} + \Delta_{\text{Dol-Cal}}$ for calcite and dolomite samples in Location 8, grouped according to rock type.	94
Figure 6.4. $\delta^{13}\text{C}$ vs. $\delta^{18}\text{O}_{\text{Dol}}$ or $\delta^{18}\text{O}_{\text{Cal}} + \Delta_{\text{Dol-Cal}}$ for calcite and dolomite samples in Location 7, grouped according to rock type.	95
Figure 6.5. $\delta^{18}\text{O}_{\text{Dol}}$ or $\delta^{18}\text{O}_{\text{Cal}} + \Delta_{\text{Dol-Cal}}$ vs. elevation for calcite and dolomite.....	97
Figure 6.6. $\delta^{13}\text{C}$ vs. elevation for calcite and dolomite.....	98
Figure 7.1. Fe vs. Mn concentrations in diffuse effluent (DE) from the TAG site on the Mid-Atlantic Ridge.....	106
Figure 7.2. Zn vs. Mn concentrations in diffuse effluent (DE) from the TAG site on the Mid-Atlantic Ridge.....	107
Figure 7.3. Cu vs. Mn concentrations in diffuse effluent (DE) from the TAG site on the Mid-Atlantic Ridge.....	108
Figure 8.1. Fluid inclusion homogenization temperatures for Latemar dolomite.	111
Figure 9.1. Model diffuse effluent chemistries (DE1-DE3) based on Mn content.....	119
Figure 9.2. Simple model of the distance of each isotope reaction front from the fluid source (distance = 0) in relation to the dolomite front at 1 km.	130
Figure 10.1. Temperature profiles across Location 7.	136
Figure 10.2. East and west temperature profiles for Location 7.....	137

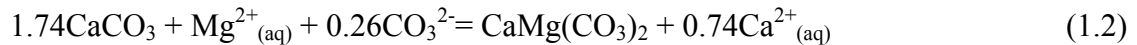
Chapter 1

Introduction

The formation of dolomite is a long-standing problem (Morrow, 1982; Land, 1985; Machel and Mountjoy, 1986; Hardie, 1987; Budd, 1997; Arvidson and Mackenzie, 1999; Warren, 2000). There are no active surficial processes that produce massive, stoichiometric, ordered dolomite. Primary Ca-rich disordered dolomite does form in some contemporary surficial environments, such as sabkhas and hot springs (Wells, 1962; Curtis et al., 1963; Rosen et al., 1989), and in anoxic lagoons due to microbial influence (Vasconcelos and McKenzie, 1997; van Lith et al., 2002). However, the texture, composition, and volume of these primary dolomite precipitates are unlike occurrences of most dolomite in the geologic record. It is more likely that massive dolomitization is usually due to the replacement of calcite, where dolomite forms by a reaction between an Mg-rich fluid and limestone that approximately is:



or



Reactions 1.1 and 1.2 represent the two end-member processes envisioned: replacement of calcite by dolomite at constant C and O (Equation 1.1) or at constant volume (Equation 1.2). Dolomite can form by replacement of calcite limestone provided there is access to a

fluid with sufficient Mg, and a flow mechanism capable of delivering Mg to and removing Ca from the site of reaction (Land, 1985).

Dolomite has been synthesized in the laboratory at temperatures $\geq 100^\circ\text{C}$ (Graf and Goldsmith, 1956; Katz and Matthews, 1977; Gaines, 1980; Gregg and Sibley, 1984; Sibley et al., 1994; Lumsden et al., 1995; Arvidson and Mackenzie, 1999). Partially ordered, nonstoichiometric dolomite has been precipitated at low temperatures through the actions of sulphate-reducing bacteria under anoxic conditions (Vasconcelos et al., 1995; Warthmann et al., 2000) or with repeated fluctuations in pH (Deelman, 1999) or temperature (Nordeng and Sibley, 1993). Disordered, Ca-rich “protodolomite” has been synthesized at $T < 100^\circ\text{C}$ (Kelleher and Redfern, 2002). However, stoichiometric, ordered dolomite has not been synthesized in the laboratory under Earth surface conditions (1 atmosphere and $\sim 25^\circ\text{C}$), either by direct precipitation or replacement of calcite. A variety of dolomitizing fluid chemistries, such as those of evaporative brines, mixtures of freshwater and seawater, seawater modified by extensive sulfate reduction, the degradation of organic matter by sulfate-reducing bacteria, and solutions enriched in Li have been proposed to explain the replacement of calcite by dolomite at surface conditions (Siegel, 1961; Wells, 1962; Curtis et al., 1963; Friedman and Sanders, 1967; Zenger, 1972; Badiozamani, 1973; Folk and Land, 1975; Gaines, 1980; Baker and Kastner, 1981; Morrow and Ricketts, 1988; Slaughter and Hill, 1991; Brady et al., 1996). Although evaporative brines may produce primary dolomite or cause replacement of aragonite mud by dolomite in arid carbonate environments (Hardie, 1987), the volume of brine required to produce the amount of dolomite seen in the rock record would be immense, and the environments that produce such brines are relatively rare.

Environments within a freshwater-seawater mixing zone are thermodynamically suited to produce ordered dolomite (Badiozamani, 1973), but there is little evidence for precipitation of ordered dolomite or replacement of calcite by dolomite even in well-documented modern freshwater-seawater mixing zones (Plummer et al., 1976; Steinen et al., 1978; Halley and Harris, 1979; Hanshaw and Back, 1980; Gebelein et al., 1980). Furthermore, if the mixing zone model is evaluated using thermodynamic data for disordered or weakly ordered dolomite and takes the partial pressure of CO₂ and temperature into account, the range of fluid chemistries capable of producing dolomite is quite restricted (Plummer, 1975; Hardie, 1987). The experimental results of Seigel (1961), that suggest that sulfate is necessary to precipitate dolomite, are contradicted by those of Baker and Kastner (1971), Morrow and Ricketts (1988), and work by Slaughter and Hill (1991) that instead suggest that the presence of sulfate ions inhibits the replacement of calcite by dolomite. Experiments by Brady et al. (1996) have determined that although sulfate inhibits dolomite growth in sulfate-poor (< 5 mM) solutions, it accelerates dolomite growth in sulfate rich (>5 mM) solutions. The applicability of these experiments to massive dolomite bodies as a whole is even more uncertain because field studies document that dolomite is found in both high-sulfate and low-sulfate environments (Jones, 1965; Bathurst, 1975; Eugster and Hardie, 1978; Kelts and McKenzie, 1982; Garrison et al., 1984; Kohut et al., 1995; Brady et al., 1996). As sulfate reduction is a common reaction, one would expect to see more sulfate reduction-related dolomite than is observed in the geologic record (Land, 1985). Organogenic dolomite, formed by decomposition of organic matter via sulfate reducing bacteria (Slaughter and Hill, 1991), cannot explain the presence of massive replacement dolomite because most

evaporative environments do not contain enough available organic matter (Brady et al., 1996). Furthermore, any dolomite formed in a sulfate reducing environment would be depleted in ^{13}C , and most massive dolomite in the rock record does not exhibit this (Land, 1980). Solutions enriched in Li (0.5 M) or dioxane cause dolomitization to occur more rapidly (Gaines, 1980; Oomori and Kitano, 1987), but are very unusual in the natural environment.

Work by Fanning et al. (1981), Saller (1984), Aharon et al. (1987), and Flood et al. (1996) on the dolomitization of the bases of carbonate banks and atolls has shown that normal seawater at elevated temperatures is capable of driving the calcite to dolomite reaction. It is therefore more likely that replacement dolomite forms at depth and at elevated temperature via a dolomitizing fluid, and that kinetic factors are more important than special fluid chemistries for the calcite-dolomite reaction (Hardie, 1987; Brady et al., 1996). From this, it appears that the primary requirement for dolomitization is sufficient supply of Mg-bearing dolomitizing fluid and temperatures elevated above surface conditions.

Adequate supply of Mg to the site of dolomitization and removal of Ca, in turn, requires some long-lived fluid flow system. Many mechanisms to drive fluid flow have been proposed, including density-driven flow from brine reflux (Adams and Rhodes, 1960; Simms, 1984; Jones and Rostron, 2000; Jones et al., 2004), topography-driven flow (Garven and Freeze, 1984; Garven, 1985; Gregg, 1985; Yao and Demicco, 1997), compaction-driven flow during burial (Illing, 1959; Jodry, 1969), and thermal convection caused either by the geothermal gradient (Kohout, 1967; Fanning et al., 1981; Saller, 1984; Simms, 1984; Aharon et al., 1987; Morrow, 1998; Wilson et al., 2001) or by

igneous activity (Wilson et al., 1990; Spencer-Cervato and Mullis, 1992; Antonelli and Mollema, 2000; Nader et al., 2004). Each of these flow mechanisms will produce distinctive patterns of dolomitization, with characteristic volumes and textures of dolomite, provided they can pump sufficient Mg through the system to complete the calcite-dolomite reaction. For a discussion of the limitations of each flow mechanism, see Land (1985), Machel and Mountjoy (1986), Hardie (1987), Budd (1997), and Morrow (2000).

Critical to understanding specific occurrences of dolomite is identification of both the dolomitizing fluid and the mechanism for driving fluid flow. A variety of data can be used to identify the fluid source and pump for specific occurrences of dolomitization: the distribution of dolomite in the field area, trace element geochemistry, stable and radiogenic isotope geochemistry, and fluid inclusion freezing and homogenization temperatures. In his review Budd (1997), however, noted that these efforts often cannot uniquely explain dolomitization because individual geochemical or isotopic species are considered individually in isolation from the others. Rather, an integrated interpretation of field relations, trace element and isotopic analyses, combined with transport theory and knowledge of the hydrologic regime, is called for to test hypotheses for the fluid source and driving mechanism that forms replacement dolomite.

Metamorphic petrologists have utilized such methods for many years, and can offer a fresh perspective on the problem of massive replacement dolomitization. Much progress has been made in the last decade in metamorphic petrology in applying the theory of reactive transport in porous media to interpret the chemical, isotopic, and mineralogic effects of fluid-rock reactions in metamorphic terranes (for example, see

review by Ferry and Gerdes, 1998, and Baumgartner and Valley, 2001). It is an ideal time to apply these methods to the role of limestone-fluid reactions in dolomite formation. Application of these methods, in principle, can lead to constraints on the source of dolomitizing fluid, the driving force for fluid flow, the geometry and amount of flow, the thermal structure of the flow system, and the control of fluid flow on the spatial distribution of the isotope compositions of dolomite.

This research specifically applies methods of metamorphic petrology to the formation of replacement dolomite in the Latemar carbonate buildup, Dolomites, northern Italy. The carbonate sedimentology and the replacement dolomitization in the Latemar have been studied extensively by sedimentary petrologists, which makes it an ideal location to apply current theories of metamorphic petrology and to evaluate previous models for replacement dolomitization. This is the first time that the methods of metamorphic petrology have been applied to a classic sedimentology problem.

Chapter 2

Geology

Regional Geology

The Dolomites, part of the Southern Alps in northern Italy (Figure 2.1), are largely composed of Mesozoic shallow water carbonates that have been studied extensively for more than 100 years (De Dolomieu, 1791; Richthofen, 1860; Mojsisovics, 1879; Vardebasso, 1930; Leonardi, 1955; Rossi, 1967; Bosellini and Hsü, 1973; Bosellini and Rossi, 1974a; Bosellini and Rossi, 1974b; Gaetani et al, 1981; Bosellini, 1984; Blendinger, 1985; Doglioni, 1987; Doglioni and Bosellini, 1987; Goldhammer, 1987; Goldhammer et al., 1987; Bosellini and Hardie, 1988; Goldhammer et al, 1990; Gianolla et al., 1998; Masetti and Trombetta, 1998; and Bosellini et al, 2003).

The earliest sedimentary rocks preserved in the Dolomites formed in the Middle/Upper Permian when the Paleotethys transgressed eastward across the region, depositing the Gardena Sandstone (terrestrial red beds, alluvial fan conglomerates, sandstones, and siltstones) on top of the Paleozoic metamorphic basement. In some areas, these continental sediments overlie thick localized accumulations of felsic volcanics (Bosellini and Rossi, 1974). The felsic volcanics (the Bozener Porphyry Plateau), formed during early Permian rifting and block faulting, and created structural highs which somewhat restricted the alluvial sedimentation. As the Paleotethys transgressed further eastwards, transitional marine sediments of the Permian Bellerophon Formation (black shales, evaporites, micritic skeletal limestones) were next deposited. They represent a variety of depositional environments ranging from coastal sabkha to

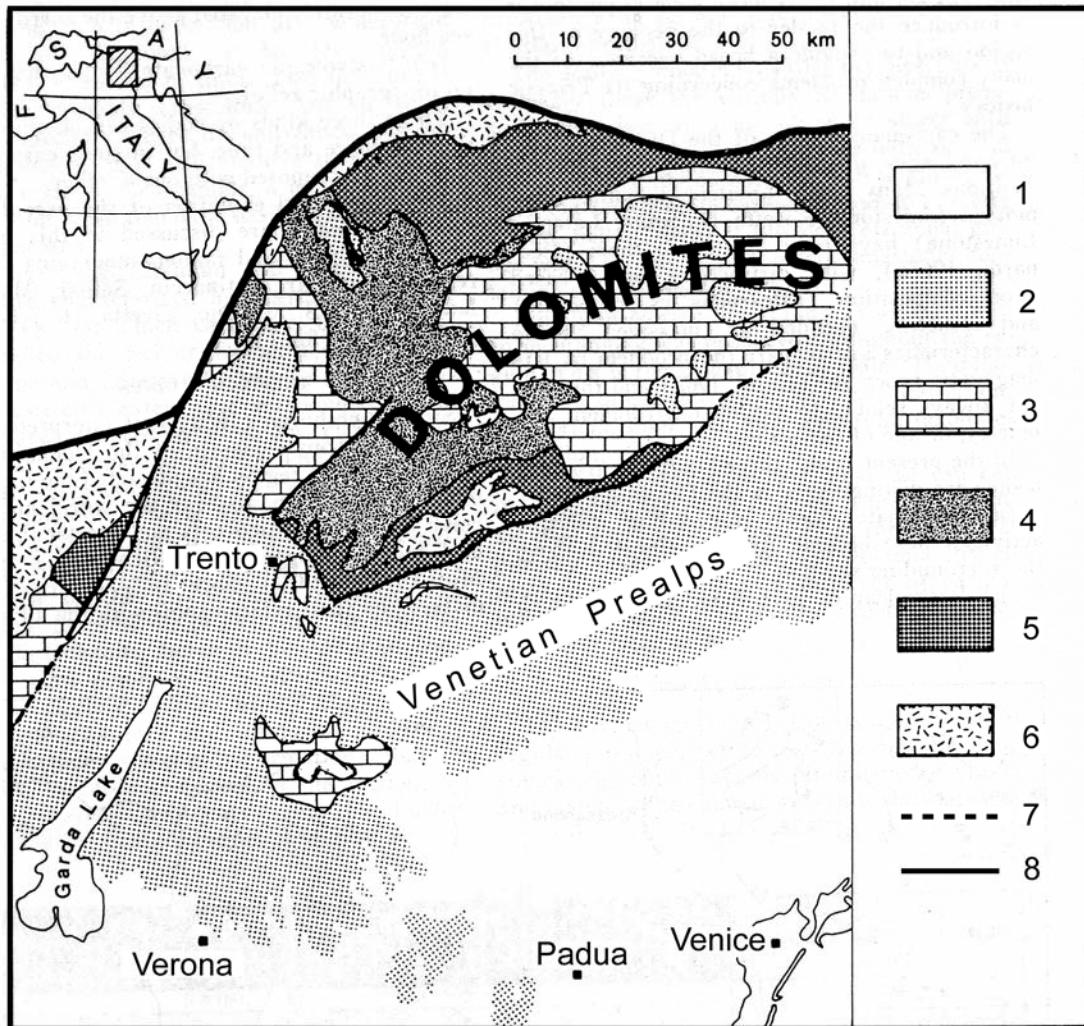


Figure 2.1. Regional geological setting of the Dolomites (adapted from Bosellini and Rossi, 1974a). 1, Alluvial plain; 2, Tertiary and Jurassic; 3, Triassic (with the buildups); 4, Permian ignimbrites; 5, Metamorphic basement; 6, Intrusions; 7, Major faults; 8, Tectonic boundary of the Southern Alps.

shallow shelf (Bosellini and Hardie, 1973; Massari and Neri, 1997). The Lower Triassic (Scythian) Werfen Formation, a highly variable sequence of shallow-water carbonates and alluvial sediments, unconformably overlies the Permian strata (Bosellini and Rossi, 1974; Goldhammer, 1987).

Regional strike-slip faulting in the Upper Anisian/Lower Ladinian (early Middle Triassic) caused localized block faulting with uplift, subaerial exposure, and erosion in some areas, and subsidence in others. Carbonate platforms and buildups nucleated on the structural highs. Three main carbonate platforms formed on top of the Lower Serla Dolomite, a widespread tidal flat unit overlying much of the area: the Monte Rite Formation and the Upper Serla Dolomite in the east and the Contrin Formation in the west. Both the Monte Rite Formation and Upper Serla Dolomite were drowned during late Anisian subsidence of the eastern Dolomites, but in the west, where uplift and westward marine transgression occurred, the Richtofen Conglomerate (a thin, local, conglomerate), and the Morbiac Limestone (a lagoonal-basinal carbonate) developed, followed by the Contrin Formation (a shallow-water platform rich in dasycladacean algae and trace fossils) that prograded over these formations on the structural highs (Bosellini et al, 2003; Goldhammer, 1987).

Continued subsidence in the late Anisian caused the upward growth of these buildups, although the growth of the eastern platforms was terminated by drowning caused by more rapid subsidence. Aggradation continued on the Contrin in isolated structural highs in the west, produced by strike-slip faulting along the Stava and Trodena Lines (Doglioni, 1984; Blendinger, 1985). The increasing relative sea level allowed thick carbonate platforms to develop (Latemar, Agnello, Marmolada, Catinaccio, Pale di San

Martino) with deposition of cherty limestone in the surrounding basins (Livinallongo Formation). The strike-slip faulting that caused the structural highs and platform growth was associated with Ladinian volcanic activity and localized plutonic intrusions such as the Predazzo and Monzoni complexes. The platforms were cut by mafic dikes, and submarine volcanics overlapped and partially filled the surrounding depositional basins. Some platforms in the western Dolomites (Latemar, Agnello, Marmolada) were buried beneath these volcanics, and a rapidly-subsiding caldera developed (Blendinger, 1985; Goldhammer, 1987). Carbonate production in the west was terminated or temporarily halted by this volcanic event, while areas to the east did not experience any interruption in carbonate production (Goldhammer, 1987; Bosellini et al, 2003). After Ladinian volcanism and plutonism, sedimentation continued with the Wengen Formation; the Carnian Cassian Dolomite (and its basinal equivalent, the San Cassiano Formation), Durrenstein Formation, and Raibl Formation; the Norian Dolomia Principale; the Lower Jurassic Calcari Grigi; and Upper Jurassic and Cretaceous deep water carbonates (Figure 2.2).

The Latemar Carbonate Buildup

The focus of this study is the Middle Triassic Latemar carbonate buildup, a small massif located northwest of the town of Predazzo, in the Trentino-Alto Adige province, (Figure 2.3). The Latemar is a series of vertically stacked platform carbonate deposits surrounded by reef and foreslope deposits (Figure 2.4) that totals 10-12 km³ in volume (Wilson et al., 1990).

Period	Stage	Time (m.y.)	Stratigraphic Stage	Thickness (m)
Cretaceous	Lower Cretaceous	120	Deepwater Carbonates	200
	Malm	141	Deepwater Carbonates	53
Jurassic	Dogger	149	Deepwater Carbonates	39
	Liassic	178	Calcari Grigi	300
	Rhaetian	190	(unconformity)	
Triassic	Norian	215	Dolomia Principale	200
	Carnian	225	Platform Carbonates, Raibl Fm.	150
	Upper Anisian, Ladinian	228	Latemar Limestone, Lower Edifice	700
	Lower Anisian	242	Richthofen Cglm., Contrin Fm.	120
	Scythian	244	Werfen Fm.	300
	Mid-Upper Permian	248	Gardena Sandstone, Bellerophon Fm.	400
	Lower Permian	258	Volcanics	1500
		286		

Figure 2.2. Stratigraphic column of the Trento Plateau, southern Alps (adapted from Goldhammer, 1987). Wavy lines indicate unconformity bounded sequence.

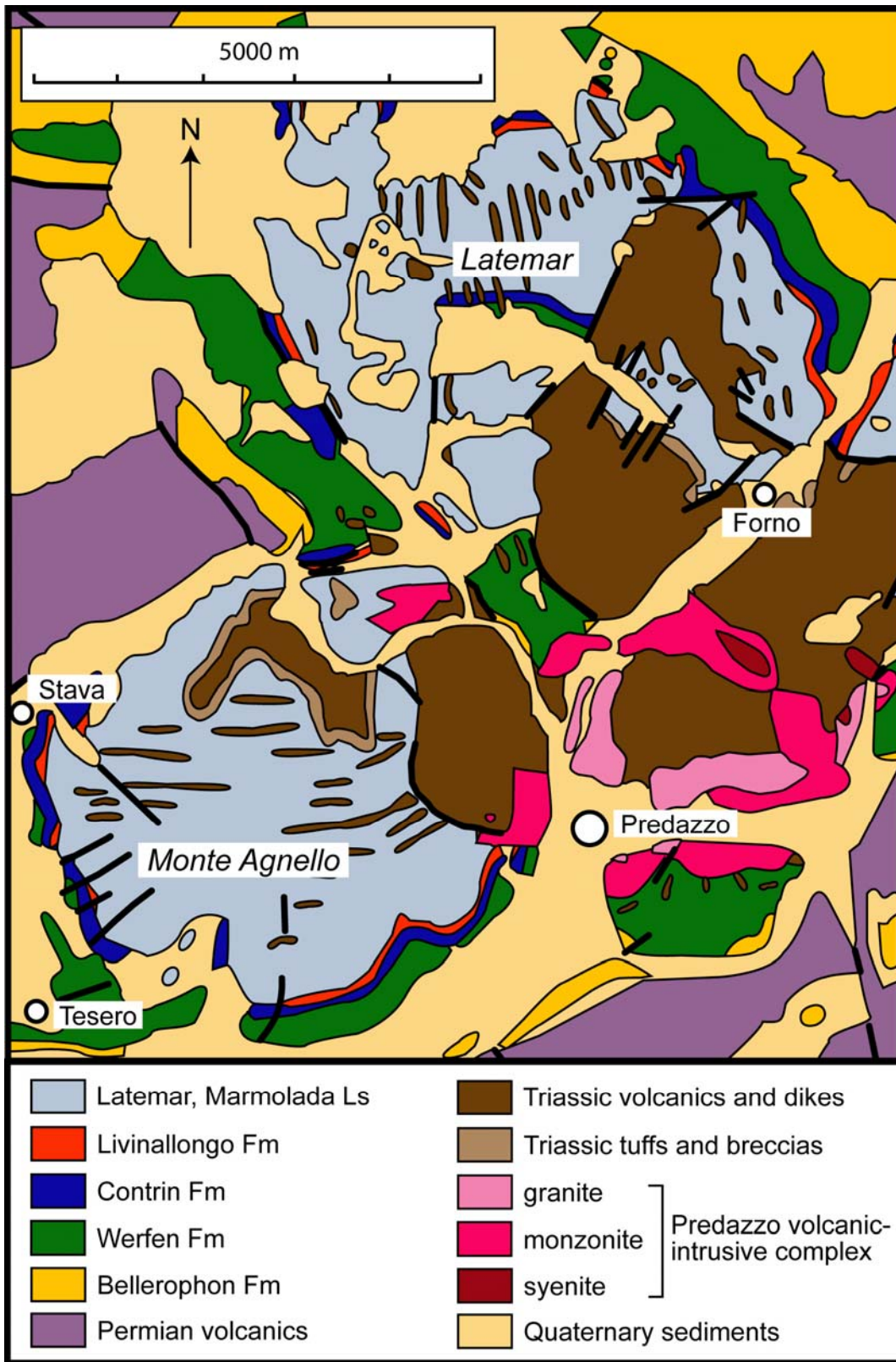


Figure 2.3. Geologic map of Latemar and adjacent buildups (adapted from Leonardi, 1955). Circles are locations of towns.

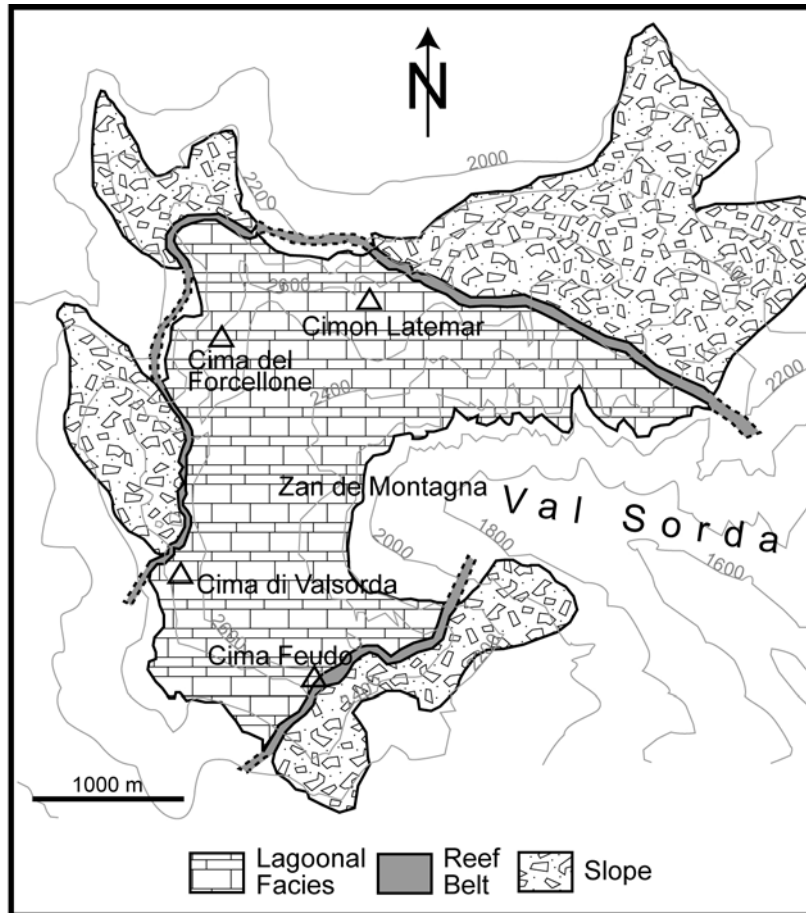


Figure 2.4. Reef structure of the Latemar (adapted from Egenhoff et al., 1999).

Numerous stratigraphic studies have been conducted on the Latemar (Rossi, 1967; Cros, 1977; Goldhammer, 1987; Harris, 1988; Dunn, 1991; Yose, 1993; Brack et al., 1996; Egenhoff et al., 1999; Preto et al, 2001), which records Middle Triassic shallow water carbonate deposition from the Upper Anisian to the Lower Ladinian. The buildup is comprised of three stratigraphic units: the Latemar Limestone and Lower Edifice (together constituting ~ 700 m of vertically stacked platform deposits), and the Marmolada Limestone (reef and foreslope breccias and grainstones). The platform carbonates are stratigraphically equivalent to the Livinallongo Formation (adjacent basinal shales and turbidites). The lower 300 m of the Latemar platform facies, the Lower Edifice, consists of flat-lying, thinly bedded grainstones of dasycladacean algae and represent Late Anisian shallow subtidal deposition and cementation. The upper 400 m, the Latemar Limestone, consists of cyclic carbonate layers (subtidal grainstones with cm-scale dolomite caps) and represent repeated subaerial exposure of the platform during the Ladinian (Hardie et al., 1986; Goldhammer, et al., 1987, 1990).

The Predazzo volcanic-intrusive complex intruded adjacent to and beneath the Latemar buildup in the Late Ladinian at 232-238 Ma (from U-Pb and $^{40}\text{Ar}/^{39}\text{Ar}$ dating of igneous minerals by Laurenzi and Visona, 1996; Mundil et al., 1996; and Visona, 1997). This igneous activity was contemporaneous with carbonate production, and produced a plutonic core, dikes, lava flows, volcanoclastic material that filled the adjacent basins and covered the other buildups, volcanic breccias containing carbonate rock fragments derived from these buildups, and a ring dike complex that intruded the Latemar and nearby buildups including the Monte Agnello and the Marmolada platforms. Igneous activity resulted in a down-drop of the southeastern portion of the Latemar buildup along

a circular caldera fault system (Vardebasso, 1930; Blendinger, 1985). Lavas and volcaniclastic rocks covered the Latemar buildup and permanently terminated carbonate deposition on the platform and in the surrounding basin.

The Latemar has been partially dolomitized, and the dolomitization, based on field relations, is considered contemporaneous with this igneous activity (Wilson et al, 1990; Riva and Stefani, 2003). Although the Dolomites were deformed by folding and thrust faulting during the Tertiary Alpine orogeny, the Latemar and surrounding region was largely unaffected by Alpine deformation and entirely unaffected by Alpine regional metamorphism (Blendinger, 1985; Doglioni, 1987).

Chapter 3

Methods of Investigation

A total of 263 samples of limestone and dolomite were collected from thirteen outcrops and along six traverses, giving a distribution of samples from the meter scale to the km scale (Figure 3.1). Dolomite-limestone contacts and sample positions were mapped at the meter-scale to centimeter-scale accuracy in nine of the thirteen outcrops using a Laser Technology, Inc. laser range finder and digital fluxgate compass or using digital photographs. Sample locations and contacts between dolomite, limestone, and igneous rocks along the traverses were mapped with a laser rangefinder, hand-held Magellan GPS device, and Brunton compass. Sample locations are listed in Appendix I.

Mineral assemblages were determined for 137 samples in polished thin sections with back-scattered electron (BSE) imaging using the JEOL JXA-8600 electron microprobe at Johns Hopkins University. Mineral modes were measured for each sample by setting up a square 4×4 1 cm^2 grid, and taking a digital BSE image of the area surrounding each node at 150X magnification (1024×800 pixels, $0.725 \text{ }\mu\text{m/pixel}$). These images were analyzed in Adobe Photoshop by assigning a range of grayscale values to each mineral as well as to porosity. The grayscale values for each mineral and porosity were determined separately for each sample using Photoshop's Threshold tool. The total number of pixels for each grayscale range was determined using the Histogram tool, and the modal distribution of each sample was calculated by weighting each grayscale range against the total number of pixels per image. Uncertainties in mineral identification were resolved by obtaining an energy-dispersive X-ray spectrum. Charging

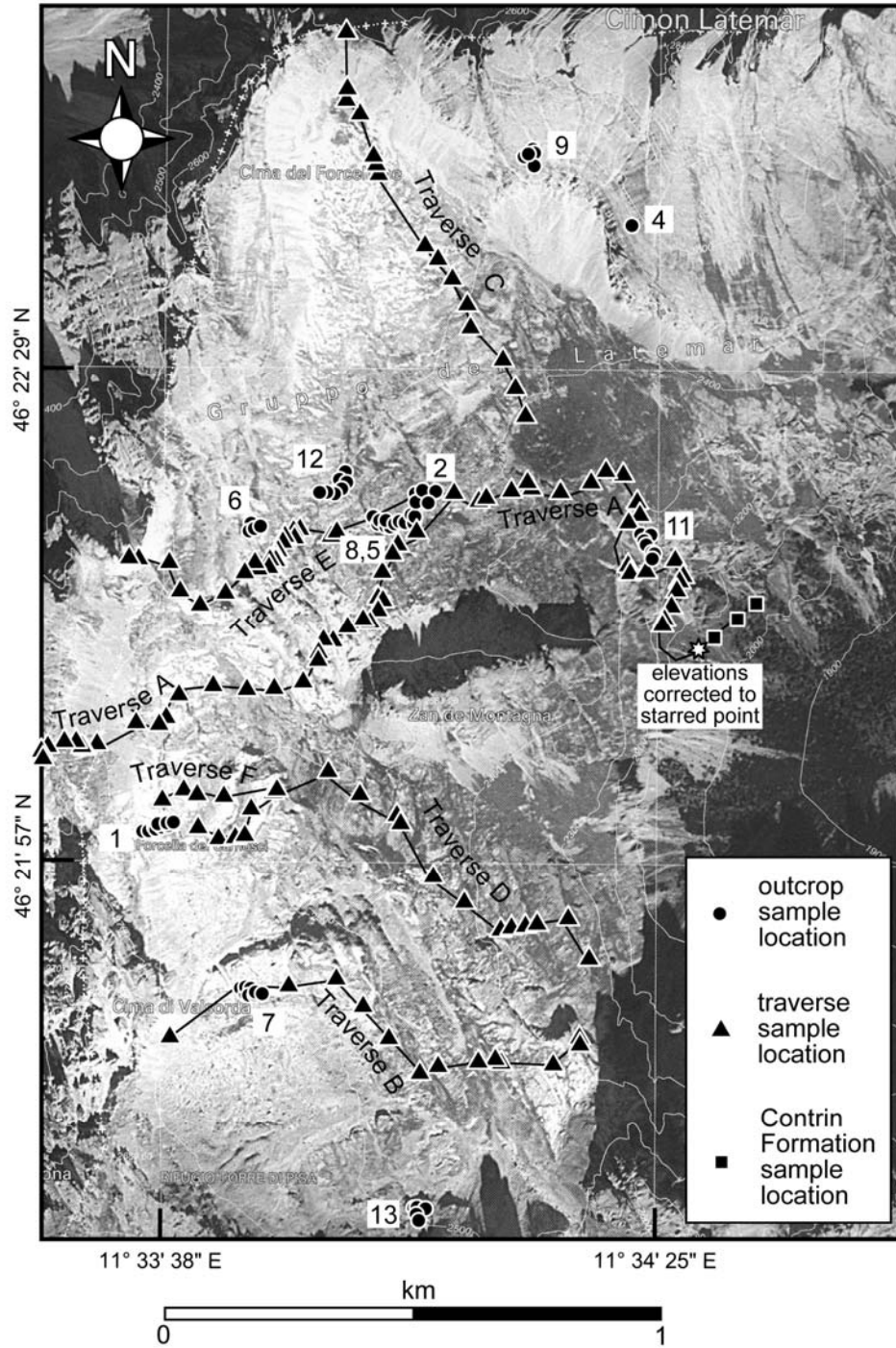


Figure 3.1. Orthographic aerial photograph with sample locations.

or shadows on the surface of the specimen were not included in the total pixel sum. Tests demonstrated that the precision of mineral modes measured in this way is comparable to or better than modes measured by counting $\geq 2,000$ points in thin section using BSE imaging with the electron microprobe. Mineral compositions were measured by wavelength-dispersive X-ray spectrometry with the electron microprobe at Johns Hopkins University using natural mineral standards and a ZAF correction scheme (Armstrong, 1988). Because most samples were monominerallic, minerals were analyzed at the nodes of square $4 \times 4 \text{ } 1 \text{ cm}^2$ grids, with additional spots analyzed if needed. All 263 samples were analyzed for carbon and oxygen isotope compositions, using polished slabs that had been stained for calcite and dolomite. Monominerallic powder was drilled from each slab with a 1 or 2 mm diameter diamond-tipped drill. The powders were dissolved in phosphoric acid at 90°C , and the released CO_2 was purified and analyzed for oxygen and carbon isotopic compositions with the dual-inlet gas source Micromass Isoprime mass spectrometer in the laboratory of A. J. Kaufman at the University of Maryland. The values for $\delta^{18}\text{O}$ and $\delta^{13}\text{C}$ are reported relative to VSMOW and VPDB respectively. Calcite standards (NBS-19 and Lincoln Limestone, an in-house working standard) were analyzed multiple times during each analytical session to verify that the analytical precision for both carbon and oxygen isotopes was $\pm 0.1\%$ (1σ). Duplicate analyses were made of over half the samples, and analyses were accepted only when they agreed within measurement error.

Selected major, minor, and trace element (Ca, Cr, Mn, Fe, Co, Ni, Cu, Zn, Rb, Sr, Ba, Pb) compositions were measured for carbonate minerals in 36 samples using $100\mu\text{m}$ thick sections, the ThermoFinnigan Element 2 LA-ICPMS, and the NIST-610 silicate

glass standard in the laboratory of W. F. McDonough at the University of Maryland. The spectra for some major and minor elements (Ca, Mn, Fe, Rb, Sr) were first collected using a 6-7 Hz laser with a 15-30 μm spot size. Minor and trace element (Cr, Co, Ni, Cu, Zn, Sr, Ba, Pb) spectra were then collected from immediately adjacent locations using a 6-8 Hz laser with a 65-70 μm spot size. Each mineral in a sample was analyzed in approximately 8 pairs of spots within a 1 inch diameter circular thick section. The spectra obtained from these analyses were processed using LAMTRACE, a Lotus 1-2-3 data reduction spreadsheet and macro designed by Jackson et al. (1997). The spectra for each pair of microsampling spots were analyzed for spikes, trace mineral interferences, breakthrough (when the laser burns through the sample and ablates the underlying glass slide) and background counts. A measurement was taken every 389 milliseconds, and the spectra were averaged over every three measurements, giving average values for every 1.16 seconds. Particle bombardment spikes in both the background and in the ablation spectra were removed manually. Data for each analysis were processed taking the detection limit as three times the standard deviation of the background. Spectra from different isotopes of the same element (eg., ^{65}Cu and ^{63}Cu) were compared for each microsampling spot to ensure that the average values obtained in the analyses were not artificially high due to particle bombardment. Only values for the more abundant isotope are reported (^{63}Cu , ^{66}Zn , ^{86}Sr , ^{138}Ba , ^{208}Pb). Major element spectra were processed using the mineral's average CaO content, previously obtained from microprobe analyses, as the calibration point. The resulting ^{86}Sr values from the first set of analyses at each microsampling location were used to calibrate the second set of trace element spectra.

Element concentrations in the NIST 610 silicate glass standards generally have a 1-3% uncertainty. Analyses were considered unreliable if the relative standard deviation (RSD) of the glass standard was >5% for Mn, Sr, Co, Zn, Cu, Ba, Pb, >6% for Ni, >7% for Fe, and >10% for Cr, and the data for that element were discarded. In some cases, volatilization of calcite samples during previous analyses caused anomalously high ^{57}Fe backgrounds, making the concentration of ^{57}Fe in the sample to appear to be below the detection limit of the instrument. Therefore, Fe analyses are not reported for samples analyzed under these conditions.

Several samples were imaged on an ELM-3 Luminoscope, using an Olympus Magnafire Imaging System, in the cathodoluminescence laboratory of Sorena Sorenson at the Smithsonian Institute.

Chapter 4

Distribution of Dolomite

The Latemar dolomites are distinguished from the surrounding limestones by color and texture. Latemar limestones are grey to white in color and compact with typically <9% pore space. Limestones in the Lower Edifice are dominated by skeletal grainstones (primarily consisting of dasycladacean algae) with minor interbedded peloidal wackestones, while limestones in the overlying Latemar Limestone are skeletal-peloidal wackestones and packstones consisting of dasycladacean algae, cyanobacteria, foraminifera, ostracods, gastropods, and bivalves as well as non-skeletal peloids and lithoclasts. Limestone stratigraphy and petrography is described in greater detail by Goldhammer (1987) and Dunn (1991).

There are three types of dolomite in the Latemar: replacement dolomite, diagenetic (cycle cap) dolomite, and saddle dolomite. The majority of dolomite in the Latemar (>99%) is replacement dolomite. It is tan to orange in color with a sugary texture and up to 16% porosity. The color of replacement dolomite depends on the amount of Fe and Mn; samples with high Fe and Mn contents are orange, and stain bright blue in potassium ferrocyanide solution, while samples with lesser Fe and Mn contents are tan and stain lavender-beige. Replacement dolomite is coarsely crystalline, with individual dolomite grains ranging from microns up to 1 mm in diameter. Existing sedimentary structures are typically destroyed by massive replacement dolomitization. In contrast, cycle cap dolomite forms thin (1 to 15 cm thick) diagenetic caps on the tops of the cyclic deposits of the Latemar Limestone. It is restricted to exposed cap horizons that

have undergone vadose diagenesis. Like replacement dolomite, it is yellow in color but is microcrystalline, contains low porosity, individual grain sizes range from 1-10 microns in diameter, and preserves original micrite layers and structures in the limestones. The petrography of cycle cap dolomite petrography is described in greater detail by Goldhammer (1987), Wilson (1989), and Schubel (1997). Saddle dolomite is dolomite with a warped crystal lattice (Radke and Mathis, 1980). It occurs at the edges of open pores and vugs as a pore-filling cement. It forms zoned crystals on the mm scale, with inclusions of Fe-oxides outlining the zones. Occurrences and petrography of saddle dolomite are described exhaustively in Wilson (1989) and Schubel (1997). Because cycle cap dolomite and saddle dolomite formed during diagenesis and make up a volumetrically insignificant percentage of the Latemar dolomite (<1%), they are not considered further in this study.

Limestone-dolomite contacts

Dolomitization is easily visible in the field both on the meter and km scale due to the color difference (Figure 4.1). Dolomitized areas are 100% dolomite (or nearly so), and areas of limestone are likewise ~100% limestone with little or (more typically) no dolomite (Figure 4.2). The transition from unreacted or nearly unreacted limestone to completely or almost completely reacted dolomite is sharp at the scale of the buildup (<~0.5 m) (Figure 4.3). In the transition zone, dolomite occurs as an anastomosing network of veins in unreacted or nearly unreacted limestone, and the dolomite-limestone contact is sharp even at the mm scale (Figure 4.4). Limestone-dolomite contacts have the same sharpness regardless of geometry or orientation of the dolomite body.

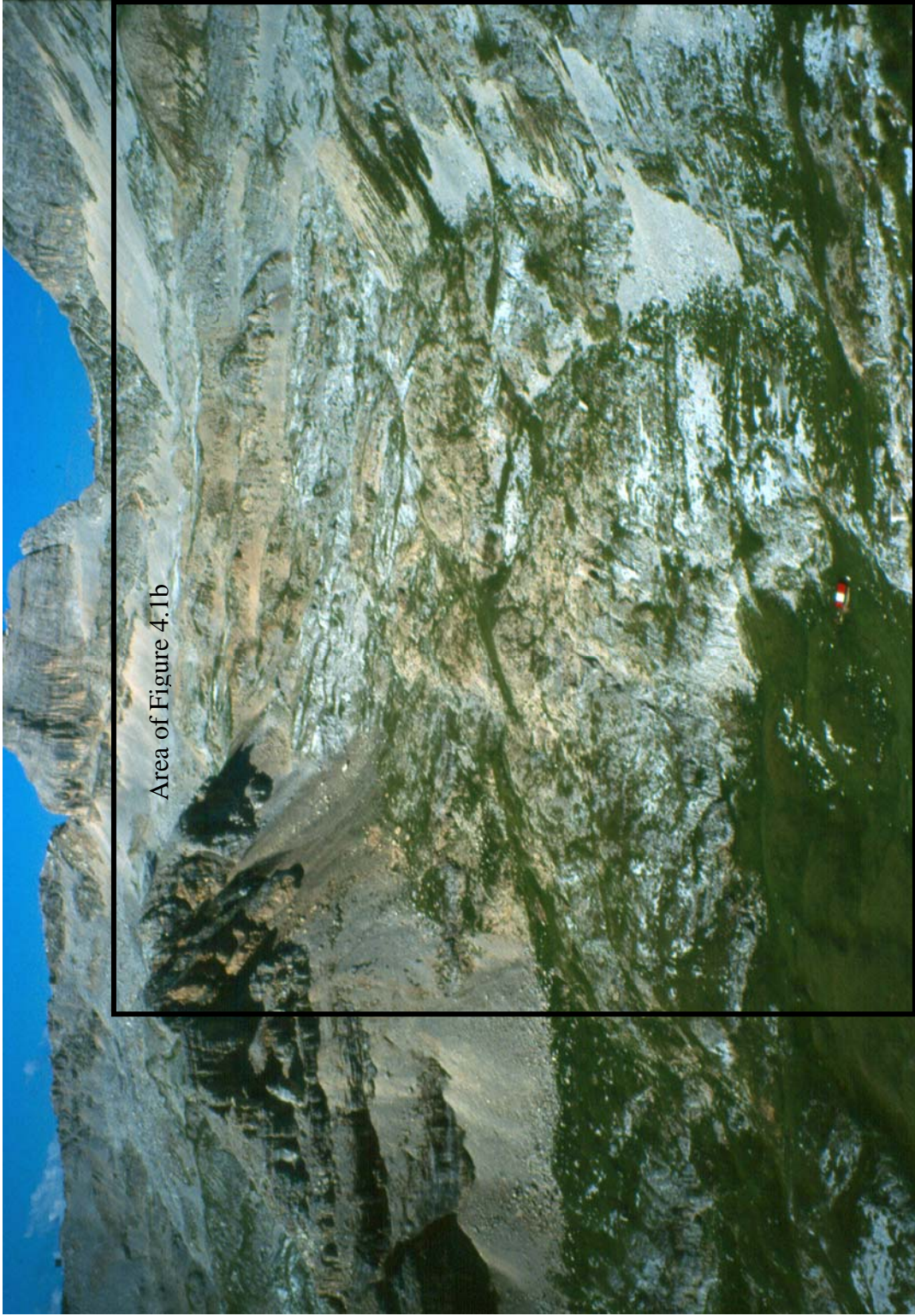


Figure 4.1a. Panoramic photo of platform interior, facing west. Topographic relief ~ 500 m; width of field of view 1-2 km, depending on distance from point of photograph. Gray rocks are limestone, orange rocks are dolomite.

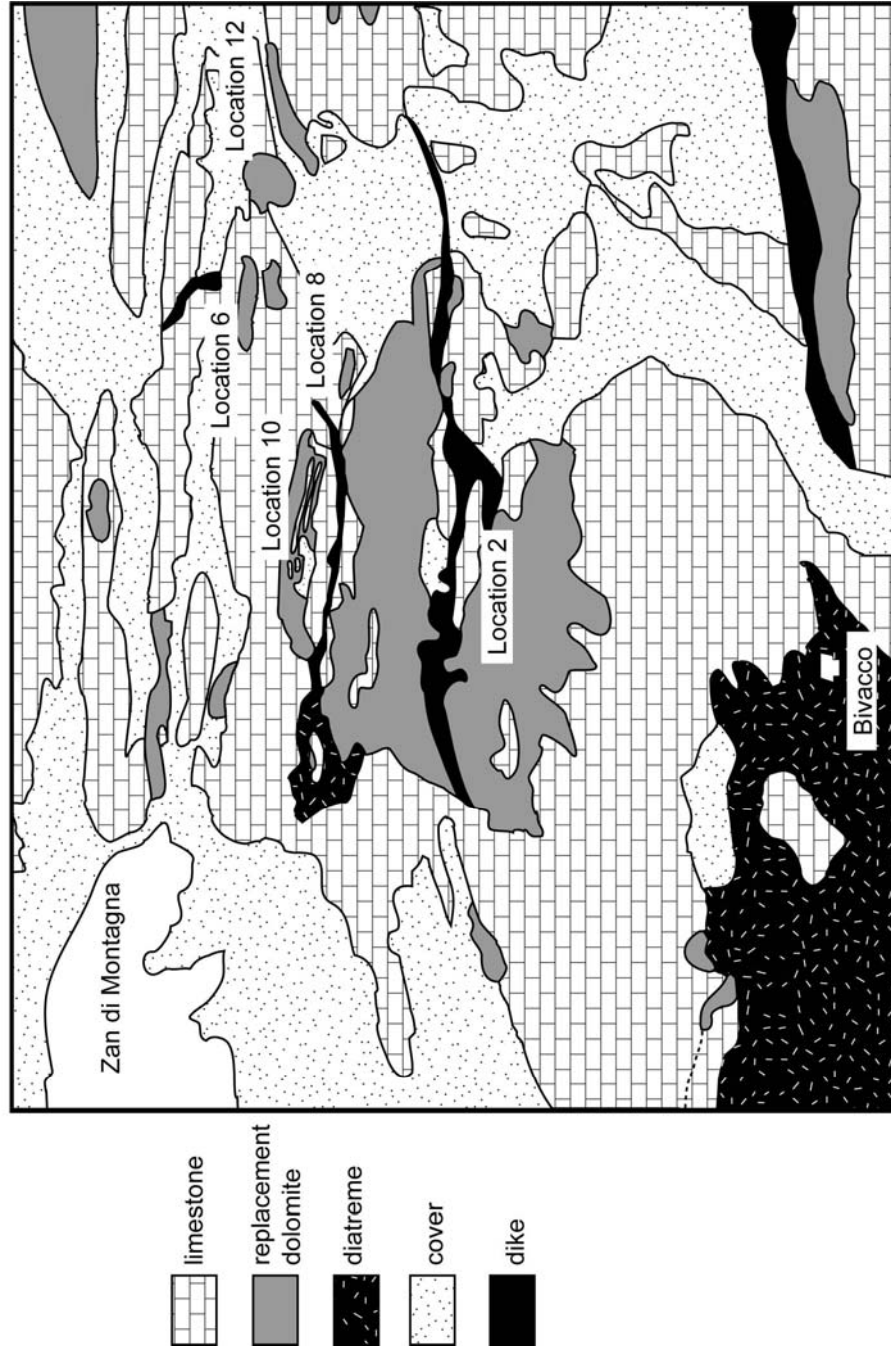


Figure 4.1b. Panoramic map of the platform interior facing west (tracing of digital photo in Figure 4.1a). Geologic relationships in the area of Zan di Montagna are obscured by topography and shadow. Dolomite is heterogeneously distributed in discrete bodies at a variety of spatial scales separated by completely unreacted limestone. Detailed maps at locations 2-12 appear in later figures.

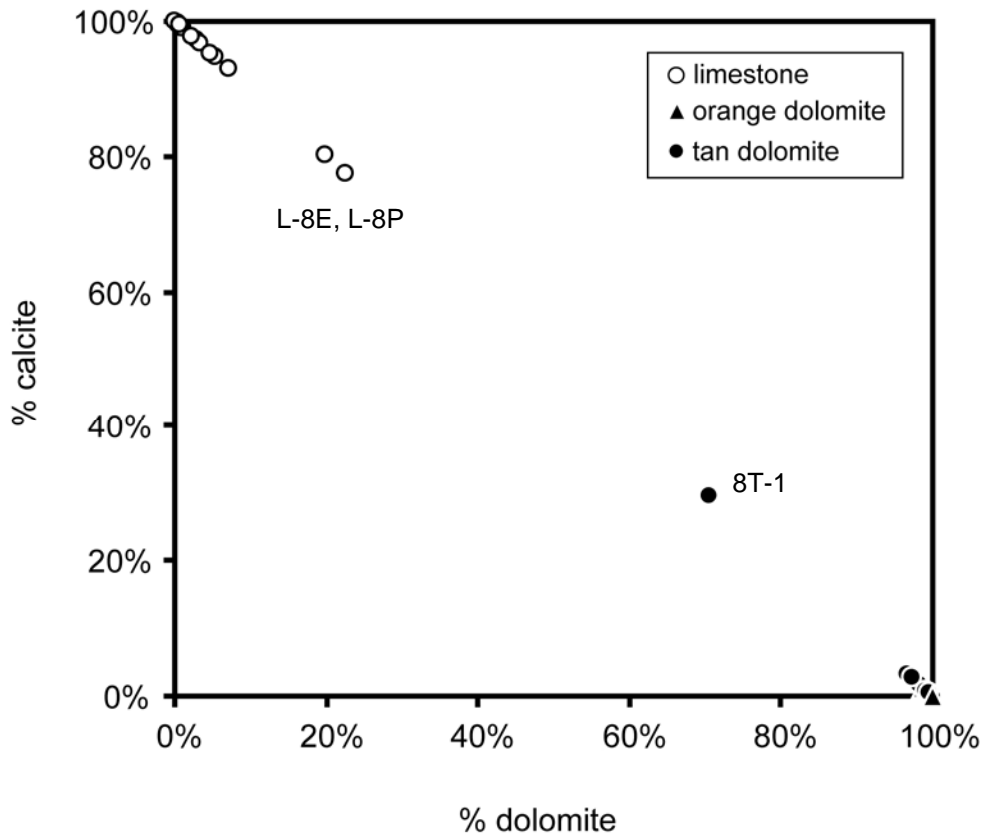


Figure 4.2. Normalized modes of dolomites and limestones. L-8E, L-8P, and 8T-1 all occur at contacts between limestone and dolomite. X-axis is $\frac{\text{dolomite}}{\text{dolomite} + \text{calcite}} \times 100\%$ and Y-axis is $\frac{\text{calcite}}{\text{dolomite} + \text{calcite}} \times 100\%$.

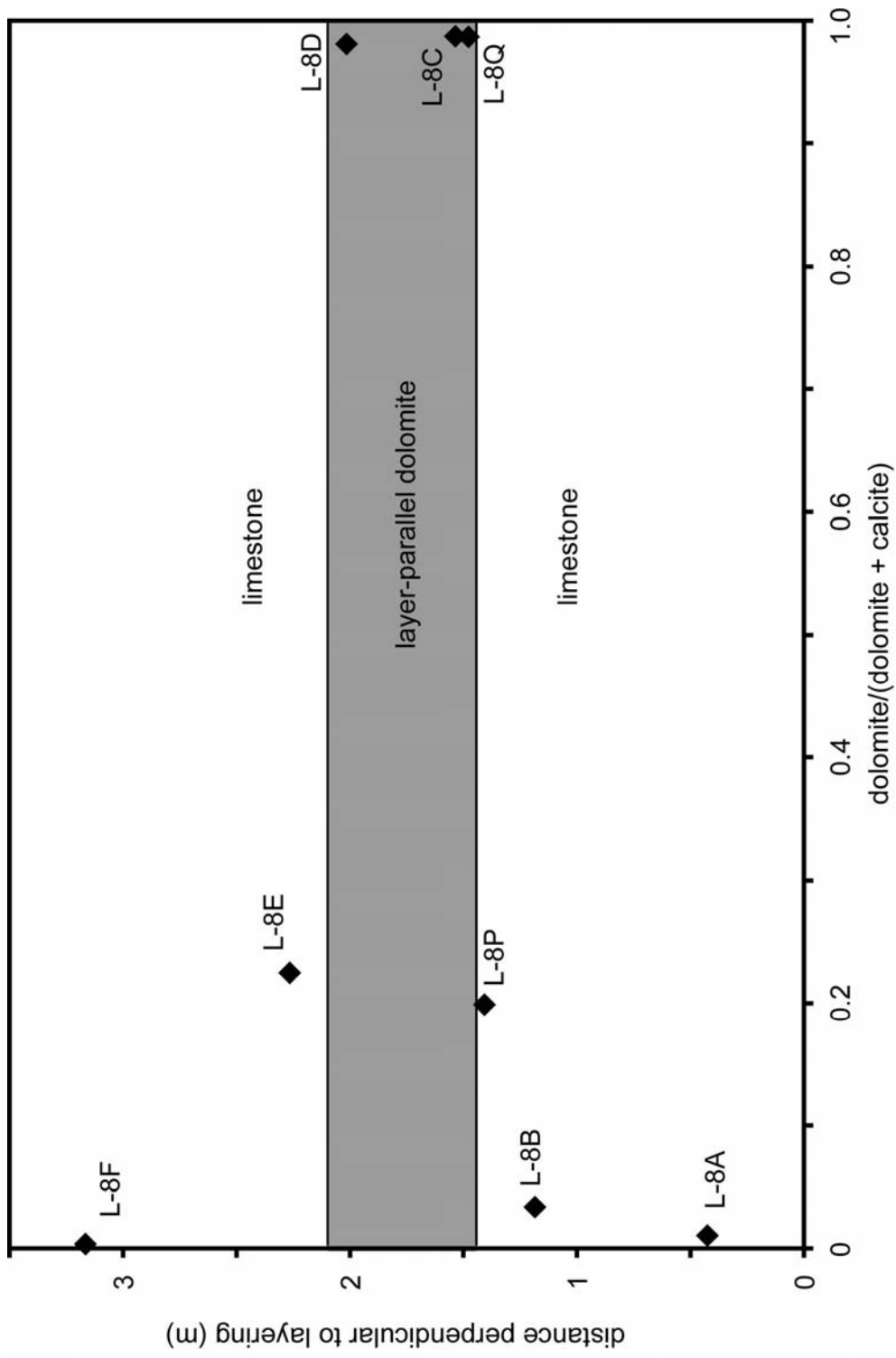


Figure 4.3. Distribution of limestone and dolomite at the meter scale at two limestone-dolomite contacts (Location 8). Layering is approximately horizontal. Transition from nearly completely unreacted limestone to nearly completely reacted dolomite occurs over $< \sim 0.5$ m perpendicular to the limestone-dolomite contact. Sample locations as in Figure 4.5.

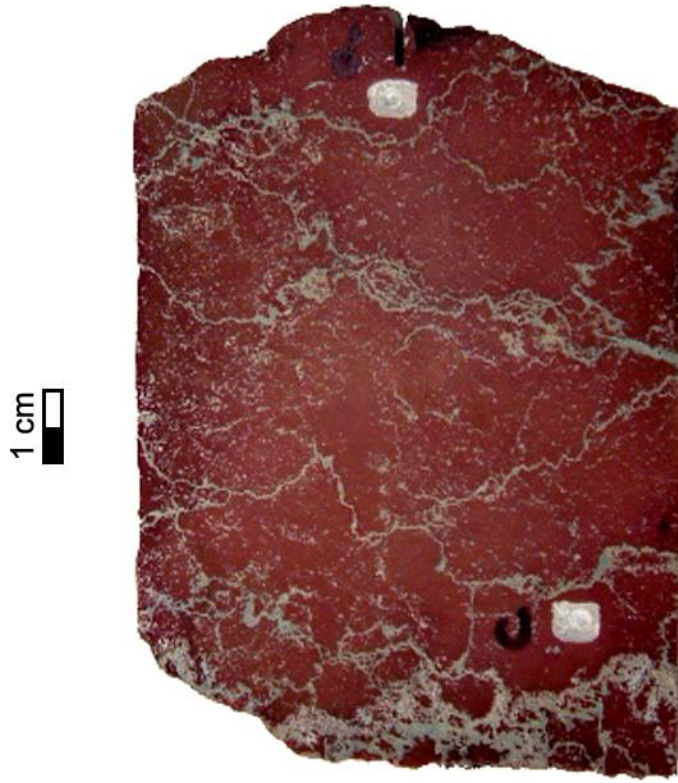


Figure 4.4. Digital photograph of polished surface of sample L-8P (Figure 4.2), stained for calcite (red) and dolomite (blue), showing dolomite veins in limestone. Lettered spots are drill sites sampled for stable isotope analysis. C indicates side of sample near the dolomite contact.

Outcrop scale field relations

On the outcrop scale, field observations correspond closely to those reported by Wilson (1989). At elevations above ~2300 m, replacement dolomite predominantly forms layer-parallel bodies on the outcrop scale (Figures 4.5 - 4.7). Dolomite crops out as parallel bands in cross-section that correspond to sheet-like bodies almost exactly parallel to bedding in limestone. Dolomite occasionally crosscuts limestone at the cm-scale. The layer-parallel sheet-like bodies can have horizontal dimensions $> \sim 10^4 \text{ m}^2$ (Figure 4.8). Sheets at different levels occasionally can be seen interconnected by vertical dolomite bodies that in some cases are sheets (Figure 4.5) but in other cases may be tubes. Bodies that appear in cross section as isolated dolomite pods that line up exactly along the same bedding plane appear to be layer-parallel tube-shaped bodies, or finger-like extensions of a dolomite sheet exposed in cross section (Figure 4.5). Where sheet-like bodies are observed connected to vertical bodies, they always extend from vertical bodies in the up-dip direction (Figures 4.5., 4.6). Layer-parallel dolomite bodies are located largely in the structurally higher part of the buildup, above the contact between the massive Lower Edifice and the well-layered cyclic structures of the Latemar Limestone.

Dolomite also occurs as breccias with dolomite and limestone blocks up to several m in diameter set in a dolomite cement matrix (Figure 4.9). Breccias are the predominant occurrence of dolomite below ~2300 m in elevation, below the Lower Edifice - Latemar Limestone contact. They also occur above ~2300 m, but are much less abundant. At the 10-100 m scale the contact between limestone and dolomite breccia contacts is irregular and shows no preferred orientation (Figures 4.10, 4.11). At the $> 100 \text{ m}$ scale the

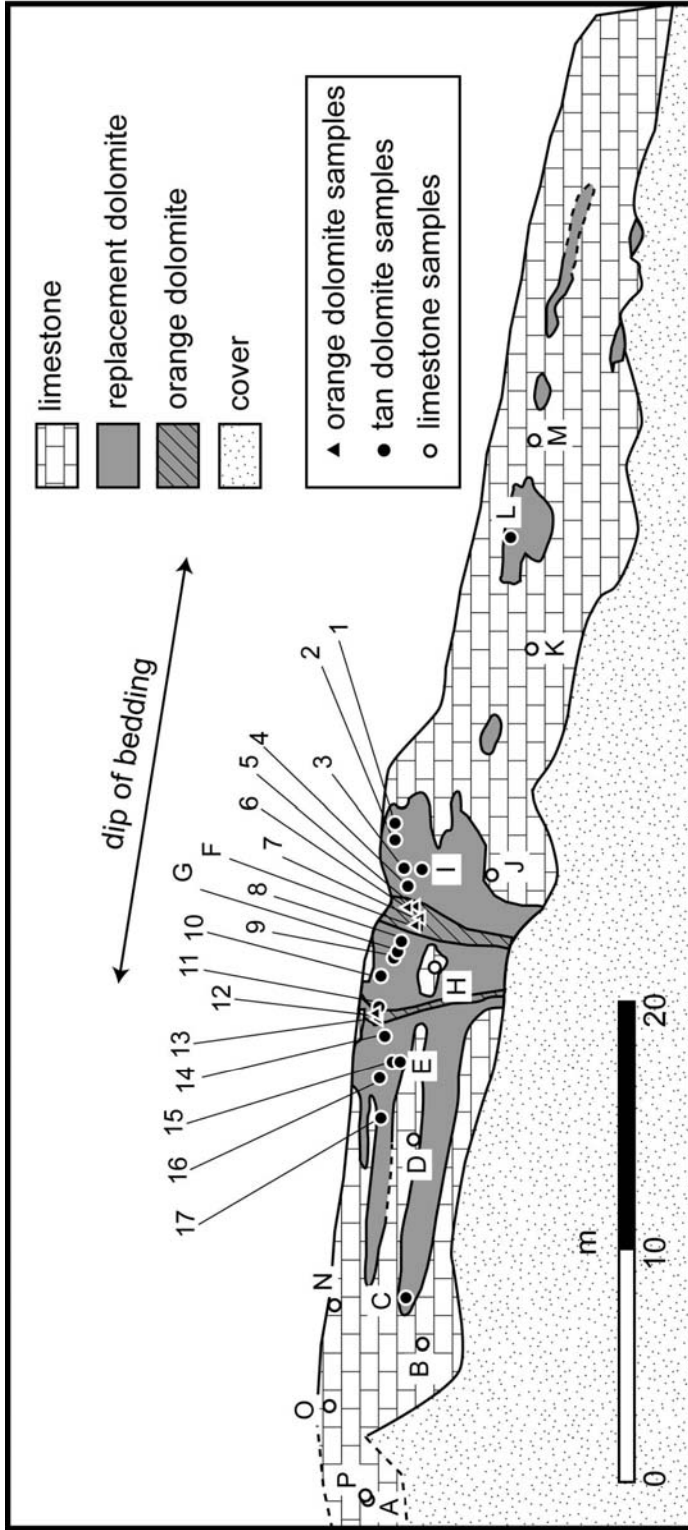


Figure 4.5. Sheet-like bodies of dolomite parallel to bedding planes in limestone (Location 7). Field relations exposed on the steep face of a gully mapped using a laser rangefinder and digital fluxgate compass and projected onto a vertical plane with E-W strike parallel to the length of the gully. Contacts are dashed where approximate. Sample location numbers omit the L-7 and the 7T prefixes in text and tables. Bands of dolomite are cross-sections through bedding parallel sheet-like bodies. Isolated dolomite pods that line up along the same bedding horizon are cross sections through bedding-parallel tube-like bodies. Sheet-like bedding-parallel bodies preferentially develop up-dip from two vertical fracture-controlled sheet-like bodies of orange dolomite.

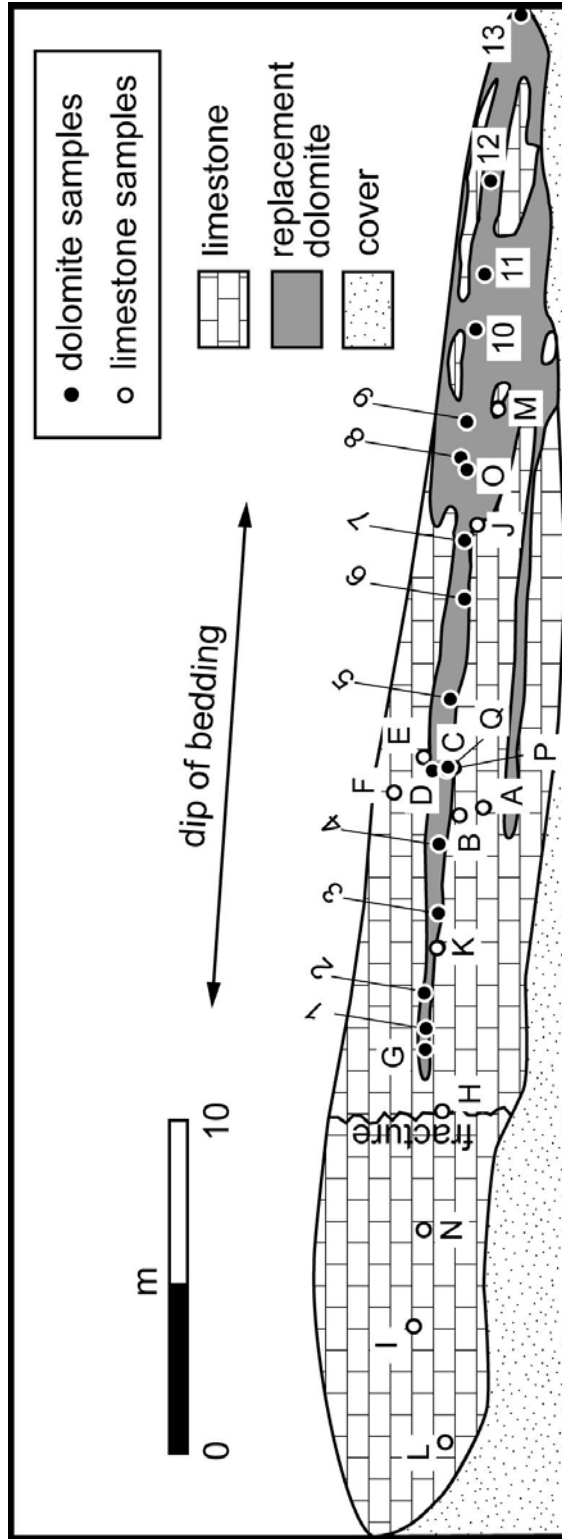


Figure 4.6. Sheet-like bodies of dolomite parallel to bedding planes in limestone (Location 8). Field relations exposed on the steep face of an outcrop, mapped using a laser rangefinder and digital fluxgate compass and projected onto a vertical plane with E-W strike parallel to outcrop face. A vertical fracture occurs on the west side of the outcrop. Sample location numbers omit the L-8 and 8T prefixes in text and tables.

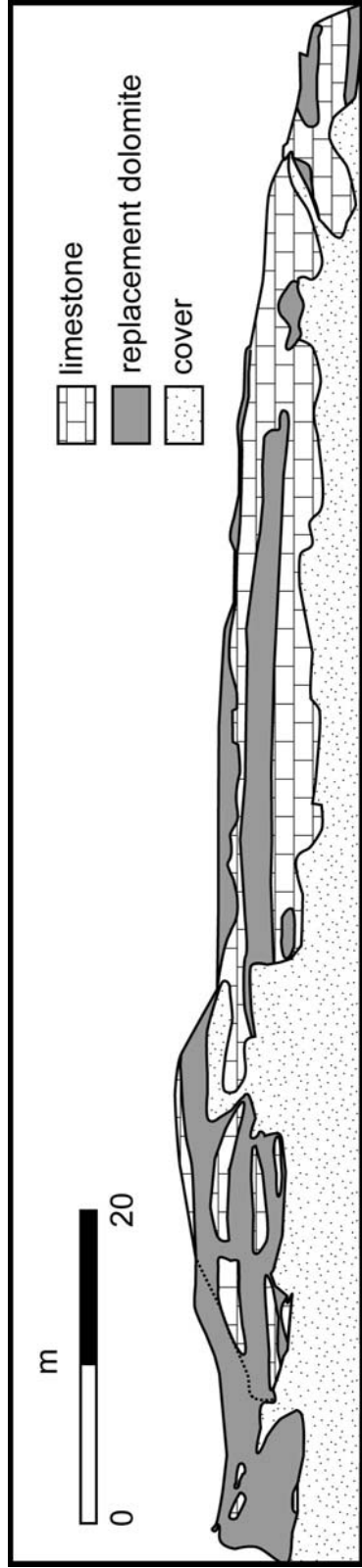


Figure 4.7. Sheet-like bodies of dolomite parallel to bedding planes in limestone (Location 10). Field relations exposed on the steep face of an outcrop, mapped using a laser rangefinder and digital fluxgate compass and projected onto a vertical plane with N-S strike parallel to outcrop face. Dotted line separates features that appear in contact from the viewpoint of the rangefinder but that are separated in three dimensions.

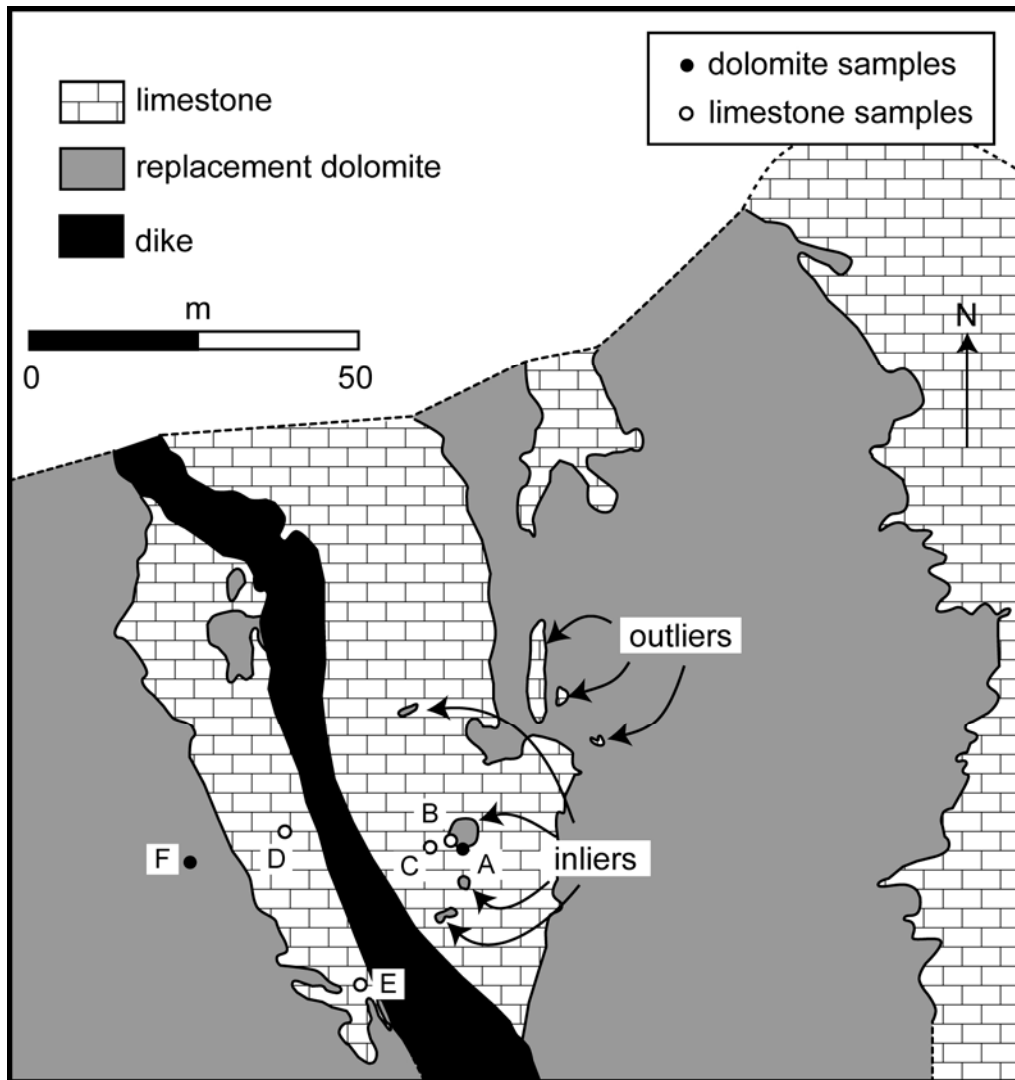


Figure 4.8. Map of Location 2 showing bedding-parallel sheets of dolomite. The eastern dolomite sheet, exposed both where it is almost exactly parallel to the topographic surface and in inliers through overlying limestone, has a horizontal dimension $>\sim 10^4 \text{ m}^2$. Contacts and sample locations mapped with laser rangefinder and digital floodgate compass. Dashed lines indicate edge of area mapped. Sample location letters omit the L-2 prefix in text and tables.



Figure 4.9. Photograph of dolomite breccia showing limestone and dolomite blocks (base of Traverse B). Width of field of view in foreground ~10 m.

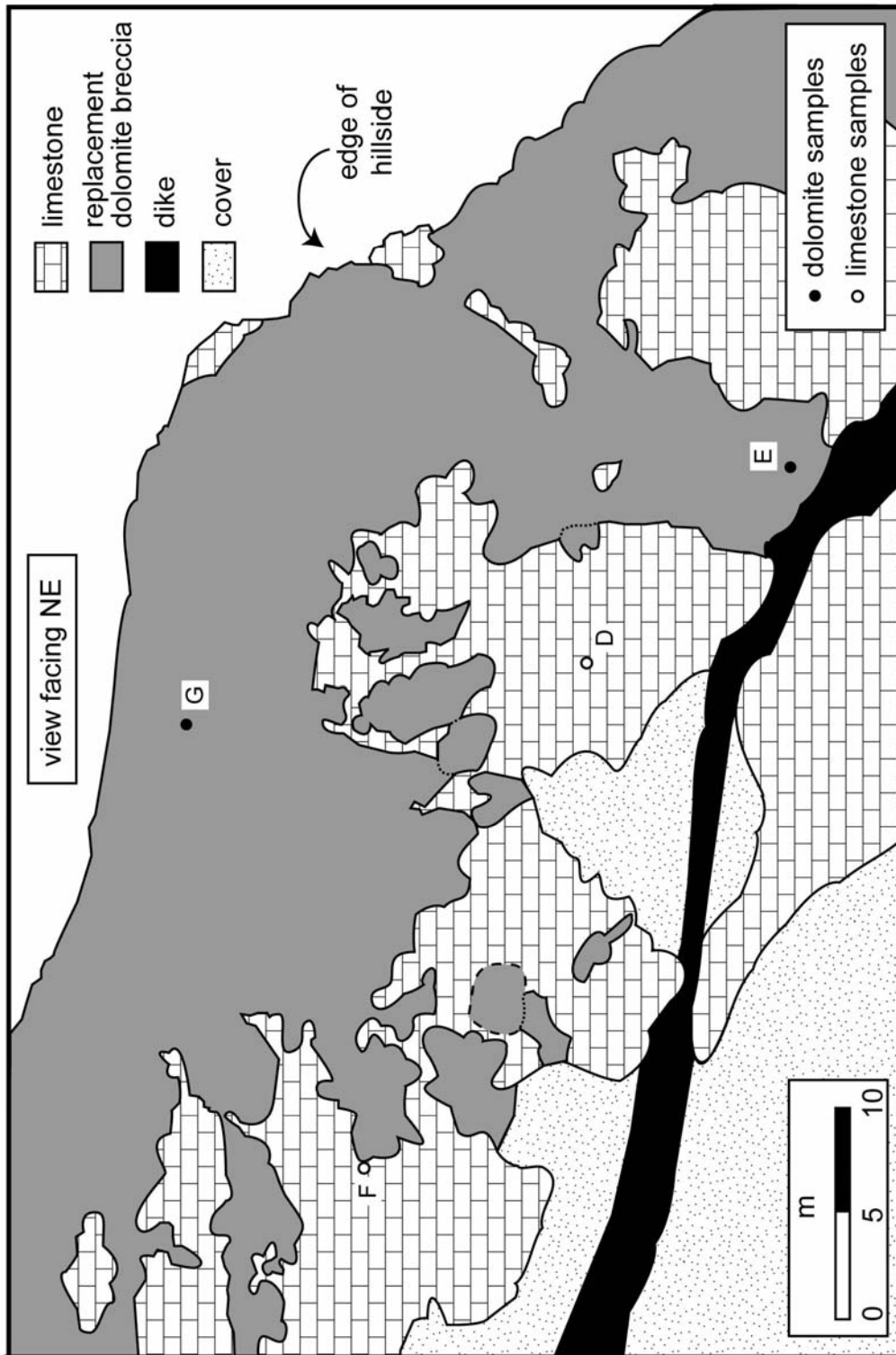


Figure 4.10. Dolomite breccia (Location 11). Geologic relations traced from a digital photograph. Dashed and dotted contacts as in Figure 4.6. Sample location letters omit the L-11 prefix in text and tables.

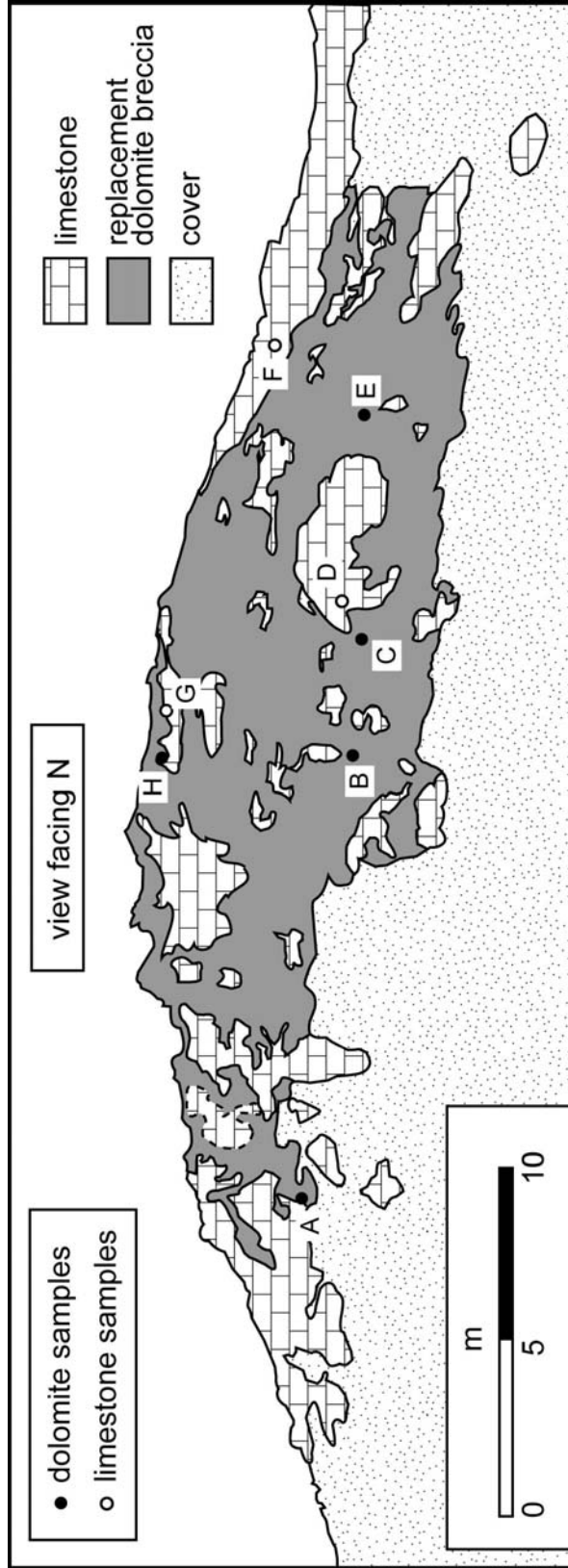


Figure 4.11. Dolomite breccia exposed on hill (Location 12). Geologic relations traced from a digital photograph. Dashed contacts as in Figure 4.6. Dolomite breccia is approximately circular in map view and columnar in three dimensions. Sample location letters omit the L-12 prefix in text and tables.

dolomite breccias form vertical columns with diameters of ~10-50 m and heights > 100 m (Figure 4.12). Riva and Stefani (2003) have established that these breccias are associated with extensional faulting caused by distension of the underlying magma chamber of the Predazzo volcanic-intrusive complex. These dolomite breccias are not restricted to the Latemar; work by Zempolich and Hardie (1997) in the Venetian Alps has shown that they are common in Mesozoic basinal sediments and are associated with faults and fractures. Zempolich (1995) concluded from the work of Doglioni (1990) and Elder (1977) that formation of these vertical breccia pipes occurred prior to dolomitization in other parts of the Dolomites. Sharp contacts between limestone blocks and dolomite cement matrix at some locations (Location 12, Figure 4.11), however, suggest that brecciation and dolomitization may have been contemporaneous at least in some cases in the Latemar buildup. Undeformed dolomite cement that forms the matrix of the dolomite breccias rules out brecciation after dolomitization.

Dolomite bodies are also associated with basalt dikes (Figure 4.13), occurring in map view as bands parallel to dikes, and in 3D as sheets parallel to dikes. Dolomite bodies associated with dikes primarily occur in the upper part of the buildup above the Lower Edifice - Latemar Limestone contact. Even in the same outcrop, some limestone-dike contacts are dolomitized and others are not (see also Figure 4.8). The parallel alignment of the dolomite bodies and dikes indicates that dolomitization postdates intrusion of the dikes at Location 1. Other occurrences of dikes that cross-cut dolomite are described in Wilson (1989), and Wilson et al. (1990) concluded some dikes were emplaced after dolomitization. Overall, emplacement of dikes and dolomitization appears to be broadly synchronous (Wilson et al., 1990).



Figure 4.12. Photograph looking south to base of Traverse A. Topographic relief ~ 500 m; width of field of view ~ 1 km. Dolomite breccia forms a vertical column, the top of which is illustrated in Figure 4.8, is >100 m tall, with a diameter of ~50 m (outlined in black).

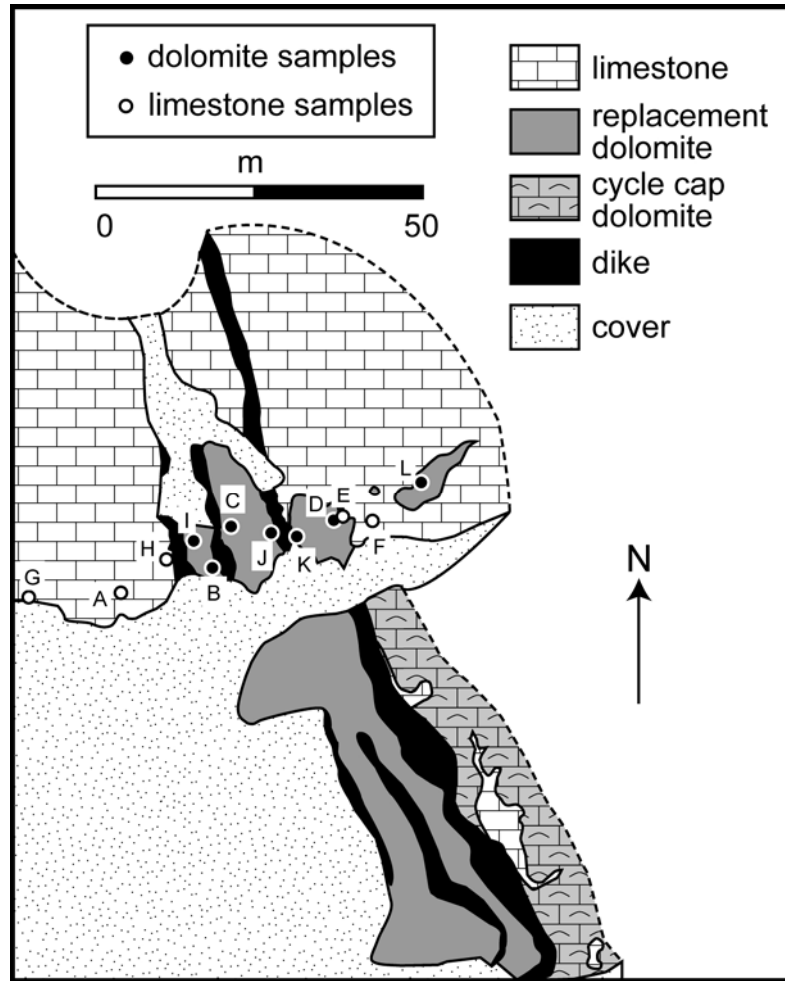


Figure 4.13. Map view of Location 1. Contacts and sample locations mapped with laser rangefinder and digital floodgate compass. Dashed lines indicate edge of area mapped. Sample location letters omit the L-1 prefix in text and tables.

Interconnected near-vertical and near-horizontal dolomite bodies can form irregular shapes (Figure 4.14, 4.15). The near-horizontal portions are not exactly layer-parallel, and the near-vertical portions have neither uniform orientation nor width. They occur in the upper part of the buildup, above the Lower Edifice - Latemar Limestone contact.

Regional scale field relations

Figure 4.1 shows an oblique view of the Latemar Limestone with ~500 m vertical relief and a width of field of view of 1-2 km. The contact between the Latemar Limestone and the Lower Edifice is located approximately at the base of the photograph and map, near the Bivacco Latemar. At the 100 m to km scale dolomite bodies show the same kind of heterogeneous distribution as at the outcrop scale.

The amount of dolomite and orientation of the dolomite-limestone contacts were recorded along six traverses in order to determine if there is any systematic change in the amount or geometry of dolomite throughout the buildup over 700 m elevation. To compare all data, spatial positions in 3D were projected parallel to layering (using average strike and dip of bedding in the buildup) to a single position in map view (Figure 3.1). The cumulative dolomite/(dolomite+limestone) vs. elevation curve (Figure 4.16) suggests that there is more dolomite in the lowest part of the buildup than in the upper parts of the system. This may in part be an artifact, however, that only a single path allows access to elevations $< \sim 120$ m, and the path lies in dolomite. Limestone is visible from a distance in vertical cliffs at elevations $< \sim 120$ m (Figure 4.12). Nevertheless, even ignoring curves below ~ 120 , the dolomite/(dolomite+limestone) curve steadily decreases

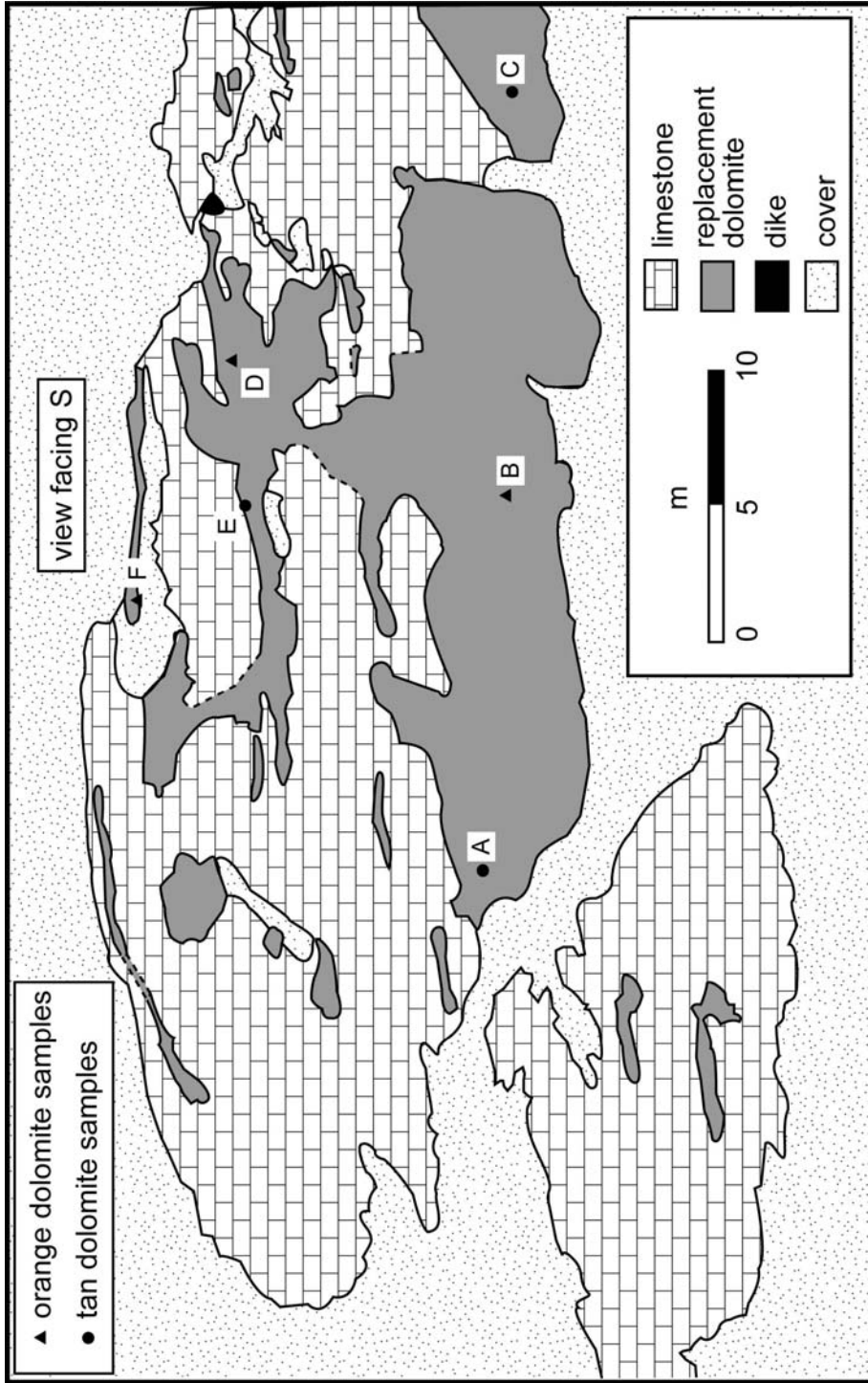


Figure 4.14. Irregularly shaped dolomite bodies with sub-vertical and sub-horizontal contacts developed in limestone approximately horizontal layers at Location 13. Geologic relations traced from a digital photograph. Dashed contacts as in Figure 4.7. Sample location letters omit the L-13 prefix in text and tables.

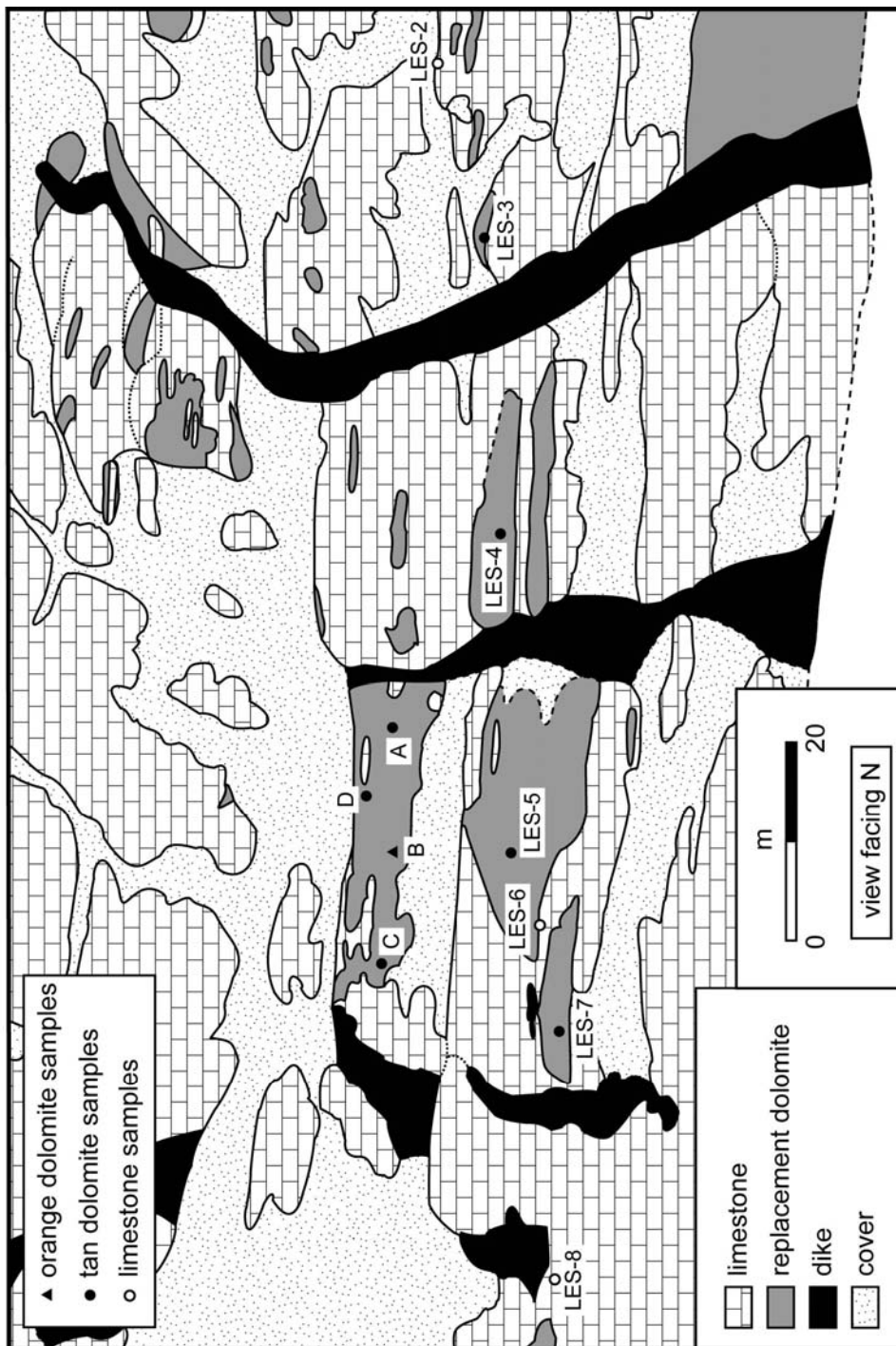


Figure 4.15. Panoramic view of irregularly shaped dolomite bodies in Location 6 traced from a digital photograph. Sample location letters omit the L-6 prefix in text and tables. Contacts are dashed where approximate. Dotted line separates features that appear in contact from the viewpoint of the photographer, but that are separated in three dimensions. LES series samples are part of Traverse E, that passes through Location 6.

in slope with increasing elevation while the limestone/(dolomite+limestone) curve steadily increases in slope, indicating that the amount of dolomite decreases with increasing elevation.

The slope of the curve of the cumulative fraction of horizontal contacts between limestone and dolomite decreases with increasing elevation above 120 m with a major change at ~321 m (Figure 4.17). This confirms the qualitative observation at the outcrop scale that more vertical contacts occur in the lower part of the system and more horizontal contacts occur in the upper part of the system. The change at ~321 m corresponds to the Lower Edifice - Latemar Limestone contact. The massive, poorly bedded character of the Lower Edifice is probably the reason for the predominance of vertical contacts at the lower elevations. The well-developed, meter scale layering in the Latemar Limestone accounts for the predominance of layer-parallel contacts at higher elevations that are horizontal or nearly so.

Summary

Replacement dolomite occurs at all elevations between the base of the Lower Edifice at 1979 m to the peak of the Cima Latemar Piccolo at 2845 m. It forms an interconnected orthogonal lattice composed of near-horizontal sheets and tubes and near-vertical sheets and tubes (Figure 4.18). There is a strong control on dolomite geometry by preexisting structures including bedding planes, fractures, dike-limestone contacts, and breccia pipes (to the extent that they pre-date dolomitization). The orientations of near-horizontal sheets and tubes are controlled by bedding planes, while the orientations of vertical sheets are controlled by fractures and dike-limestone contacts. Vertical tubes

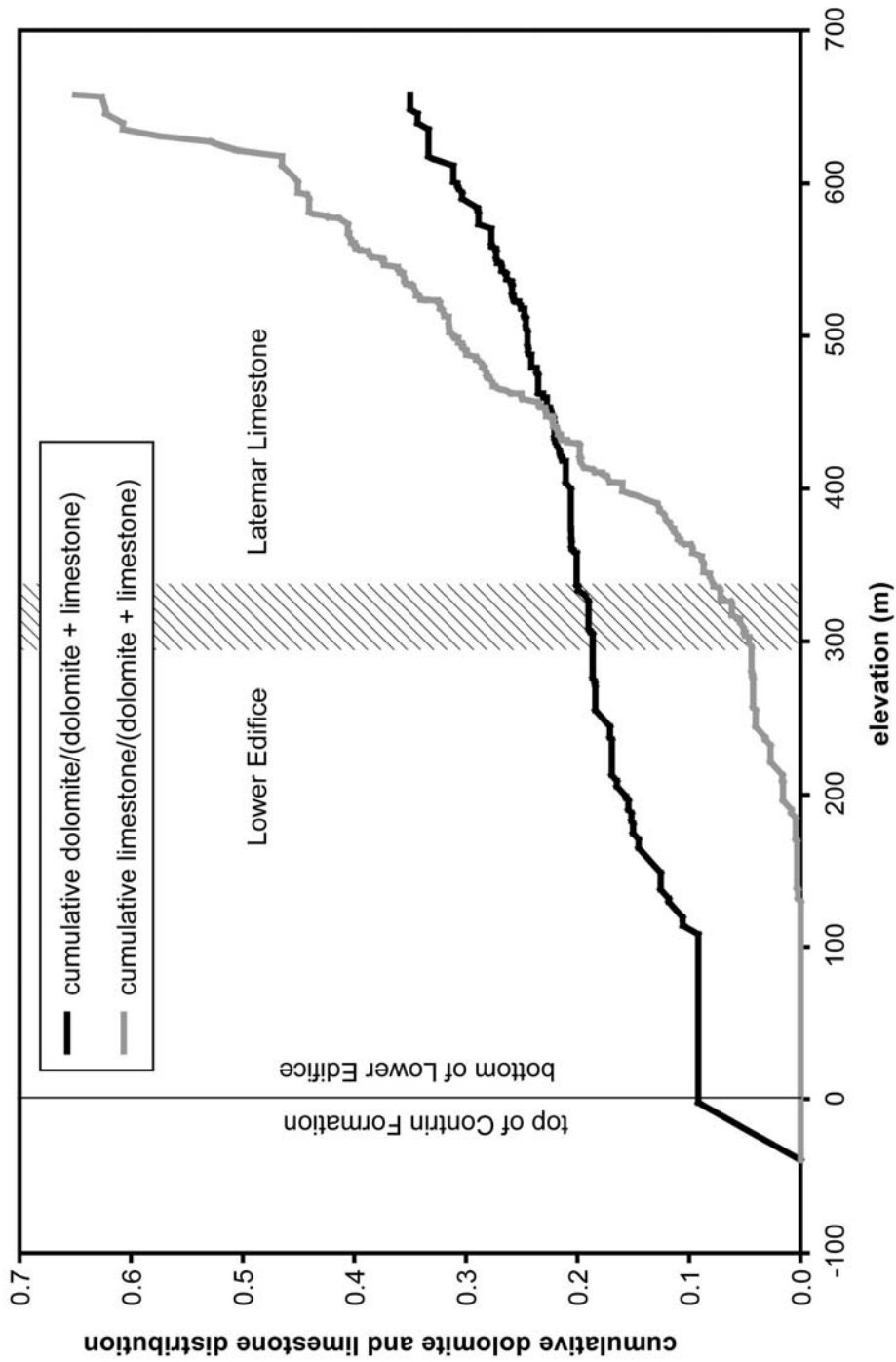


Figure 4.16. Cumulative fraction of dolomite (black) and limestone (gray) as a function of elevation in the Latemar buildup. Elevation measured relative to base of the Lower Edifice. Contact between the Lower Edifice and Latemar Limestone represented as a band because it is gradational. Curves combined all measured data along six traverses (Figure 3.1), projected parallel to bedding to a single map position. Total length of traverses measured along the ground surface = 9.7 km.

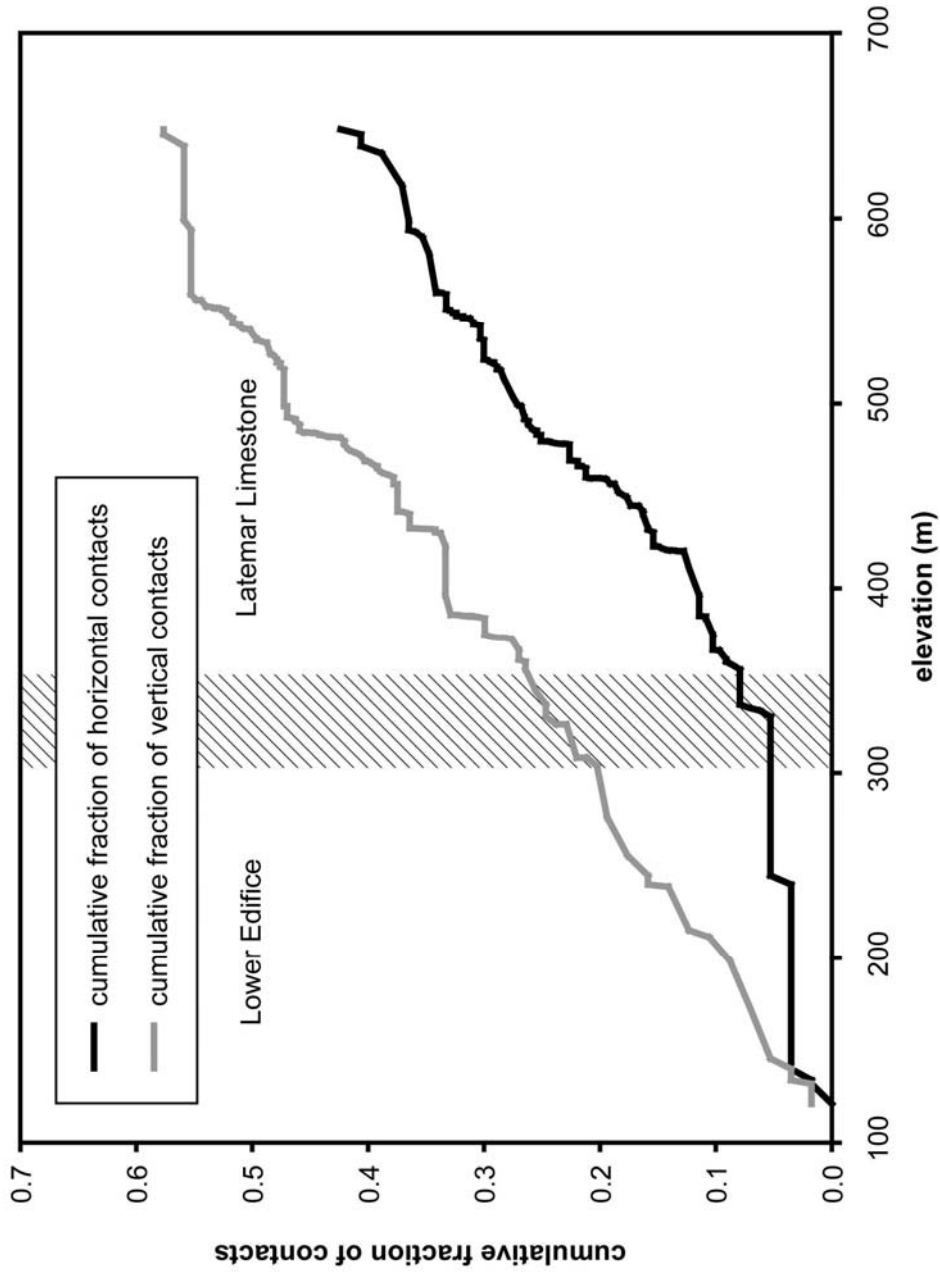


Figure 4.17. Cumulative fraction of horizontal or nearly horizontal (black) and vertical or nearly vertical (gray) dolomite-limestone contacts as a function of elevation in the Latemar buildup. Elevation scale same as in Figure 4.15. Curves combined all measured data along six traverses (Figure 3.1), projected parallel to bedding to a single map position. Total length of traverses measured along the ground surface = 9.7 km.

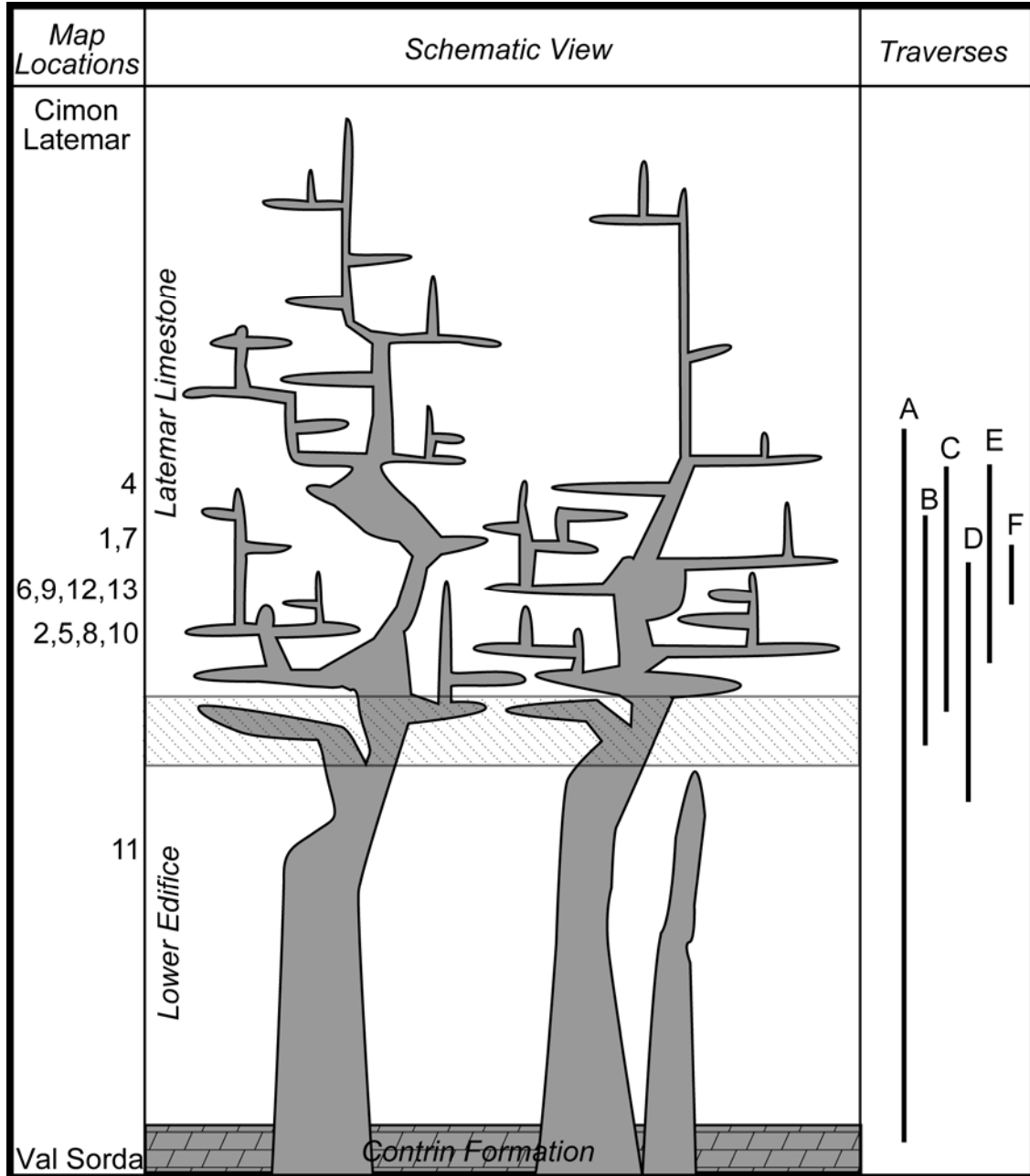


Figure 4.18. Schematic diagram of trellis-like structure of replacement dolomite illustrated in cross section. Map locations are shown on the left, while vertical extent of traverses A-F are shown on the right. The ruled area in the middle represents the gradational Lower Edifice - Latemar Limestone contact at ~321 m elevation (measured elevation 2300 m). The Contrin Formation is completely composed of dolomite.

of dolomite breccia are controlled by breccia pipes and possibly intersections of fractures.

Wilson et al. (1990) proposed three zones of replacement dolomitization in the Latemar: a dolomite breccia, an intensely dolomitized zone, and a sparsely dolomitized zone. They conclude these zones of dolomitization form a large mushroom shape, approximately 2.5 km across and 700 m high, with meter-scale dolomite “fingers” stretching along certain preferred directions, with a total volume of dolomite approaching 2 to 3 km³ (Wilson et al., 1990). The regional-scale field observations in this study do not appear to show any evidence for this large mushroom shape of dolomitized rock. Similarity between the distribution of dolomite on the outcrop scale (Figures 4.5 - 4.15) and on the regional scale (Figure 4.1) implies that there is a trellis-like structure of replacement dolomite rock at the outcrop and all larger scales.

Chapter 5

Mineralogy, Texture, and Mineral Chemistry of Dolomites and Limestones

Mineralogy and Textures

The Latemar dolomites and limestones are almost entirely composed of dolomite and/or calcite. Trace minerals of diagenetic and/or hydrothermal origin include iron oxides, K-feldspar, quartz, or pyrite. Trace minerals of detrital origin include K-feldspar, quartz, rutile, biotite, zircon, apatite, gypsum, anhydrite, ilmenite, fluorite, monazite, corundum, and garnet. Some dolomite samples have hydrocarbon coatings on the inside of the pore spaces. Except in the narrow transition zone between limestone and dolomite, typical Latemar dolomites contain 81-97 modal % dolomite, 0-3% calcite, and 3-16% pore space (Table 5.1, Figure 4.2). Typical Latemar limestones contain 91-99 modal % calcite, 0-7% dolomite, and 1-9% pore space. Amounts of other trace minerals in both dolomite and limestone never exceed, with one exception, 0.2 modal %.

Almost all analyzed samples of Latemar limestone samples have low porosity (average = 3%, range = 1-4%) and are composed almost entirely of calcite with scattered euhedral, K-feldspar grains (Figure 5.1). The euhedral K-feldspar crystals are considered authigenic rather than detrital, because of their shape and K-rich composition (Spötl et al., 1996; Sandler et al., 2004). Many limestone samples also contain small amounts of dolomite (~5%), either as isolated grains (Figure 5.2) or as crystals decorating fractures (Figure 5.3). Figures 5.4-5.9 illustrate textures and occurrences of trace minerals in several uncommon samples of limestone. A few samples show preferential dolomitization of aragonitic fossils such as dasycladacean algae (Figures 5.4 and 5.5).

Table 5.1. Modal distribution of minerals in limestone, orange (Fe-rich) dolomite, and tan (Fe-poor) dolomite.

rock type	Sample	% Calcite	% Dolomite	% Pore Space	% Accessory [†]
limestone	L-1E	93.56%	5.18%	1.32%	0.08%
limestone	L-1F	96.19%	2.84%	1.07%	0.05%
limestone	L-8A	96.26%	1.02%	2.76%	0.03%
limestone	L-8B	94.55%	3.31%	2.23%	0.09%
limestone	L-8E*	75.44%	21.89%	3.11%	0.05%
limestone	L-8F	96.99%	0.35%	2.68%	0.17%
limestone	L-8H	97.60%	0.95%	1.73%	0.08%
limestone	L-8I	91.89%	0.53%	8.75%	0.00%
limestone	L-8L	91.18%	4.58%	4.30%	0.03%
limestone	L-8P*	78.94%	19.61%	1.54%	0.07%
limestone	LAS-39	97.29%	0.00%	2.75%	0.01%
limestone	LAS-44	91.43%	6.97%	1.84%	0.01%
limestone	L-1A	98.93%	0.42%	0.85%	0.06%
limestone	LAS-1	94.95%	2.20%	2.92%	0.03%
limestone	LAS-17	97.50%	0.00%	2.74%	0.04%
limestone	LAS-35	96.59%	0.57%	3.00%	2.95%
Fe-rich dolomite	L-1C	1.28%	92.75%	6.10%	0.04%
Fe-rich dolomite	L-1D	0.00%	91.64%	9.31%	0.05%
Fe-rich dolomite	LAS-43	0.01%	90.54%	9.58%	0.00%
tan dolomite	8T-1*	27.84%	66.37%	6.27%	0.00%
tan dolomite	8T-12	0.35%	92.83%	6.99%	0.00%
tan dolomite	8T-2	1.68%	88.28%	10.31%	0.00%
tan dolomite	8T-9	2.78%	80.90%	16.41%	0.00%
tan dolomite	L-1B	1.77%	91.09%	7.24%	0.02%
tan dolomite	L-8C	1.22%	93.84%	4.98%	0.00%
tan dolomite	L-8D	1.72%	88.98%	9.44%	0.00%
tan dolomite	L-8Q*	1.23%	92.40%	6.52%	0.02%
tan dolomite	LAS-24	1.55%	89.77%	9.24%	0.00%
tan dolomite	LAS-34	2.48%	90.68%	6.98%	0.00%
tan dolomite	LAS-5	0.00%	91.22%	8.92%	0.02%
tan dolomite	LAS-51	0.00%	96.94%	3.14%	0.01%
tan dolomite	LAS-52	0.81%	95.04%	4.20%	0.00%
tan dolomite	LAS-54	0.47%	93.69%	5.89%	0.00%

Notes: * indicates samples that are in the narrow transition zone between limestone and dolomite. [†] accessory minerals include K-feldspar, iron oxides, pyrite, quartz, apatite, rutile, zircon, biotite, gypsum, anhydrite, ilmenite, sphalerite, fluorite, monazite, corundum, and garnet.

Rare limestone samples exhibit an unusual texture of strings of dolomite and K-feldspar formed along stylolites (Figures 5.6, 5.7). Still other rare samples contain areas of dolomitization that are associated with the occurrence of K-feldspar and Fe-oxide (Figures 5.7 and 5.8). In these, K-feldspar occurs as ropy, twisted aggregates and tend to be associated with stylolites. In other areas dolomite occurs as isolated grains and Fe-oxide occurs along the calcite grain boundaries and cleavage planes (Figure 5.9). This association of Fe-oxide with K-feldspar tends to occur in samples where dolomite is not otherwise present.

Almost all analyzed samples of Latemar dolomites are nearly entirely composed of the mineral dolomite. Textures and chemical zoning in dolomite is variable. Texture and zoning is unrelated to porosity. Dolomites are more porous than limestones, although the degree of porosity is variable. Most dolomites are composed of compositionally zoned dolomite crystals with anhedral cores full of calcite inclusions and euhedral, inclusion-free, concentric, chemically zoned rims (Figure 5.10). Others samples contain compositionally zoned dolomite with calcite inclusions scattered throughout the grain (Figure 5.11). The number of concentric chemical zones in each dolomite crystal is usually >15 , and the zones have widths that vary over an order of magnitude, from 1 μm to 50 μm . These zoning patterns are localized on the mm scale within each sample, and adjacent dolomite crystals generally exhibit the same zoning pattern.

Less commonly, dolomites are composed of unzoned dolomite crystals (Figure 5.12) or crystals with patchy rather than concentric compositional zoning (Figure 5.13). In general, the unzoned or patchy dolomite crystals contain fewer calcite inclusions than

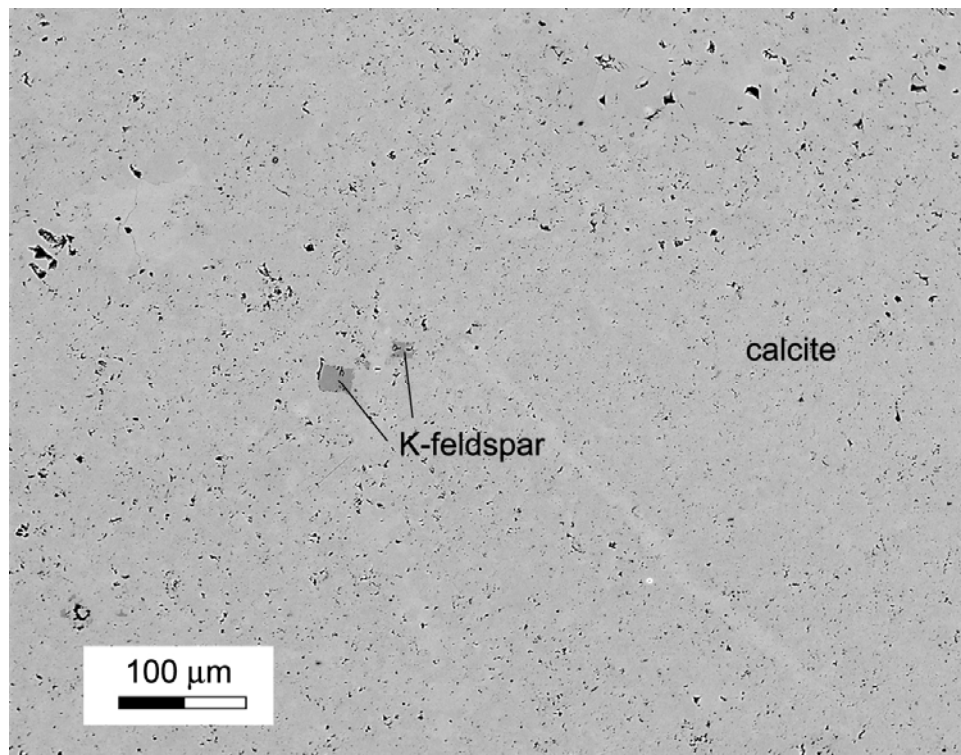


Figure 5.1. BSE image of representative dolomite-free limestone with trace euhedral K-feldspar (sample LAS-17).

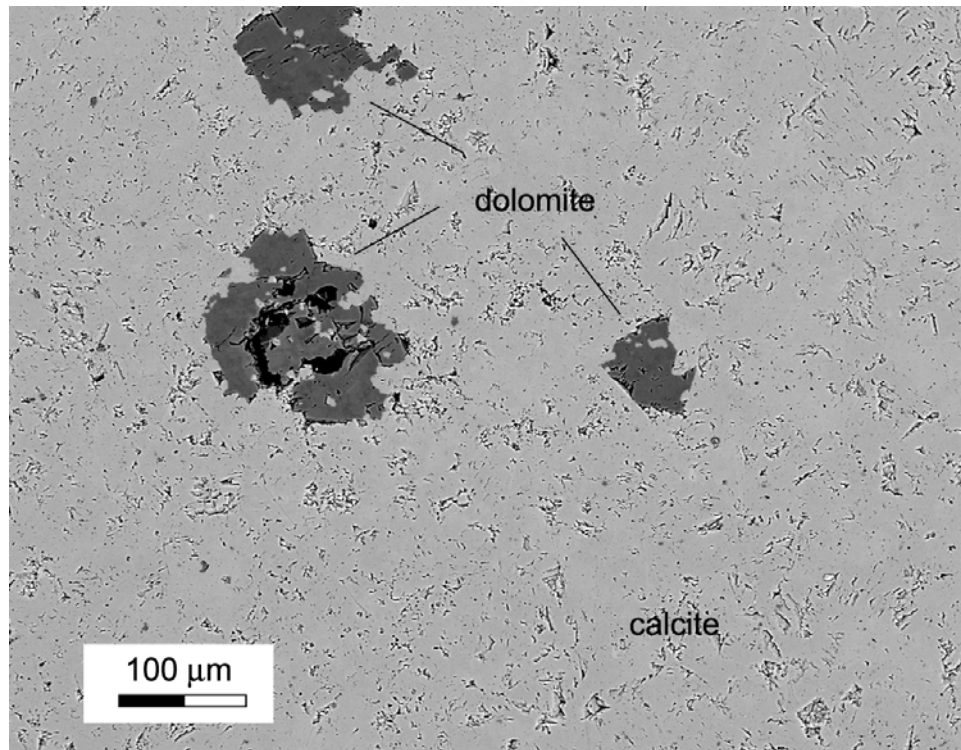


Figure 5.2. Representative BSE image of dolomite grains in dolomite-poor limestone (sample L-11F).

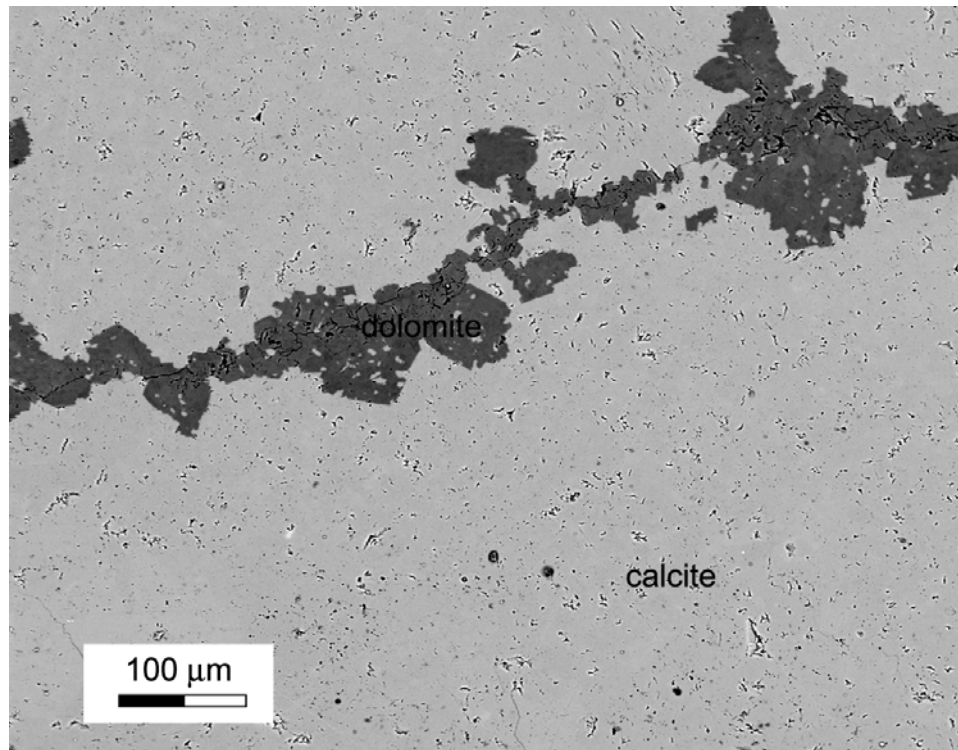


Figure 5.3. BSE image of dolomite developed along fracture in limestone (sample L-12F).

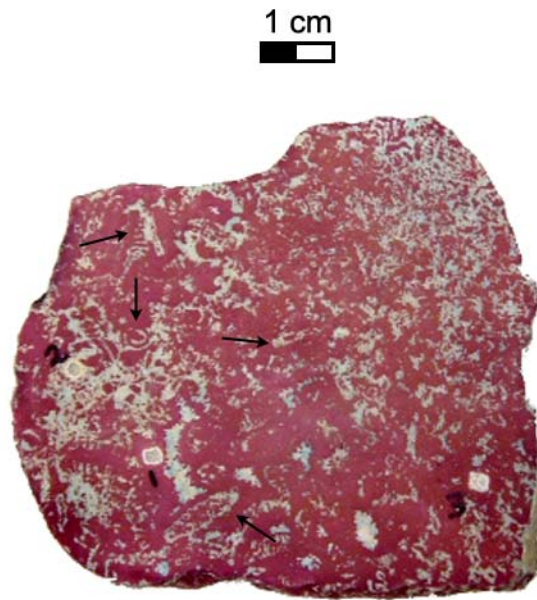


Figure 5.4. Digital photograph of polished surface of sample LAS-7, stained for calcite (red) and dolomite (blue), showing preferential dolomitization of aragonitic dasycladacean algae fossils (arrows). Numbered spots are drill sites sampled for stable isotope analysis.

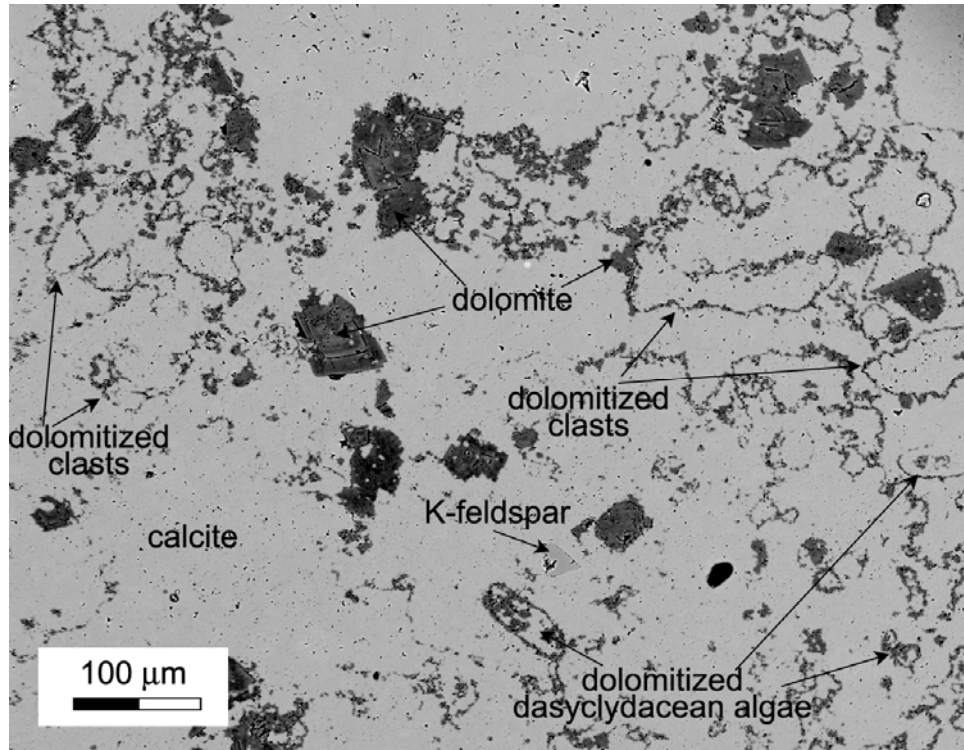


Figure 5.5. BSE image of preferential dolomitization of aragonitic dasycladacean algae and possibly aragonitic carbonate clasts (sample L-12D).

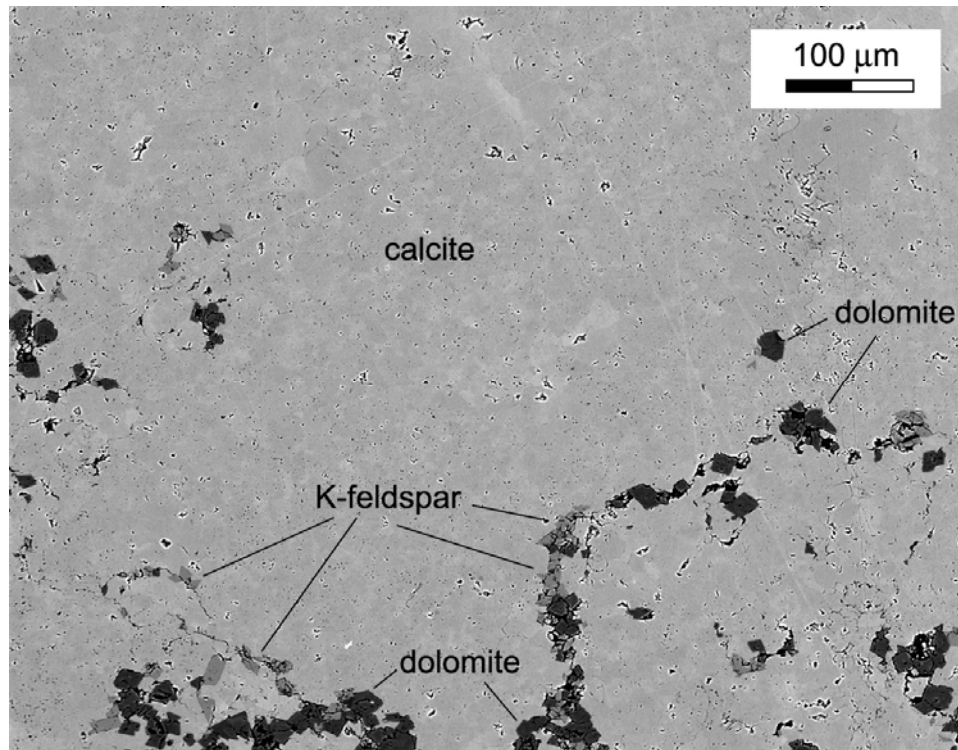


Figure 5.6. BSE image of strings of dolomite and K-feldspar developed along stylolite in limestone (sample LES-8).

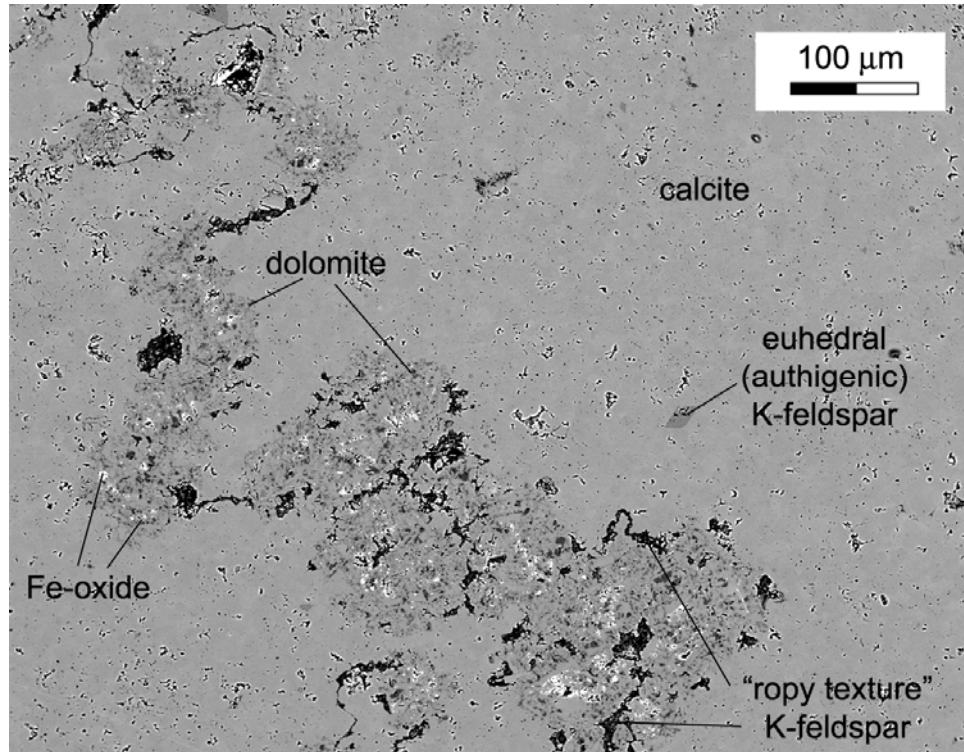


Figure 5.7. BSE image of K-feldspar and Fe-oxide developed with dolomite along stylolite in limestone (sample L-8H).

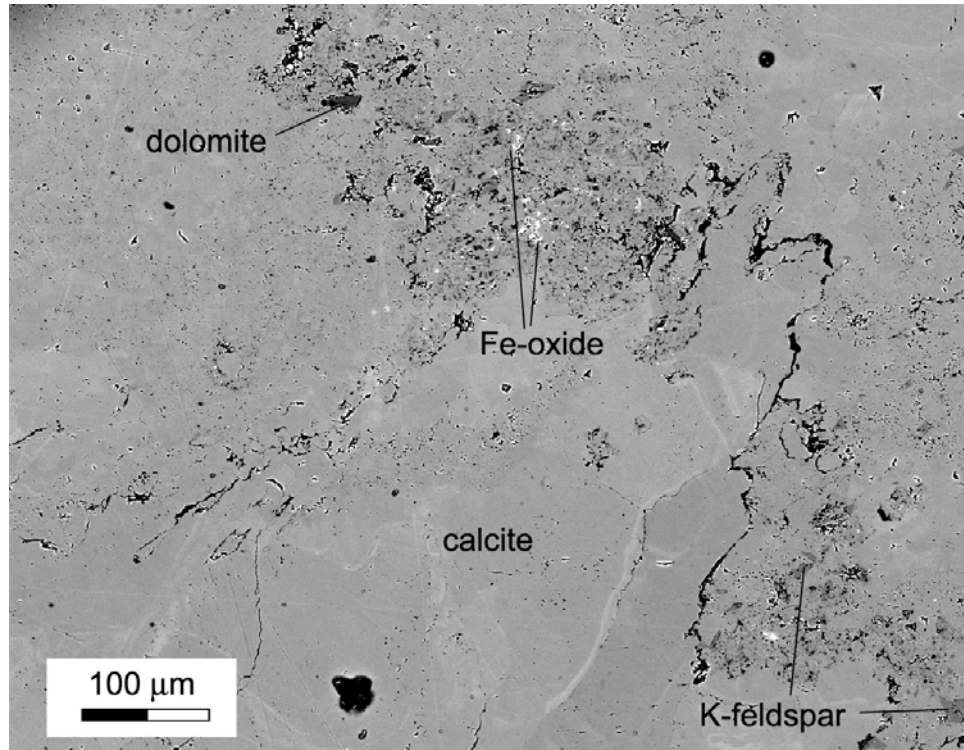


Figure 5.8. BSE image of dolomite associated with Fe-oxide and K-feldspar (sample LAS-31).

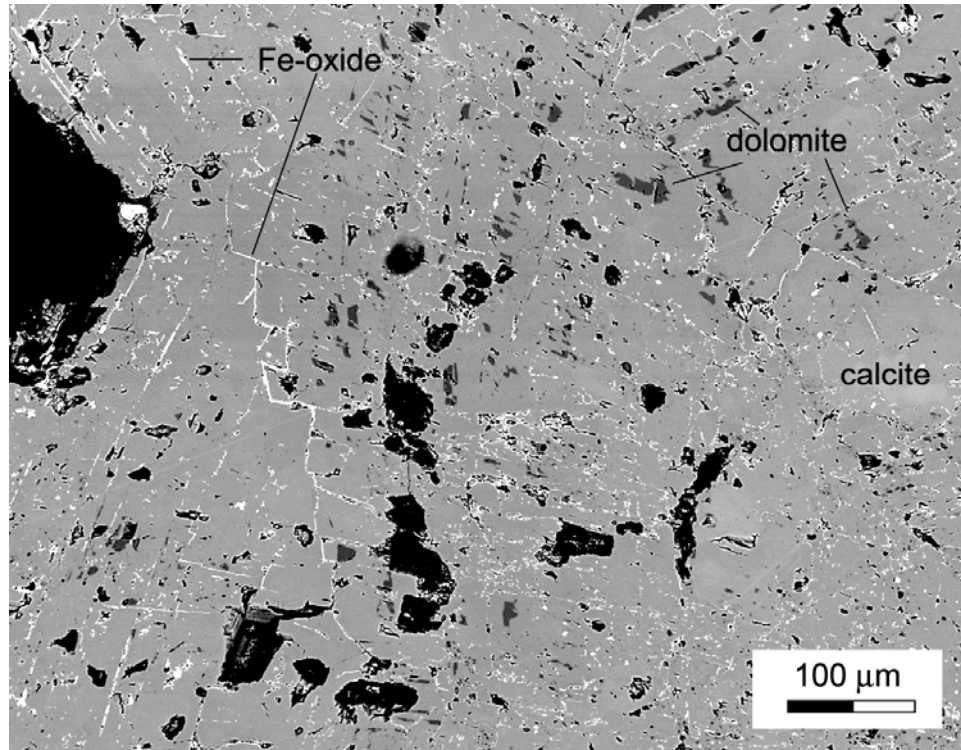


Figure 5.9. BSE image of dolomite associated with Fe-oxide in limestone (sample L-1H). Black areas are pores and pluck marks. Fe-oxide occurs along grain boundaries and cleavage planes of calcite.

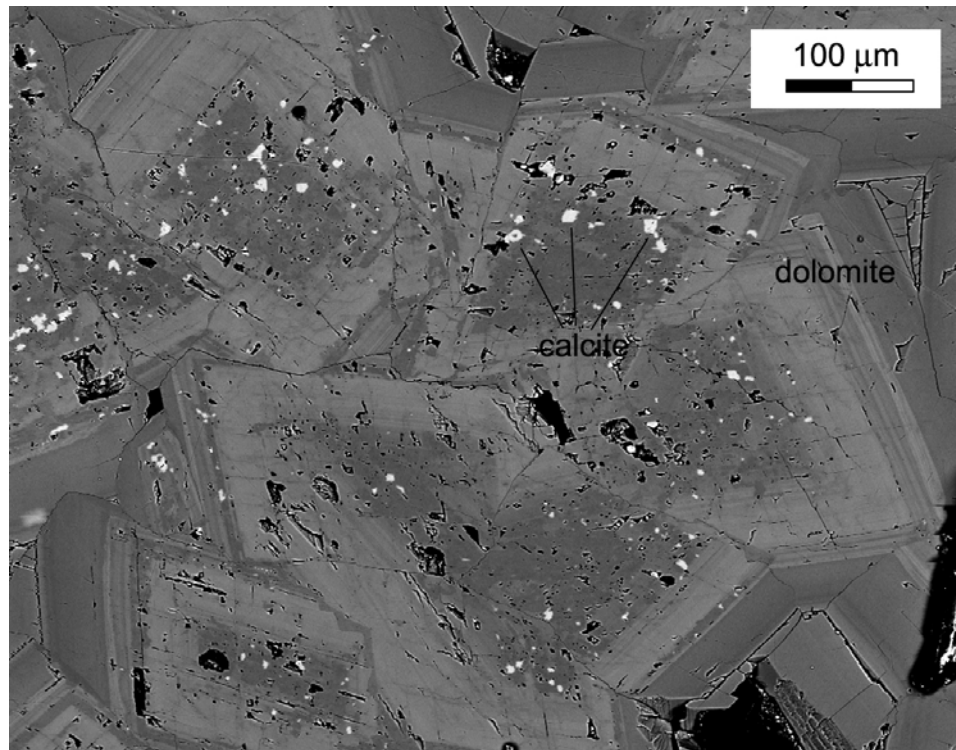


Figure 5.10. Representative BSE image of zoned dolomite grains, that have calcite inclusion-rich cores and concentrically zoned, inclusion-free rims (sample L-1C). Black areas are pores and pluck marks.

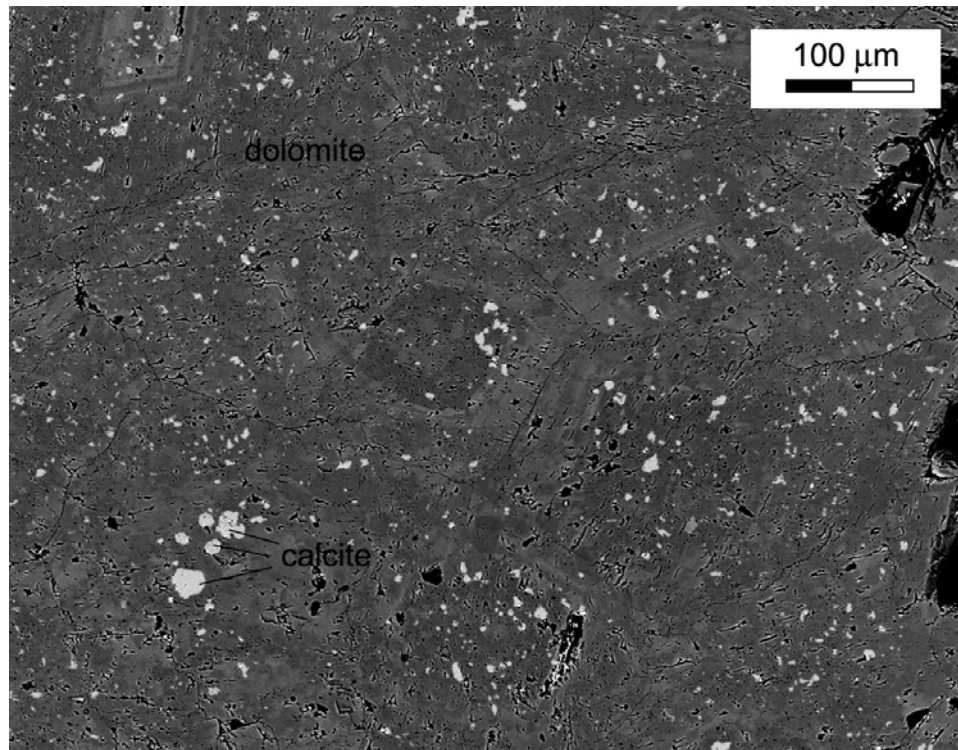


Figure 5.11. BSE image of example of concentric compositionally zoned, tan, Fe-poor dolomite, with calcite inclusions scattered throughout the dolomite (sample 8T-4). Black areas are pores and pluck marks.

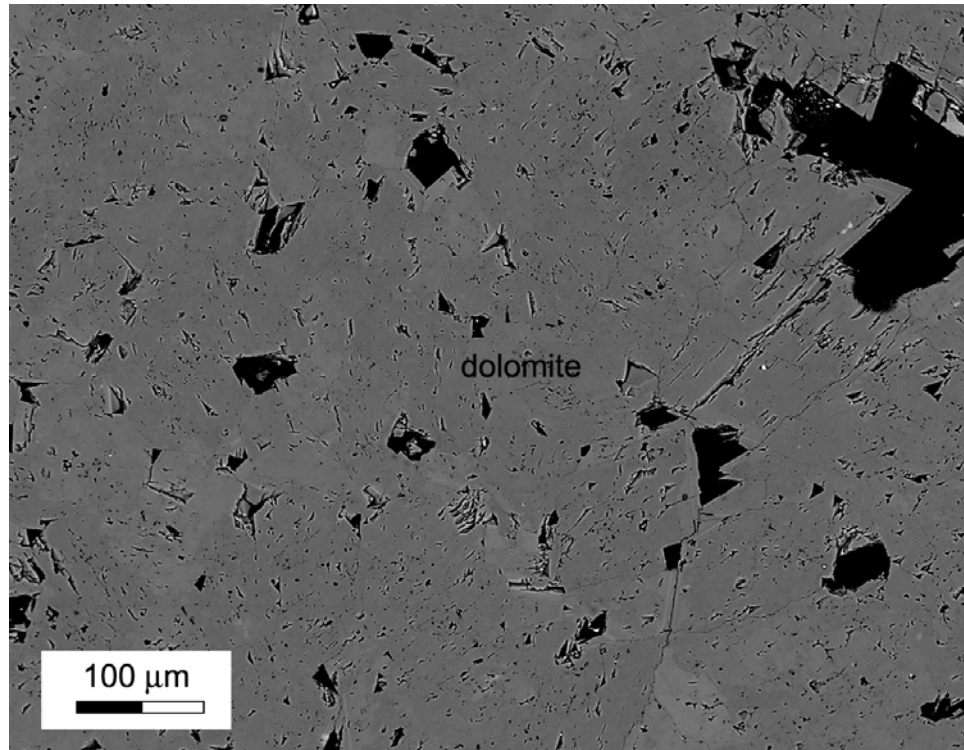


Figure 5.12. Representative BSE image of unzoned, tan, Fe-poor dolomite (sample LAS-5). Black areas are pores and pluck marks.

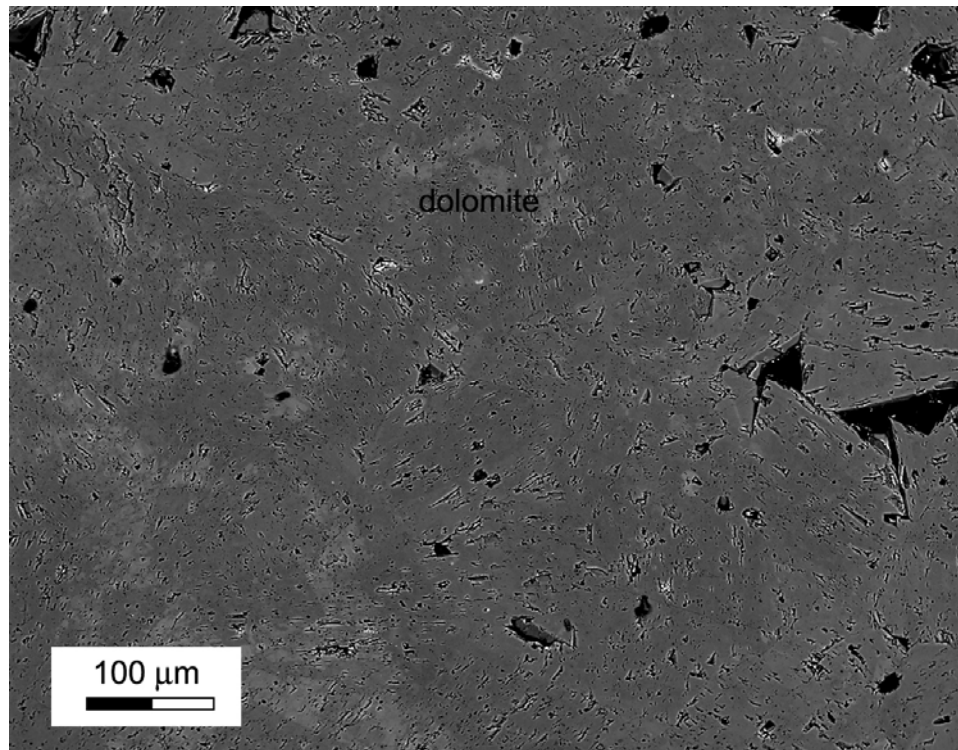


Figure 5.13. BSE image of example of orange, Fe-poor dolomite exhibiting patchy rather than concentric compositional zoning (sample L-13B). Black areas are pores and pluck marks.

their concentrically zoned counterparts, or they may not contain any calcite. A few dolomite samples contain rare scattered euhedral quartz crystals. The quartz crystals are surrounded by unzoned dolomite, and may or may not contain calcite and dolomite inclusions (Figures 5.14 and 5.15).

The concentric compositional zoning observed in the BSE images of Latemar dolomite is visible in cathodoluminescence images as well (Figure 5.16).

Major Element Chemistry

The Latemar limestones and dolomites can be grouped by field occurrence (Table 5.2). The groups include (1) outcrops that are entirely limestone (Locations 4, 9), (2) limestone and dolomite samples from outcrops that contain both limestone and dolomite (Locations 1, 2, 5, 6, 7, 8, 11, 12, 13), (3) outcrops of dolomite breccia (Locations 11, 12), (4) limestone and dolomite samples from Traverses A-F, and (5) orange dolomite regardless of location. A summary of the major element chemistry of calcite and dolomite, measured by electron microprobe and arranged by occurrence, is presented in Table 5.2. Major element chemistry data for each sample is listed in Appendix II.

The calcites are nearly pure CaCO_3 (Figures 5.17-5.20), although calcites in dolomite samples contain more Mg than calcites from limestone samples (Figure 5.19), which may be an artifact of analyzing small calcite grains in a dolomite matrix. The Mg enrichment in the calcites in these dolomite samples may be due to ablation of the calcite and penetration of the electron beam into underlying dolomite during microprobe analysis. Most dolomites are enriched in Fe relative to calcite, with orange dolomites

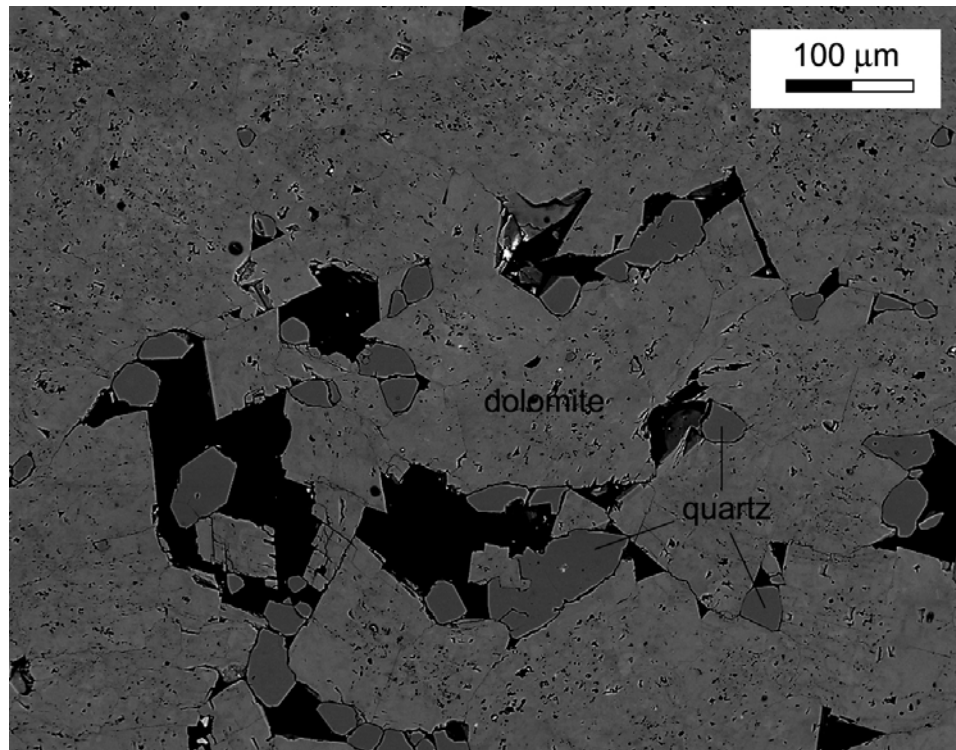


Figure 5.14. BSE image of inclusion-free quartz in unzoned, Fe-rich, inclusion-free dolomite (sample L-6B). Black areas are pores and pluck marks.

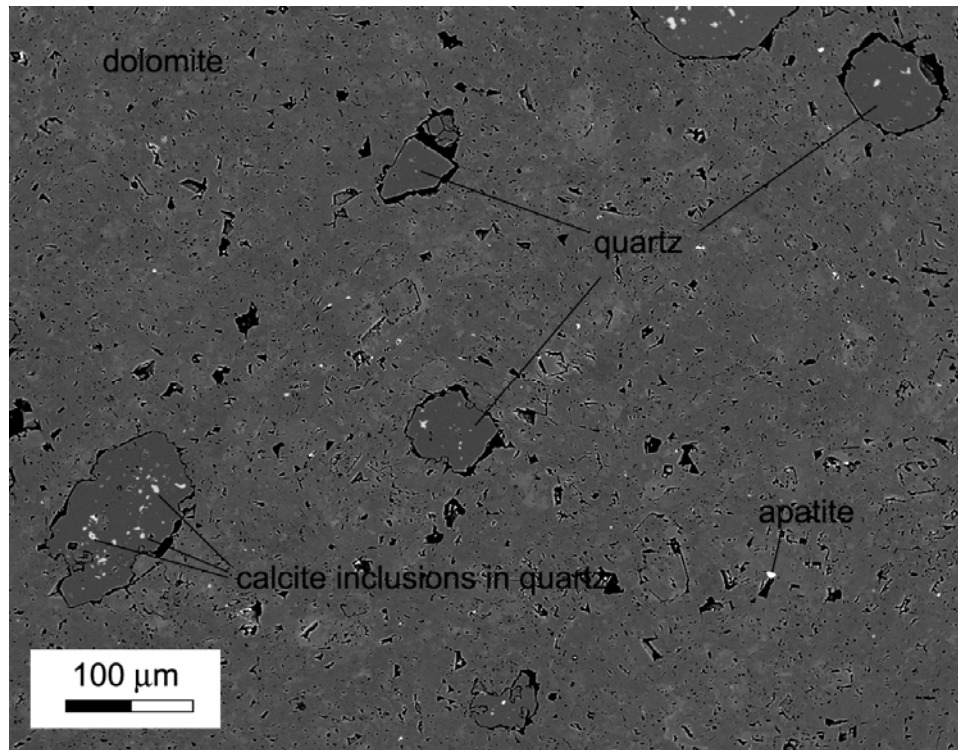


Figure 5.15. BSE image of quartz with calcite inclusions in tan, Fe-poor, unzoned dolomite (sample LES-14). Black areas are pores and pluck marks.

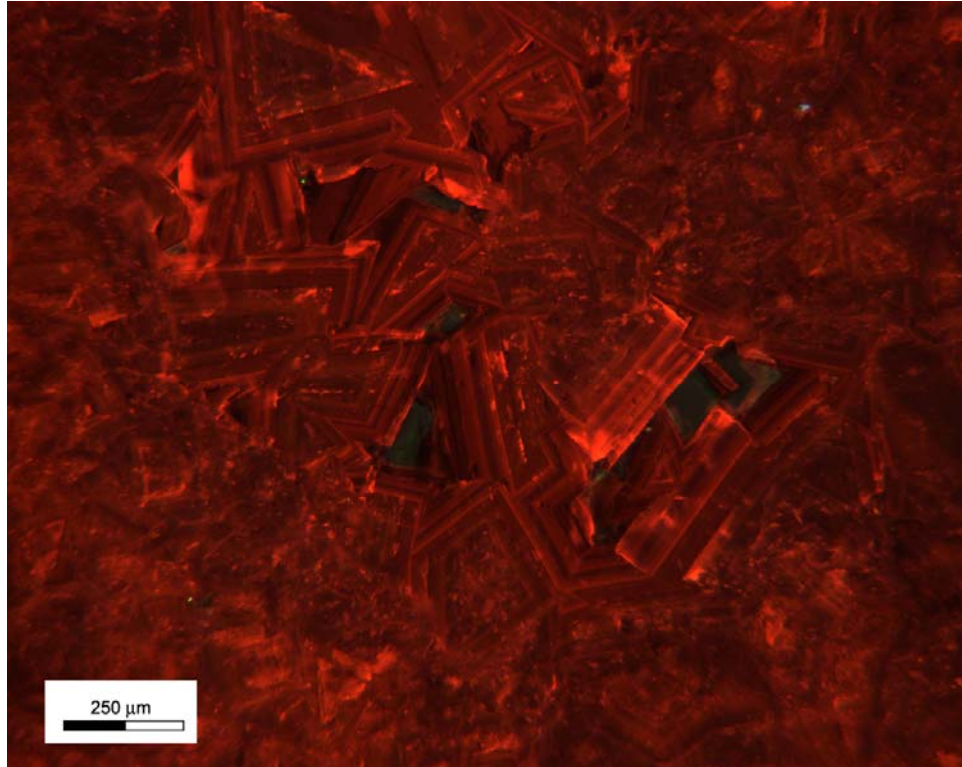


Figure 5.16. CL image of compositional zoning in tan, Fe-poor dolomite (sample L-12B).

Table 5.2. Average major element chemistry (Ca, Mg, Fe) of limestone and dolomite according to protolith, in cations per CO₃. Sr and Mn are below detection limit.

Field occurrence	Rock type	Mineral	Ca	Mg	Fe
(1) limestone outcrops	limestone	calcite	0.993	0.124	$2.80 \cdot 10^{-4}$
(2) outcrops with limestone and dolomite	dolomite	calcite	0.983	0.022	$6.68 \cdot 10^{-4}$
		dolomite	0.574	0.489	$6.44 \cdot 10^{-3}$
	limestone	calcite	0.992	0.123	$4.38 \cdot 10^{-4}$
		dolomite	0.588	0.473	$5.93 \cdot 10^{-3}$
(3) dolomite breccia	dolomite	dolomite	0.578	0.493	$3.65 \cdot 10^{-3}$
(4) traverses A-F	limestone	calcite	0.995	0.138	$3.52 \cdot 10^{-4}$
		dolomite	0.584	0.481	$7.91 \cdot 10^{-3}$
	dolomite	calcite	0.977	0.304	$7.51 \cdot 10^{-4}$
		dolomite	0.563	0.506	$7.72 \cdot 10^{-3}$
(5) orange dolomite	dolomite	dolomite	0.556	0.496	$1.66 \cdot 10^{-2}$

particularly so (Figures 5.21-5.24). The orange, Fe-rich dolomites generally do not exhibit compositional zoning in backscatter images or in CL images (e.g., Figures 5.12-5.15). Dolomites with lower Fe contents typically show concentric zoning on crystal rims (e.g., Figures 5.11, 5.16).

X-ray maps of zoned dolomite demonstrate that the compositional zoning observed in BSE images is primarily caused by variations in Fe content rather than variations in the Ca or Mg content (Figure 5.25). Traverses across zoned dolomite crystals with the electron microprobe reveal that the Fe variation across the compositional zones ranges from 0.002 to 0.016 Fe atoms per CO₃.

Trace Element Chemistry

Twenty six samples of dolomite and twelve samples of calcite (seven with whole rock $\delta^{18}\text{O} > 26\text{‰}$) were analyzed for selected major and trace elements using LA-ICPMS (Table 5.3; Figures 5.26-5.34). Measurements for individual samples are listed in Appendix III. Elements are plotted against Mn in Figures 5.26-5.34 because among the trace and minor elements in calcite and dolomite, Mn is the most likely conserved during mixing of seawater and seafloor hydrothermal fluids (Von Damm and Lilley, 2004).

Like the major element Mg, the first group of elements (Fe, Mn, Zn) display significant enrichment in dolomite compared to calcite. In addition, there are positive correlations among their concentrations in dolomite. For all analyzed dolomite samples, 91%, 84%, and 71% have Fe, Mn, and Zn contents, respectively, greater than the range of all analyzed calcite samples (Figures 5.26, 5.27).

calcite in isotopically unaltered limestone

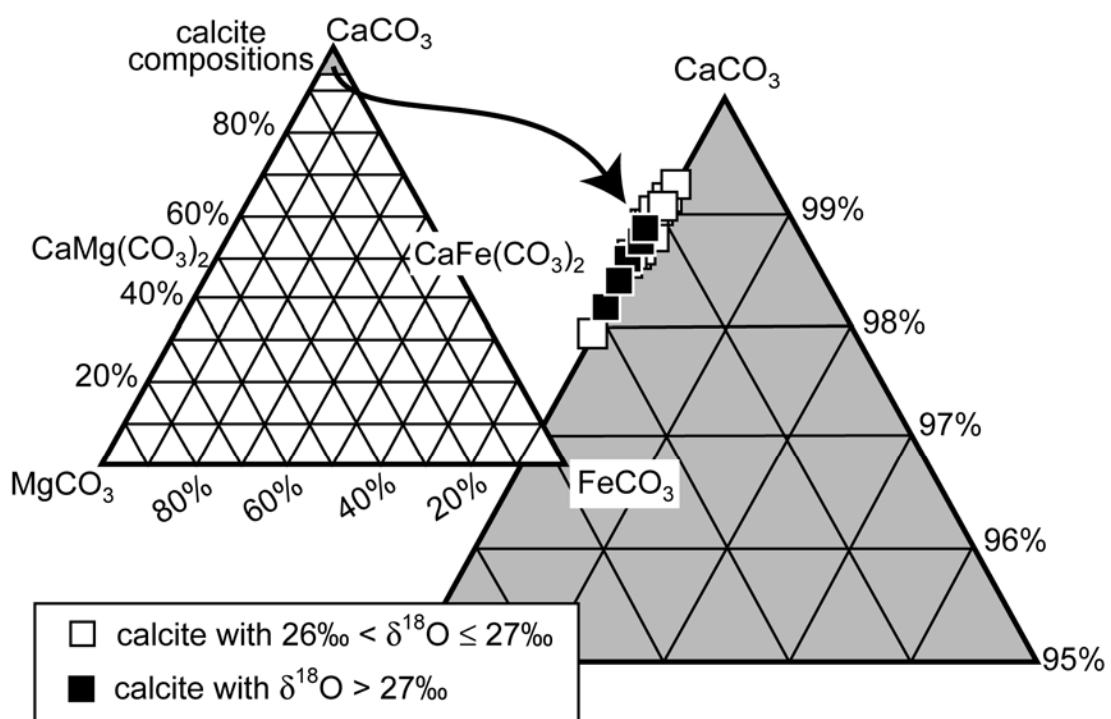


Figure 5.17. Major element composition of calcite in isotopically unaltered limestone (whole rock $\delta^{18}\text{O} > 26\text{‰}$).

calcite in limestone only outcrops

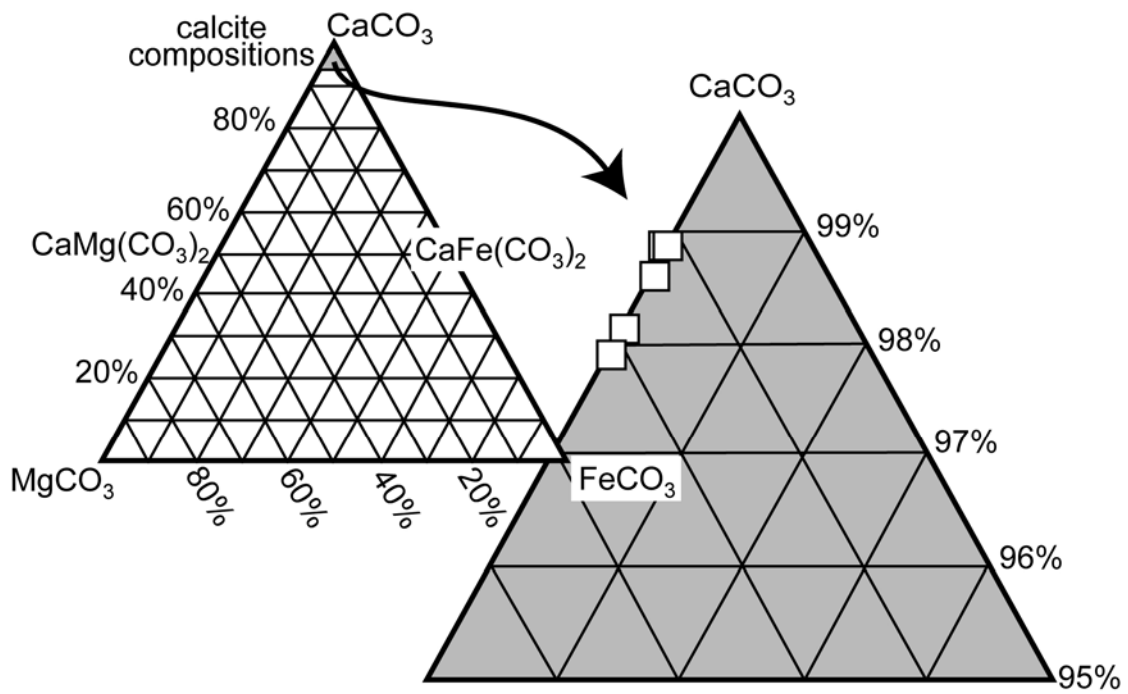


Figure 5.18. Major element composition of calcite in dolomite-free limestone.

calcite in outcrops of mixed limestone and dolomite

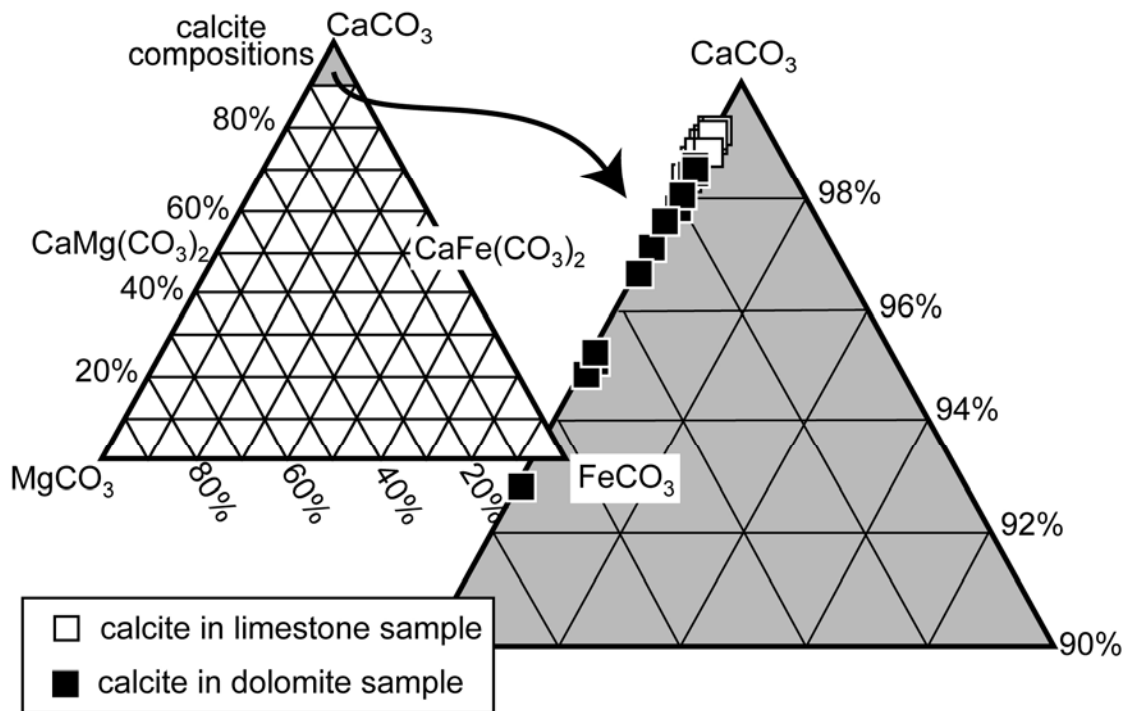


Figure 5.19. Major element composition of calcite from outcrops that contain both limestone and dolomite. High Mg content of calcite in some dolomite samples is likely an artifact of analyzing small calcite grains in a dolomite matrix.

calcite in limestone along traverses

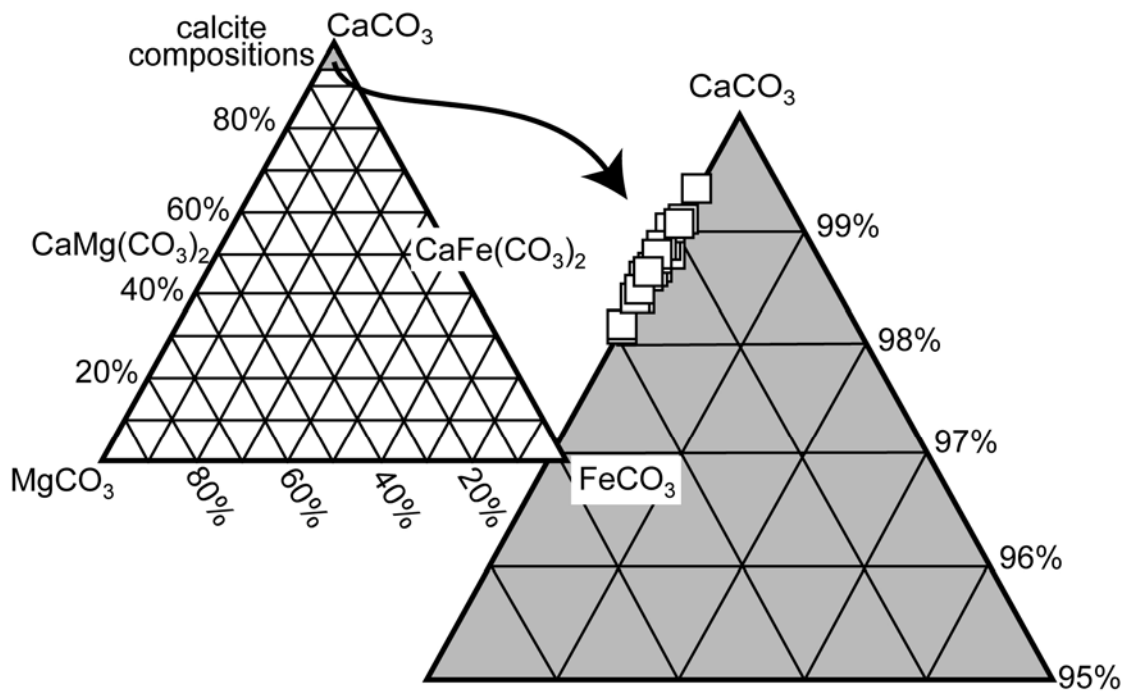


Figure 5.20. Major element composition of calcite from limestone outcrops in Traverses A-F.

dolomite in outcrops of mixed limestone and dolomite

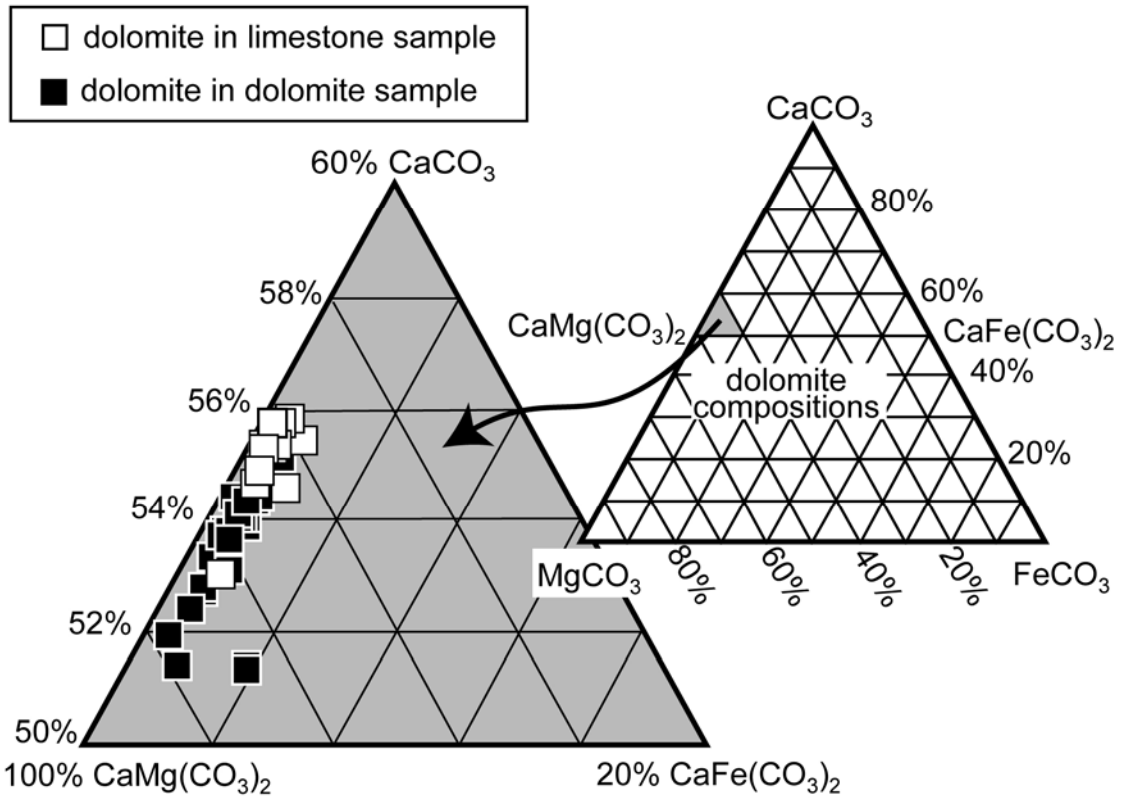


Figure 5.21. Major element composition of dolomite from outcrops that contain both limestone and dolomite.

dolomite along traverses in outcrops of mixed limestone and dolomite

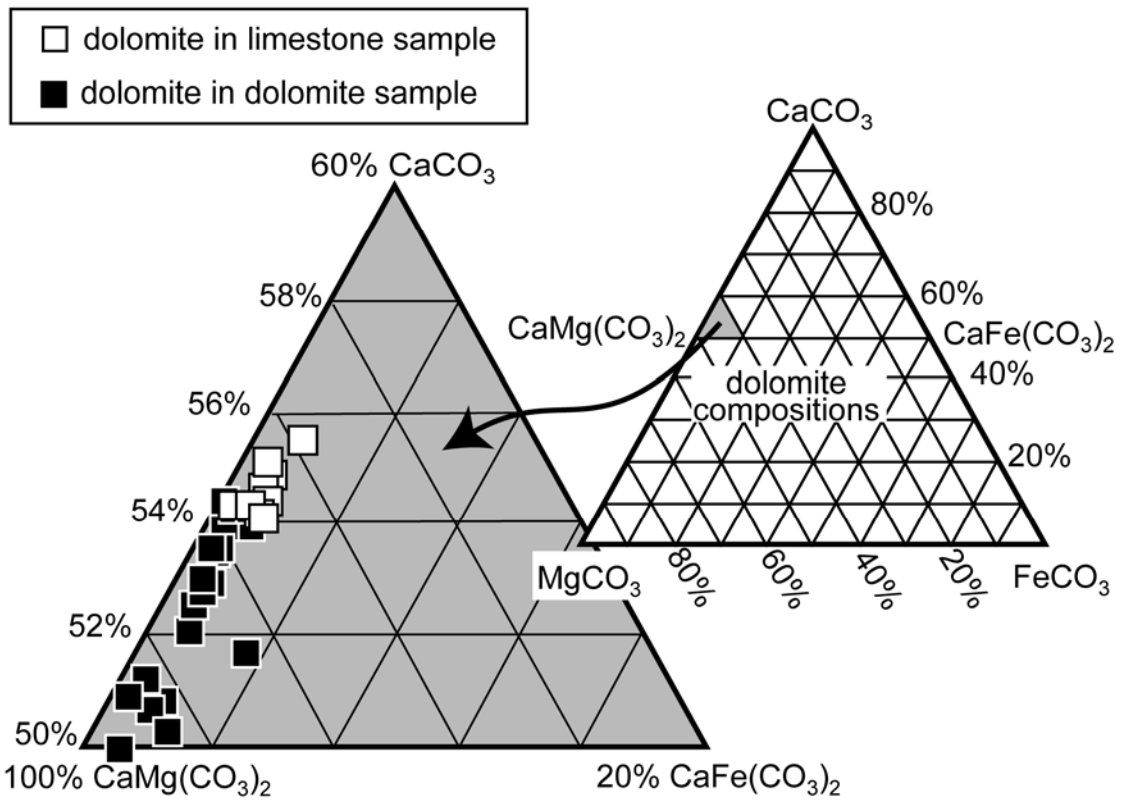


Figure 5.22. Major element composition of dolomite from dolomite outcrops in Traverses A-F.

dolomite in dolomite breccia

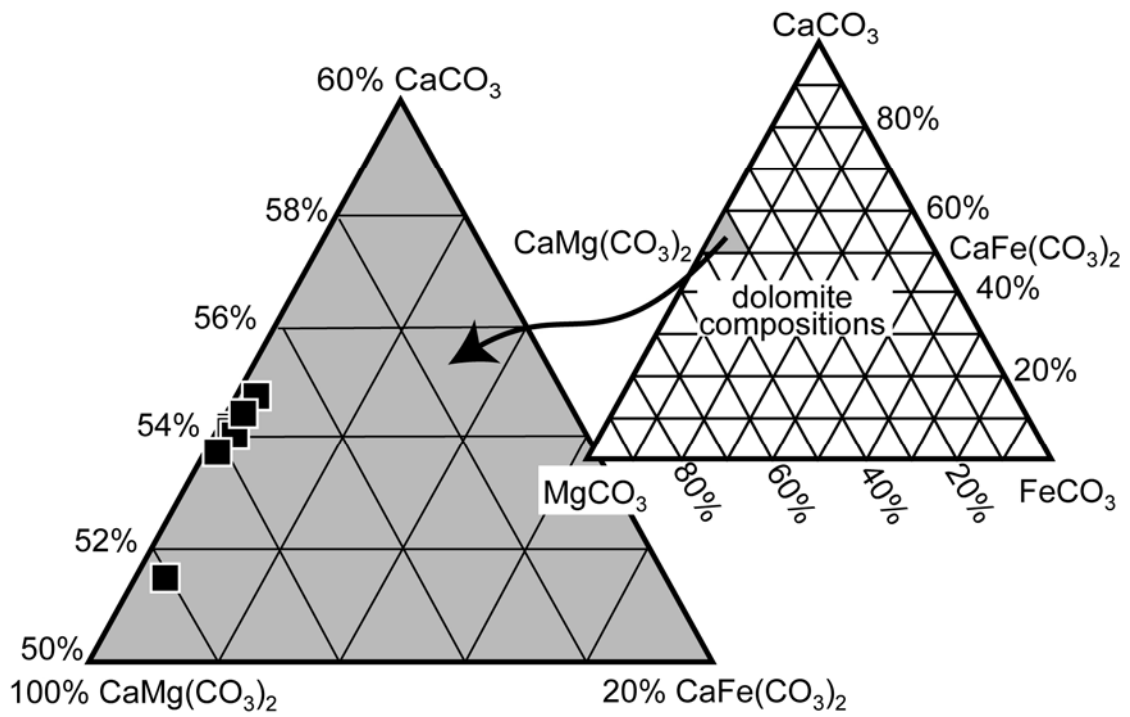


Figure 5.23. Major element composition of dolomite in outcrops of dolomite breccia.

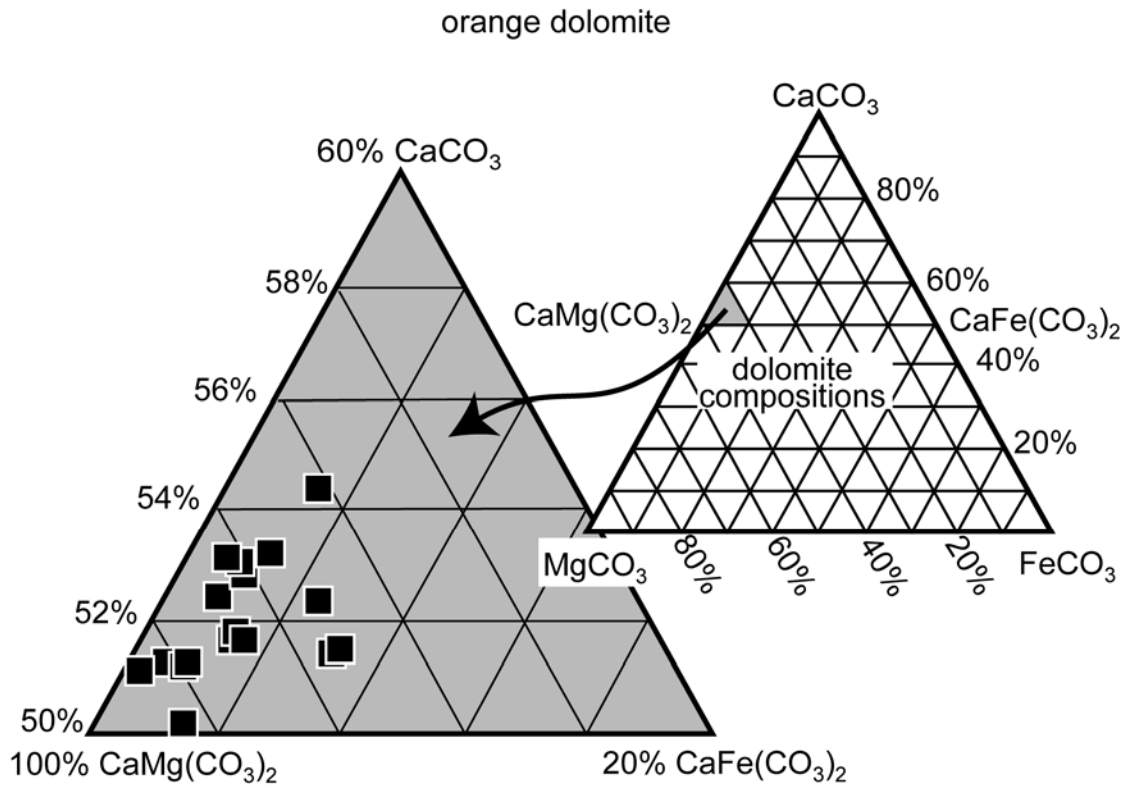


Figure 5.24. Major element composition of orange dolomite.

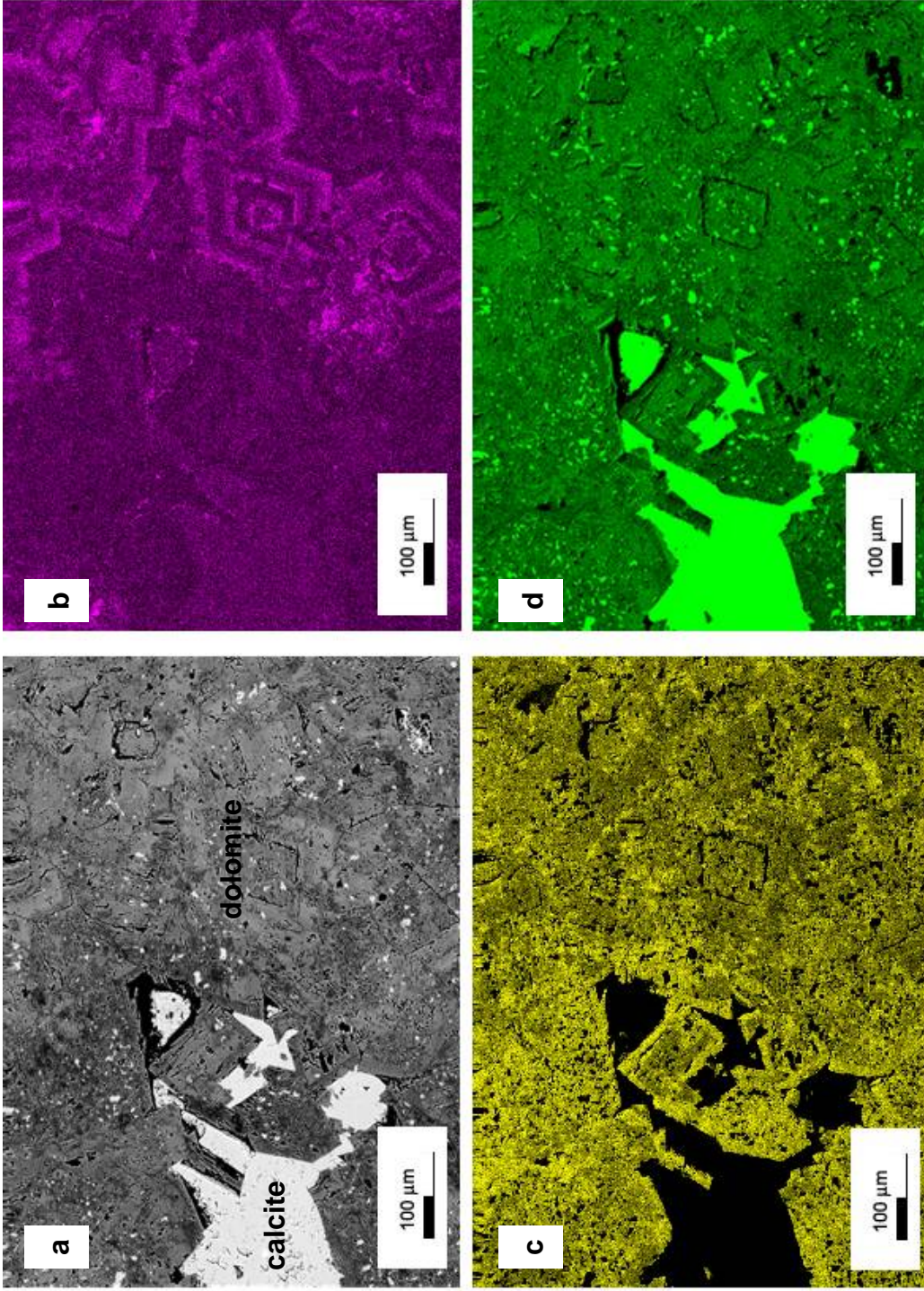


Figure 5.25. BSE image and X-ray maps of dolomite zoning in sample 7T-3, (a) BSE image, (b) Fe X-ray map, (c) Mg X-ray map, and (d) Ca X-ray map.

The positive correlation between Fe and Mn is well-defined and approximately linear; the correlation between Mn and Zn is distinct but weaker. The correlations among Fe, Mn, and Zn in dolomite indicate that Fe, Mn, and Zn were added in approximately constant proportions during the conversion of calcite to dolomite.

A second group of elements (Ca, Sr) display significant depletion in dolomite compared to calcite. 79% of dolomite samples have Sr contents less than the range of all analyzed calcite (Figure 5.28). Strontium was lost from calcite during its conversion to dolomite. Loss of Sr during the calcite-dolomite reaction is explained by its ionic radius (1.16Å) that is similar to that of Ca (1.00Å) but much larger than Mg (0.72Å) (Shannon and Prewitt, 1969).

A third group of elements (Co, Ni, Cr, and Cu) have completely or nearly completely overlapping concentrations in both dolomite and calcite (Figures 5.29-5.32), showing no evidence for either enrichment or depletion during the conversion of calcite to dolomite.

The fourth group of elements (Ba and Pb) sometimes have values greater in dolomite than the range in calcite values (13% of dolomite samples for Ba, 5% for Pb), but the Ba and Pb values of calcite and dolomite largely overlap (Figures 5.33 and 5.34). Although data are somewhat equivocal, there is no compelling evidence for either enrichment or depletion of Ba or Pb during the conversion of calcite to dolomite.

Table 5.3. Average LA-ICPMS and microprobe data for Latemar calcites and dolomites, in cations per CO₃. Values in parentheses after the average value are the standard deviation. The total range of measured values is given on the second line.

Cations per CO ₃		calcite in isotopically unaltered limestone*	tan dolomite	orange dolomite	% of dolomite samples outside of range of calcite values [†]
Ca	average range	9.86·10 ⁻¹ (2.73·10 ⁻³) 9.82·10 ⁻¹ - 9.90·10 ⁻¹	5.26·10 ⁻¹ (1.50·10 ⁻²) 5.05·10 ⁻¹ - 5.49·10 ⁻¹	5.19·10 ⁻¹ (9.00·10 ⁻³) 5.10·10 ⁻¹ - 5.46·10 ⁻¹	100%
Mg	average range	1.33·10 ⁻² (2.65·10 ⁻³) 9.89·10 ⁻³ - 1.67·10 ⁻²	4.68·10 ⁻¹ (1.40·10 ⁻²) 4.47·10 ⁻¹ - 4.87·10 ⁻¹	4.60·10 ⁻¹ (1.10·10 ⁻²) 4.34·10 ⁻¹ - 4.75·10 ⁻¹	100%
Mn	average range	2.69·10 ⁻⁵ (2.01·10 ⁻⁵) 2.89·10 ⁻⁶ - 1.13·10 ⁻⁴	2.76·10 ⁻⁴ (1.82·10 ⁻⁴) 3.60·10 ⁻⁵ - 1.17·10 ⁻³	5.57·10 ⁻⁴ (1.58·10 ⁻⁴) 8.36·10 ⁻⁵ - 8.53·10 ⁻⁴	91%
Fe	average range	4.46·10 ⁻⁴ (1.93·10 ⁻⁴) 1.89·10 ⁻⁴ - 8.79·10 ⁻⁴	6.43·10 ⁻³ (6.36·10 ⁻³) 4.15·10 ⁻⁴ - 4.50·10 ⁻²	2.29·10 ⁻² (6.15·10 ⁻³) 9.85·10 ⁻³ - 3.55·10 ⁻²	84%
Zn	average range	1.20·10 ⁻⁶ (2.88·10 ⁻⁷) 6.26·10 ⁻⁷ - 1.70·10 ⁻⁶	5.05·10 ⁻⁶ (3.02·10 ⁻⁶) 1.05·10 ⁻⁶ - 1.35·10 ⁻⁵	1.22·10 ⁻⁵ (6.69·10 ⁻⁶) 1.90·10 ⁻⁶ - 2.57·10 ⁻⁵	71%
Sr	average range	1.85·10 ⁻⁴ (3.89·10 ⁻⁵) 6.92·10 ⁻⁵ - 2.76·10 ⁻⁴	4.72·10 ⁻⁵ (2.21·10 ⁻⁵) 1.69·10 ⁻⁵ - 9.92·10 ⁻⁵	3.30·10 ⁻⁵ (1.16·10 ⁻⁵) 1.84·10 ⁻⁵ - 6.82·10 ⁻⁵	79%
Cr	average range	9.18·10 ⁻⁶ (6.26·10 ⁻⁶) 5.11·10 ⁻⁶ - 2.43·10 ⁻⁵	8.68·10 ⁻⁶ (3.80·10 ⁻⁶) 2.85·10 ⁻⁶ - 1.81·10 ⁻⁵	4.80·10 ⁻⁶ (2.51·10 ⁻⁶) 2.24·10 ⁻⁶ - 1.38·10 ⁻⁵	1%
Co	average range	1.20·10 ⁻⁶ (1.22·10 ⁻⁶) 1.44·10 ⁻⁷ - 3.39·10 ⁻⁶	5.42·10 ⁻⁷ (4.86·10 ⁻⁷) 1.26·10 ⁻⁷ - 2.21·10 ⁻⁶	1.41·10 ⁻⁶ (1.04·10 ⁻⁶) 1.63·10 ⁻⁷ - 3.18·10 ⁻⁶	0%

Table 5.3. cont.

Ni	average range	$1.98 \cdot 10^{-5}$ ($1.43 \cdot 10^{-5}$) $6.69 \cdot 10^{-6}$ - $5.46 \cdot 10^{-5}$	$1.51 \cdot 10^{-5}$ ($9.43 \cdot 10^{-6}$) $4.23 \cdot 10^{-6}$ - $3.60 \cdot 10^{-5}$	$1.97 \cdot 10^{-5}$ ($1.89 \cdot 10^{-5}$) $4.90 \cdot 10^{-6}$ - $6.20 \cdot 10^{-5}$	3%
Cu	average range	$7.24 \cdot 10^{-7}$ ($5.13 \cdot 10^{-7}$) $1.88 \cdot 10^{-7}$ - $1.63 \cdot 10^{-6}$	$9.58 \cdot 10^{-7}$ ($1.38 \cdot 10^{-6}$) $1.28 \cdot 10^{-7}$ - $1.09 \cdot 10^{-5}$	$8.83 \cdot 10^{-7}$ ($1.13 \cdot 10^{-6}$) $1.46 \cdot 10^{-7}$ - $7.08 \cdot 10^{-6}$	3%
Ba	average range	$6.15 \cdot 10^{-7}$ ($2.61 \cdot 10^{-7}$) $2.03 \cdot 10^{-7}$ - $1.23 \cdot 10^{-6}$	$8.32 \cdot 10^{-7}$ ($5.72 \cdot 10^{-7}$) $1.70 \cdot 10^{-7}$ - $3.66 \cdot 10^{-6}$	$7.36 \cdot 10^{-7}$ ($3.36 \cdot 10^{-7}$) $1.90 \cdot 10^{-7}$ - $1.79 \cdot 10^{-6}$	13%
Pb	average range	$8.60 \cdot 10^{-7}$ ($4.02 \cdot 10^{-8}$) $2.76 \cdot 10^{-8}$ - $1.76 \cdot 10^{-7}$	$1.06 \cdot 10^{-7}$ ($9.84 \cdot 10^{-8}$) $2.17 \cdot 10^{-8}$ - $6.11 \cdot 10^{-7}$	$1.03 \cdot 10^{-7}$ ($6.86 \cdot 10^{-8}$) $2.79 \cdot 10^{-8}$ - $4.56 \cdot 10^{-7}$	5%

Notes:

* whole rock $\delta^{18}\text{O} > 26\text{‰}$

† % analyzed dolomite samples with concentration of an element that is greater than or less than the range of measured calcite values.

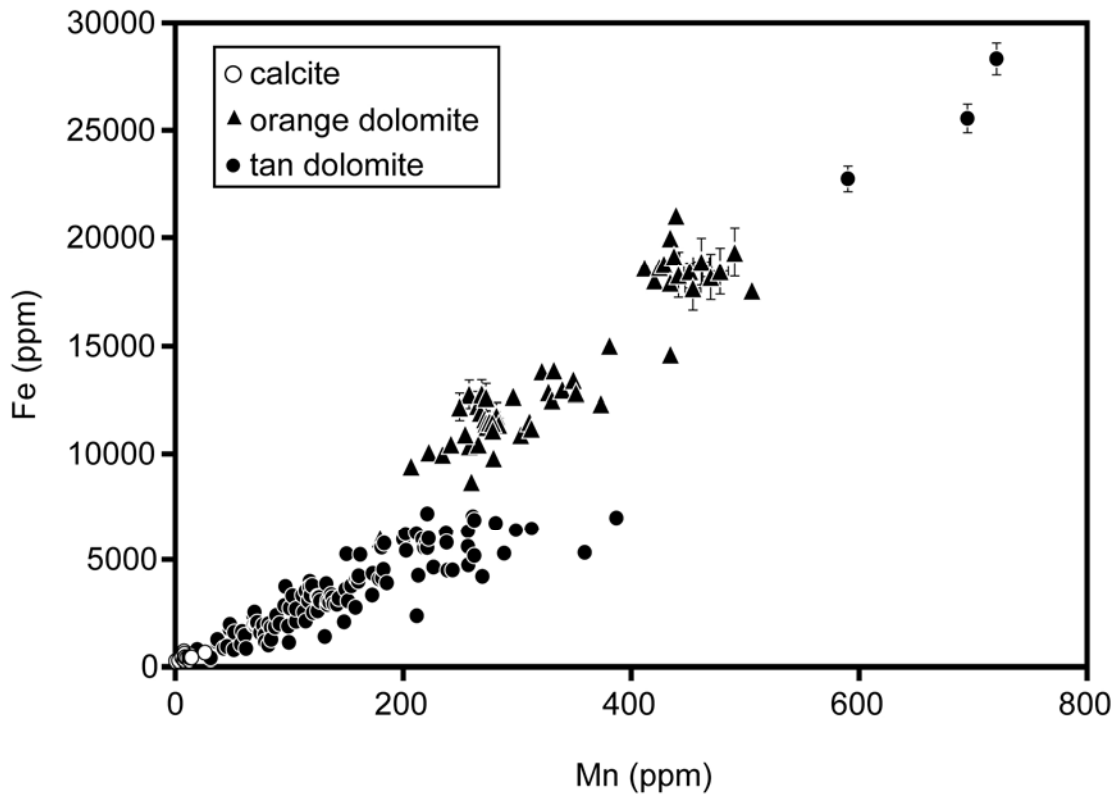


Figure 5.26. Concentrations of Fe and Mn in calcite and dolomite, measured by LA-ICPMS. Error bars (standard error propagation) are shown where error is larger than the size of the symbol.

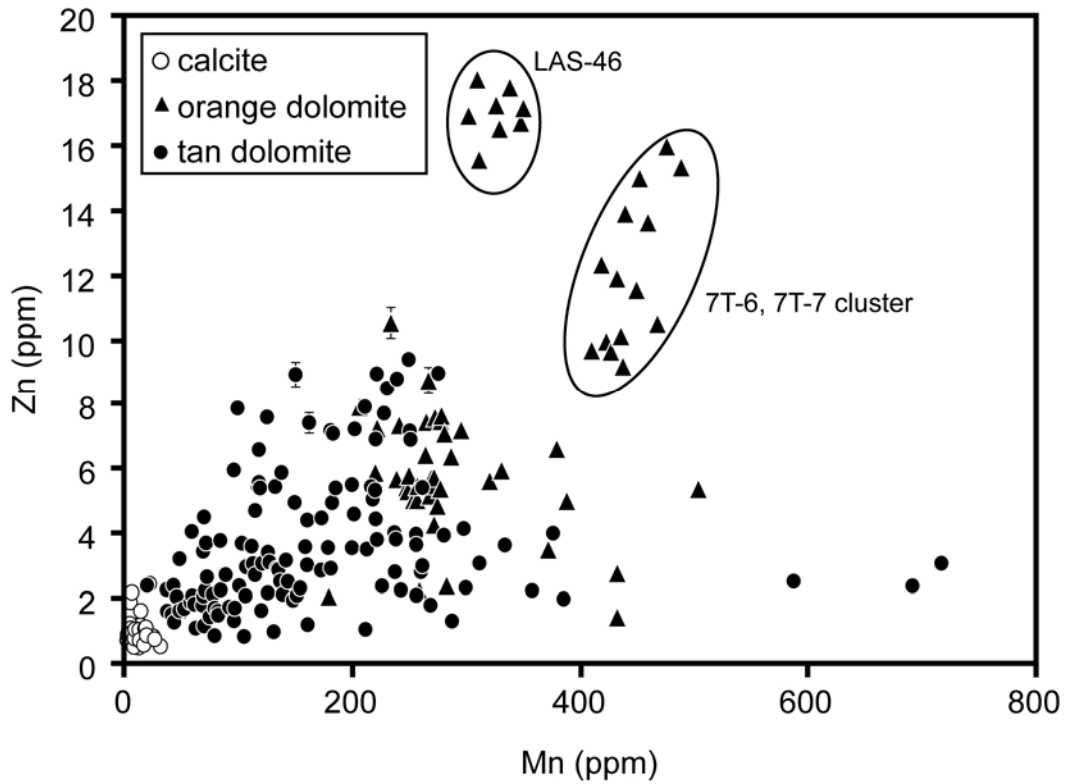


Figure 5.27. Concentrations of Zn and Mn in calcite and dolomite, measured by LA-ICPMS. Error bars (standard error propagation) are shown where error is larger than the size of the symbol.

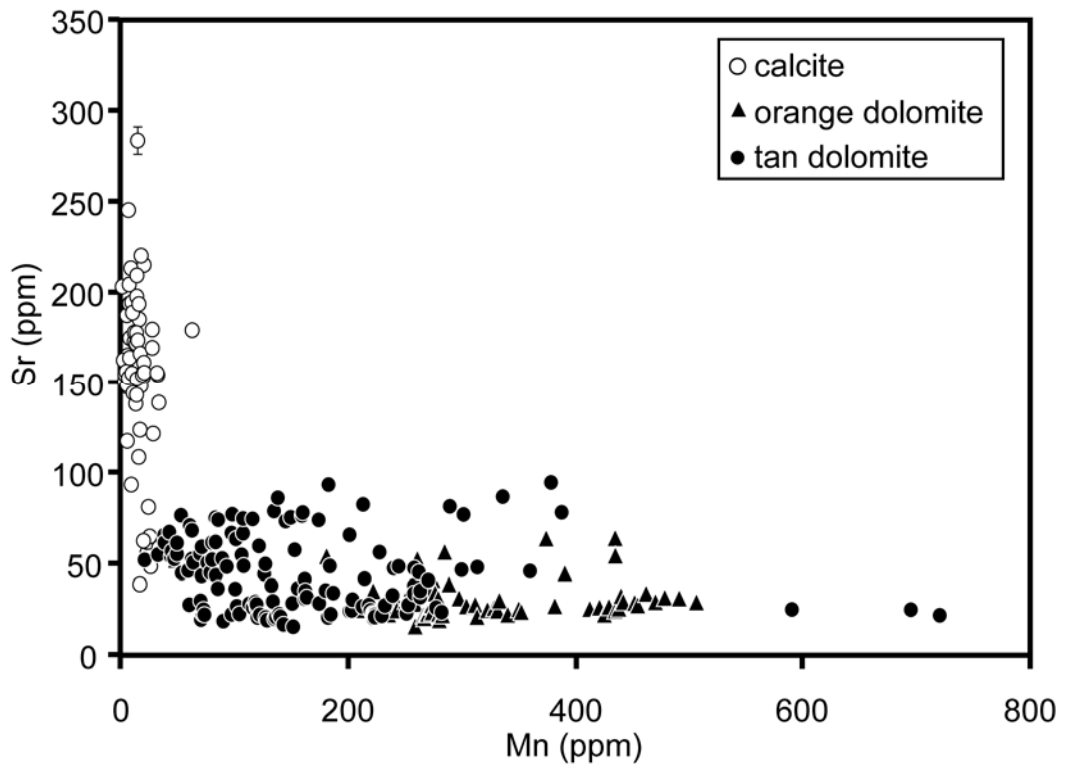


Figure 5.28. Concentrations of Sr and Mn in calcite and dolomite, measured by LA-ICPMS. Error bars (standard error propagation) are shown where error is larger than the size of the symbol.

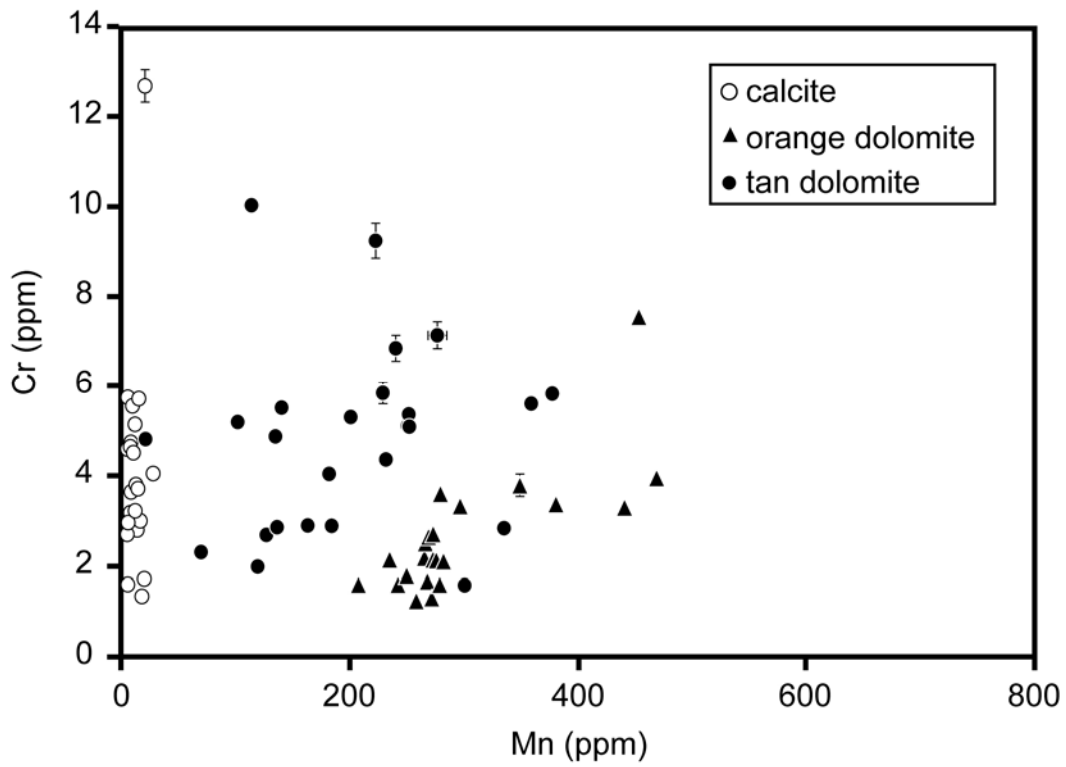


Figure 5.29. Concentrations of Cr and Mn in calcite and dolomite, measured by LA-ICPMS. Error bars (standard error propagation) are shown where error is larger than the size of the symbol.

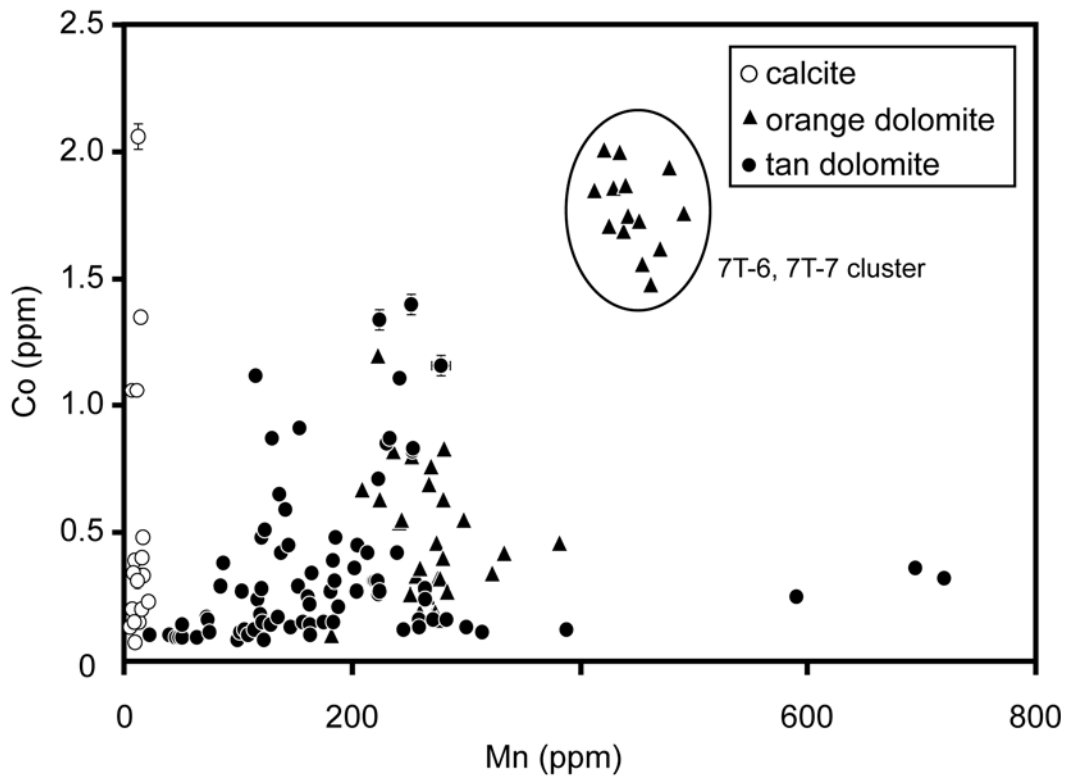


Figure 5.30. Concentrations of Co and Mn in calcite and dolomite, measured by LA-ICPMS. Error bars (standard error propagation) are shown where error is larger than the size of the symbol.

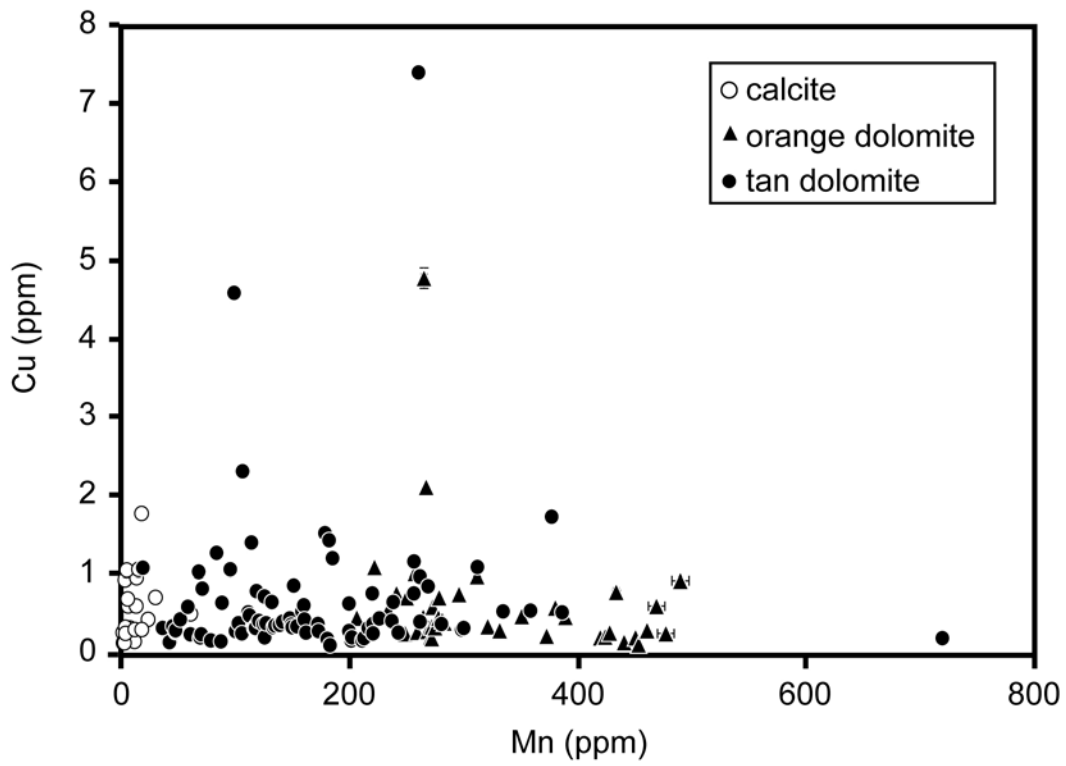


Figure 5.31. Concentrations of Cu and Mn in calcite and dolomite, measured by LA-ICPMS. Error bars (standard error propagation) are shown where error is larger than the size of the symbol.

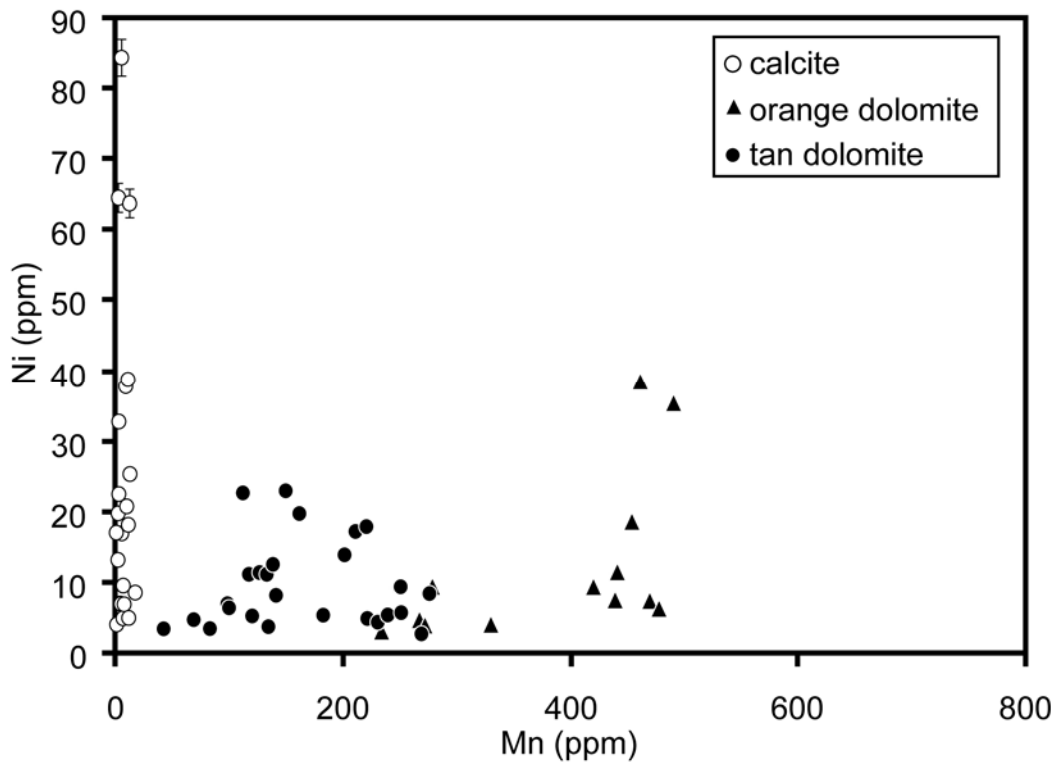


Figure 5.32. Concentrations of Ni and Mn in calcite and dolomite, measured by LA-ICPMS. Error bars (standard error propagation) are shown where error is larger than the size of the symbol.

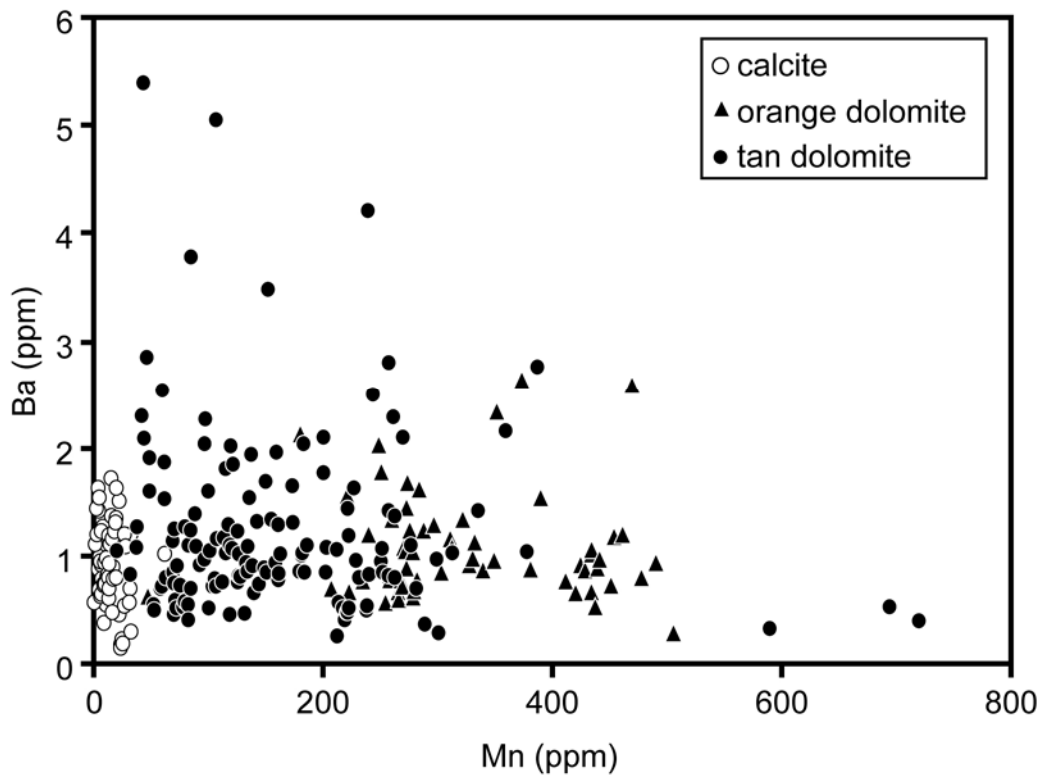


Figure 5.33. Concentrations of Ba and Mn in calcite and dolomite, measured by LA-ICPMS. Error bars (standard error propagation) are shown where error is larger than the size of the symbol.

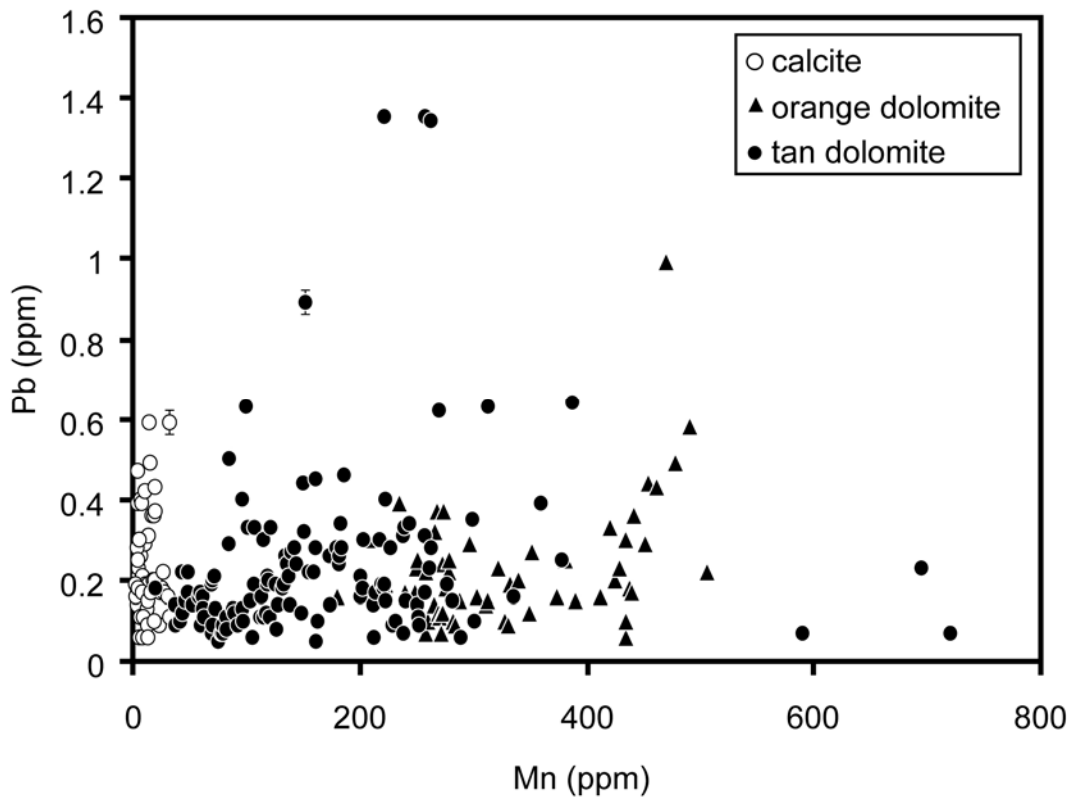


Figure 5.34. Concentrations of Pb and Mn in calcite and dolomite, measured by LA-ICPMS. Error bars (standard error propagation) are shown where error is larger than the size of the symbol.

Chapter 6

Stable Isotopes

All measurements of $\delta^{13}\text{C}$ (‰ VPDB) and $\delta^{18}\text{O}$ (‰ VSMOW) for calcite and dolomite samples are listed in Appendix IV. Measured $\delta^{18}\text{O}$ values range from 23.4 to 28.9‰ VSMOW for calcite (Figure 6.1), from 21.5 to 25.5‰ VSMOW for tan dolomite, and from 22.6 to 26.5‰ VSMOW for orange dolomite. Measured $\delta^{13}\text{C}$ values range from 1.1 to 4.0‰ VPDB for calcite, from 1.9 to 4.0‰ VPDB for tan dolomite, and from 2.4 to 4.6‰ VPDB for orange dolomite.

In any discussion of the $\delta^{18}\text{O}$ of calcite and dolomite within a single outcrop or across the entire buildup, it is necessary to correct one or the other value for the fractionation of ^{18}O and ^{16}O between the two minerals so they may be directly compared. The less numerous values of $\delta^{18}\text{O}_{\text{Cal}}$ were corrected for direct comparison with measured $\delta^{18}\text{O}_{\text{Dol}}$. The relevant correction added to all measured $\delta^{18}\text{O}_{\text{Cal}}$ values is

$$\Delta_{\text{Dol-Cal}} = \delta^{18}\text{O}_{\text{Cal}} - \delta^{18}\text{O}_{\text{Dol}} = 0.45 \times \left(\frac{10^6}{T^2} \right) - 0.40 \quad (6.1)$$

(Sheppard and Schwarcz, 1970). The values of T (25-53°C) used to compute values of $\Delta_{\text{Dol-Cal}}$ for each calcite sample are explained in Chapter 8. Values of $\Delta_{\text{Dol-Cal}}$ calculated from Equation 6.1 are comparable to those computed from the vibrational frequencies of calcite and dolomite given in Deines (2004)

$$\Delta_{\text{Dol-Cal}} = \delta^{18}\text{O}_{\text{Cal}} - \delta^{18}\text{O}_{\text{Dol}} = 0.52 \times \left(\frac{10^6}{T^2} \right) - 0.50 \quad (6.2)$$

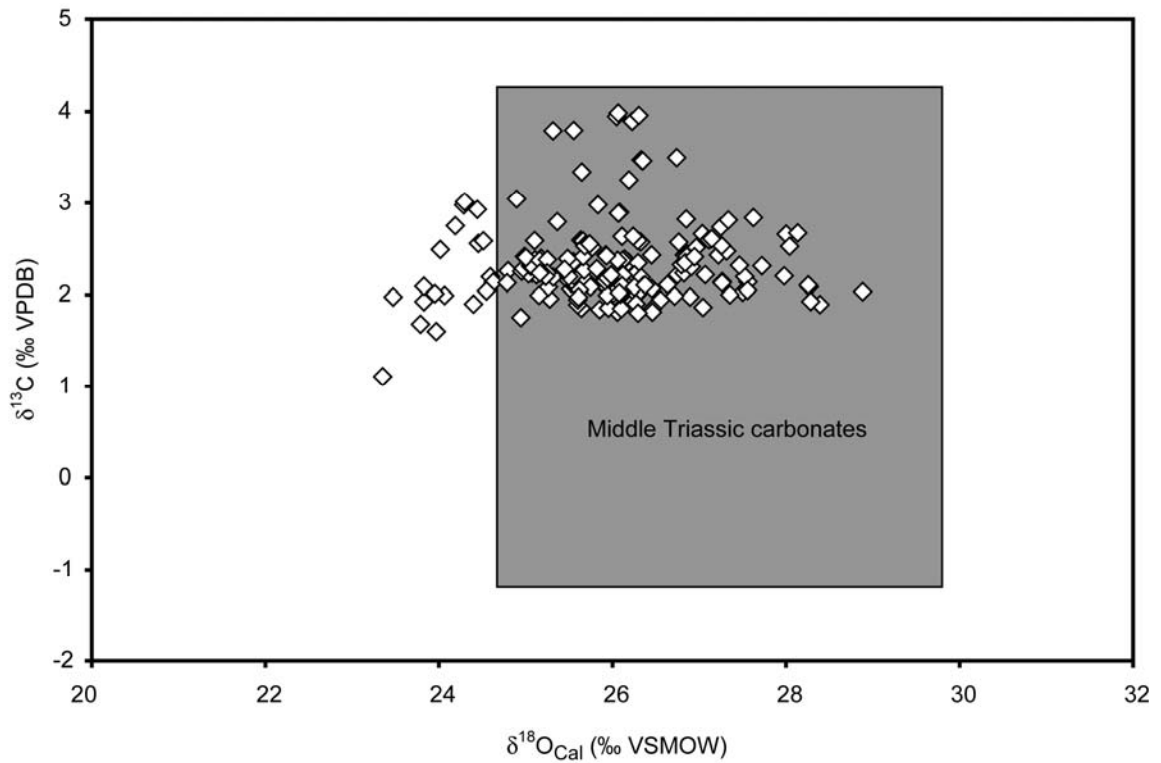


Figure 6.1. Measured $\delta^{13}\text{C}$ vs. $\delta^{18}\text{O}_{\text{Cal}}$ for calcite samples. Most fall in the range of normal Middle Triassic carbonates (gray box based on measurements of whole rock and brachiopod samples, Korte et al., 2005).

(from Chacko, personal communication). The difference in the fractionation factors calculated from Equations 6.1 and 6.2, between -0.37 and +0.20 for $T \leq 100^\circ\text{C}$, are small compared to the measured range in $\delta^{18}\text{O}_{\text{Cal}}$. All measured values of $\delta^{13}\text{C}$ and $\delta^{18}\text{O}_{\text{Dol}}$ and calculated $\delta^{18}\text{O}_{\text{Cal}} + \Delta_{\text{Dol-Cal}}$ values for calcite and dolomite are presented in Figure 6.2. The range in $\delta^{18}\text{O}$ is very large compared to the range in $\delta^{13}\text{C}$, which is nearly constant for all samples. The $\delta^{18}\text{O}$ of dolomite is significantly lower than the corrected $\delta^{18}\text{O}$ of calcite, with virtually no overlap between the dolomite values and the calcite values. Calcite $\delta^{18}\text{O}$ values indicate ^{18}O depletion of a few limestones relative to typical Middle Triassic marine carbonates (Figure 6.1) (Veizer and Hoefs, 1976; Korte et al., 2005). In contrast, all of the dolomites are depleted in ^{18}O relative to calcites. On the other hand, there is an almost complete overlap in the $\delta^{13}\text{C}$ values of calcite and the dolomite. The $\delta^{13}\text{C}$ data indicate that the $\delta^{13}\text{C}$ of most of the dolomite samples was inherited from the limestone protolith. The $\delta^{13}\text{C}$ of all samples is within the range of the $\delta^{13}\text{C}$ of normal Triassic marine carbonates (Veizer and Hoefs, 1976; Korte et al., 2005).

The variation in $\delta^{18}\text{O}$ within single outcrops (Figures 6.3-6.4) is nearly as great as the variation across the entire buildup. Data from Location 8 (Figure 6.3) demonstrate particularly well at the outcrop scale that $\delta^{13}\text{C}_{\text{Dol}}$ was normally inherited directly from the precursor calcite in limestone but that the $\delta^{18}\text{O}$ of dolomite is significantly less than the calcite precursor. The single exception to this generalization that $\delta^{13}\text{C}_{\text{Dol}}$ was inherited directly from the precursor calcite in limestone is found in Location 7 (Figure 6.4). The $\delta^{13}\text{C}_{\text{Dol}}$ of all but one orange dolomite is $\sim 2\text{‰}$ higher than $\delta^{13}\text{C}$ of both tan dolomite and calcite in the same outcrop. The $\delta^{13}\text{C}$ of these orange dolomite samples overlaps the

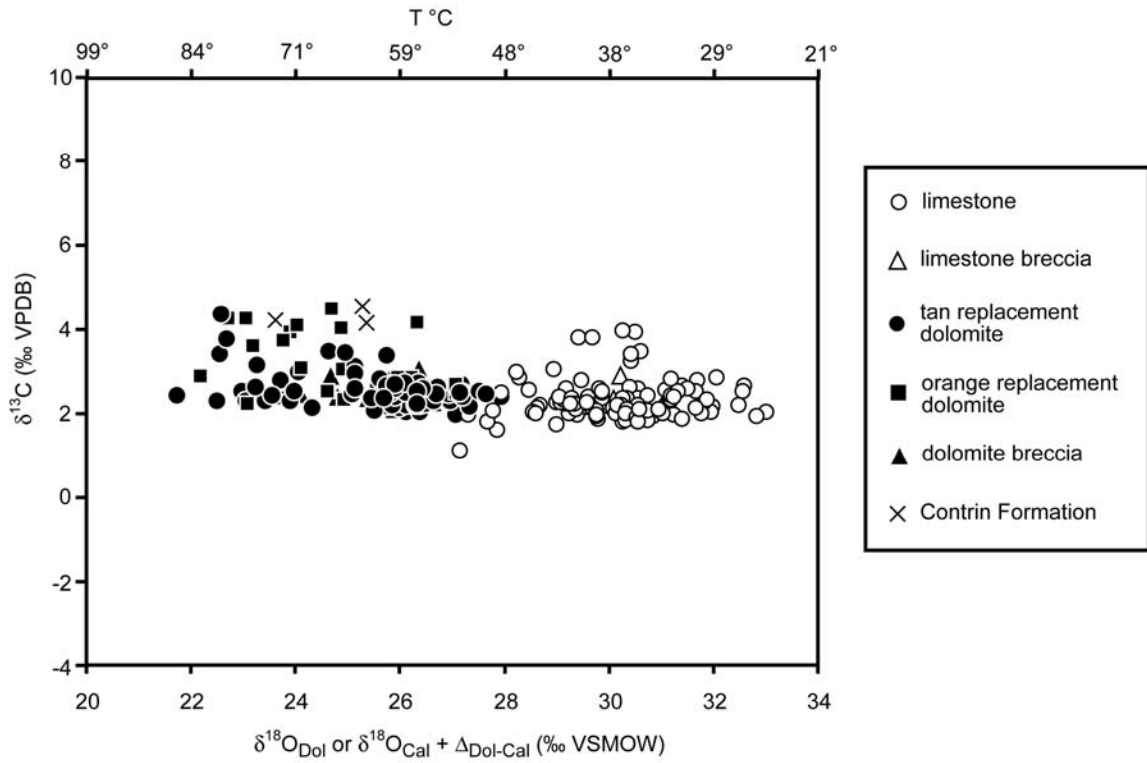


Figure 6.2. $\delta^{13}\text{C}$ vs. $\delta^{18}\text{O}_{\text{Dol}}$ or $\delta^{18}\text{O}_{\text{Cal}} + \Delta_{\text{Dol-Cal}}$ for calcite and dolomite samples, grouped according to rock type. All analyzed samples in the study area are plotted.

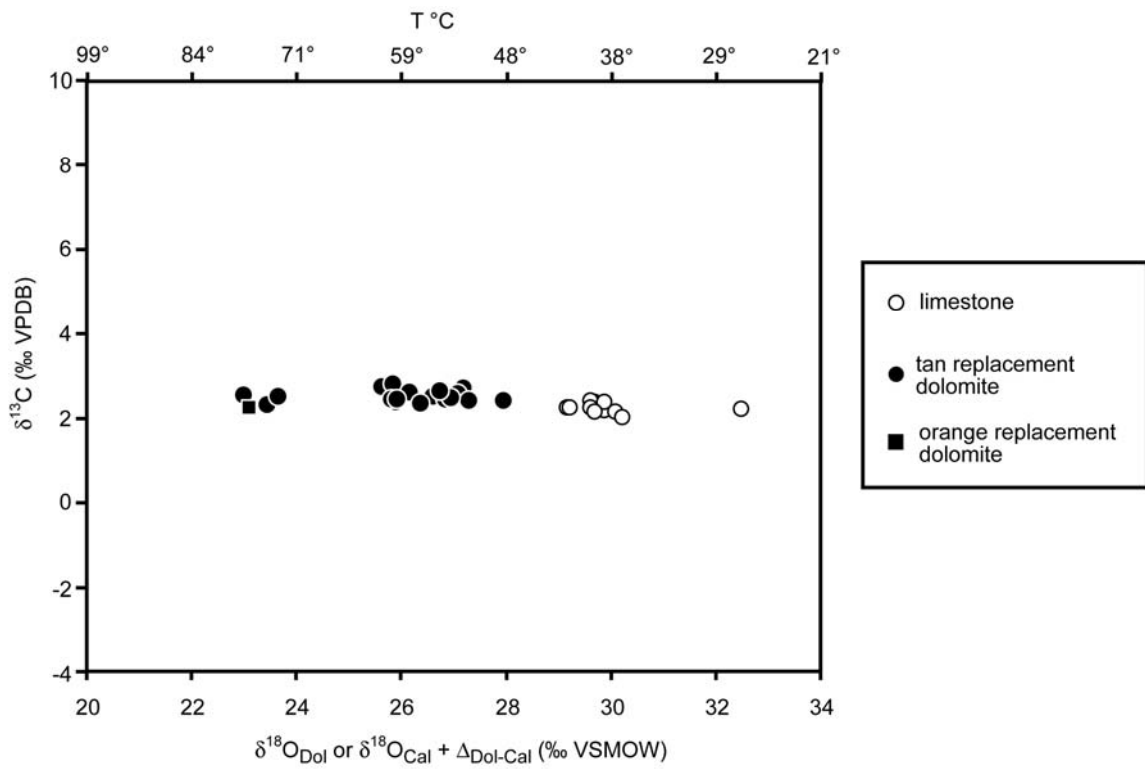


Figure 6.3. $\delta^{13}\text{C}$ vs. $\delta^{18}\text{O}_{\text{Dol}}$ or $\delta^{18}\text{O}_{\text{Cal}} + \Delta_{\text{Dol-Cal}}$ for calcite and dolomite samples in Location 8, grouped according to rock type.

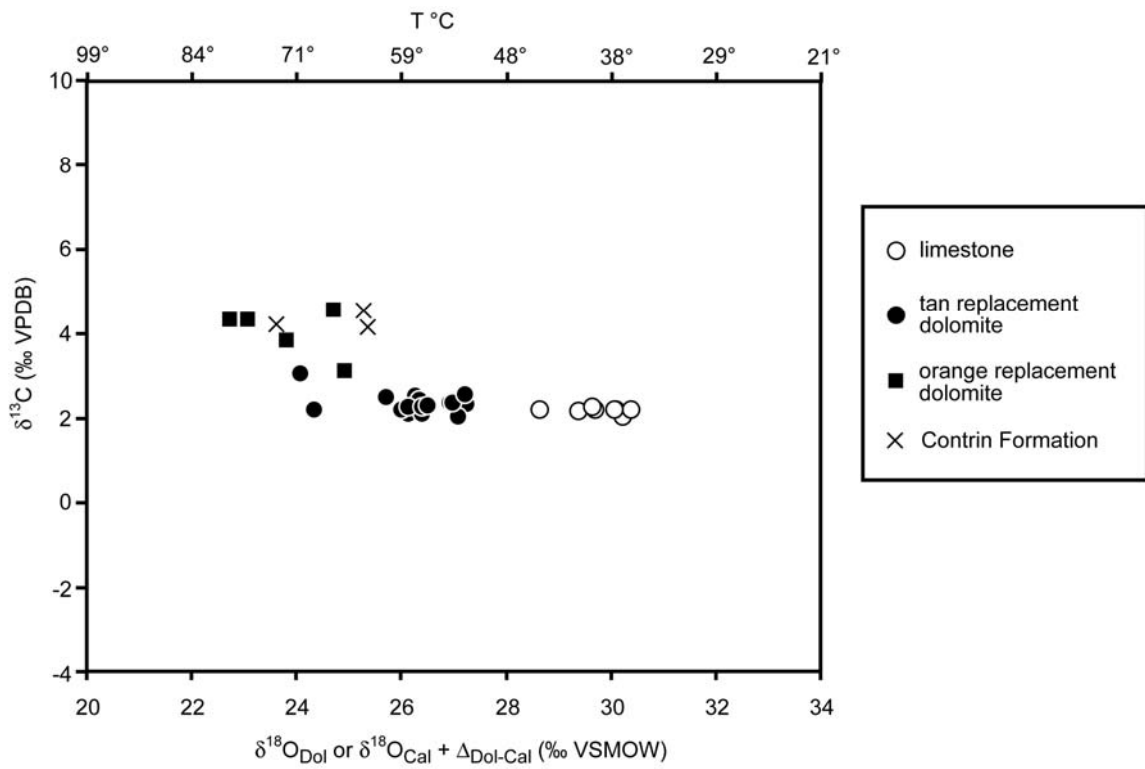


Figure 6.4. $\delta^{13}\text{C}$ vs. $\delta^{18}\text{O}_{\text{Dol}}$ or $\delta^{18}\text{O}_{\text{Cal}} + \Delta_{\text{Dol-Cal}}$ for calcite and dolomite samples in Location 7, grouped according to rock type.

range of $\delta^{13}\text{C}$ values for dolomite in the underlying Contrin Formation. This relationship is explained later in Chapter 9.

There is also no systematic change in $\delta^{18}\text{O}$ with elevation in calcite (Figure 6.5), although there is a weak trend of increasing $\delta^{18}\text{O}_{\text{Dol}}$ with elevation that probably reflects increasing average temperature with depth. This weak trend (approximately $-50^\circ\text{C}/\text{km}$) is used to constrain dT/dz in time-integrated fluid flux estimates in Chapter 9. There is a trend of decreasing $\delta^{13}\text{C}$ with increasing elevation for both calcite and dolomite (Figure 6.6). The lower ^{13}C in almost all calcite samples and many dolomite samples above 350 m, which corresponds to the stratigraphic contact between the Lower Edifice and the Latemar Limestone, may simply correspond to a change in the primary $\delta^{13}\text{C}$ across the stratigraphic boundary.

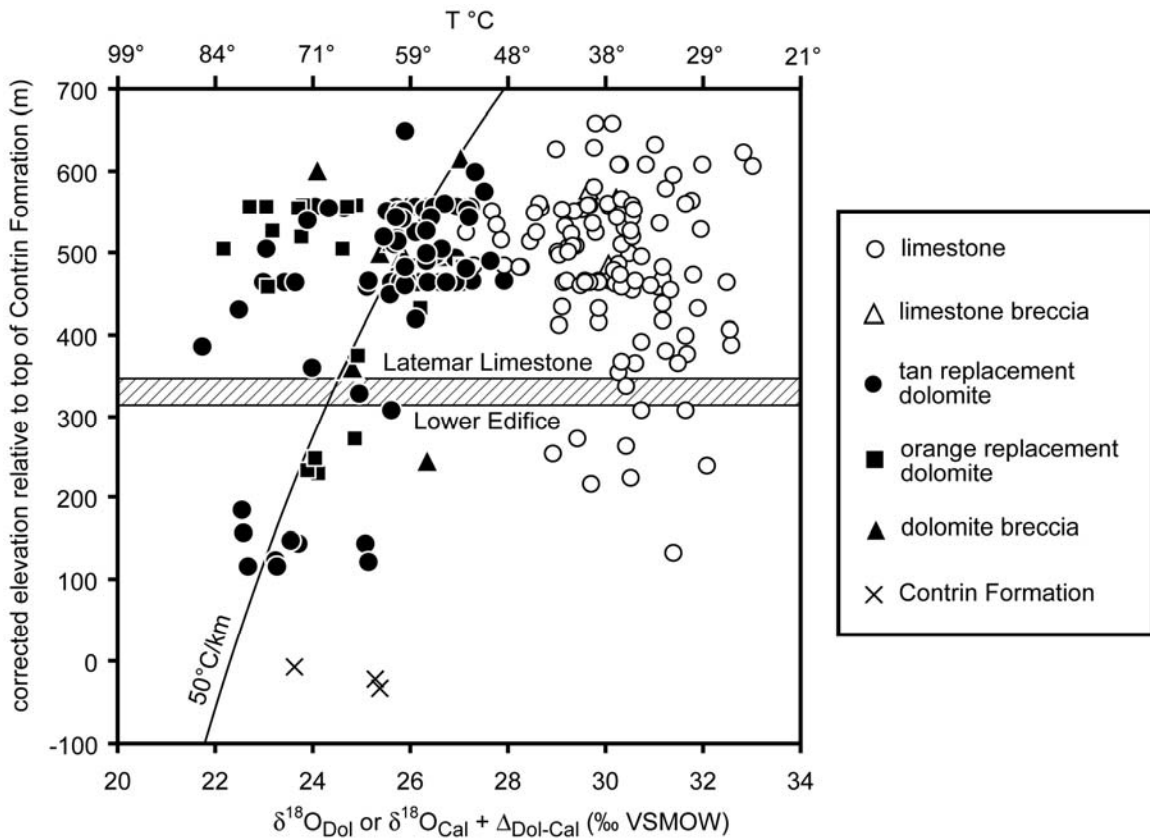


Figure 6.5. $\delta^{18}\text{O}_{\text{Dol}}$ or $\delta^{18}\text{O}_{\text{Cal}} + \Delta_{\text{Dol-Cal}}$ vs. elevation for calcite and dolomite. There is no systematic change in $\delta^{18}\text{O}$ for calcite with increasing elevation. There is a weak trend in $\delta^{18}\text{O}$ for dolomite; with the exception of one sample, all the analyzed dolomite below 350 m has $\delta^{18}\text{O} < 26\text{‰}$. The $\delta^{18}\text{O}$ gradient in dolomite corresponds to a temperature increase of 50°C/km with depth.

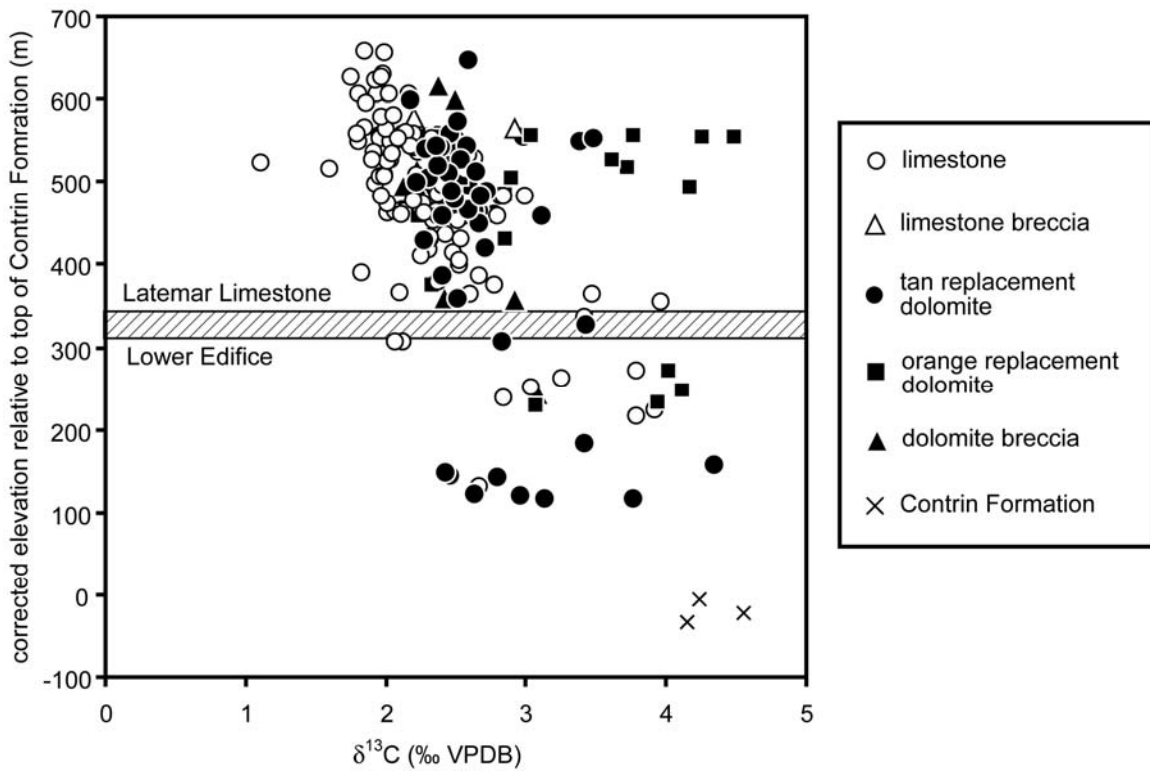


Figure 6.6. $\delta^{13}\text{C}$ vs. elevation for calcite and dolomite. $\delta^{13}\text{C}$ in most samples is lower at elevations above ~ 350 m, corresponding to the Lower Edifice - Latemar Limestone stratigraphic (Anisian-Ladinian) boundary, than those below ~ 350 m.

Chapter 7

Source of Dolomitizing Fluid

The $^{87}\text{Sr}/^{86}\text{Sr}$ and trace element compositions of replacement dolomite and limestone protolith, the salinity of fluid inclusions in dolomite, and the estimated Ca/Mg ratio of fluid required to convert limestone to dolomite all constrain the source and nature of the dolomitizing fluids in the Latemar.

$^{87}\text{Sr}/^{86}\text{Sr}$

For unaltered calcite ($\text{Fe} < 500$ ppm, and $\text{Sr}/\text{Mn} < 5$), $^{87}\text{Sr}/^{86}\text{Sr}$ isotope ratios range from 0.707430 to 0.707580, with higher $^{87}\text{Sr}/^{86}\text{Sr}$ in the Lower Edifice than in the Latemar Limestone (Pursell, 1997). The $^{87}\text{Sr}/^{86}\text{Sr}$ in replacement dolomite ranges from 0.707552 to 0.707867 (Wilson et al., 1990). Although the $^{87}\text{Sr}/^{86}\text{Sr}$ values of dolomite reported by Wilson et al. (1990) are generally higher than those for calcite measured by Pursell (1997), both sets are within the 0.70740 - 0.70790 range of values for Triassic seawater given by Burke et al. (1982). The dolomitizing fluid must have had the same $^{87}\text{Sr}/^{86}\text{Sr}$ as Triassic seawater.

Fluid Inclusions

Freezing temperatures measured by Wilson (1989) for fluid inclusions in replacement dolomite indicate that the salinity of the dolomitizing fluid corresponds to 3.5 to 5.1 weight percent NaCl. Modern seawater has a 3.5 weight percent NaCl equivalent salinity. The dolomitizing fluid must have had a similar salinity.

Ca/Mg ratio

Given the temperature of dolomitization, it is possible to calculate the Ca/Mg ratio of the fluid needed to drive the calcite - dolomite reaction. Assuming reaction temperatures of 50-90°C (the range temperatures of dolomitization, given by oxygen isotopes, are discussed in Chapter 8), the Ca/Mg ratio for the fluid coexisting with calcite and dolomite can be computed from

$$\log \frac{a_{\text{Ca}^{++}}}{a_{\text{Mg}^{++}}} = -0.22 + \frac{7.21 \cdot T(^{\circ}\text{C})}{1000} \quad (7.1)$$

(Hyeong and Capuano, 2001). Equation 7.1, fit to the Ca/Mg ratios in natural pore waters where calcite and dolomite are in equilibrium at 43-150°C, gives Ca/Mg ratios of fluid that are similar to but higher than those predicted by SUPCRT92 for disordered dolomite and calcite (Johnson et al., 1992, using data from Helgesen et al., 1978), and inferred from experimental data of Rosenberg et al. (1967) and Rosenberg and Holland (1964) for calcite-dolomite-fluid equilibrium (Table 7.1). The relation of Hyeong and Capuano (2001) is preferred over those derived from experimental and thermodynamic data for three reasons. First, equations based on experiments extrapolate data from elevated temperatures (>275°C) to the lower temperature of dolomitization (50-90°C) in the Latemar. The data of Hyeong and Capuano (2001) overlap in temperature with the temperature of dolomitization in the Latemar. Second, equations based on experiments and thermodynamic data assume mineral-fluid equilibrium during dolomitization while the empirical equation of Hyeong and Capuano (2001) does not (although Hyeong and Capuano do conclude that the pore fluids they analyzed were close to equilibrium with coexisting calcite and dolomite). Third, the thermodynamic calculations assume completely disordered dolomite and the experiments involved dolomite of an unknown

Table 7.1. Ca/Mg of fluid coexisting with calcite and dolomite.

Source	150°C	90°C	80°C	70°C	50°C
Rosenberg, et al. (1967): $\log \frac{m_{Ca^{2+}}}{m_{Mg^{2+}}} = \frac{-1.14 \times 10^3}{T(^{\circ}K)} + 3.15$ (for 295-420°C, 1M)	2.85	1.02	0.83	0.67	0.42
Rosenberg and Holland (1964): $\log \frac{m_{Ca^{2+}}}{m_{Mg^{2+}}} = \frac{-1.00 \times 10^3}{T(^{\circ}K)} + 2.98$ (for 275-420°C, 2M)	4.13	1.68	1.40	1.16	0.77
SUPCRT disordered dolomite (Johnson et al., 1992)	4.37	1.68	1.55	1.28	0.83
Hyeong and Capuano (2001): $\log \frac{a_{Ca^{++}}}{a_{Mg^{++}}} = -0.22 + \frac{7.21 \cdot T(^{\circ}C)}{1000}$ (for 43-150°C)	7.27	2.68	2.27	1.93	1.38

ordering state. It is not known how well this represents partially disordered dolomite ($s=0.4$) like that found in the Latemar (Schubel, 1997). Regardless of method used to estimate the Ca/Mg of the fluid coexisting with calcite and dolomite during formation of replacement dolomite, the Ca/Mg was almost certainly in the range of 0.42-2.68 for dolomitization at 50-90°C. The dolomitizing fluid therefore must have had a Ca/Mg < 0.42-2.68. The preferred estimate is Ca/Mg < 1.38 based on Equation 7.1.

Trace Elements

Replacement dolomite in the Latemar is enriched in Fe, Mn, and Zn relative to the limestone protolith. The positive correlation in these elements indicates that Fe, Mn, and Zn were added in approximately constant proportions during the conversion of calcite to dolomite. Dolomite is neither enriched in Co, Ni, Cr, Cu, Pb, and Ba relative to calcite, nor are there correlations between any of these elements and Fe, Mn, or Zn. Dolomitizing fluid therefore should contain significant Fe, Mn, and Zn but not Co, Ni, Cr, Cu, Pb, or Ba and should exhibit variable Fe, Mn, and Zn contents but approximately constant Fe/Mn and Zn/Mn.

Considering the trace element chemistry of the dolomite, the salinity estimated from fluid inclusions, the $^{87}\text{Sr}/^{86}\text{Sr}$ of dolomite, and the low Ca/Mg of fluid required for dolomitization, it is possible to identify a plausible modern analog to the dolomitizing fluid (Table 7.2). The dolomitizing fluid (“target” fluid, Table 7.2) must have a Ca/Mg < 1.38, significant amounts of Fe, Mn, and Zn that are variable in space and/or time, $^{87}\text{Sr}/^{86}\text{Sr} = 0.707552 - 0.707867$, and salinity near that of seawater (~546 mM Cl).

Triassic seawater, an obvious candidate for the dolomitizing fluid, has appropriate salinity, $^{87}\text{Sr}/^{86}\text{Sr}$, and Ca/Mg (Hardie, 1990; Burke, 1982), but has too small concentrations of Fe, Mn, and Zn. A more detailed analysis of this will be presented later in Chapter 9.

Conversely, Red Sea brines, Salton Sea geothermal fluids, Gulf Coast oil field brines, and Creede Ag-Pb-Zn ore fluids all have high Fe, Mn, and Zn concentrations but their Cl concentrations and Ca/Mg are much too high to have been viable dolomitizing fluids (Skinner, 1997; Zierenberg, 1990). Although many Ag-Pb-Zn ore fluids are commonly associated with Fe, Mn, and Zn enrichment in carbonates and have a positive correlation within the dolomites surrounding the ore deposit, the $\delta^{18}\text{O}$ and $\delta^{13}\text{C}$ in these dolomites are much lower ($\delta^{18}\text{O} = +11\text{‰}$ SMOW and $\delta^{13}\text{C} = -5\text{‰}$ PDB) than those of the Latemar dolomite (Large and McGoldrick, 1999). Additionally, these fluids are unlikely to be found in a geologic setting such as the Latemar.

Mid-ocean ridge black-smoker vent fluids have chloride concentrations that are similar to the target chloride concentrations of the dolomitizing fluid, and contain significant amounts of Fe, Mn, and Zn (Von Damm, 1990). However, their Ca/Mg $\sim \infty$ is impossibly high to form dolomite (Mg is stripped out of seawater in mid-ocean ridge hydrothermal systems and is not present in black smoker and white smoker type vent fluids). Additionally, the high temperatures (up to $\sim 350^\circ\text{C}$) of mid-ocean-ridge fluids cause many of these trace metals to form sulfide complexes upon mixing with cold ambient seawater, thereby removing them from solution. The $^{87}\text{Sr}/^{86}\text{Sr}$ in modern vent fluid, which represents seawater exchange with MOR-type basalts, is also lower than that measured in the Latemar dolomite.

Table 7.2. Potential modern analogues to dolomitizing fluids.

	Target	Triassic seawater ^{1,2}	Red Sea brine ^{3,4}	Salton Sea fluid ⁵	Oil field brine ⁵	Creede ore fluid ⁵	EPR vent fluid ^{6,7}	Diffuse effluent ^{8,9}
Cl (mM)	≈546	546	<i>4410</i>	<i>4260</i>	<i>4460</i>	<i>1312</i>	490	570
Ca/Mg	<1.38	0.29	3.8	<i>489</i>	<i>12.8</i>	8	∞	0.33
⁸⁷ Sr/ ⁸⁶ Sr	0.707552 - 0.707867	0.70740 - 0.70790	0.70696 - 0.70782	NA	NA	NA	0.7037 - 0.7045	0.70758 - 0.7092
Fe (mM)	(+)	1×10^{-3}	1500	27,900	5340	NA	1660	710
Mn (mM)	(+)	5×10^{-4}	1500	26,400	NA	12,600	960	170
Zn (mM)	(+)	6×10^{-3}	46	7920	4590	19,900	106	10

Notes: (+) indicates a significant amount is required. Values in italics represent values that do not match the target requirements.

¹ Hardie (1996)

² Burke et al. (1982)

³ Zierenberg (1990)

⁴ Pierret et al. (2001)

⁵ Skinner (1997)

⁶ 21N EPR, sample OBS, Von Damm (1990)

⁷ Ravizza et al. (2001)

⁸ TAG 1995 site 2896-2, sample HT20, GSA data repository 9667, James and Elderfield (1996)

⁹ Kelley et al. (2005)

On the other hand, diffuse effluent (a hydrothermal fluid that flows diffusely from the flanks of mid-ocean ridges, at $T = 50-100^{\circ}\text{C}$ and that is approximately a mixture between seawater and black smoker type vent fluid) is a fluid that fits all the target fluid characteristics. It has chloride concentrations of $\sim 570 \text{ mM}$, $^{87}\text{Sr}/^{86}\text{Sr}$ in the range of the Latemar dolomites (Kelley et al., 2005), $\text{Ca}/\text{Mg} < 1.38$, and significant quantities of Fe, Mn, and Zn (James and Elderfield, 1996). Additionally, the Fe, Mn, and Zn concentrations vary but occur in nearly constant proportion (Figures 7.1-7.2). Data from the TAG mound on the Mid-Atlantic ridge (black circles) were taken from various sites along the ridge flank at the same time (James and Elderfield, 1996), while data from $9^{\circ}50'\text{N}$ East Pacific Rise (white circles) are taken at the same sampling site over a period of eleven years (Von Damm and Lilley, 2004). The variations in Fe, Mn, and Zn contents occur over both space and time in diffuse effluent. Furthermore, there is very little Cu in diffuse effluent (Figure 7.3) (James and Elderfield, 1996) and no correlation between Cu and Mn (or Fe or Zn) contents. The absence of published data for the Co, Ni, Cr, Pb, and Ba contents of diffuse effluent does not allow for testing the prediction that diffuse effluent should contain very small concentrations of these elements with no correlations of their concentrations with those of Mn, Fe, and Zn. The Predazzo volcanic-intrusive complex likely drove the hydrothermal system that produced diffuse effluent. Located structurally below the Latemar, it was active at the time of dolomitization and provided a source of heat, Fe, Mn, and Zn added to the Triassic seawater circulating through it.

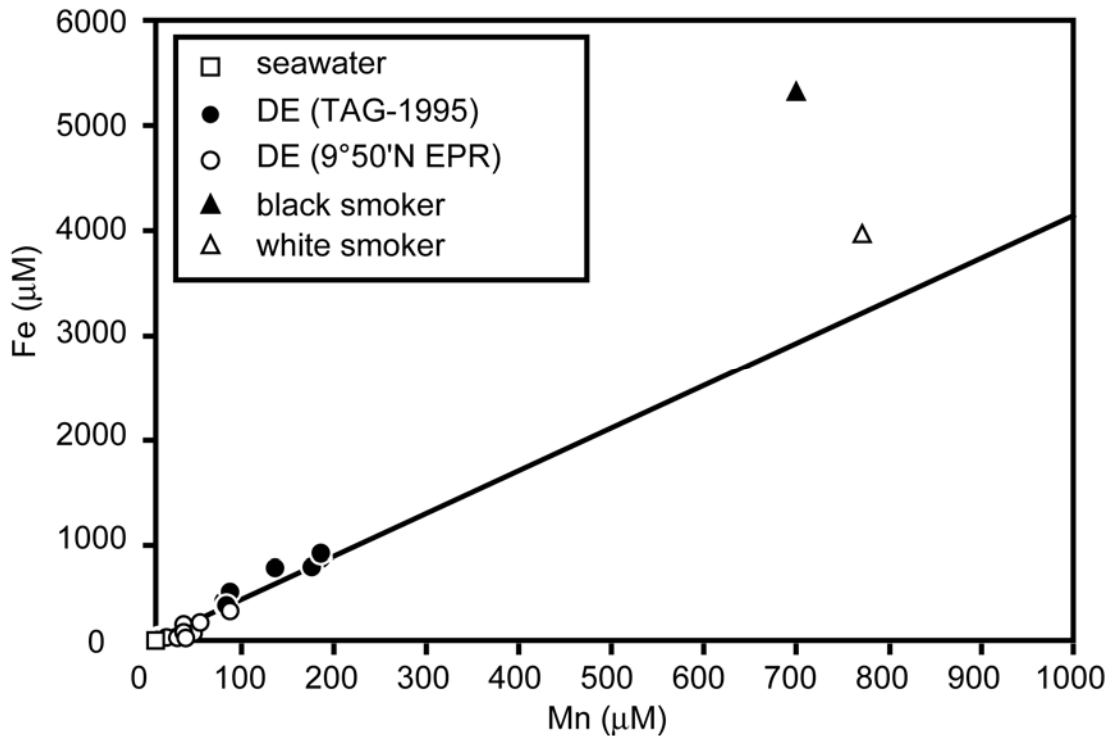


Figure 7.1. Fe vs. Mn concentrations in diffuse effluent (DE) from the TAG site on the Mid-Atlantic Ridge (black circles; James and Elderfield, 1996) and 9°50'N East Pacific Rise (white circles; Von Damm and Lilley, 2004). Seawater (white square) from Von Damm (1990), black smoker (black triangle) and white smoker (white triangle) from Edmond et al. (1995) for reference. The TAG site data represent samples taken at the same time in different locations across the Mid-Atlantic Ridge flank, and the East Pacific Rise data points represent samples taken at the same location over a period of 11 years. There is a similar positive correlation between Fe and Mn in both sets of DE samples, indicating that Fe and Mn vary in both space and time but occur in an approximately constant proportion.

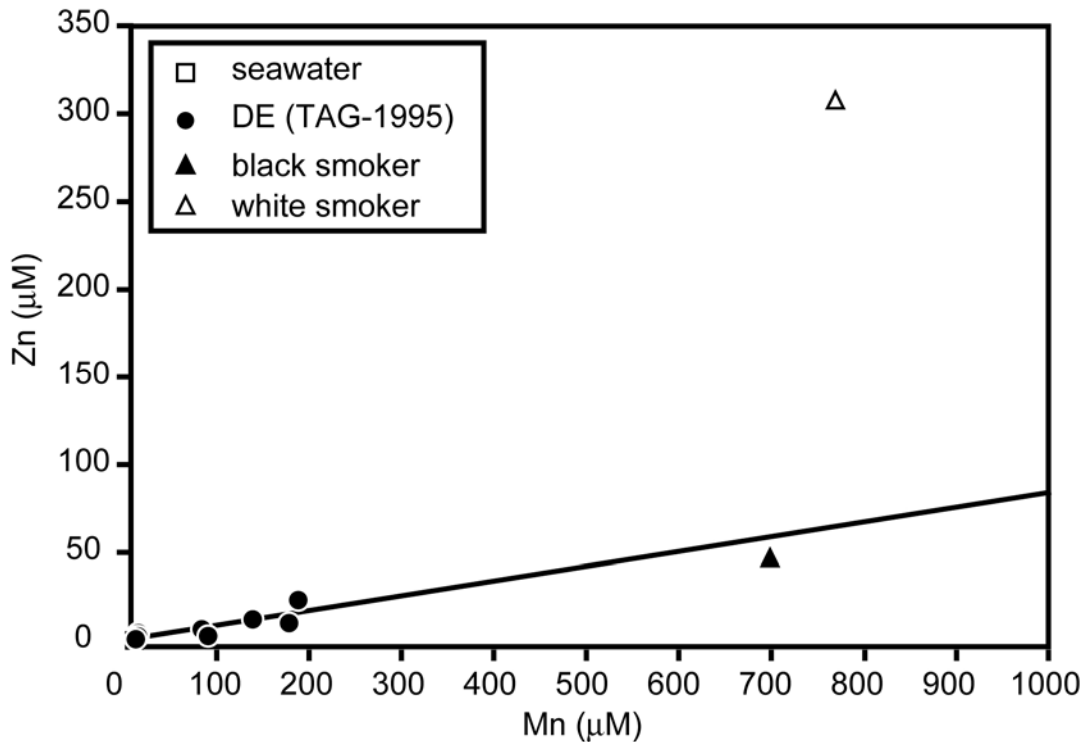


Figure 7.2. Zn vs. Mn concentrations in diffuse effluent (DE) from the TAG site on the Mid-Atlantic Ridge (black circles; James and Elderfield, 1996). Seawater (white square) from Von Damm (1990), black smoker (black triangle) and white smoker (white triangle) from Edmond et al. (1995) for reference. The TAG site data points represent samples taken at the same time in different locations across the Mid-Atlantic Ridge flank. There is a positive correlation between Zn and Mn in the TAG DE data, indicating that Zn and Mn vary in space but occur in an approximately constant proportion. There are no Zn data from the 9°50'N East Pacific Rise site.

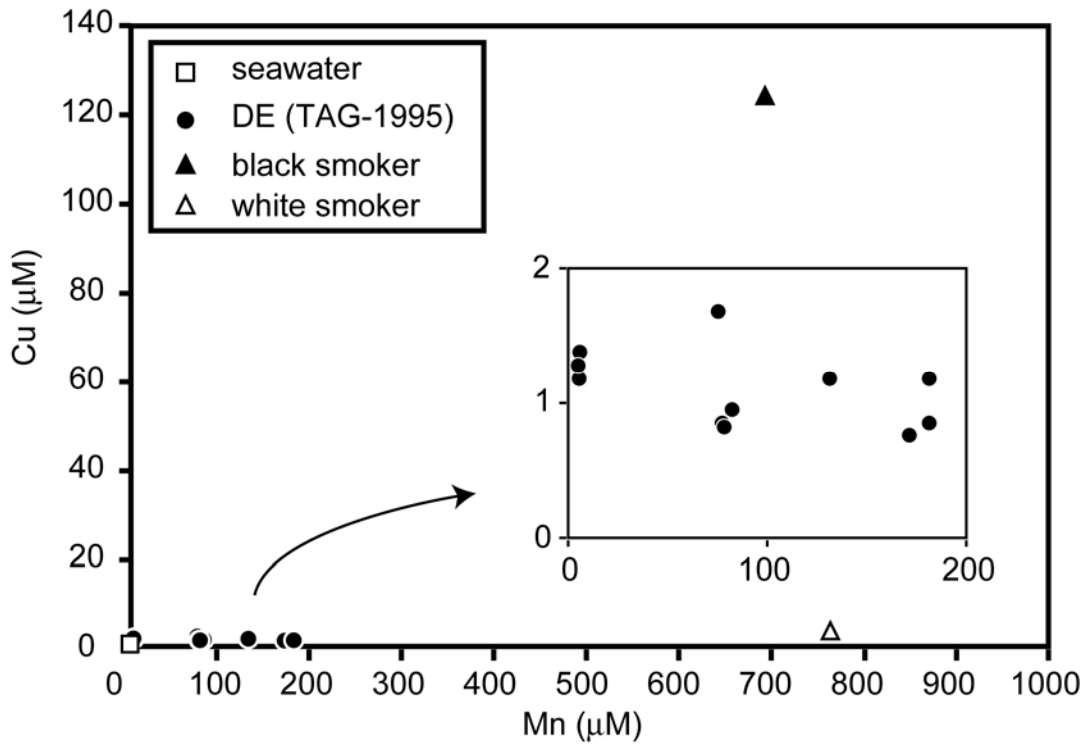


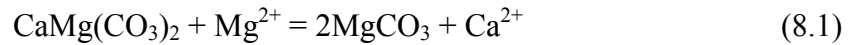
Figure 7.3. Cu vs. Mn concentrations in diffuse effluent (DE) from the TAG site on the Mid-Atlantic Ridge (black circles; James and Elderfield, 1996). Seawater (white square) from Von Damm (1990), black smoker (black triangle) and white smoker (white triangle) from Edmond et al. (1995) for reference. Inset is a magnified view of the Cu vs. Mn data for DE near the origin. The TAG site data points represent samples taken at the same time in different locations across the Mid-Atlantic Ridge flank. There is no correlation between Cu and Mn in the TAG DE data. There are no Cu data from the 9°50'N East Pacific Rise site.

Chapter 8

Temperature of Dolomitization

Fluid Inclusions

Wilson (1989) analyzed 55 fluid inclusions in seven samples of replacement dolomite in the Latemar. These samples exhibit homogenization temperatures of 72-220°C, that were interpreted by Wilson (1989), Wilson et al. (1990), and Hardie et al. (1991) as the temperature of dolomitization. Thermodynamic data for the equilibrium



however, indicate that magnesite forms from disordered dolomite at ~130°C (SUPCRT92, Johnson et al., 1992) in the presence of a fluid with the Ca/Mg ratio of Triassic seawater (Hardie, 1996). Thus, at the temperatures of dolomitization indicated by the fluid inclusions, magnesite rather than dolomite should be stable in the Latemar. The absence of magnesite from the 131 dolomite samples collected in this study suggests that measured homogenization temperatures do not represent the temperature of dolomitization. Furthermore, the temperature of dolomitization more likely was <90°C.

Fluid inclusions may give anomalously high homogenization temperatures in carbonates if stresses from burial, uplift, deformation, or later heating events, cause stretching or leakage of the fluid inclusion (Presbindowski and Larese, 1987). Experiments performed by Prezbindowski and Larese (1987) with calcite have shown that external increases in pressure and temperature can change the homogenization temperatures of entire populations of primary fluid inclusions without visible evidence of alteration. It is not unlikely that similar effects could occur in dolomite. Additionally,

fluid inclusion arrays with variable sizes of inclusions require that 90% the homogenization temperatures in the assemblage are within 10-15°C of each other in order to rule out stretching and leakage (Goldstein, 2001). The fluid inclusions in the Latemar dolomites do not meet this criterion (Figure 8.1), indicating that leakage or stretching may have occurred in many of the inclusions that have high homogenization temperatures. Possible causes include release of overburden during uplift and erosion, increase in temperature from post-dolomitization igneous activity, and/or effects of Tertiary alpine deformation (Blendinger, 1985; Doglioni, 1987).

Oxygen Isotopes

In this study, the measured $\delta^{18}\text{O}$ of calcite and dolomite were used to estimate fluid-rock equilibration temperatures (see Chapter 6). These calculations assume oxygen isotopic exchange equilibrium between mineral and fluid, and are justified by studies by Milliken et al. (1981) of calcite and dolomite in the Texas Gulf Coast oil fields, by Kelley et al. (2005) of aragonite chimneys forming from diffuse effluent in the Lost City hydrothermal field 15 km from the Mid-Atlantic Ridge, and by numerous studies of foraminifera tests in deep sea sediments (Emiliani and Edwards, 1953; Savin et al., 1975; Matthews and Poore, 1980; Miller and Katz, 1987) that all indicate carbonate-fluid ^{18}O - ^{16}O exchange equilibrium at $<100^\circ\text{C}$. The experimentally determined calcite-water fractionation (O'Neil et al., 1969),

$$\Delta_{\text{Cal-H}_2\text{O}} = \delta^{18}\text{O}_{\text{Cal}} - \delta^{18}\text{O}_{\text{H}_2\text{O}} = 2.78 \times \left(\frac{10^6}{T^2} \right) - 2.89 \quad (8.2)$$

was combined with a dolomite-calcite fractionation (Sheppard and Schwarcz, 1970)

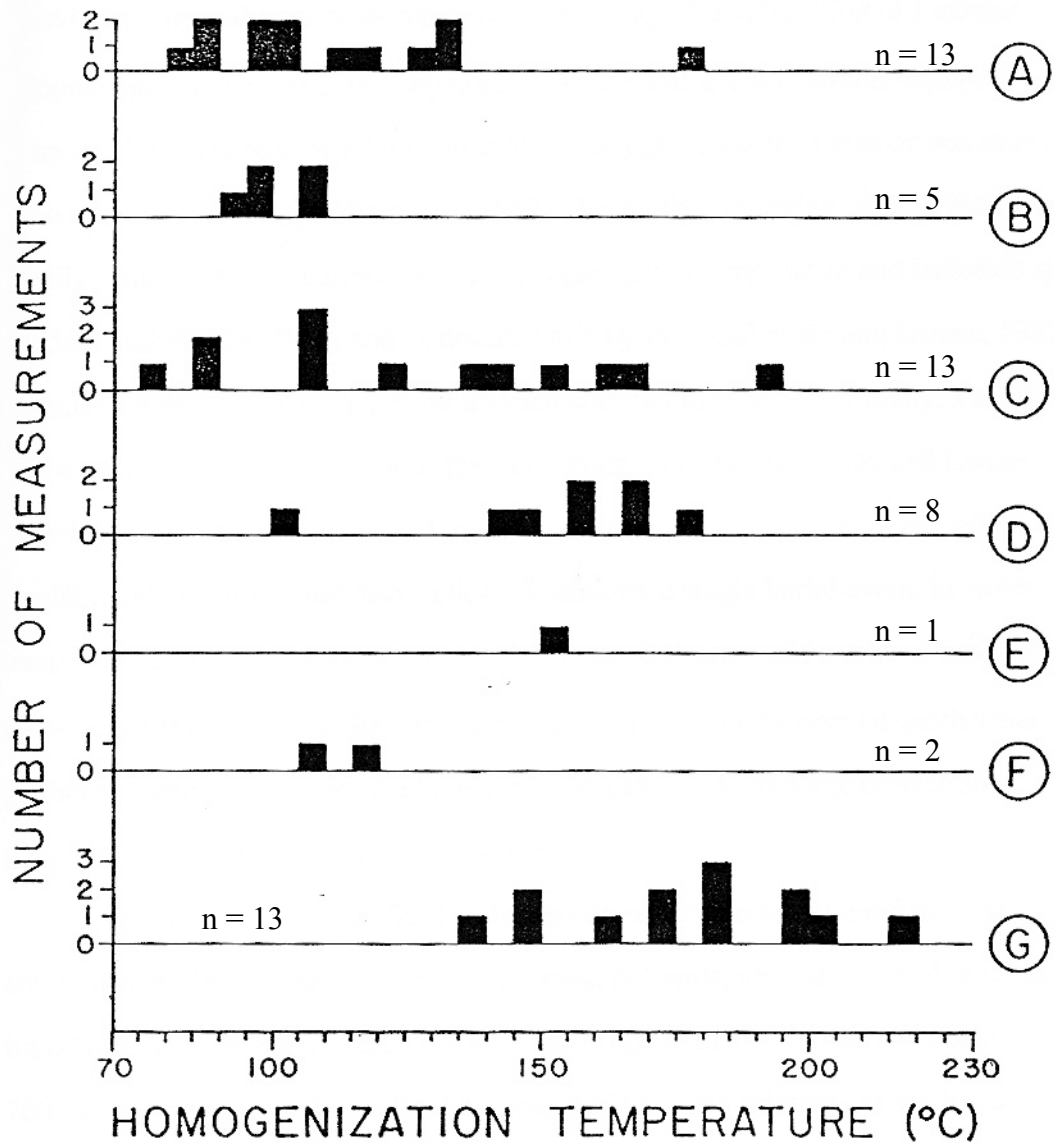


Figure 8.1. Fluid inclusion homogenization temperatures for Latemar dolomite (from Wilson, 1989). The range of values in a single sample, such as Sample C, may be almost as large as the entire data set.

$$\Delta_{\text{Dol-Cal}} = \delta^{18}\text{O}_{\text{Cal}} - \delta^{18}\text{O}_{\text{Dol}} = 0.45 \times \left(\frac{10^6}{T^2} \right) - 0.40 \quad (8.3)$$

to obtain a dolomite-water fractionation,

$$\Delta_{\text{Dol-H}_2\text{O}} = \delta^{18}\text{O}_{\text{Dol}} - \delta^{18}\text{O}_{\text{H}_2\text{O}} = 3.23 \times \left(\frac{10^6}{T^2} \right) - 3.29 \quad (8.4)$$

Diffuse effluent, the most likely candidate for a dolomitizing fluid (discussed in Chapter 7), has $\delta^{18}\text{O}_{\text{H}_2\text{O}}$ averaging $\sim 0\%$ VSMOW (Elderfield et al., 1999; Kelley et al., 2005).

Equations 8.2 and 8.4 were used to calculate the temperature of equilibration between fluid and calcite or dolomite, respectively. Results appear in Appendix IV, Table 8.1, and Figures 6.2-6.5).

Values of $\Delta_{\text{Dol-Cal}}$ calculated from Equation 8.3 are comparable to those computed from the vibrational frequencies of calcite and dolomite given in Deines (2004)

$$\Delta_{\text{Dol-Cal}} = \delta^{18}\text{O}_{\text{Cal}} - \delta^{18}\text{O}_{\text{Dol}} = 0.52 \times \left(\frac{10^6}{T^2} \right) - 0.50 \quad (8.5)$$

(from Chacko, personal communication). The difference in the fractionation factors calculated from Equations 8.3 and 8.5 is $<0.5^\circ\text{C}$ for $T \leq 100^\circ\text{C}$. Dolomite temperatures calculated using Equations 8.2 and 8.5 have temperatures only 2-3 $^\circ\text{C}$ higher than those calculated using Equation 8.4 (Table 8.1).

Since Equations 8.2-8.4 are based on experimental data for oxygen isotope exchange at high temperatures, it is useful to compare these fractionation equations with those calibrated at lower temperatures. The calcite-water oxygen isotope fractionation

$$\Delta_{\text{Cal-H}_2\text{O}} = \delta^{18}\text{O}_{\text{Cal}} - \delta^{18}\text{O}_{\text{H}_2\text{O}} = 18.03 \times \left(\frac{10^3}{T} \right) - 32.42 \quad (8.6)$$

Table 8.1. Temperatures calculated from $\delta^{18}\text{O}$ of calcite and dolomite using Equations 8.2-8.9

	measured $\delta^{18}\text{O}$						
	maximum	minimum					
calcite	28.88	23.35					
dolomite	27.94	21.51					
range	<i>Equation 8.2</i>	<i>Equation 8.6</i>					
calcite T°C	25 - 52	23 - 50					
range	<i>Equation 8.4</i>	<i>Equations</i>	<i>Equations</i>	<i>Equations</i>	<i>Equation 8.7</i>	<i>Equation 8.8</i>	<i>Equation 8.9</i>
dolomite T°C	(8.2 + 8.3) 50 - 86	8.2 + 8.5 53 - 89	8.3 + 8.6 47 - 82	8.5 + 8.6 50 - 85	42 - 83	58 - 98	54 - 103

Notes:

- Equation 8.2 O'Neil et al. (1969)
Equation 8.3 Sheppard and Schwarcz (1970)
Equation 8.4 combination of Equations 8.1 and 8.2
Equation 8.5 Deines (2005), Chacko (personal communication)
Equation 8.6 Kim and O'Neil (1997)
Equation 8.7 Vasconcelos et al. (2005)
Equation 8.8 Northrop and Clayton (1966)
Equation 8.9 Schmidt et al. (2005)

from experimental data at temperatures of 10-40°C (Kim and O'Neil, 1997) gives temperatures only ~2°C lower than Equation 8.2 for calcites (Table 8.1).

A dolomite-water fractionation has been calibrated by Vasconcelos et al. (2005) for dolomite precipitated in microbial cultures and natural environments at temperatures of 25-45°C:

$$\Delta_{\text{Dol-H}_2\text{O}} = \delta^{18}\text{O}_{\text{Dol}} - \delta^{18}\text{O}_{\text{H}_2\text{O}} = 2.73 \times \left(\frac{10^6}{T^2} \right) + 0.26 \quad (8.7)$$

It gives almost identical results to Equation 8.4 for the highest temperature of dolomitization although ~ 7°C lower than the lowest dolomitization temperature (Table 8.1). The dolomite-water fractionation of Northrop and Clayton (1966),

$$\Delta_{\text{Dol-H}_2\text{O}} = \delta^{18}\text{O}_{\text{Dol}} - \delta^{18}\text{O}_{\text{H}_2\text{O}} = 3.20 \times \left(\frac{10^6}{T^2} \right) - 1.50 \quad (8.8)$$

is not generally used because it averages two different fractionation expressions for different dolomites (Friedman and O'Neil, 1977). Schmidt et al. (2005) have experimentally determined another dolomite-water fractionation,

$$\Delta_{\text{Dol-H}_2\text{O}} = \delta^{18}\text{O}_{\text{Dol}} - \delta^{18}\text{O}_{\text{H}_2\text{O}} = 2.63 \times \left(\frac{10^6}{T^2} \right) + 3.12 \quad (8.9)$$

which is based on experiments with disordered, amorphous Ca-Mg carbonates precipitated from a hypersaline solution at low temperatures (40-80°C). This fractionation gives temperatures for the highest $\delta^{18}\text{O}_{\text{Dol}}$ values similar to those calculated from Equation 8.4, but temperatures up to 17°C higher for the lowest $\delta^{18}\text{O}_{\text{Dol}}$. However, amorphous carbonate is unlike dolomite in the Latemar, and crystallization from hypersaline fluids does not match the conditions in which replacement dolomite formed from diffuse effluent.

Regardless of the expression for calcite-water and dolomite-water fractionation used, calculated temperatures are all in the range of ~40-100°C. Preferred values of temperature are those calculated from Equations 8.2 and 8.4. These range from 25 to 52°C in calcite, from 50 to 86°C for tan dolomite, and from 57 to 80 °C for orange dolomite. Calculated temperatures for dolomite are interpreted as temperatures of dolomitization. Temperatures for calcite with $\delta^{18}\text{O} < 26$ ($T > 37^\circ\text{C}$) are interpreted as a record of elevated temperature caused by flow associated with dolomitization. Oxygen isotope temperatures $< 90^\circ\text{C}$ recorded by dolomite are consistent with development of dolomite but not magnesite from reaction of limestone with diffuse effluent. Thermodynamic data indicate that disordered dolomite will form from calcite at $\sim 50^\circ\text{C}$ (SUPCRT92, Johnson et al., 1992) from a fluid with a Ca/Mg ratio of Triassic seawater (Hardie, 1996) as well as diffuse effluent (James and Elderfield, 1996; Von Damm and Lilley, 2004). This temperature boundary is seen in the Latemar dolomites and limestones. However, Equation 7.1 gives a very different temperature barrier ($< 0^\circ\text{C}$).

On the outcrop scale, there can be almost as much range in temperature as there is over the entire buildup (Figures 6.2-6.4). The high variability in temperature on the outcrop scale indicates that there were multiple fluid flow events at variable temperature rather than a single, uniform, pervasive fluid flow event. There is no systematic change in temperature recorded by calcite with elevation (Figure 6.5). There is a weak trend in decreasing temperature increasing with elevation recorded by dolomite: only dolomite located ≥ 450 m above the Contrin Formation records $T < 59^\circ\text{C}$. The average decrease in dolomite temperature with elevation corresponds to a thermal gradient during dolomitization of $\sim -50^\circ\text{C}/\text{km}$. The high variability in temperature on the outcrop scale,

combined with the scattered values in temperature as a function of elevation indicates that the pervasive, uniform fluid flow event described by Wilson (1989), Wilson et al. (1990), and Hardie et al. (1991) was unlikely on a regional as well as on an outcrop scale. It is more likely that multiple, spatially restricted fluid pulses at variable temperature traveled along channels with higher permeability. The chemical heterogeneity in dolomite (described in Chapter 5) supports the notion of pulses of fluid flow with variable temperature and fluid chemistry.

Chapter 9

Time-integrated Fluid Flux: Estimation and Applications

Reaction Mechanism

Replacement dolomite forms by reaction of calcite in limestone with fluid, provided the fluid has a sufficiently high Mg/Ca, and there is a flow mechanism capable of delivering Mg to and removing Ca from the site of reaction (Land, 1985). In more detail, field relationships indicate that dolomitization in the Latemar is due to the replacement of calcite caused by fluid flow through an interconnected orthogonal lattice composed of near-horizontal sheets and tubes and near-vertical sheets and tubes. There are two possible reaction mechanisms: the equilibrium gradient flow mechanism or the disequilibrium flow mechanism (Ferry and Gerdes, 1998). A gradient flow mechanism is expected to produce a gradual transition from limestone to dolomite with distance in the field along the flow path. The sharp interface between unreacted limestone and completely reacted dolomite in the Latemar (Figures 4.3, 4.4) therefore indicates that the disequilibrium flow mechanism is the likelier mechanism (Ferry and Gerdes, 1998). The disequilibrium flow mechanism occurs when an infiltrating fluid is not in chemical equilibrium with the rock through which it flows. The fluid reacts with the rock until they are in chemical equilibrium or at steady state, which results in isotopic, chemical, and mineralogical reaction fronts. Reaction fronts are interfaces perpendicular to the flow direction where discontinuities in mineralogy, mineral chemistry, and isotopic compositions develop. Upstream from a reaction front, rocks have compositions that reflect equilibration with the input fluid, and the downstream samples have compositions

of the original unaltered rock (Ferry and Gerdes, 1998). In the Latemar, the reaction front for Mg is visible in the field as the transition from unaltered limestone to dolomite. There are additional reaction fronts that are not visible, however, and correspond to other chemical tracers in the fluid. These include the isotopic tracers $^{87}\text{Sr}/^{86}\text{Sr}$, $\delta^{18}\text{O}$ and $\delta^{13}\text{C}$, as well as trace elements, Fe, Mn, Cu, and Zn, among others. The locations of the isotope reaction fronts can be predicted if the total amount of fluid that has passed through the system, or time-integrated fluid flux is known. Fe, Mn, Cu, and Zn fronts can be predicted in principle, but not in practice.

Amount of fluid as a time-integrated fluid flux: Replacement at constant C and O

Because the amount of dolomite along an inferred flow path (i.e., distance along the flow path to the Mg reaction front) is a function of the time-integrated fluid flux, or q , the simplest way to estimate the amount of fluid flow is to measure the spatial extent of dolomitization in the field. The estimate, in turn, leads to a first-order quantitative interpretation of other isotopic tracers in Latemar dolomites. Determination of q requires knowledge of mineral chemistry and the composition of the dolomitizing fluid. As discussed in Chapter 7, the dolomitizing fluid is most likely analogous to modern diffuse effluent. Because diffuse effluent is variable in chemistry, it is appropriate to consider model diffuse effluent chemistries based on a single parameter, such as Mn content. Three models of diffuse effluent (DE 1-3) were calculated from data from James and Elderfield (1996) and Von Damm and Lilley (2004), in order of increasing Mn (Figure 9.1). These model compositions are given in Table 9.1.

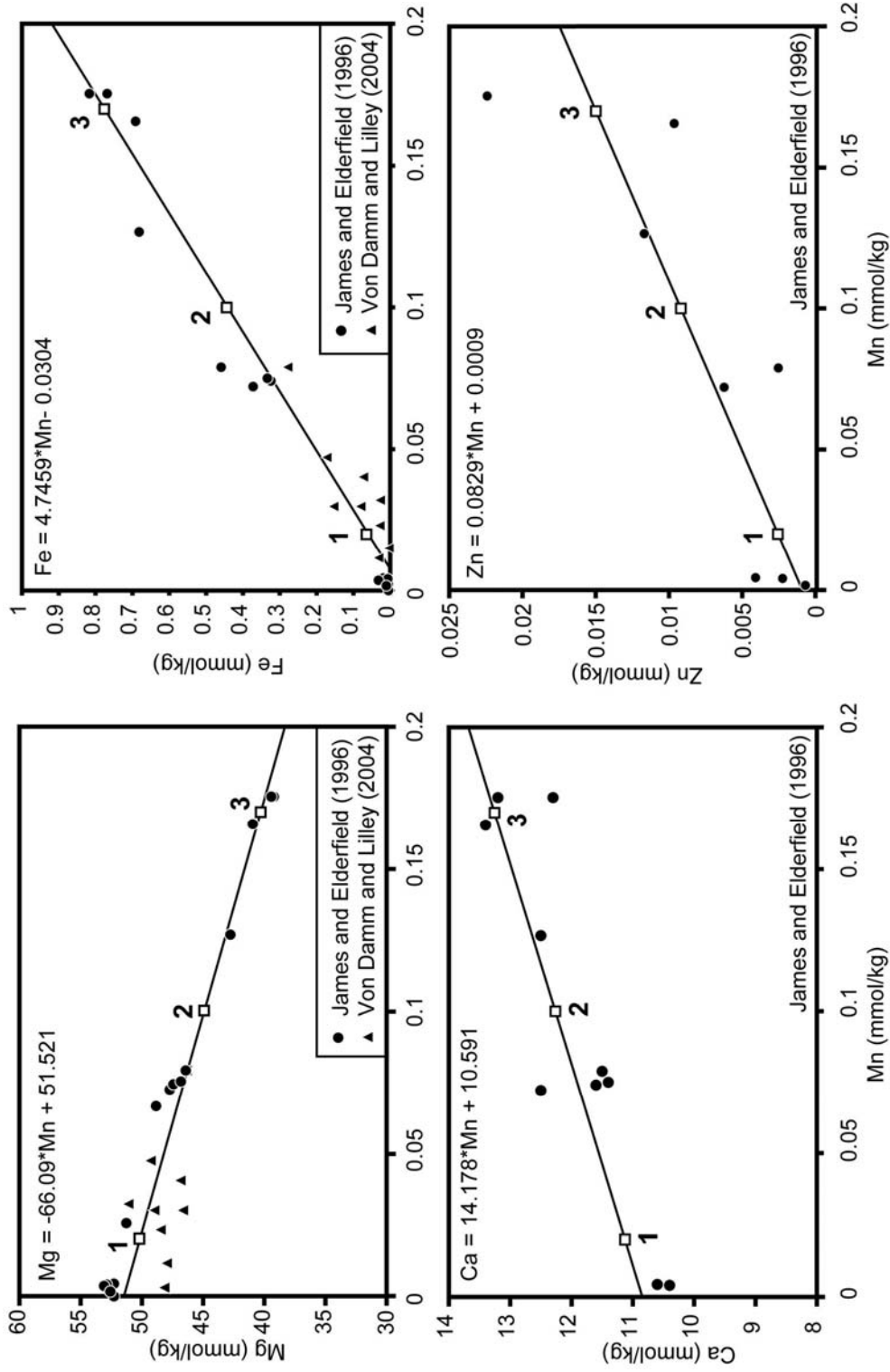


Figure 9.1. Model diffuse effluent chemistries (DE1-DE3) based on Mn content. DE 1 has low Mn, Fe, Ca and high Mg concentrations, DE 3 has a high Mn, Fe, Ca, and low Mg concentrations, and DE 2 has intermediate concentrations. Lines are linear fits to the data and equations for the fits are shown in each panel.

Table 9.1a. Compositions of calcite and dolomite used to calculate the time-integrated fluid flux.

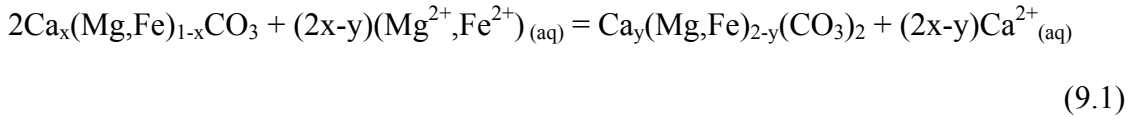
	calcite	tan dolomite	orange dolomite
Mn (ppm)	20	200	300
Fe (ppm)	300	4000	14000
Sr (ppm)	200	40	30
Zn (ppm)	1	4	10
Mg (cations per CO ₂)	0.01	0.47	0.45
Ca (cations per CO ₂)	0.99	0.52	0.51

Table 9.1b. Compositions of fluids used to calculate the time-integrated fluid flux.

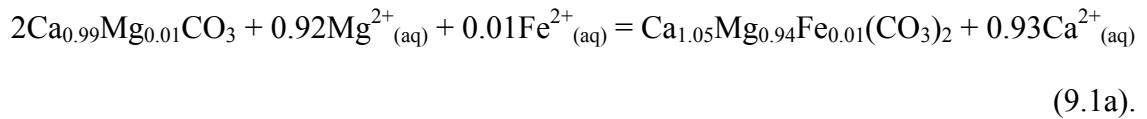
	DE1	DE2	DE3	Triassic Seawater
Mg (mol/cm ³)	$5.15 \cdot 10^{-5}$	$4.61 \cdot 10^{-5}$	$4.07 \cdot 10^{-5}$	$1.05 \cdot 10^{-4}$
Ca (mol/cm ³)	$1.12 \cdot 10^{-5}$	$1.23 \cdot 10^{-5}$	$1.35 \cdot 10^{-5}$	$2.98 \cdot 10^{-5}$
Fe (mol/cm ³)	$6.62 \cdot 10^{-8}$	$4.56 \cdot 10^{-7}$	$8.46 \cdot 10^{-7}$	$1.00 \cdot 10^{-12}$
Mn (mol/cm ³)	$2.05 \cdot 10^{-8}$	$1.03 \cdot 10^{-7}$	$1.85 \cdot 10^{-7}$	$6.00 \cdot 10^{-12}$
Sr (mol/cm ³)	$9.05 \cdot 10^{-8}$	$8.76 \cdot 10^{-8}$	$8.47 \cdot 10^{-8}$	$8.90 \cdot 10^{-8}$
Zn (mol/cm ³)	$2.63 \cdot 10^{-9}$	$9.43 \cdot 10^{-9}$	$1.62 \cdot 10^{-8}$	$6.00 \cdot 10^{-12}$
CO ₂ (mol/cm ³)	$5.56 \cdot 10^{-6}$	$1.19 \cdot 10^{-5}$	$1.82 \cdot 10^{-5}$	$2.36 \cdot 10^{-6}$

Notes: Diffuse Effluent fluid chemistries DE1-DE3 are calculated from trends in Figure 9.1. Model CO₂ values calculated against Mg measurements from Von Damm and Lilley (2004), and normalized against Mn. Triassic Seawater Mg and Ca concentrations from Hardie (1996); Fe, Mn, Sr, and Zn values from Millero and Sohn (1992); CO₂ values from Von Damm and Lilley (2004).

For replacement of calcite by dolomite at constant O and C, the general reaction is:



where other cations in abundance <0.002 cations per mineral formula unit (Mn, Zn, Sr, etc.) are ignored for simplicity. Taking the limestone-dolomite reaction given by Reaction 9.1, where $x = 0.99$, $y = 1.05$, and $\text{Mg}/(\text{Mg}+\text{Fe}) = 1.00$ and 0.99 for typical Latemar calcite and dolomite, respectively,



To convert 1 cm^3 of porous limestone with $\sim 3\%$ porosity (the average porosity of unaltered limestone) into dolomite with the composition $\text{Ca}_{1.05}\text{Mg}_{0.94}\text{Fe}_{0.01}(\text{CO}_3)_2$ by Reaction 9.1a, 1.21×10^{-2} moles of Mg^{2+} are required. There are 2.64×10^{-2} moles of Ca in 1 cm^3 of the porous limestone; 1.21×10^{-2} of these will be replaced by Mg, and 1.32×10^{-4} will be replaced by Fe. From this, it is possible to calculate how much fluid is necessary to convert 1 cm^3 of calcite + porosity into dolomite. This value will depend on the Mg and Ca contents of the dolomitizing fluid and the fluid that coexists with calcite and dolomite following the reaction.

Take the dolomitizing fluid as DE 2 (44.9 mmol/kg Mg, 12.0 mmol/kg Ca), for example, and the Ca/Mg of the fluid following reaction as that calculated for coexisting with calcite and dolomite at a representative 70°C using Equation 7.1 from Hyeong and Capuano (2001). With the Ca + Mg of the input fluid and the Ca/Mg ratio of 1.93 in the

output fluid, 2.61×10^{-5} moles Mg/cm³ of input fluid are required for the calcite to dolomite reaction. Because 1.21×10^{-2} moles of Mg are required to turn 1 cm³ of porous limestone into dolomite, 1 cm of dolomitization along the flow path requires a time-integrated fluid flux of ~ 26 moles fluid/cm² rock, or ~ 460 cm³ fluid/cm² rock.

Assuming that the dolomitization (Mg) front traveled ~ 1 km (from the spatial extent of dolomite distribution in the Latemar), the molar time-integrated fluid flux q_{mol} is 2.57×10^6 moles fluid/cm² rock and the volumetric time-integrated fluid flux q_{vol} is 4.63×10^7 cm³ fluid/cm² rock (Table 9.2).

Table 9.3 lists values for the volumetric and molar time-integrated fluid fluxes, q_{vol} and q_{mol} , for a variety of dolomitization distances, temperatures, and fluid chemistries, estimated from diffuse effluent chemistries measured by Von Damm and Lilley (2004) and James and Elderfield (1996) (Figure 9.1; Table 9.1), as well as from Triassic seawater, calculated using the method in Table 9.2. For diffuse effluents (DE1-3), values of q_{vol} range from 1.9×10^7 to 1.4×10^8 cm³ fluid/cm² rock, and values of q_{mol} range from 1.1×10^6 to 7.5×10^6 moles fluid/cm² rock. For unaltered Triassic seawater, values of q_{vol} range from 9.6×10^6 to 5.0×10^7 cm³ fluid/cm² rock, and values of q_{mol} range from 5.3×10^5 to 2.8×10^6 moles fluid/cm² rock.

Calculations in Tables 9.2 and 9.3 assume constant temperature along the flow path and do not account for cooling as the fluid moves away from its source. Table 9.4 lists values for q that consider fluid flow along a temperature gradient of $-50^\circ\text{C}/\text{km}$, which is estimated from temperatures recorded by the $\delta^{18}\text{O}$ of dolomite (Figure 6.5). For diffuse effluents (DE1-DE3), values of q_{vol} range from 2.0×10^7 to 9.2×10^7 cm³ fluid/cm² rock, and values of q_{mol} range from 1.1×10^6 to 5.1×10^6 moles fluid/cm² rock.

Table 9.2. Calculation of time-integrated fluid flux using diffuse effluent (DE2) at 70°C, ($\rho_{DE2}=1.0265 \text{ g/cm}^3$) as a dolomitizing fluid.

input fluid: $m_{Mg^{++}} = 44.91 \text{ mmol/kg} = 4.61 \times 10^{-5} \text{ mol/cm}^3$

$$m_{Ca^{++}} = 12.01 \text{ mmol/kg} = 1.23 \times 10^{-5} \text{ mol/cm}^3$$

$$m_{Mg^{++}} + m_{Ca^{++}} = 5.84 \times 10^{-5} \text{ mol/cm}^3$$

output fluid: $\log \frac{a_{Ca^{++}}}{a_{Mg^{++}}} = -0.22 + \frac{7.21 \cdot T(^{\circ}\text{C})}{1000}$ (Hyeong and Capuano, 2001)

$$T = 70^{\circ}\text{C}$$

$$\frac{m_{Ca^{++}}}{m_{Mg^{++}}} = 1.93$$

$$m_{Mg^{++}}$$

combining input and output fluids:

$$m_{Mg^{++},output} + 1.93m_{Mg^{++},output} = 5.84 \times 10^{-5} \text{ mol/cm}^3$$

$$m_{Mg^{++},output} = 2.00 \times 10^{-5} \text{ mol/cm}^3$$

$$\Delta m_{Mg^{++}} = m_{Mg^{++},input} - m_{Mg^{++},output} = 2.61 \times 10^{-5} \text{ mol/cm}^3$$

limestone to dolomite reaction using DE2:

$$\frac{1.21 \times 10^{-2} \text{ mol Mg required}}{2.61 \times 10^{-5} \text{ mol Mg/cm}^3 \text{ used in reaction}} = 463 \text{ cm}^3 \text{ DE2}$$

= amount of fluid required to convert 1 cm³ calcite with ~3% porosity into dolomite

time-integrated fluid flux based on 1 km dolomite along flow path:

$$q_{vol} = \frac{(463 \text{ cm}^3 \text{ DE2})(10^5 \text{ cm})}{\text{cm}^2 \text{ rock}} = \frac{4.6 \times 10^7 \text{ cm}^3 \text{ DE2}}{\text{cm}^2 \text{ rock}}$$

$$q_{mol} = \frac{q_{vol}}{\bar{V}_{DE2}} = \frac{4.63 \times 10^7 \text{ cm}^3 \text{ DE2/cm}^2 \text{ rock}}{18 \text{ cm}^3 \text{ DE2/mol}} = 2.6 \times 10^6 \text{ mol DE2/cm}^2 \text{ rock}$$

Table 9.3. Calculated time-integrated fluid flux of dolomitization, using three diffuse effluent chemistries (DE1-DE3) and Triassic seawater at a range of T = 50-150°C.

distance of dolomitization along the flow path (km)	T°C	<i>input Ca²⁺</i> <i>mol/cm³</i>	Diffuse Effluent			Triassic SW
			<i>DE1</i>	<i>DE2</i>	<i>DE3</i>	
			<i>input Mg²⁺</i> <i>mol/cm³</i>			
			5.15·10 ⁻⁵	4.61·10 ⁻⁵	4.07·10 ⁻⁵	1.05·10 ⁻⁴
			1.12·10 ⁻⁵	1.23·10 ⁻⁵	1.35·10 ⁻⁵	2.98·10 ⁻⁵
0.7	150	q _{vol}	1.9·10 ⁷	2.2·10 ⁷	2.5·10 ⁷	9.6·10 ⁶
		q _{mol}	1.1·10 ⁶	1.2·10 ⁶	1.4·10 ⁶	5.3·10 ⁵
0.7	90	q _{vol}	2.5·10 ⁷	2.8·10 ⁷	3.3·10 ⁷	1.2·10 ⁷
		q _{mol}	1.4·10 ⁶	1.6·10 ⁶	1.8·10 ⁶	6.9·10 ⁵
0.7	80	q _{vol}	2.6·10 ⁷	3.0·10 ⁷	3.5·10 ⁷	1.3·10 ⁷
		q _{mol}	1.5·10 ⁶	1.7·10 ⁶	2.0·10 ⁶	7.4·10 ⁵
0.7	70	q _{vol}	2.8·10 ⁷	3.2·10 ⁷	3.8·10 ⁷	1.4·10 ⁷
		q _{mol}	1.6·10 ⁶	1.8·10 ⁶	2.1·10 ⁶	8.0·10 ⁵
0.7	50	q _{vol}	3.4·10 ⁷	3.9·10 ⁷	4.7·10 ⁷	1.8·10 ⁷
		q _{mol}	1.9·10 ⁶	2.2·10 ⁶	2.6·10 ⁶	9.8·10 ⁵
1	150	q _{vol}	2.8·10 ⁷	3.1·10 ⁷	3.5·10 ⁷	1.4·10 ⁷
		q _{mol}	1.5·10 ⁶	1.7·10 ⁶	2.0·10 ⁶	7.6·10 ⁵
1	90	q _{vol}	3.5·10 ⁷	4.0·10 ⁷	4.7·10 ⁷	1.8·10 ⁷
		q _{mol}	1.9·10 ⁶	2.2·10 ⁶	2.6·10 ⁶	9.9·10 ⁵
1	80	q _{vol}	3.7·10 ⁷	4.3·10 ⁷	5.0·10 ⁷	1.9·10 ⁷
		q _{mol}	2.1·10 ⁶	2.4·10 ⁶	2.8·10 ⁶	1.1·10 ⁶
1	70	q _{vol}	4.0·10 ⁷	4.6·10 ⁷	5.5·10 ⁷	2.1·10 ⁷
		q _{mol}	2.2·10 ⁶	2.6·10 ⁶	3.0·10 ⁶	1.1·10 ⁶
1	50	q _{vol}	4.8·10 ⁷	5.6·10 ⁷	6.7·10 ⁷	2.5·10 ⁷
		q _{mol}	2.7·10 ⁶	3.1·10 ⁶	3.7·10 ⁶	1.4·10 ⁶
2	150	q _{vol}	5.5·10 ⁷	6.2·10 ⁷	7.1·10 ⁷	2.7·10 ⁷
		q _{mol}	3.1·10 ⁶	3.4·10 ⁶	3.9·10 ⁶	1.5·10 ⁶
2	90	q _{vol}	7.0·10 ⁷	8.0·10 ⁷	9.3·10 ⁷	3.5·10 ⁷
		q _{mol}	3.9·10 ⁶	4.4·10 ⁶	5.2·10 ⁶	2.0·10 ⁶
2	80	q _{vol}	7.5·10 ⁷	8.6·10 ⁷	1.0·10 ⁸	3.8·10 ⁷
		q _{mol}	4.2·10 ⁶	4.8·10 ⁶	5.6·10 ⁶	2.1·10 ⁶
2	70	q _{vol}	8.0·10 ⁷	9.3·10 ⁷	1.1·10 ⁸	4.1·10 ⁷
		q _{mol}	4.5·10 ⁶	5.1·10 ⁶	6.1·10 ⁶	2.3·10 ⁶
2	50	q _{vol}	9.6·10 ⁷	1.1·10 ⁸	1.3·10 ⁸	5.0·10 ⁷
		q _{mol}	5.3·10 ⁶	6.2·10 ⁶	7.5·10 ⁶	2.8·10 ⁶

Notes: q_{mol} has units of moles fluid/cm² rock, q_{vol} has units of cm³ fluid/cm² rock. Values in box are those from the sample calculation in Table 9.2.

Table 9.4. Calculated time-integrated fluid flux of dolomitization, using Triassic seawater and three diffuse effluent chemistries based on variable Fe content as a dolomitizing fluid, at variable input temperatures and a temperature gradient of $-50^{\circ}\text{C}/\text{km}$ along the flow path.

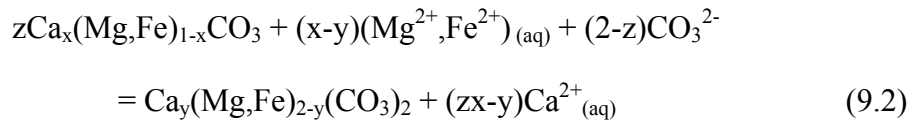
distance of dolomitization along the flow path (km)	T $^{\circ}\text{C}$	<i>input</i> Ca^{2+} mol/cm^3	Diffuse Effluent			Triassic SW
			<i>DE1</i>	<i>DE2</i>	<i>DE3</i>	
			<i>input</i> Mg^{2+} mol/cm^3			
0.7	100	q_{vol}	$2.6 \cdot 10^7$	$3.0 \cdot 10^7$	$3.5 \cdot 10^7$	$1.3 \cdot 10^7$
		q_{mol}	$1.4 \cdot 10^6$	$1.6 \cdot 10^6$	$1.9 \cdot 10^6$	$7.3 \cdot 10^5$
0.7	150	q_{vol}	$2.0 \cdot 10^7$	$2.3 \cdot 10^7$	$2.6 \cdot 10^7$	$1.0 \cdot 10^7$
		q_{mol}	$1.1 \cdot 10^6$	$1.3 \cdot 10^6$	$1.5 \cdot 10^6$	$5.6 \cdot 10^5$
1	100	q_{vol}	$3.9 \cdot 10^7$	$4.5 \cdot 10^7$	$5.3 \cdot 10^7$	$2.0 \cdot 10^7$
		q_{mol}	$2.2 \cdot 10^6$	$2.5 \cdot 10^6$	$3.0 \cdot 10^6$	$1.1 \cdot 10^6$
1	150	q_{vol}	$3.0 \cdot 10^7$	$3.4 \cdot 10^7$	$3.9 \cdot 10^7$	$1.5 \cdot 10^7$
		q_{mol}	$1.7 \cdot 10^6$	$1.9 \cdot 10^6$	$2.2 \cdot 10^6$	$8.3 \cdot 10^5$
2	150	q_{vol}	$6.9 \cdot 10^7$	$7.9 \cdot 10^7$	$9.2 \cdot 10^7$	$3.5 \cdot 10^7$
		q_{mol}	$3.8 \cdot 10^6$	$4.4 \cdot 10^6$	$5.1 \cdot 10^6$	$1.9 \cdot 10^6$

Notes: q_{mol} has units of moles fluid/ cm^2 rock, q_{vol} has units of cm^3 fluid/ cm^2 rock. Calculations for 2 km of dolomitization and an input T= 100°C are not considered because it requires dolomitization at $T < 50^{\circ}\text{C}$, which is not observed.

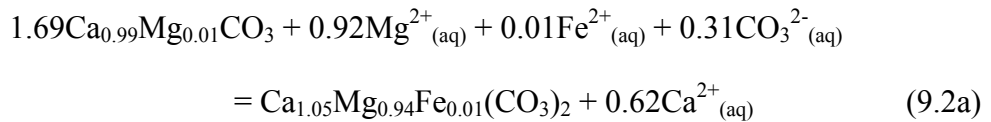
For Triassic seawater, values of q_{vol} range from 1.0×10^7 to 3.5×10^7 cm³ fluid/cm² rock, and values of q_{mol} range from 5.6×10^5 to 1.9×10^6 moles fluid/cm² rock.

Amount of fluid as a time-integrated fluid flux: Replacement at constant volume

Reaction 9.1 is for replacement of calcite by dolomite at constant O and C, creating porosity of ~ 13% in the dolomite. Many Latemar dolomites, however, have porosities as low as 3%, indicating that replacement at constant O and C did not occur. As the typical limestone porosity is 3%, it is likely that some dolomites may have formed by replacement at constant volume, where the reaction is:



with $z=(1-\phi)(\bar{V}_{\text{Dol}}/\bar{V}_{\text{Cal}})$, where ϕ = porosity of the original limestone, \bar{V}_{Dol} and \bar{V}_{Cal} are the molar volumes of dolomite and calcite, and other cations in abundance <0.002 cations per mineral formula unit (Mn, Zn, Sr, etc.) are ignored for simplicity. Taking, as before, $\phi = 0.03$, $x = 0.99$, $y = 1.05$, and $\text{Mg}/(\text{Mg}+\text{Fe}) = 1.00$ and 0.99 for typical Latemar calcite and dolomite, respectively,



In order to convert 1 cm³ limestone with 3% porosity to 1 cm³ dolomite by Reaction 9.2a, 1.43×10^{-2} moles of Mg^{2+} are required. Methods to compute the time-integrated fluid flux then follow those in Table 9.2. Because the only difference in the calculations is the amount of Mg required, calculated time-integrated flux is simply larger by a factor of

1.18 (because $\frac{1.43 \times 10^{-2} \text{ moles Mg}^{2+}}{1.21 \times 10^{-2} \text{ moles Mg}^{2+}} = 1.18$) for a constant volume reaction compared to

those listed in Tables 9.3 and 9.4 for replacement at constant C and O. Specifically, for diffuse effluents (DE1-DE3), values of q_{vol} range from 2.4×10^7 to $1.8 \times 10^8 \text{ cm}^3$ fluid/cm² rock, and values of q_{mol} range from 1.3×10^6 to 6.1×10^6 moles fluid/cm² rock. For Triassic seawater, values of q_{vol} range from 1.2×10^7 to $4.2 \times 10^7 \text{ cm}^3$ fluid/cm² rock, and values of q_{mol} range from 6.7×10^5 to 2.6×10^6 moles fluid/cm² rock. These values of q (calculated for both constant temperature as well as a temperature gradient of $\sim -50^\circ\text{C}/\text{km}$) almost completely overlap the values given in Tables 9.3 and 9.4. Thus calculated time-integrated fluid fluxes are not critically dependent on whether the reaction was constant volume, constant C and O, or something in between.

Because dolomitization by Reaction 9.2a requires the addition of 4.8×10^{-3} moles of C per cm³ rock, the dolomitizing fluid must contain enough C. To form 1 km of dolomite at constant volume, q_{vol} must contain at least 480 moles of C. Triassic seawater has ~ 40 -60 moles of C for $q_{\text{vol}} = 1.8 \times 10^7$ - $2.4 \times 10^7 \text{ cm}^3$ fluid/cm² rock, DE1 has 200-270 moles C for $q_{\text{vol}} = 3.5 \times 10^7$ - $4.8 \times 10^7 \text{ cm}^3$ fluid/cm² rock, DE2 has 420-570 moles C for $q_{\text{vol}} = 3.5 \times 10^7$ - $4.8 \times 10^7 \text{ cm}^3$ fluid/cm² rock, and DE3 has 650-870 moles C for $q_{\text{vol}} = 4.6 \times 10^7$ - $6.5 \times 10^7 \text{ cm}^3$ fluid/cm² rock (q_{vol} calculated for 1 km of dolomite with an input $T=150^\circ\text{C}$ and a temperature gradient of $-50^\circ\text{C}/\text{km}$, and with a constant $T=70^\circ\text{C}$, respectively). Triassic seawater does not contain nearly enough C to form dolomite at constant volume. The C content of DE1 is not quite high enough to account for constant volume dolomitization, although DE2 has barely enough C, and DE3 potentially has sufficient C to form dolomite by Equation 9.2 (depending on how much C in the fluid is available for Reaction 9.2a). It is possible that dolomite with low porosity formed

through a constant volume reaction, provided the dolomitizing fluid was like DE3. This is consistent with the lower porosity of Fe-rich orange dolomite compared to Fe-poor tan dolomite. Dolomite with high porosity, on the other hand, must have formed through replacement with constant O and C.

Latemar dolomites have porosities of 3-16% (Table 5.1). It is likely that dolomites with ~16% porosity replaced limestone with 3% porosity at constant moles of C and O, which increased the original porosity by 13%. Dolomites with porosities ~3% likely replaced the precursor calcite at constant volume. Most dolomites have intermediate porosities, however, indicating replacement by some mechanism intermediate between Reactions 9.1a and 9.2a. The presence of stylolites in the dolomite and limestone samples indicates that compaction has occurred, and it cannot be discounted that compaction in the rock combined with replacement at constant moles C and O may alternatively account for some of the intermediate dolomite porosities.

Isotope Reaction Fronts

With the values of q constrained, the location of isotopic reaction fronts can be calculated relative to the position of the dolomitization front following Dipple and Ferry (1992) and Ferry and Gerdes (1998). For a given q , the displacement of any isotope reaction front relative to the dolomitizing front depends on the concentrations of the relevant tracer species in the dolomitizing fluid, calcite, and dolomite (Table 9.5).

Figure 9.2 represents fluid flow and mineral-fluid reaction in the Latemar with a simple one-dimensional model for replacement at constant O and C, where the dolomite reaction front is 1 km from the fluid source (summary of results in Tables 9.2, 9.4, and

Table 9.5. Location of isotope reaction fronts calculated following Dipple and Ferry (1992) using DE2 diffuse effluent chemistry at 70°C along an isothermal flow path for 1 km of dolomitization.

$\delta^{18}\text{O}$ (calculated for calcite limestone):	
$V_{\text{O,calcite}} = \frac{\text{moles O in CaCO}_3}{\text{molar volume CaCO}_3} = \frac{3}{36.934 \text{ cm}^3} = 0.081 \text{ mol O/cm}^3 \text{ rock}$	
$n_{\text{O,SW}} = 1 \text{ mol O/mol DE2}$ (assumes pure H_2O)	
$q_{\text{mol}} = 2.6 \times 10^6 \text{ mol fluid/cm}^2 \text{ rock}$	
$\Delta z_{\text{O}} = \frac{q_{\text{mol}} n_{\text{O,DE2}}}{V_{\text{O,calcite}}} = 3.2 \times 10^7 \text{ cm} = 320 \text{ km}$	
$\delta^{13}\text{C}$ (calculated for dolomite):	
$V_{\text{C,dolomite}} = \frac{\text{moles C in CaMg(CO}_3)_2}{\text{molar volume CaMg(CO}_3)_2} = \frac{2}{64.365 \text{ cm}^3} = 0.0311 \text{ mol C/cm}^3 \text{ rock}$	
$n_{\text{C,SW}} = \frac{1.19 \times 10^{-5} \text{ mol C/cm}^3 \text{ DE2}}{5.55 \times 10^{-2} \text{ mol DE2/cm}^3 \text{ DE2}} = 2.14 \times 10^{-4} \text{ mol C/mol DE2}$	
$q_{\text{mol}} = 2.6 \times 10^6 \text{ mol fluid/cm}^2 \text{ rock}$	
$\Delta z_{\text{C}} = \frac{q_{\text{mol}} n_{\text{C,DE2}}}{V_{\text{C,calcite}}} = 1.8 \times 10^4 \text{ cm} = 180 \text{ m}$	
$^{87}\text{Sr}/^{86}\text{Sr}$ (calculated for calcite limestone):	
$V_{\text{Sr,calcite}} = 1.87 \times 10^{-6} \text{ mol Sr/cm}^3 \text{ rock}$	
$n_{\text{Sr,SW}} = \frac{8.76 \times 10^{-8} \text{ mol Sr/cm}^3 \text{ DE2}}{5.55 \times 10^{-2} \text{ mol DE2/cm}^3 \text{ DE2}} = 1.58 \times 10^{-6} \text{ mol Sr/mol DE2}$	
$q_{\text{mol}} = 2.6 \times 10^6 \text{ mol fluid/cm}^2 \text{ rock}$	
$\Delta z_{\text{Sr}} = \frac{q_{\text{mol}} n_{\text{Sr,DE2}}}{V_{\text{Sr,calcite}}} = 2.2 \times 10^6 \text{ cm} = 22 \text{ km}$	

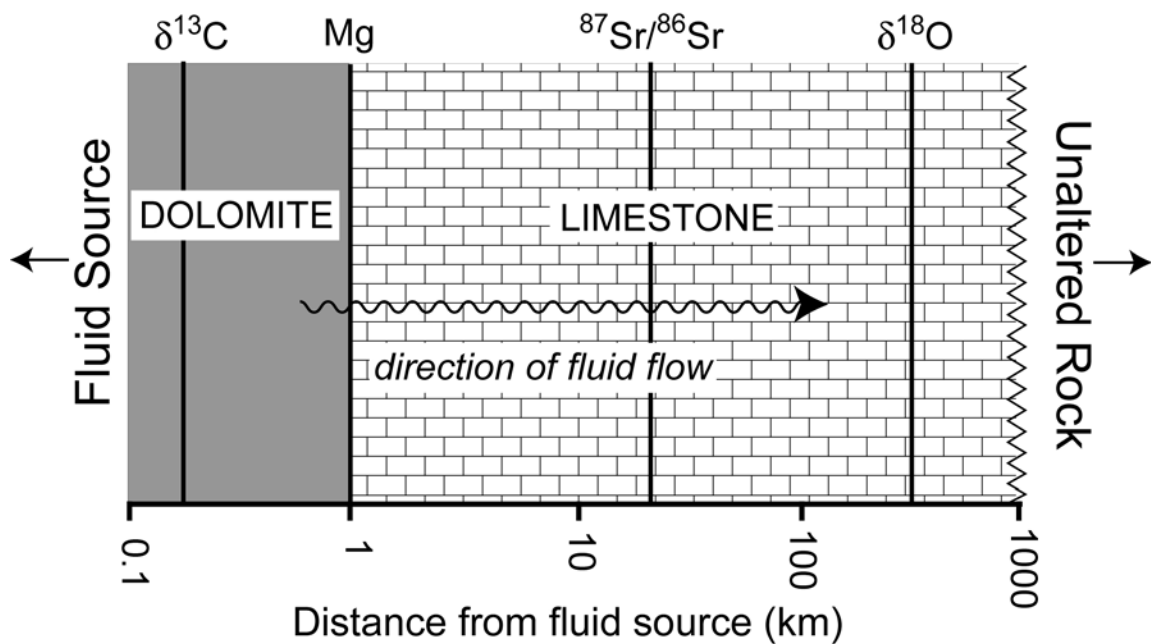


Figure 9.2. Simple model of the distance of each isotope reaction front from the fluid source (distance = 0) in relation to the dolomite front at 1 km. Distance coordinate parallel to direction of fluid flow. Distances calculated based on $q_{\text{mol}} = 2.6 \times 10^6$ mol fluid/cm² rock and $T = 70^\circ\text{C}$ with no temperature gradient. Results for other values of q and T , with and without a temperature gradient and 3% porosity in limestone, are similar.

9.5). The calculated locations of the isotope reaction fronts for diffuse effluent (DE2) occur over a distance range of >3 orders of magnitude. The predicted $\delta^{13}\text{C}$ reaction front is located >800 m behind the dolomite front, while the $\delta^{18}\text{O}$ and $^{87}\text{Sr}/^{86}\text{Sr}$ reaction fronts are 320 to 22 km further from the fluid source than the dolomite front, respectively. Results do not significantly differ whether q is based on constant volume replacement, or whether limestone of 0 or 3% porosity is considered, and are nearly the same regardless of which values of q in Tables 9.3 or 9.4 are used. In more detail, if the dolomite front occurs at any location $\neq 1$ km from the inlet, isotope fronts adopt the same relative positions as those calculated in Table 9.5 and illustrated in Figure 9.2. The $\delta^{18}\text{O}$ and $^{87}\text{Sr}/^{86}\text{Sr}$ of dolomite therefore record equilibration with the input fluid while the $\delta^{13}\text{C}$ of dolomite is inherited (with few exceptions, discussed below) from the limestone protolith. Figure 9.2 justifies interpreting $\delta^{18}\text{O}$ of dolomite in terms of temperature of formation from a dolomitizing fluid and $^{87}\text{Sr}/^{86}\text{Sr}$ in terms of the Sr-isotope composition of the dolomitizing fluid.

In a field area the size of the Latemar (less than 3 km in diameter), it would be unlikely that any of the reaction fronts except the dolomite reaction front would be exposed. However, reaction sides are exposed (Yardley and Lloyd, 1995), and can be seen in Figures 4.5-4.14.

Although the $\delta^{13}\text{C}$ reaction front is located <200 m from the fluid input for a time-integrated fluid flux of $q_{\text{mol}} = 2.6 \times 10^6$ mol fluid/cm² rock (calculated for DE2), there is evidence that a carbon isotope reaction front passed through some rocks in Location 7 (Figure 6.4). Several samples of orange dolomite in the middle of a fractured, Fe-rich dolomitized channel have elevated $\delta^{13}\text{C}$ compared to the other dolomite and calcite

samples in the outcrop. The $\delta^{13}\text{C}$ of these orange dolomite samples is the same as the underlying Contrin Formation, suggesting sufficient fluid passed that the $\delta^{13}\text{C}$ of the Contrin Formation was advected upward at least to the elevation of Location 7. In order for the $\delta^{13}\text{C}$ of the Contrin to overprint the pre-existing $\delta^{13}\text{C}$ of the limestone in Location 7, 555 m above the Contrin Formation, q_{mol} in the channel must have been 3.2×10^7 mol fluid/cm² rock (for dolomitizing fluid DE1), 1.5×10^7 mol fluid/cm² rock (for dolomitizing fluid DE2), or 9.7×10^6 mol fluid/cm² rock (for dolomitizing fluid DE3). These values of q_{mol} require that locally 3-14 times more fluid passed through the rocks with altered $\delta^{13}\text{C}$ than passed through rocks that retained the original $\delta^{13}\text{C}$ of the limestone protolith.

Trace Element Requirements of Dolomitization

Trace elements in dolomite, such as Mn, Zn, and Fe, can be used in conjunction with calculated q , to confirm a source of dolomitizing like modern diffuse effluent as opposed to Triassic seawater (Table 9.6). These trace elements had to be present in the dolomitizing fluid at high enough concentrations to form dolomite enriched in Mn, Fe, and Zn. In general, there is sufficient Mn, Fe, and Zn in DE1-DE3 for $q_{\text{vol}} = 2.5\text{-}3.4 \times 10^6$ cm³ fluid/cm² rock (exceptions discussed below). On the other hand, these trace elements are present at such low concentrations in Triassic seawater that there is no possibility that Triassic seawater could have formed the Latemar dolomite. For the values of q_{vol} given in Table 9.8, DE1-DE3 have more than enough Zn to account for the Zn enrichment in both orange and tan dolomite. DE2 and DE3 have enough Mn to account for Mn enrichment in both orange and tan dolomite. The concentration of Mn in

DE1 is just under the requirement for tan dolomite and does not contain enough Mn to form orange dolomite. DE3 contains enough Fe to account for the Fe enrichment in tan dolomite, but not for orange dolomite. DE1 and DE2 do not contain enough Fe to form orange dolomite, and are just under the required concentrations to form tan dolomite. However, increasing q_{vol} by a factor of 2 to 5 will provide enough Fe to account for the Fe enrichment in orange dolomite. Because some of the orange, Fe-rich dolomite is present in channels that have experienced a higher fluid flux (their $\delta^{13}\text{C}$ has been overprinted by the $\delta^{13}\text{C}$ of the Contrin Formation), this localized higher fluid flux is expected. In samples of orange dolomite with a $\delta^{13}\text{C}$ that still reflects the $\delta^{13}\text{C}$ of the limestone protolith, the upper bound on the local time-integrated fluid flux is that the flux had to be high enough to account for the Fe enrichment, but low enough to retain the $\delta^{13}\text{C}$ of the limestone protolith. Additionally, the samples in Location 7 with high Fe and a $\delta^{13}\text{C}$ that has been overprinted by the $\delta^{13}\text{C}$ of the Contrin Formation have low porosity (~3%), indicating that dolomite formed via constant volume replacement (Reaction 9.2) rather than replacement at constant moles of C and O (Reaction 9.1). Because constant volume replacement requires locally elevated time-integrated fluid fluxes, the low porosity of orange dolomite is further evidence that these rocks did experience elevated flow of dolomitizing fluid needed to account for their high Fe contents. It is also possible, however, that the equivalent to diffuse effluent produced by reaction of seawater with the Predazzo volcanic intrusive complex contained more Fe than diffuse effluent in modern mid-ocean ridge environments, and that no increase in fluid flux is necessary to account for the Fe enrichment in the Latemar dolomite samples.

Table 9.6. Budget of trace elements.

moles needed to convert 1 cm ² × 1 km of calcite into dolomite:				
	tan dolomite	orange dolomite		
Mn (mol/km)	0.9	1.5		
Fe (mol/km)	19	65		
Zn (mol/km)	0.013	0.039		
Diffuse Effluent Chemistry				
	Triassic SW	1	2	3
at 70°C, no temperature gradient				
q _{vol} (cm ³ fluid/cm ² rock)	2.06·10 ⁷	4.0·10 ⁷	4.6·10 ⁷	5.5·10 ⁷
moles Mn contained in q _{vol}	2.11·10 ⁻⁵	0.8	4.1	7.4
moles Fe contained in q _{vol}	2.11·10 ⁻⁵	3	18	34
moles Zn contained in q _{vol}	2.11·10 ⁻⁴	0.11	0.38	0.65
at a temperature gradient of 50°C/km, with an input fluid at T=150°C				
q _{vol} (cm ³ fluid/cm ² rock)	1.5·10 ⁷	3.0·10 ⁷	3.4·10 ⁷	3.9·10 ⁷
moles Mn contained in q _{vol}	1.54·10 ⁻⁵	0.6	3.1	5.5
moles Fe contained in q _{vol}	1.54·10 ⁻⁵	2	14	25
moles Zn contained in q _{vol}	1.54·10 ⁻⁴	0.08	0.28	0.49

Chapter 10

Mechanism and Duration of Reactive Flow

Wilson (1989), Wilson et al. (1990), and Hardie et al. (1991) concluded that dolomitization of the Latemar was caused by slow, pervasive, uniform fluid flow that resulted in smooth gradients in temperature in both vertical and horizontal dimensions at the 100 m to km scale. As discussed in Chapter 8, the high variability in estimated temperature at the outcrop scale, combined with the lack of a well-defined systematic trend in temperature with elevation, indicates that this is not the case. It is more likely that dolomitization resulted from spatially restricted, discrete fluid pulses at variable temperature traveling within regions of higher permeability. This is documented at Location 7, where sheet-like bedding-parallel dolomite bodies preferentially developed up-dip from two near-vertical fracture-controlled sheet-like bodies of orange dolomite (Figure 4.5). These orange dolomite bodies record oxygen isotope temperatures that are higher than the surrounding tan dolomite (Figure 10.1), and are interpreted as near-vertical, approximately planar flow channels with high flux of hot fluid. The development and preservation of the temperature anomalies preserved by these flow channels indicates that the fluid flux was relatively large and the duration of fluid flow was relatively short.

Using heat transport theory (Brady, 1988), it is possible to estimate the total duration of flow (t) and local volumetric fluid flux (J_{Tv}) that is required to produce and preserve the two temperature anomalies recorded in Location 7. Consider vertical flow

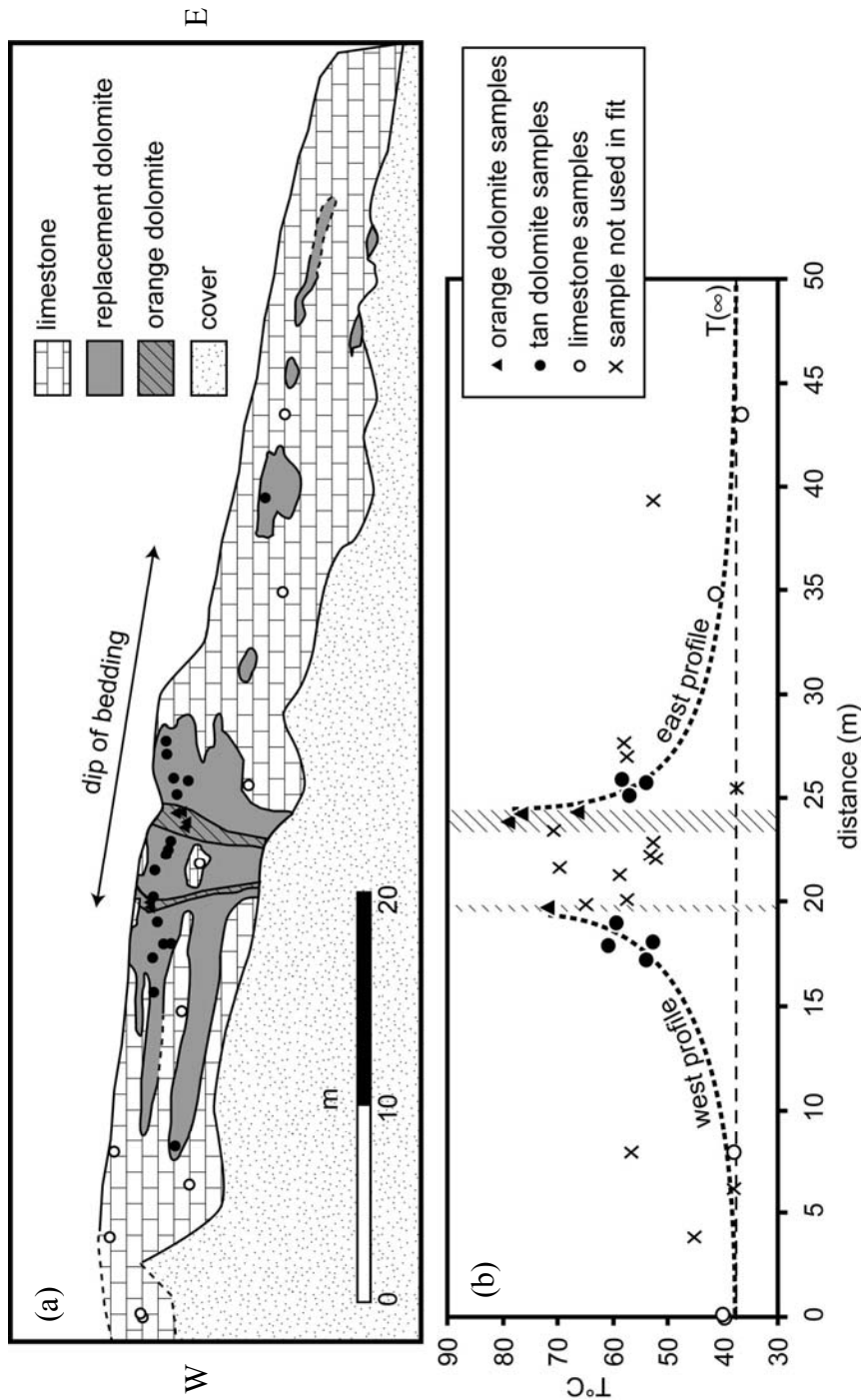


Figure 10.1. Temperature profile across Location 7. (a) Cross-section view as in Figure 4.5. (b) East and west temperature profiles. $T(\infty)$ estimated from T recorded by limestone samples away from orange dolomite (open circles). $T(0)$ estimated from samples of orange dolomite recording highest T in each orange dolomite body (filled triangles). Fit parameter, a , estimated from samples of tan dolomite closest to the orange dolomite bodies along the line of traverse where most samples were collected (filled circles). The two images are lined up such that the sample locations in (a) are directly above the sample locations in (b). The hatched area in (b) represents the location of the near-vertical sheet-like bands of orange dolomite.

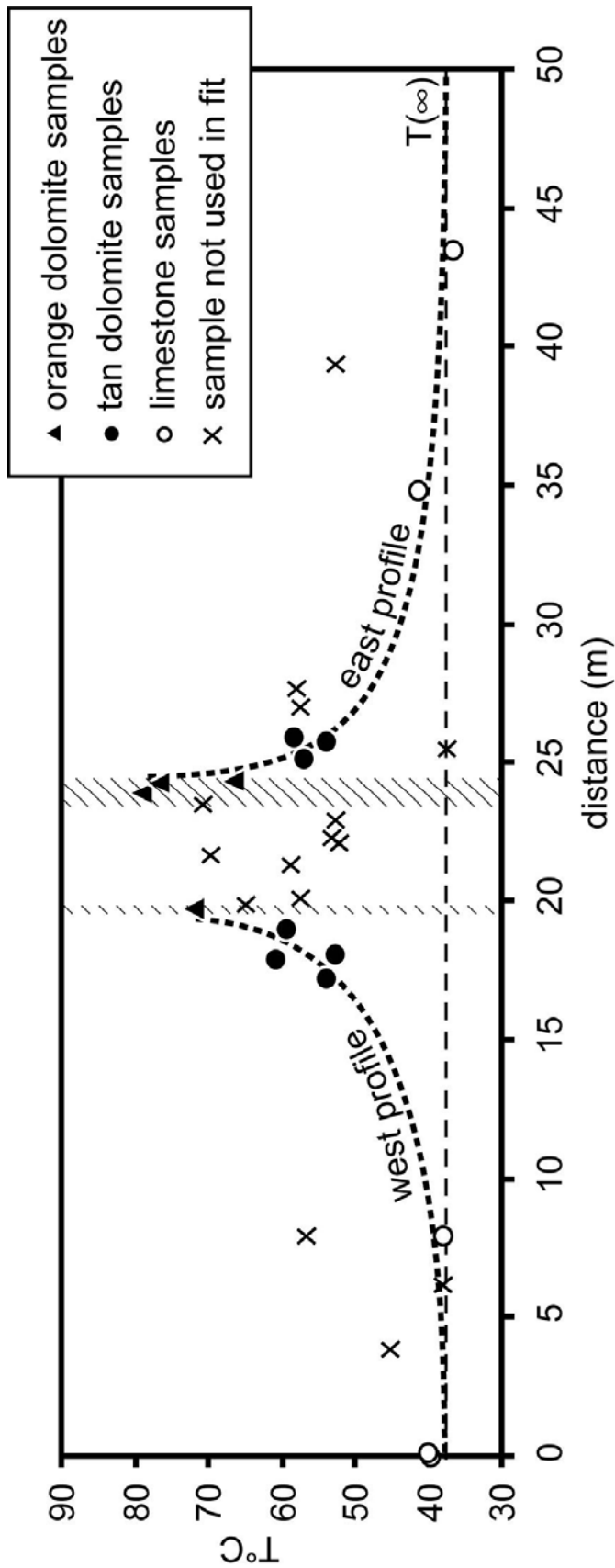


Figure 10.2. East and west temperature profiles for Location 7. $T(\infty)$ estimated from limestone samples away from orange dolomite (open circles). $T(0)$ estimated from samples of orange dolomite recording highest T in each orange dolomite body (filled triangles). Fit parameter, a , estimated from samples of tan dolomite closest to the orange dolomite bodies along the line of traverse where most samples were collected (filled circles).

with average Darcy flux J_{TV} in vertical channels corresponding to what is now orange dolomite in outcrop at Location 7. Spatial coordinates are x (horizontal measured perpendicular to the flow channel) with 0 at the channel margin and vertical measured parallel to fluid flow. The observed temperature profiles first were fit to

$$T(x) = T(\infty) + \Delta T e^{-ax} \quad (10.1)$$

where $T(x)$ is temperature at distance x from the channel, $T(\infty)$ is the far-field temperature, $\Delta T = T(0) - T(\infty)$, and a is an empirical fit parameter. Symbols for variables used in Equation 10.1 and the following analysis are listed and defined in Table 10.1. Numerical values of the variables used in calculations are listed in Table 10.2. Values of the a parameter were computed from T recorded by tan dolomite samples closest to the inferred flow channel (orange dolomite).

The time-integrated conductive heat flux out of the channel and into the surrounding rock, ΔQ , is

$$\Delta Q = c_r \rho_r \int_0^{\infty} T'(x) dx = c_r \rho_r \int_0^{\infty} \Delta T e^{-ax} dx = c_r \rho_r \frac{\Delta T}{a} \quad (10.2)$$

where $T'(x) = T(x) - T(\infty)$. From Equation (11) of Brady (1988), the duration of flow in the channel is

$$t = \left(\frac{2c_r \rho_r}{aK_r} \right)^2 \frac{\kappa}{\pi} \quad (10.3)$$

where c_r , ρ_r , K_r , and κ are the specific heat, density, thermal conductivity, and thermal diffusivity of the rock. For east and west profiles, $t = 0.08$ years and 0.18 years, equivalent to 28 and 65 days, respectively (Table 10.2).

Table 10.1. Symbols in Equations 10.1-10.4.

ρ_r, ρ_f	g/cm^3	density (r, rock; f, fluid)
$T(0)$	$^{\circ}\text{C}$	temperature within channel
$T(\infty)$	$^{\circ}\text{C}$	far-field temperature (average recorded by unaltered calcite)
ΔT	$^{\circ}\text{C}$	difference in temperature between channel and far-field
a	$1/\text{cm}$	empirical fit parameter in equation for temperature profile
c_r, c_f	J/gK	specific heat (r, rock; f, fluid)
W	cm	channel half width
$\partial T/\partial z$	$^{\circ}\text{K/cm}$	temperature gradient along vertical flow path
κ_r	cm^2/s	thermal diffusivity of rock
K_r	J/cmKs	thermal conductivity of rock
ΔQ	J/cm^2	time-integrated conductive heat flux out of channel
q_{Tv}	$\text{cm}^3 \text{ fluid/cm}^2 \text{ rock}$	time-integrated fluid flux to produce temperature anomaly
t	s	duration of flow in channel
J_{Tv}	cm/s	average Darcy flux in vertical flow channel
q_{vol}	$\text{cm}^3 \text{ fluid/cm}^2 \text{ rock}$	time-integrated fluid flux of dolomitization

Table 10.2. Input values and calculated results from Equations 10.1-10.4.

	east profile	west profile	source
T(0)	78	72	Figure 10.2
T(∞)	38	38	Figure 10.2
ΔT	40	34	
a	0.68	0.45	fit to data, Figure 10.2
$c_f \rho_f$	4.04	4.04	Brady (1988)
c_r	0.815	0.815	Holland and Powell (1998)
ρ_r	2.71	2.71	Holland and Powell (1998)
W	53	15	Figure 10.2
$\partial T / \partial z$	$-5 \cdot 10^{-4}$	$-5 \cdot 10^{-4}$	Figure 6.5
κ_r	$1.13 \cdot 10^{-2}$	$1.13 \cdot 10^{-2}$	$K_r / c_r \rho_r$
K_r	$2.5 \cdot 10^{-2}$	$2.5 \cdot 10^{-2}$	Brady (1988)
ΔQ	$1.28 \cdot 10^{12}$	$1.66 \cdot 10^{12}$	Equation 10.2
q_{Tv}	$1.21 \cdot 10^5$	$5.34 \cdot 10^5$	$J_{Tv} \cdot t$
t (seconds)	$2.43 \cdot 10^6$	$5.61 \cdot 10^6$	Equation 10.3
t (years)	0.08	0.18	Equation 10.3
J_{Tv}	$5 \cdot 10^{-2}$	$1 \cdot 10^{-1}$	Equation 10.4
q_{vol}	$4.63 \cdot 10^7$	$4.63 \cdot 10^7$	Table 9.3
# pulses	384	87	q_{vol} / q_{Tv}
total duration of flow (years)	30	15	$t \cdot \# \text{ pulses}$

Using Equation (10) of Brady (1988), the average Darcy flux (J_{Tv}) in the flow channel is

$$J_{Tv} = \frac{\Delta Q}{tWc_f\rho_f\left(-\frac{\partial T}{\partial z}\right)} \quad (10.4)$$

where W is the half-width of the flow channel, c_f and ρ_f are the specific heat and density of the fluid, and $(\partial T/\partial z)$ is the geothermal gradient. For east and west profiles, $J_{Tv} = 0.05$ and 0.10 cm/s, respectively. The values calculated for J_{Tv} are similar to a direct measurement of diffuse effluent flux on the seafloor of 0.02 cm/s (Mottl et al., 1998). The time-integrated fluid flux associated with the temperature anomalies ($q_{Tv} = J_{Tv}t$) are $1.21 \cdot 10^5$ cm³ fluid/cm² rock (east profile) and $5.34 \cdot 10^5$ cm³ fluid/cm² rock (west profile) (Table 10.2).

Because t and q_{Tv} represent the duration of flow and time-integrated fluid flux to produce the temperature anomalies in Figure 10.1, it is possible to constrain the total duration of flow and the number of fluid pulses required to form the Latemar dolomite in its entirety. Dividing q_{vol} (from Table 9.3 or 9.4), the time-integrated fluid flux for dolomitization, by q_{Tv} gives the number of pulses of flow (of size q_{Tv}) that are required. Approximately 380 pulses of fluid, the size of that to produce the east temperature profile in Figure 10.1 were required for dolomitization of the Latemar, and ~90 pulses of fluid the size of that to produce the west temperature profile would be required. Because flow was unusually high in the channels (evidenced by high Fe, low porosity, altered $\delta^{13}C$), these are minimum values. Overall, thousands of pulses may be expected. Multiplying the number of pulses by the duration of each pulse gives the total duration of active dolomitization: 30 years using the east channel temperature profile, and 15 years using

the west channel profile. For the same reason, these are minimum values, but duration of flow and reaction nevertheless must have been short, probably no more than hundreds or thousands of years. Although the total duration of flow is very short for both profiles, especially in the context of geologic time, it is likely that flow was not continuous, and the pulses of flow were spread out over a much longer time period. This is expected for a geologic setting in which fluid like diffuse effluent is venting. Using the diffuse effluent flux (0.02 cm/s) measured by Mottl et al. (1998) gives a total duration of flow of only two years.

Although the estimates of the number of fluid pulses required for dolomitization of the Latemar is dependent on the temperature profile and width of flow channel used, pulsed flow is clearly the mechanism of dolomitization. There is as much variation in $\delta^{18}\text{O}$ across a single outcrop as there is across the entire buildup (Figures 6.3 and 6.4), which in itself is indicative of pulses of flow at variable temperature rather than a single, pervasive fluid flow event. Furthermore, the highly variable flow of hydrothermal vent systems in both space and time is well-known (Von Damm, 1995; Von Damm, 2004), and this temporal variability is also seen in diffuse effluent (Von Damm and Lilley, 2004), the most likely candidate for the dolomitizing fluid.

Appendix I. Sample Locations

Location	Sample	Rock Unit	Easting Gauss-Boaga	Northing Gauss-Boaga	Longitude (WGS84)	Latitude (WGS84)	elevation (m)	dip-corrected elevation (m)
Location 1	L-1A	LS	1696971.87	5138061.87	11°33'37.57	46°22'02.38	2530.93	552.27
Location 1	L-1B	DOL	1696986.47	5138065.82	11°33'38.26	46°22'02.49	2529.18	550.52
Location 1	L-1C	DOL	1696989.44	5138072.44	11°33'38.41	46°22'02.70	2532.12	553.46
Location 1	L-1D	DOL	1697005.80	5138073.41	11°33'39.17	46°22'02.71	2528.04	549.38
Location 1	L-1E	LS	1697007.24	5138074.02	11°33'39.24	46°22'02.73	2527.44	548.78
Location 1	L-1F	LS	1697011.98	5138073.30	11°33'39.46	46°22'02.70	2525.80	547.14
Location 1	L-1G	LS	1696957.20	5138061.16	11°33'36.88	46°22'02.37	2532.44	553.78
Location 1	L-1H	LS	1696979.37	5138067.00	11°33'37.93	46°22'02.53	2530.36	551.70
Location 1	L-1I	DOL	1696983.47	5138070.13	11°33'38.12	46°22'02.63	2531.67	553.01
Location 1	L-1J	DOL	1696995.86	5138071.12	11°33'38.70	46°22'02.65	2530.02	551.36
Location 1	L-1K	DOL	1696999.92	5138070.84	11°33'38.89	46°22'02.64	2528.68	550.02
Location 1	L-1L	DOL	1697019.73	5138079.69	11°33'39.83	46°22'02.90	2528.32	549.66
Location 2	L-2A	DOL	1697548.32	5138749.18	11°34'05.56	46°22'24.02	2411.74	433.08
Location 2	L-2B	LS	1697546.51	5138750.48	11°34'05.48	46°22'24.06	2411.88	433.22
Location 2	L-2C	LS	1697543.34	5138749.46	11°34'05.33	46°22'24.03	2412.86	434.20
Location 2	L-2D	LS	1697521.22	5138751.82	11°34'04.30	46°22'24.13	2417.04	438.38
Location 2	L-2E	LS	1697532.71	5138728.60	11°34'04.80	46°22'23.37	2419.97	441.31
Location 2	L-2F	DOL	1697506.80	5138747.17	11°34'03.62	46°22'23.99	2424.16	445.50
Location 4	L-4A	LS	1697943.63	5139292.47	11°34'24.88	46°22'41.18	2585.00	606.34
Location 4	L-4B	LS	1697943.63	5139292.47	11°34'24.88	46°22'41.18	2585.00	606.34
Location 4	L-4C	LS	1697943.63	5139292.47	11°34'24.88	46°22'41.18	2585.00	606.34

Appendix I. cont.

Location	Sample	Rock Unit	Easting Gauss-Boaga	Northing Gauss-Boaga	Longitude (WGS84)	Latitude (WGS84)	elevation (m)	dip-corrected elevation (m)
Location 4	L-4D	LS	1697943.63	5139292.47	11°34'24.88	46°22'41.18	2585.00	606.34
Location 5	L-5A	LS	1697438.98	5138692.40	11°34'00.36	46°22'22.29	2445.89	467.23
Location 5	L-5B	LS	1697441.32	5138690.88	11°34'00.47	46°22'22.24	2445.07	466.41
Location 5	L-5C	LS	1697445.57	5138691.15	11°34'00.67	46°22'22.25	2444.63	465.97
Location 5	L-5D	DOL	1697446.39	5138692.66	11°34'00.71	46°22'22.29	2444.91	466.25
Location 5	L-5E	DOL	1697447.98	5138691.88	11°34'00.78	46°22'22.27	2444.61	465.95
Location 5	L-5F	DOL	1697450.94	5138693.16	11°34'00.93	46°22'22.31	2444.33	465.67
Location 6	L-6A	DOL	1697193.10	5138680.14	11°33'48.85	46°22'22.15	2470.62	491.96
Location 6	L-6B	DOL	1697180.63	5138675.75	11°33'48.26	46°22'22.03	2471.64	492.98
Location 6	L-6C	DOL	1697170.10	5138670.21	11°33'47.76	46°22'21.86	2474.29	495.63
Location 6	L-6D	DOL	1697173.32	5138685.83	11°33'47.93	46°22'22.36	2474.19	495.53
Location 7	L-7A	LS	1697156.42	5137744.43	11°33'45.72	46°21'51.91	2535.47	556.81
Location 7	L-7B	LS	1697162.77	5137739.13	11°33'46.00	46°21'51.73	2533.32	554.66
Location 7	L-7C	DOL	1697164.40	5137739.73	11°33'46.08	46°21'51.75	2534.07	555.41
Location 7	L-7D	LS	1697171.20	5137738.28	11°33'46.40	46°21'51.69	2533.66	555.00
Location 7	L-7E	DOL	1697174.54	5137738.79	11°33'46.55	46°21'51.71	2534.16	555.50
Location 7	L-7F	DOL	1697179.92	5137738.14	11°33'46.81	46°21'51.68	2533.48	554.82
Location 7	L-7G	DOL	1697178.86	5137738.44	11°33'46.76	46°21'51.69	2534.23	555.57
Location 7	L-7H	DOL	1697178.11	5137736.84	11°33'46.72	46°21'51.64	2532.67	554.01
Location 7	L-7I	DOL	1697182.26	5137736.70	11°33'46.91	46°21'51.63	2533.34	554.68
Location 7	L-7J	LS	1697181.96	5137733.06	11°33'46.89	46°21'51.51	2530.44	551.78

Appendix I. cont.

Location	Sample	Rock Unit	Easting Gauss-Boaga	Northing Gauss-Boaga	Longitude (WGS84)	Latitude (WGS84)	elevation (m)	dip-corrected elevation (m)
Location 7	L-7K	LS	1697191.29	5137729.37	11°33'47.32	46°21'51.38	2528.77	550.11
Location 7	L-7L	DOL	1697195.86	5137729.98	11°33'47.54	46°21'51.40	2529.61	550.95
Location 7	L-7M	LS	1697199.96	5137729.90	11°33'47.73	46°21'51.39	2528.64	549.98
Location 7	L-7N	LS	1697164.35	5137742.32	11°33'46.08	46°21'51.83	2536.86	558.20
Location 7	L-7O	LS	1697160.27	5137742.67	11°33'45.89	46°21'51.85	2537.07	558.41
Location 7	L-7P	LS	1697156.56	5137744.19	11°33'45.72	46°21'51.90	2535.56	556.90
Location 7	7T-1	DOL	1697184.14	5137737.39	11°33'47.00	46°21'51.65	2534.36	555.70
Location 7	7T-2	DOL	1697183.51	5137737.47	11°33'46.97	46°21'51.65	2534.32	555.66
Location 7	7T-3	DOL	1697182.37	5137737.53	11°33'46.92	46°21'51.66	2533.99	555.33
Location 7	7T-4	DOL	1697181.58	5137737.72	11°33'46.88	46°21'51.66	2533.84	555.18
Location 7	7T-5	DOL	1697180.72	5137737.98	11°33'46.84	46°21'51.67	2533.54	554.88
Location 7	7T-6	DOL	1697180.67	5137738.38	11°33'46.84	46°21'51.69	2533.85	555.19
Location 7	7T-7	DOL	1697180.26	5137737.91	11°33'46.82	46°21'51.67	2533.35	554.69
Location 7	7T-8	DOL	1697179.33	5137737.98	11°33'46.78	46°21'51.67	2534.13	555.47
Location 7	7T-9	DOL	1697178.67	5137738.74	11°33'46.75	46°21'51.70	2534.36	555.70
Location 7	7T-10	DOL	1697177.90	5137739.65	11°33'46.71	46°21'51.73	2534.90	556.24
Location 7	7T-11	DOL	1697176.62	5137739.70	11°33'46.65	46°21'51.73	2534.98	556.32
Location 7	7T-12	DOL	1697176.34	5137739.98	11°33'46.64	46°21'51.74	2535.08	556.42
Location 7	7T-13	DOL	1697176.15	5137740.01	11°33'46.63	46°21'51.74	2535.05	556.39
Location 7	7T-14	DOL	1697175.42	5137739.45	11°33'46.60	46°21'51.73	2534.78	556.12
Location 7	7T-15	DOL	1697174.34	5137739.23	11°33'46.55	46°21'51.72	2534.49	555.83

Appendix I. cont.

Location	Sample	Rock Unit	Easting Gauss-Boaga	Northing Gauss-Boaga	Longitude (WGS84)	Latitude (WGS84)	elevation (m)	dip-corrected elevation (m)
Location 7	7T-16	DOL	1697173.68	5137739.81	11°33'46.52	46°21'51.74	2535.00	556.34
Location 7	7T-17	LS	1697172.03	5137739.80	11°33'46.44	46°21'51.74	2534.95	556.29
Location 8	L-8A	LS	1697451.67	5138679.49	11°34'00.94	46°22'21.86	2440.43	461.77
Location 8	L-8B	LS	1697451.43	5138680.04	11°34'00.93	46°22'21.88	2441.19	462.53
Location 8	L-8C	DOL	1697452.85	5138680.63	11°34'01.00	46°22'21.90	2441.54	462.88
Location 8	L-8D	DOL	1697452.83	5138680.92	11°34'00.99	46°22'21.91	2442.02	463.36
Location 8	L-8E	LS	1697453.21	5138682.32	11°34'01.01	46°22'21.95	2442.27	463.61
Location 8	L-8F	LS	1697452.11	5138687.29	11°34'00.97	46°22'22.11	2443.17	464.51
Location 8	L-8G	DOL	1697444.34	5138683.55	11°34'00.60	46°22'22.00	2442.23	463.57
Location 8	L-8H	LS	1697442.44	5138684.72	11°34'00.51	46°22'22.04	2441.72	463.06
Location 8	L-8I	LS	1697435.94	5138686.33	11°34'00.21	46°22'22.10	2442.57	463.91
Location 8	L-8J	LS	1697460.24	5138682.04	11°34'01.34	46°22'21.94	2440.66	462.00
Location 8	L-8K	DOL	1697447.43	5138680.99	11°34'00.74	46°22'21.92	2441.83	463.17
Location 8	L-8L	LS	1697432.41	5138686.53	11°34'00.05	46°22'22.11	2441.61	462.95
Location 8	L-8M	LS	1697464.17	5138685.13	11°34'01.53	46°22'22.03	2440.14	461.48
Location 8	L-8N	LS	1697438.87	5138685.87	11°34'00.35	46°22'22.08	2442.27	463.61
Location 8	L-8O	DOL	1697461.92	5138684.47	11°34'01.43	46°22'22.01	2440.97	462.31
Location 8	L-8P	LS	1697452.85	5138680.63	11°34'01.00	46°22'21.90	2441.41	462.75
Location 8	L-8Q	DOL	1697452.85	5138680.63	11°34'01.00	46°22'21.90	2441.48	462.82
Location 8	L-8R	LS	1697504.25	5138689.14	11°34'03.41	46°22'22.12	2432.17	453.51
Location 8	L-8S	DOL	1697503.50	5138688.13	11°34'03.38	46°22'22.09	2432.38	453.72

Appendix I. cont.

Location	Sample	Rock Unit	Easting Gauss-Boaga	Northing Gauss-Boaga	Longitude (WGS84)	Latitude (WGS84)	elevation (m)	dip-corrected elevation (m)
Location 8	L-8T	DOL	1697503.27	5138697.72	11°34'03.38	46°22'22.40	2430.08	451.42
Location 8	L-8U	DOL	1697506.03	5138698.28	11°34'03.51	46°22'22.41	2429.57	450.91
Location 8	L-8V	DOL	1697499.71	5138697.73	11°34'03.21	46°22'22.40	2431.86	453.20
Location 8	L-8W	DOL	1697502.52	5138701.40	11°34'03.35	46°22'22.52	2433.13	454.47
Location 8	L-8X	DOL	1697499.93	5138702.17	11°34'03.23	46°22'22.55	2434.08	455.42
Location 8	8T-1	DOL	1697444.98	5138682.42	11°34'00.63	46°22'21.96	2442.22	463.56
Location 8	8T-2	DOL	1697446.06	5138681.73	11°34'00.68	46°22'21.94	2442.28	463.62
Location 8	8T-3	DOL	1697448.48	5138681.49	11°34'00.79	46°22'21.93	2441.84	463.18
Location 8	8T-4	DOL	1697450.58	5138681.08	11°34'00.89	46°22'21.91	2441.82	463.16
Location 8	8T-5	DOL	1697455.04	5138680.83	11°34'01.10	46°22'21.90	2441.48	462.82
Location 8	8T-6	DOL	1697458.03	5138681.32	11°34'01.24	46°22'21.91	2441.06	462.40
Location 8	8T-7	DOL	1697459.81	5138682.04	11°34'01.32	46°22'21.94	2441.05	462.39
Location 8	8T-8	DOL	1697462.35	5138684.77	11°34'01.45	46°22'22.02	2441.20	462.54
Location 8	8T-9	DOL	1697463.40	5138685.67	11°34'01.50	46°22'22.05	2440.98	462.32
Location 8	8T-10	DOL	1697466.22	5138686.98	11°34'01.63	46°22'22.09	2440.67	462.01
Location 8	8T-11	DOL	1697467.89	5138687.33	11°34'01.71	46°22'22.10	2440.46	461.80
Location 8	8T-12	DOL	1697470.73	5138687.65	11°34'01.84	46°22'22.11	2440.26	461.60
Location 8	8T-13	DOL	1697475.86	5138689.59	11°34'02.09	46°22'22.16	2439.29	460.63
Location 8	8T-14	DOL	1697489.54	5138691.01	11°34'02.73	46°22'22.20	2435.83	457.17
Location 9	L-9A	LS	1697724.04	5139430.70	11°34'14.82	46°22'45.89	2497.55	518.89
Location 9	L-9B	LS	1697734.43	5139433.84	11°34'15.31	46°22'45.98	2501.54	522.88

Appendix I. cont.

Location	Sample	Rock Unit	Easting Gauss-Boaga	Northing Gauss-Boaga	Longitude (WGS84)	Latitude (WGS84)	elevation (m)	dip-corrected elevation (m)
Location 9	L-9C	LS	1697734.79	5139435.91	11°34'15.33	46°22'46.05	2505.74	527.08
Location 9	L-9D	LS	1697745.12	5139438.60	11°34'15.81	46°22'46.12	2507.46	528.80
Location 9	L-9E	LS	1697744.50	5139412.18	11°34'15.74	46°22'45.27	2509.72	531.06
Location 9	L-9F	LS	1697741.14	5139445.90	11°34'15.64	46°22'46.36	2513.73	535.07
Location 11	L-11A	LS	1697988.40	5138617.77	11°34'25.94	46°22'19.30	2201.89	223.23
Location 11	L-11B	DOL	1697989.40	5138627.16	11°34'26.00	46°22'19.60	2208.01	229.35
Location 11	L-11C	DOL	1697986.66	5138630.65	11°34'25.88	46°22'19.72	2210.43	231.77
Location 11	L-11D	LS	1697973.57	5138651.64	11°34'25.30	46°22'20.41	2230.52	251.86
Location 11	L-11E	DOL	1697975.80	5138645.96	11°34'25.40	46°22'20.23	2223.20	244.54
Location 11	L-11F	LS	1697963.37	5138666.77	11°34'24.85	46°22'20.91	2240.12	261.46
Location 11	L-11G	DOL	1697984.38	5138663.07	11°34'25.82	46°22'20.77	2250.77	272.11
Location 11	L-11H	LS	1697943.43	5138688.88	11°34'23.95	46°22'21.65	2250.33	271.67
Location 12	L-12A	DOL	1697344.73	5138746.75	11°33'56.04	46°22'24.15	2478.58	499.92
Location 12	L-12B	DOL	1697359.58	5138755.35	11°33'56.75	46°22'24.41	2474.11	495.45
Location 12	L-12C	DOL	1697362.66	5138760.22	11°33'56.90	46°22'24.57	2473.79	495.13
Location 12	L-12D	LS	1697363.31	5138762.94	11°33'56.93	46°22'24.66	2475.70	497.04
Location 12	L-12E	DOL	1697368.98	5138768.32	11°33'57.21	46°22'24.82	2474.07	495.41
Location 12	L-12F	LS	1697364.53	5138790.89	11°33'57.03	46°22'25.56	2485.48	506.82
Location 12	L-12G	LS	1697353.86	5138777.67	11°33'56.51	46°22'25.14	2493.20	514.54
Location 12	L-12H	DOL	1697353.13	5138775.47	11°33'56.48	46°22'25.07	2493.09	514.43
Location 12	L-12I	LS	1697328.68	5138749.45	11°33'55.29	46°22'24.26	2487.02	508.36

Appendix I. cont.

Location	Sample	Rock Unit	Easting Gauss-Boaga	Northing Gauss-Boaga	Longitude (WGS84)	Latitude (WGS84)	elevation (m)	dip-corrected elevation (m)
Location 12	L-12J	LS	1697316.17	5138749.49	11°33'54.71	46°22'24.27	2484.36	505.70
Location 13	L-13A	DOL	1697533.42	5137297.76	11°34'02.66	46°21'37.05	2482.58	503.92
Location 13	L-13B	DOL	1697521.89	5137298.14	11°34'02.13	46°21'37.08	2481.92	503.26
Location 13	L-13C	DOL	1697509.74	5137300.06	11°34'01.56	46°21'37.15	2482.55	503.89
Location 13	L-13D	DOL	1697514.98	5137286.92	11°34'01.79	46°21'36.72	2495.85	517.19
Location 13	L-13E	DOL	1697520.38	5137285.62	11°34'02.04	46°21'36.68	2495.65	516.99
Location 13	L-13F	DOL	1697522.13	5137273.37	11°34'02.10	46°21'36.28	2504.68	526.02
Traverse A	LAS-1	LS	1697893.86	5138794.69	11°34'21.79	46°22'25.13	2332.33	353.67
Traverse A	LAS-2	LS	1697863.86	5138768.28	11°34'20.35	46°22'24.30	2342.36	363.70
Traverse A	LAS-3	LS	1697803.33	5138751.00	11°34'17.49	46°22'23.81	2353.87	375.21
Traverse A	LAS-4	LS	1697742.67	5138758.34	11°34'14.67	46°22'24.11	2364.88	386.22
Traverse A	LAS-5	DOL	1697735.80	5138768.20	11°34'14.36	46°22'24.43	2363.85	385.19
Traverse A	LAS-6	LS	1697702.74	5138752.05	11°34'12.79	46°22'23.95	2376.92	398.26
Traverse A	LAS-7	LS	1697648.93	5138736.25	11°34'10.25	46°22'23.49	2392.57	413.91
Traverse A	LAS-8	DOL	1697638.01	5138732.33	11°34'09.73	46°22'23.38	2397.02	418.36
Traverse A	LAS-9	DOL	1697585.30	5138747.35	11°34'07.29	46°22'23.92	2407.44	428.78
Traverse A	LAS-10	DOL	1697509.12	5138671.30	11°34'03.61	46°22'21.54	2426.52	447.86
Traverse A	LAS-11	LS	1697473.53	5138641.21	11°34'01.90	46°22'20.60	2431.43	452.77
Traverse A	LAS-12	DOL	1697463.53	5138625.86	11°34'01.41	46°22'20.11	2436.99	458.33
Traverse A	LAS-13	LS	1697440.94	5138587.18	11°34'00.30	46°22'18.89	2435.91	457.25
Traverse A	LAS-14	LS	1697433.34	5138535.85	11°33'59.86	46°22'17.23	2436.49	457.83

Appendix I. cont.

Location	Sample	Rock Unit	Easting Gauss-Boaga	Northing Gauss-Boaga	Longitude (WGS84)	Latitude (WGS84)	elevation (m)	dip-corrected elevation (m)
Traverse A	LAS-15	DOL	1697438.27	5138531.12	11°34'00.09	46°22'17.07	2436.17	457.51
Traverse A	LAS-16	LS	1697433.52	5138507.78	11°33'59.83	46°22'16.32	2435.81	457.15
Traverse A	LAS-17	LS	1697415.81	5138487.67	11°33'58.97	46°22'15.69	2445.30	466.64
Traverse A	LAS-18	LS	1697404.64	5138486.78	11°33'58.45	46°22'15.67	2451.09	472.43
Traverse A	LAS-19	LS	1697371.42	5138476.47	11°33'56.88	46°22'15.38	2462.61	483.95
Traverse A	LAS-20	LS	1697341.87	5138449.24	11°33'55.46	46°22'14.53	2461.94	483.28
Traverse A	LAS-21	DOL	1697323.85	5138448.95	11°33'54.61	46°22'14.53	2466.82	488.16
Traverse A	LAS-22	LS	1697313.72	5138415.16	11°33'54.09	46°22'13.45	2478.05	499.39
Traverse A	LAS-23	DOL	1697312.20	5138409.08	11°33'54.01	46°22'13.26	2482.44	503.78
Traverse A	LAS-24	DOL	1697282.15	5138365.55	11°33'52.54	46°22'11.88	2501.55	522.89
Traverse A	LAS-25	DOL	1697224.13	5138351.06	11°33'49.80	46°22'11.47	2519.25	540.59
Traverse A	LAS-26	LS	1697168.03	5138348.75	11°33'47.17	46°22'11.46	2526.90	548.24
Traverse A	LAS-27	DOL	1697099.30	5138357.24	11°33'43.97	46°22'11.80	2517.37	538.71
Traverse A	LAS-28	LS	1697029.81	5138337.00	11°33'40.69	46°22'11.22	2531.09	552.43
Traverse A	LAS-29	DOL	1697003.81	5138290.34	11°33'39.41	46°22'09.74	2537.22	558.56
Traverse A	LAS-30	LS	1696990.27	5138280.02	11°33'38.76	46°22'09.42	2541.19	562.53
Traverse A	LAS-31	LS	1696944.48	5138281.63	11°33'36.62	46°22'09.52	2537.82	559.16
Traverse A	LAS-32	LS	1696862.78	5138235.70	11°33'32.73	46°22'08.12	2555.86	577.20
Traverse A	LAS-34	DOL	1696831.55	5138232.06	11°33'31.26	46°22'08.03	2577.26	598.60
Traverse A	LAS-33	LS	1696838.64	5138229.11	11°33'31.59	46°22'07.93	2573.51	594.85
Traverse A	LAS-35	LS	1696822.71	5138241.20	11°33'30.87	46°22'08.34	2583.72	605.06

Appendix I. cont.

Location	Sample	Rock Unit	Easting Gauss-Boaga	Northing Gauss-Boaga	Longitude (WGS84)	Latitude (WGS84)	elevation (m)	dip-corrected elevation (m)
Traverse A	LAS-36	LS	1696797.54	5138241.86	11°33'29.69	46°22'08.38	2600.39	621.73
Traverse A	LAS-37	DOL	1696764.65	5138231.02	11°33'28.14	46°22'08.07	2625.93	647.27
Traverse A	LAS-38	LS	1696750.79	5138216.65	11°33'27.47	46°22'07.62	2636.52	657.86
Traverse A	LAS-39	LS	1696756.12	5138206.68	11°33'27.70	46°22'07.29	2635.15	656.49
Traverse A	LAS-40	LS	1697927.11	5138786.34	11°34'23.33	46°22'24.82	2314.67	336.01
Traverse A	LAS-41	DOL	1697956.80	5138732.22	11°34'24.64	46°22'23.04	2284.52	305.86
Traverse A	LAS-42	LS	1697942.32	5138588.40	11°34'23.74	46°22'18.40	2216.26	237.60
Traverse A	LAS-43	DOL	1697938.13	5138598.29	11°34'23.56	46°22'18.72	2225.53	246.87
Traverse A	LAS-44	LS	1697973.05	5138592.74	11°34'25.19	46°22'18.51	2193.93	215.27
Traverse A	LAS-45	LS	1698033.86	5138614.52	11°34'28.06	46°22'19.15	2161.78	183.12
Traverse A	LAS-46	DOL	1698049.99	5138579.51	11°34'28.76	46°22'18.00	2135.43	156.77
Traverse A	LAS-47	DOL	1698037.85	5138554.88	11°34'28.16	46°22'17.21	2121.74	143.08
Traverse A	LAS-48	DOL	1698037.67	5138554.41	11°34'28.15	46°22'17.20	2121.59	142.93
Traverse A	LAS-49	DOL	1698043.30	5138569.00	11°34'28.44	46°22'17.66	2126.28	147.62
Traverse A	LAS-50	LS	1698024.36	5138519.95	11°34'27.47	46°22'16.10	2110.51	131.85
Traverse A	LAS-51	DOL	1698013.09	5138490.77	11°34'26.90	46°22'15.16	2101.13	122.47
Traverse A	LAS-52	DOL	1698010.25	5138483.40	11°34'26.76	46°22'14.93	2098.76	120.10
Traverse A	LAS-53	DOL	1698010.89	5138483.66	11°34'26.79	46°22'14.94	2094.84	116.18
Traverse A	LAS-54	DOL	1698010.95	5138483.70	11°34'26.79	46°22'14.94	2094.54	115.88
Traverse A	LAS-55	DOL	1698114.21	5138455.58	11°34'31.58	46°22'13.92	1972.31	-6.35
Traverse A	LAS-56	DOL	1698160.66	5138495.49	11°34'33.81	46°22'15.16	1956.96	-21.70

Appendix I. cont.

Location	Sample	Rock Unit	Easting Gauss-Boaga	Northing Gauss-Boaga	Longitude (WGS84)	Latitude (WGS84)	elevation (m)	dip-corrected elevation (m)
Traverse A	LAS-57	DOL	1698198.15	5138527.71	11°34'35.61	46°22'16.16	1944.57	-34.09
Traverse B	LBS-1	DOL	1697845.30	5137638.40	11°34'17.76	46°21'47.75	2337.46	358.80
Traverse B	LBS-2	DOL	1697845.04	5137637.23	11°34'17.75	46°21'47.71	2338.70	360.04
Traverse B	LBS-3	LS	1697844.35	5137634.11	11°34'17.71	46°21'47.61	2342.01	363.35
Traverse B	LBS-4	LS	1697790.27	5137590.57	11°34'15.12	46°21'46.26	2395.18	416.52
Traverse B	LBS-5	DOL	1697681.90	5137593.81	11°34'10.06	46°21'46.48	2409.02	430.36
Traverse B	LBS-6	LS	1697676.19	5137593.98	11°34'09.79	46°21'46.49	2409.75	431.09
Traverse B	LBS-7	LS	1697639.31	5137595.09	11°34'08.07	46°21'46.57	2414.46	435.80
Traverse B	LBS-8	LS	1697557.05	5137584.95	11°34'04.20	46°21'46.33	2431.49	452.83
Traverse B	LBS-9	DOL	1697521.93	5137570.88	11°34'02.54	46°21'45.91	2443.81	465.15
Traverse B	LBS-10	LS	1697456.75	5137641.35	11°33'59.60	46°21'48.26	2460.27	481.61
Traverse B	LBS-11	LS	1697408.16	5137706.02	11°33'57.43	46°21'50.40	2472.18	493.52
Traverse B	LBS-12	LS	1697352.24	5137760.18	11°33'54.90	46°21'52.21	2501.93	523.27
Traverse B	LBS-13	LS	1697255.09	5137748.00	11°33'50.33	46°21'51.92	2520.03	541.37
Traverse B	LBS-14	LS	1697014.59	5137643.13	11°33'38.93	46°21'48.78	2542.95	564.29
Traverse B	LBS-15	LS	1697014.59	5137643.13	11°33'38.93	46°21'48.78	2558.86	580.20
Traverse C	LCS-1	LS	1697730.24	5138904.30	11°34'14.31	46°22'28.85	2368.72	390.06
Traverse C	LCS-2	LS	1697710.85	5138960.62	11°34'13.49	46°22'30.69	2388.55	409.89
Traverse C	LCS-3	LS	1697683.58	5139016.46	11°34'12.29	46°22'32.52	2410.69	432.03
Traverse C	LCS-4	LS	1697617.49	5139085.11	11°34'09.31	46°22'34.82	2442.68	464.02
Traverse C	LCS-5	LS	1697611.09	5139131.56	11°34'09.08	46°22'36.33	2474.17	495.51

Appendix I. cont.

Location	Sample	Rock Unit	Easting Gauss-Boaga	Northing Gauss-Boaga	Longitude (WGS84)	Latitude (WGS84)	elevation (m)	dip-corrected elevation (m)
Traverse C	LCS-6	LS	1697580.33	5139182.02	11°34'07.72	46°22'37.99	2491.55	512.89
Traverse C	LCS-7	LS	1697548.91	5139222.84	11°34'06.31	46°22'39.35	2500.64	521.98
Traverse C	LCS-8	DOL	1697524.61	5139251.16	11°34'05.22	46°22'40.29	2505.03	526.37
Traverse C	LCS-9	LS	1697426.57	5139413.47	11°34'00.88	46°22'45.64	2520.84	542.18
Traverse C	LCS-10	DOL	1697420.86	5139432.54	11°34'00.64	46°22'46.27	2521.38	542.72
Traverse C	LCS-11	DOL	1697432.59	5139393.34	11°34'01.13	46°22'44.99	2520.27	541.61
Traverse C	LCS-12	LS	1697391.67	5139517.18	11°33'59.40	46°22'49.04	2527.84	549.18
Traverse C	LCS-13	LS	1697366.35	5139568.62	11°33'58.30	46°22'50.73	2544.57	565.91
Traverse C	LCS-14	LS	1697365.57	5139543.71	11°33'58.22	46°22'49.92	2556.47	577.81
Traverse C	LCS-15	LS	1697364.24	5139681.53	11°33'58.37	46°22'54.39	2609.33	630.67
Traverse D	LDS-1a	LS	1697864.44	5137803.16	11°34'18.91	46°21'53.06	2284.89	306.23
Traverse D	LDS-1b	LS	1697863.77	5137804.46	11°34'18.88	46°21'53.11	2285.21	306.55
Traverse D	LDS-2	DOL	1697822.23	5137884.91	11°34'17.06	46°21'55.76	2305.08	326.42
Traverse D	LDS-3	DOL	1697758.28	5137873.77	11°34'14.05	46°21'55.46	2337.77	359.11
Traverse D	LDS-4	LS	1697736.59	5137869.83	11°34'13.03	46°21'55.36	2343.91	365.25
Traverse D	LDS-5	DOL	1697705.16	5137864.12	11°34'11.55	46°21'55.21	2352.81	374.15
Traverse D	LDS-6	LS	1697686.65	5137860.76	11°34'10.68	46°21'55.12	2358.05	379.39
Traverse D	LDS-7	LS	1697609.91	5137918.36	11°34'07.18	46°21'57.06	2383.03	404.37
Traverse D	LDS-8	LS	1697548.52	5137966.67	11°34'04.39	46°21'58.69	2409.21	430.55
Traverse D	LDS-9a	LS	1697480.58	5138078.74	11°34'01.38	46°22'02.39	2437.66	459.00
Traverse D	LDS-9b	LS	1697473.06	5138091.15	11°34'01.05	46°22'02.80	2440.81	462.15

Appendix I. cont.

Location	Sample	Rock Unit	Easting Gauss-Boaga	Northing Gauss-Boaga	Longitude (WGS84)	Latitude (WGS84)	elevation (m)	dip-corrected elevation (m)
Traverse D	LDS-10	LS	1697398.88	5138135.74	11°33'57.65	46°22'04.32	2455.46	476.80
Traverse D	LDS-11	DOL	1697332.37	5138182.19	11°33'54.61	46°22'05.89	2487.91	509.25
Traverse D	LDS-13	LS	1697221.10	5138139.46	11°33'49.34	46°22'04.63	2463.86	485.20
Traverse D	LDS-12	DOL	1697226.10	5138143.30	11°33'49.58	46°22'04.74	2462.18	483.52
Traverse D	LDS-14	DOL	1697177.61	5138106.02	11°33'47.25	46°22'03.59	2476.81	498.15
Traverse D	LDS-15	LS	1697163.54	5138052.13	11°33'46.52	46°22'01.86	2485.66	507.00
Traverse D	LDS-16	DOL	1697147.21	5138050.98	11°33'45.75	46°22'01.84	2490.84	512.18
Traverse D	LDS-17	LS	1697111.10	5138048.42	11°33'44.06	46°22'01.79	2502.29	523.63
Traverse D	LDS-18	LS	1697071.46	5138067.00	11°33'42.23	46°22'02.44	2514.38	535.72
Traverse E	LES-1	LS	1697339.17	5138663.42	11°33'55.65	46°22'21.46	2451.17	472.51
Traverse E	LES-2	LS	1697271.39	5138670.85	11°33'52.50	46°22'21.77	2460.19	481.53
Traverse E	LES-3	DOL	1697263.47	5138660.72	11°33'52.11	46°22'21.45	2457.50	478.84
Traverse E	LES-4	DOL	1697243.25	5138652.27	11°33'51.15	46°22'21.20	2458.77	480.11
Traverse E	LES-5	DOL	1697225.00	5138620.91	11°33'50.25	46°22'20.20	2461.59	482.93
Traverse E	LES-6	LS	1697224.40	5138614.11	11°33'50.21	46°22'19.98	2459.88	481.22
Traverse E	LES-7	DOL	1697220.21	5138607.77	11°33'50.01	46°22'19.78	2459.95	481.29
Traverse E	LES-8	LS	1697206.12	5138598.41	11°33'49.33	46°22'19.50	2461.16	482.50
Traverse E	LES-9	DOL	1697187.38	5138594.57	11°33'48.45	46°22'19.39	2466.46	487.80
Traverse E	LES-10	LS	1697165.10	5138586.33	11°33'47.40	46°22'19.15	2477.38	498.72
Traverse E	LES-11	LS	1697123.32	5138544.55	11°33'45.38	46°22'17.84	2505.03	526.37
Traverse E	LES-12	LS	1697074.30	5138521.69	11°33'43.05	46°22'17.15	2536.05	557.39

Appendix I. cont.

Location	Sample	Rock Unit	Easting Gauss-Boaga	Northing Gauss-Boaga	Longitude (WGS84)	Latitude (WGS84)	elevation (m)	dip-corrected elevation (m)
Traverse E	LES-13	DOL	1697033.42	5138550.31	11°33'41.19	46°22'18.12	2551.96	573.30
Traverse E	LES-14	DOL	1697009.19	5138605.82	11°33'40.14	46°22'19.94	2579.58	600.92
Traverse E	LES-15	DOL	1696930.00	5138614.33	11°33'36.45	46°22'20.30	2595.08	616.42
Traverse E	LES-16a	LS	1696947.80	5138613.26	11°33'37.28	46°22'20.25	2604.89	626.23
Traverse E	LES-16b	LS	1696947.80	5138613.26	11°33'37.28	46°22'20.25	2605.67	627.01
Traverse F	LFS-1	DOL	1697122.62	5138130.17	11°33'44.72	46°22'04.43	2496.75	518.09
Traverse F	LFS-2	LS	1697067.62	5138133.89	11°33'42.15	46°22'04.61	2511.82	533.16
Traverse F	LFS-3	DOL	1697042.04	5138145.03	11°33'40.97	46°22'04.99	2521.22	542.56
Traverse F	LFS-4	LS	1696997.27	5138124.60	11°33'38.85	46°22'04.38	2530.20	551.54

Notes: DOL, dolomite; LS, limestone; dip-corrected elevation normalized to top of Contrin Formation.

Appendix II. Major element data

Sample	L-1A	L-1C	L-1D	L-1H	L-4A
Mineral	calcite	dolomite	dolomite	calcite	calcite
MgO	0.63 (0.15)	18.92 (0.67)	20.03 (0.27)	0.60 (0.17)	0.54 (0.14)
CaO	55.96 (0.32)	32.43 (0.73)	30.57 (0.30)	55.45 (0.26)	55.51 (0.61)
FeO	0.01 (0.01)	1.20 (0.67)	1.50 (0.16)	0.04 (0.04)	0.02 (0.02)
MnO	0.02 (0.01)	0.04 (0.02)	0.03 (0.01)	0.01 (0.01)	0.01 (0.02)
SrO	0.05 (0.05)	0.05 (0.07)	0.02 (0.03)	0.02 (0.02)	0.02 (0.02)
Sum	56.66	52.64	52.16	56.11	56.11
Ca pfu	0.984 (0.004)	0.543 (0.013)	0.512 (0.005)	0.985 (0.004)	0.986 (0.003)
Mg pfu	0.015 (0.004)	0.441 (0.014)	0.467 (0.006)	0.015 (0.004)	0.013 (0.003)
Fe pfu	$7.1 \cdot 10^{-05}$ ($2.7 \cdot 10^{-04}$)	$1.6 \cdot 10^{-02}$ ($8.8 \cdot 10^{-03}$)	$2.0 \cdot 10^{-02}$ ($2.1 \cdot 10^{-03}$)	$4.6 \cdot 10^{-04}$ ($6.6 \cdot 10^{-04}$)	$2.8 \cdot 10^{-04}$ ($4.7 \cdot 10^{-04}$)
Mn pfu	$7.1 \cdot 10^{-05}$ ($2.6 \cdot 10^{-04}$)	$5.1 \cdot 10^{-04}$ ($3.6 \cdot 10^{-04}$)	$4.1 \cdot 10^{-04}$ ($2.0 \cdot 10^{-04}$)	$7.6 \cdot 10^{-05}$ ($2.8 \cdot 10^{-04}$)	$5.6 \cdot 10^{-05}$ ($2.4 \cdot 10^{-04}$)
Sr pfu	$5.0 \cdot 10^{-04}$ ($5.1 \cdot 10^{-04}$)	$5.1 \cdot 10^{-04}$ ($6.8 \cdot 10^{-04}$)	$1.6 \cdot 10^{-04}$ ($3.0 \cdot 10^{-04}$)	$7.7 \cdot 10^{-05}$ ($2.8 \cdot 10^{-04}$)	$5.7 \cdot 10^{-05}$ ($2.4 \cdot 10^{-04}$)

Sample	L-4B	L-4C	L-4D	L-6A	L-6B
Mineral	calcite	calcite	calcite	dolomite	dolomite
MgO	0.66 (0.23)	0.86 (0.27)	0.71 (0.17)	19.61 (0.78)	19.96 (0.27)
CaO	54.69 (0.36)	54.45 (0.46)	54.66 (0.38)	32.75 (0.78)	30.73 (0.26)
FeO	0.05 (0.05)	0.02 (0.02)	0.04 (0.06)	0.46 (0.16)	1.31 (0.09)
MnO	0.01 (0.01)	0.00 (0.01)	0.02 (0.03)	0.02 (0.02)	0.03 (0.01)
SrO	0.02 (0.03)	0.01 (0.01)	0.03 (0.03)	0.01 (0.01)	0.01 (0.01)
Sum	55.43	55.35	55.47	52.85	52.04
Ca pfu	0.982 (0.006)	0.977 (0.007)	0.980 (0.004)	0.542 (0.015)	0.516 (0.004)
Mg pfu	0.017 (0.006)	0.022 (0.007)	0.018 (0.005)	0.452 (0.015)	0.466 (0.004)
Fe pfu	$7.3 \cdot 10^{-04}$ ($9.9 \cdot 10^{-04}$)	$3.9 \cdot 10^{-04}$ ($5.4 \cdot 10^{-04}$)	$6.9 \cdot 10^{-04}$ ($1.0 \cdot 10^{-03}$)	$5.9 \cdot 10^{-03}$ ($2.1 \cdot 10^{-03}$)	$1.7 \cdot 10^{-02}$ ($1.2 \cdot 10^{-03}$)
Mn pfu	ND	ND	$2.3 \cdot 10^{-04}$ ($4.6 \cdot 10^{-04}$)	$2.5 \cdot 10^{-04}$ ($2.6 \cdot 10^{-04}$)	$3.5 \cdot 10^{-04}$ ($2.4 \cdot 10^{-04}$)
Sr pfu	$1.0 \cdot 10^{-04}$ ($3.3 \cdot 10^{-04}$)	ND	$2.3 \cdot 10^{-04}$ ($4.6 \cdot 10^{-04}$)	$3.6 \cdot 10^{-05}$ ($1.3 \cdot 10^{-04}$)	ND

Appendix II . (cont.)

Sample Mineral	L-7A calcite	L-7A dolomite	L-7B calcite	L-7B dolomite	L-7D calcite
MgO	0.52 (0.09)	18.60 (0.64)	0.68 (0.10)	19.28 (0.19)	0.43 (0.29)
CaO	55.97 (0.23)	33.21 (0.66)	55.71 (0.38)	33.27 (0.40)	55.64 (0.55)
FeO	0.02 (0.01)	0.59 (0.37)	0.02 (0.02)	0.31 (0.08)	0.05 (0.07)
MnO	0.01 (0.01)	0.02 (0.02)	0.00 (0.01)	0.02 (0.02)	0.01 (0.01)
SrO	0.02 (0.01)	0.01 (0.01)	0.02 (0.02)	0.01 (0.01)	0.01 (0.01)
Sum	56.54	52.43	56.43	52.89	56.14
Ca pfu	0.987 (0.002)	0.558 (0.011)	0.983 (0.003)	0.551 (0.005)	0.989 (0.007)
Mg pfu	0.013 (0.002)	0.434 (0.014)	0.017 (0.003)	0.444 (0.005)	0.011 (0.007)
Fe pfu	$6.6 \cdot 10^{-5}$ ($2.6 \cdot 10^{-4}$)	$7.8 \cdot 10^{-3}$ ($4.8 \cdot 10^{-3}$)	$1.2 \cdot 10^{-4}$ ($3.4 \cdot 10^{-4}$)	$4.0 \cdot 10^{-3}$ ($1.1 \cdot 10^{-3}$)	$7.3 \cdot 10^{-4}$ ($1.0 \cdot 10^{-3}$)
Mn pfu	ND	$3.0 \cdot 10^{-4}$ ($3.0 \cdot 10^{-4}$)	ND	$2.0 \cdot 10^{-4}$ ($2.6 \cdot 10^{-4}$)	ND
Sr pfu	ND	$5.0 \cdot 10^{-5}$ ($1.6 \cdot 10^{-4}$)	$6.2 \cdot 10^{-5}$ ($2.5 \cdot 10^{-4}$)	ND	ND

Sample Mineral	L-7F calcite	L-7F dolomite	L-7G dolomite	L-7J calcite	L-7J dolomite
MgO	0.91 (0.58)	20.11 (0.40)	19.43 (0.62)	0.67 (0.09)	19.22 (0.69)
CaO	54.71 (0.74)	30.71 (0.43)	33.02 (0.49)	55.29 (0.26)	33.27 (0.82)
FeO	0.08 (0.04)	1.47 (0.20)	0.16 (0.25)	0.02 (0.01)	0.41 (0.28)
MnO	0.02 (0.02)	0.05 (0.02)	0.01 (0.02)	0.01 (0.01)	0.02 (0.02)
SrO	0.00 (0.01)	0.00 (0.01)	0.01 (0.01)	0.02 (0.02)	0.01 (0.01)
Sum	55.72	52.34	52.64	56.00	52.95
Ca pfu	0.977 (0.014)	0.513 (0.007)	0.542 (0.010)	0.983 (0.002)	0.551 (0.014)
Mg pfu	0.022 (0.014)	0.467 (0.008)	0.456 (0.011)	0.017 (0.002)	0.443 (0.015)
Fe pfu	$9.1 \cdot 10^{-4}$ ($5.4 \cdot 10^{-4}$)	$1.9 \cdot 10^{-2}$ ($2.6 \cdot 10^{-3}$)	$2.3 \cdot 10^{-3}$ ($3.5 \cdot 10^{-3}$)	$1.3 \cdot 10^{-4}$ ($3.5 \cdot 10^{-4}$)	$5.4 \cdot 10^{-3}$ ($3.7 \cdot 10^{-3}$)
Mn pfu	$1.8 \cdot 10^{-4}$ ($4.1 \cdot 10^{-4}$)	$7.1 \cdot 10^{-4}$ ($3.2 \cdot 10^{-4}$)	$1.3 \cdot 10^{-4}$ ($3.0 \cdot 10^{-4}$)	ND	$2.5 \cdot 10^{-4}$ ($2.6 \cdot 10^{-4}$)
Sr pfu	ND	ND	$9.6 \cdot 10^{-5}$ ($2.1 \cdot 10^{-4}$)	ND	$1.1 \cdot 10^{-4}$ ($2.1 \cdot 10^{-4}$)

Appendix II . (cont.)

Sample	L-7K	L-7K	L-7L	L-7M	L-7M
Mineral	calcite	dolomite	dolomite	calcite	dolomite
MgO	0.56 (0.14)	19.32 (0.61)	19.43 (0.56)	0.69 (0.08)	19.26 (0.40)
CaO	55.57 (0.45)	33.00 (0.57)	32.56 (0.62)	55.47 (0.35)	33.32 (0.45)
FeO	0.01 (0.01)	0.41 (0.33)	0.51 (0.31)	0.02 (0.02)	0.34 (0.12)
MnO	0.01 (0.01)	0.02 (0.02)	0.03 (0.02)	0.00 (0.01)	0.01 (0.01)
SrO	0.02 (0.01)	0.01 (0.01)	0.02 (0.01)	0.01 (0.01)	0.02 (0.01)
Sum	56.17	52.77	52.54	56.19	52.95
Ca pfu	0.986 (0.003)	0.548 (0.010)	0.543 (0.011)	0.983 (0.002)	0.552 (0.008)
Mg pfu	0.014 (0.003)	0.446 (0.013)	0.450 (0.011)	0.017 (0.002)	0.444 (0.008)
Fe pfu	$7.2 \cdot 10^{-05}$ ($2.7 \cdot 10^{-04}$)	$5.4 \cdot 10^{-03}$ ($4.4 \cdot 10^{-03}$)	$6.6 \cdot 10^{-03}$ ($4.0 \cdot 10^{-03}$)	$1.4 \cdot 10^{-04}$ ($3.6 \cdot 10^{-04}$)	$4.3 \cdot 10^{-03}$ ($1.6 \cdot 10^{-03}$)
Mn pfu	ND	$3.6 \cdot 10^{-04}$ ($2.5 \cdot 10^{-04}$)	$3.7 \cdot 10^{-04}$ ($3.9 \cdot 10^{-04}$)	ND	$1.4 \cdot 10^{-04}$ ($2.3 \cdot 10^{-04}$)
Sr pfu	ND	$7.2 \cdot 10^{-05}$ ($1.9 \cdot 10^{-04}$)	$6.9 \cdot 10^{-05}$ ($1.8 \cdot 10^{-04}$)	ND	$9.1 \cdot 10^{-05}$ ($2.0 \cdot 10^{-04}$)

Sample	7T-1	7T-1	7T-2	7T-2	7T-3
Mineral	calcite	dolomite	calcite	dolomite	calcite
MgO	0.91 (0.21)	19.49 (0.68)	0.65 (0.21)	19.63 (0.48)	1.13 (0.81)
CaO	54.54 (0.34)	32.47 (0.68)	54.71 (0.41)	32.01 (0.60)	54.84 (0.98)
FeO	0.07 (0.03)	0.32 (0.28)	0.07 (0.03)	0.31 (0.09)	0.06 (0.03)
MnO	0.01 (0.02)	0.03 (0.02)	0.01 (0.01)	0.01 (0.01)	0.01 (0.01)
SrO	0.00 (0.01)	0.01 (0.01)	0.01 (0.02)	0.01 (0.02)	0.01 (0.02)
Sum	55.53	52.32	55.46	51.97	56.05
Ca pfu	0.976 (0.005)	0.543 (0.013)	0.983 (0.005)	0.537 (0.010)	0.972 (0.020)
Mg pfu	0.023 (0.005)	0.453 (0.014)	0.016 (0.005)	0.458 (0.009)	0.028 (0.020)
Fe pfu	$1.0 \cdot 10^{-03}$ ($5.8 \cdot 10^{-04}$)	$4.2 \cdot 10^{-03}$ ($3.6 \cdot 10^{-03}$)	$9.1 \cdot 10^{-04}$ ($3.2 \cdot 10^{-04}$)	$4.1 \cdot 10^{-03}$ ($1.2 \cdot 10^{-03}$)	$6.2 \cdot 10^{-04}$ ($5.0 \cdot 10^{-04}$)
Mn pfu	$1.4 \cdot 10^{-04}$ ($3.8 \cdot 10^{-04}$)	$4.0 \cdot 10^{-04}$ ($3.3 \cdot 10^{-04}$)	ND	$1.1 \cdot 10^{-04}$ ($2.1 \cdot 10^{-04}$)	$1.3 \cdot 10^{-04}$ ($3.4 \cdot 10^{-04}$)
Sr pfu	ND	$8.4 \cdot 10^{-05}$ ($1.9 \cdot 10^{-04}$)	ND	$7.3 \cdot 10^{-05}$ ($1.8 \cdot 10^{-04}$)	ND

Appendix II . (cont.)

Sample	7T-3	7T-4	7T-5	7T-6	7T-7
Mineral	dolomite	dolomite	dolomite	dolomite	dolomite
MgO	19.84 (0.68)	19.68 (0.63)	19.33 (0.23)	19.05 (0.30)	19.21 (0.17)
CaO	31.56 (0.72)	32.51 (0.80)	30.49 (0.28)	30.57 (0.16)	30.49 (0.29)
FeO	0.31 (0.32)	0.32 (0.21)	2.47 (0.19)	2.77 (0.41)	2.52 (0.10)
MnO	0.02 (0.03)	0.02 (0.02)	0.05 (0.02)	0.06 (0.02)	0.06 (0.02)
SrO	0.01 (0.01)	0.03 (0.02)	0.01 (0.01)	0.01 (0.02)	0.02 (0.02)
Sum	51.74	52.56	52.36	52.47	52.30
Ca pfu	0.531 (0.012)	0.540 (0.013)	0.514 (0.004)	0.516 (0.003)	0.515 (0.004)
Mg pfu	0.465 (0.014)	0.455 (0.014)	0.453 (0.005)	0.447 (0.006)	0.451 (0.004)
Fe pfu	$4.0 \cdot 10^{-03}$ ($4.2 \cdot 10^{-03}$)	$4.1 \cdot 10^{-03}$ ($2.8 \cdot 10^{-03}$)	$3.2 \cdot 10^{-02}$ ($2.5 \cdot 10^{-03}$)	$3.6 \cdot 10^{-02}$ ($5.4 \cdot 10^{-03}$)	$3.3 \cdot 10^{-02}$ ($1.3 \cdot 10^{-03}$)
Mn pfu	$2.3 \cdot 10^{-04}$ ($3.4 \cdot 10^{-04}$)	$3.5 \cdot 10^{-04}$ ($3.2 \cdot 10^{-04}$)	$7.5 \cdot 10^{-04}$ ($2.6 \cdot 10^{-04}$)	$7.8 \cdot 10^{-04}$ ($3.4 \cdot 10^{-04}$)	$8.1 \cdot 10^{-04}$ ($3.2 \cdot 10^{-04}$)
Sr pfu	$7.8 \cdot 10^{-05}$ ($1.9 \cdot 10^{-04}$)	$2.4 \cdot 10^{-04}$ ($2.6 \cdot 10^{-04}$)	$6.8 \cdot 10^{-05}$ ($1.8 \cdot 10^{-04}$)	$1.2 \cdot 10^{-04}$ ($2.2 \cdot 10^{-04}$)	$1.0 \cdot 10^{-04}$ ($2.1 \cdot 10^{-04}$)

Sample	7T-8	7T-8	7T-9	7T-9	7T-10
Mineral	calcite	dolomite	calcite	dolomite	calcite
MgO	1.31 (2.47)	19.47 (0.51)	0.68 (0.41)	19.52 (0.44)	1.48 (2.20)
CaO	54.50 (2.39)	32.12 (0.59)	54.85 (0.59)	32.43 (0.56)	54.34 (2.46)
FeO	0.07 (0.05)	0.46 (0.26)	0.03 (0.02)	0.35 (0.35)	0.07 (0.02)
MnO	0.01 (0.02)	0.03 (0.03)	0.01 (0.01)	0.02 (0.02)	0.02 (0.02)
SrO	0.02 (0.02)	0.01 (0.01)	0.01 (0.02)	0.02 (0.02)	0.01 (0.02)
Sum	55.91	52.09	55.59	52.34	55.92
Ca pfu	0.967 (0.058)	0.539 (0.009)	0.983 (0.010)	0.542 (0.009)	0.963 (0.052)
Mg pfu	0.031 (0.058)	0.455 (0.010)	0.017 (0.010)	0.454 (0.009)	0.036 (0.052)
Fe pfu	$1.1 \cdot 10^{-03}$ ($8.3 \cdot 10^{-04}$)	$6.0 \cdot 10^{-03}$ ($3.5 \cdot 10^{-03}$)	$3.3 \cdot 10^{-04}$ ($4.9 \cdot 10^{-04}$)	$4.5 \cdot 10^{-03}$ ($4.7 \cdot 10^{-03}$)	$9.1 \cdot 10^{-04}$ ($3.0 \cdot 10^{-04}$)
Mn pfu	$2.5 \cdot 10^{-04}$ ($4.6 \cdot 10^{-04}$)	$3.1 \cdot 10^{-04}$ ($3.3 \cdot 10^{-04}$)	$8.4 \cdot 10^{-05}$ ($2.9 \cdot 10^{-04}$)	$2.4 \cdot 10^{-04}$ ($3.2 \cdot 10^{-04}$)	$1.8 \cdot 10^{-04}$ ($4.0 \cdot 10^{-04}$)
Sr pfu	ND	$7.9 \cdot 10^{-05}$ ($1.9 \cdot 10^{-04}$)	$8.3 \cdot 10^{-05}$ ($2.9 \cdot 10^{-04}$)	$1.3 \cdot 10^{-04}$ ($2.3 \cdot 10^{-04}$)	ND

Appendix II . (cont.)

Sample	7T-10	7T-11	7T-11	7T-12	7T-13
Mineral	dolomite	calcite	dolomite	dolomite	calcite
MgO	19.54 (0.49)	0.81 (0.29)	19.14 (0.52)	20.09 (0.37)	0.94 (0.21)
CaO	32.26 (0.62)	55.39 (0.47)	32.93 (0.66)	30.83 (0.25)	54.67 (0.57)
FeO	0.31 (0.32)	0.05 (0.03)	0.25 (0.17)	1.22 (0.38)	0.07 (0.09)
MnO	0.02 (0.02)	0.01 (0.02)	0.01 (0.01)	0.05 (0.02)	0.04 (0.04)
SrO	0.02 (0.02)	0.01 (0.01)	0.01 (0.01)	0.00 (0.01)	0.01 (0.01)
Sum	52.15	56.26	52.35	52.20	55.74
Ca pfu	0.540 (0.010)	0.979 (0.007)	0.551 (0.011)	0.516 (0.003)	0.975 (0.007)
Mg pfu	0.455 (0.010)	0.020 (0.007)	0.445 (0.011)	0.468 (0.007)	0.024 (0.005)
Fe pfu	$4.1 \cdot 10^{-03}$ ($4.2 \cdot 10^{-03}$)	$6.2 \cdot 10^{-04}$ ($6.1 \cdot 10^{-04}$)	$3.4 \cdot 10^{-03}$ ($2.3 \cdot 10^{-03}$)	$1.6 \cdot 10^{-02}$ ($5.1 \cdot 10^{-03}$)	$1.0 \cdot 10^{-03}$ ($1.4 \cdot 10^{-03}$)
Mn pfu	$2.2 \cdot 10^{-04}$ ($3.3 \cdot 10^{-04}$)	$1.2 \cdot 10^{-04}$ ($3.4 \cdot 10^{-04}$)	$1.6 \cdot 10^{-04}$ ($2.4 \cdot 10^{-04}$)	$7.0 \cdot 10^{-04}$ ($3.9 \cdot 10^{-04}$)	$5.0 \cdot 10^{-04}$ ($6.8 \cdot 10^{-04}$)
Sr pfu	$1.8 \cdot 10^{-04}$ ($2.5 \cdot 10^{-04}$)	ND	$3.9 \cdot 10^{-05}$ ($1.4 \cdot 10^{-04}$)	$3.9 \cdot 10^{-05}$ ($1.4 \cdot 10^{-04}$)	ND

Sample	7T-13	7T-14	7T-14	7T-15	7T-15
Mineral	dolomite	calcite	dolomite	calcite	dolomite
MgO	19.13 (0.34)	1.01 (1.31)	19.04 (0.16)	0.76 (0.28)	19.20 (0.56)
CaO	30.85 (0.19)	55.36 (1.54)	33.44 (0.47)	55.73 (0.40)	32.85 (0.75)
FeO	1.92 (0.30)	0.03 (0.03)	0.15 (0.16)	0.02 (0.02)	0.33 (0.15)
MnO	0.06 (0.03)	0.01 (0.02)	0.02 (0.02)	0.02 (0.02)	0.02 (0.02)
SrO	0.01 (0.01)	0.01 (0.01)	0.01 (0.01)	0.01 (0.01)	0.00 (0.01)
Sum	51.97	56.43	52.66	56.54	52.40
Ca pfu	0.523 (0.003)	0.975 (0.032)	0.557 (0.005)	0.981 (0.006)	0.549 (0.012)
Mg pfu	0.451 (0.006)	0.025 (0.031)	0.441 (0.005)	0.019 (0.007)	0.446 (0.012)
Fe pfu	$2.5 \cdot 10^{-02}$ ($4.1 \cdot 10^{-03}$)	$4.1 \cdot 10^{-04}$ ($5.0 \cdot 10^{-04}$)	$2.0 \cdot 10^{-03}$ ($2.1 \cdot 10^{-03}$)	$2.8 \cdot 10^{-04}$ ($4.8 \cdot 10^{-04}$)	$4.3 \cdot 10^{-03}$ ($1.9 \cdot 10^{-03}$)
Mn pfu	$7.8 \cdot 10^{-04}$ ($3.9 \cdot 10^{-04}$)	$1.7 \cdot 10^{-04}$ ($3.9 \cdot 10^{-04}$)	$1.7 \cdot 10^{-04}$ ($2.5 \cdot 10^{-04}$)	$1.4 \cdot 10^{-04}$ ($3.7 \cdot 10^{-04}$)	$2.9 \cdot 10^{-04}$ ($3.3 \cdot 10^{-04}$)
Sr pfu	$3.9 \cdot 10^{-05}$ ($1.4 \cdot 10^{-04}$)	ND	$3.4 \cdot 10^{-05}$ ($1.3 \cdot 10^{-04}$)	ND	$3.6 \cdot 10^{-05}$ ($1.4 \cdot 10^{-04}$)

Appendix II . (cont.)

Sample	7T-16	7T-16	7T-17	L-8A	L-8A
Mineral	calcite	dolomite	calcite	calcite	dolomite
MgO	0.66 (0.36)	19.46 (0.91)	0.64 (0.36)	0.37 (0.06)	19.43 (0.39)
CaO	55.35 (0.59)	32.79 (0.82)	55.15 (0.49)	56.30 (0.23)	31.97 (0.35)
FeO	0.03 (0.03)	0.36 (0.30)	0.07 (0.11)	0.03 (0.03)	0.33 (0.17)
MnO	0.01 (0.01)	0.03 (0.03)	0.01 (0.01)	0.01 (0.01)	0.01 (0.01)
SrO	0.01 (0.01)	0.01 (0.01)	0.01 (0.01)	0.02 (0.02)	0.00 (0.00)
Sum	56.05	52.65	55.88	56.72	51.74
Ca pfu	0.983 (0.009)	0.545 (0.016)	0.983 (0.009)	0.991 (0.002)	0.539 (0.007)
Mg pfu	0.016 (0.009)	0.450 (0.017)	0.016 (0.009)	0.009 (0.002)	0.456 (0.008)
Fe pfu	$3.0 \cdot 10^{-04}$ ($6.7 \cdot 10^{-04}$)	$4.6 \cdot 10^{-03}$ ($3.9 \cdot 10^{-03}$)	$9.3 \cdot 10^{-04}$ ($1.6 \cdot 10^{-03}$)	$3.7 \cdot 10^{-04}$ ($5.1 \cdot 10^{-04}$)	$4.4 \cdot 10^{-03}$ ($2.2 \cdot 10^{-03}$)
Mn pfu	ND	$3.6 \cdot 10^{-04}$ ($4.2 \cdot 10^{-04}$)	$7.2 \cdot 10^{-05}$ ($2.7 \cdot 10^{-04}$)	ND	$2.0 \cdot 10^{-04}$ ($2.8 \cdot 10^{-04}$)
Sr pfu	ND	ND	ND	ND	ND

Sample	L-8B	L-8B	L-8D	L-8E	L-8E
Mineral	calcite	dolomite	dolomite	calcite	dolomite
MgO	0.40 (0.05)	19.19 (0.45)	19.86 (0.55)	0.37 (0.04)	19.09 (0.31)
CaO	56.18 (0.27)	32.77 (0.94)	32.00 (0.75)	56.27 (0.35)	33.58 (0.29)
FeO	0.04 (0.02)	0.45 (0.27)	0.38 (0.20)	0.03 (0.01)	0.19 (0.19)
MnO	0.00 (0.00)	0.01 (0.01)	0.02 (0.02)	0.00 (0.00)	0.01 (0.01)
SrO	0.01 (0.01)	0.01 (0.01)	0.01 (0.01)	0.02 (0.02)	0.02 (0.02)
Sum	56.62	52.43	52.27	56.68	52.88
Ca pfu	0.990 (0.001)	0.548 (0.014)	0.534 (0.012)	0.990 (0.002)	0.557 (0.004)
Mg pfu	0.010 (0.001)	0.446 (0.011)	0.461 (0.012)	0.009 (0.001)	0.441 (0.005)
Fe pfu	$5.0 \cdot 10^{-04}$ ($5.4 \cdot 10^{-04}$)	$5.9 \cdot 10^{-03}$ ($3.4 \cdot 10^{-03}$)	$5.0 \cdot 10^{-03}$ ($2.6 \cdot 10^{-03}$)	$4.0 \cdot 10^{-04}$ ($5.4 \cdot 10^{-04}$)	$2.5 \cdot 10^{-03}$ ($2.5 \cdot 10^{-03}$)
Mn pfu	ND	$2.0 \cdot 10^{-04}$ ($2.8 \cdot 10^{-04}$)	$2.4 \cdot 10^{-04}$ ($2.6 \cdot 10^{-04}$)	ND	$1.1 \cdot 10^{-04}$ ($2.2 \cdot 10^{-04}$)
Sr pfu	ND	$1.0 \cdot 10^{-04}$ ($2.3 \cdot 10^{-04}$)	$4.4 \cdot 10^{-05}$ ($1.5 \cdot 10^{-04}$)	ND	$5.6 \cdot 10^{-05}$ ($1.7 \cdot 10^{-04}$)

Appendix II . (cont.)

Sample Mineral	L-8F calcite	L-8F dolomite	L-8H calcite	L-8H dolomite	L-8I calcite
MgO	0.45 (0.14)	18.98 (0.35)	0.43 (0.08)	18.84 (0.44)	0.44 (0.05)
CaO	55.53 (0.58)	33.25 (0.42)	56.17 (0.30)	33.65 (0.58)	55.35 (0.40)
FeO	0.09 (0.27)	0.39 (0.31)	0.03 (0.01)	0.14 (0.05)	0.01 (0.02)
MnO	0.00 (0.01)	0.02 (0.01)	0.01 (0.01)	0.01 (0.01)	0.01 (0.01)
SrO	0.01 (0.01)	0.01 (0.01)	0.01 (0.01)	0.01 (0.01)	0.02 (0.01)
Sum	56.09	52.65	56.64	52.65	55.83
Ca pfu	0.987 (0.006)	0.554 (0.007)	0.989 (0.002)	0.561 (0.009)	0.989 (0.001)
Mg pfu	0.011 (0.003)	0.440 (0.007)	0.010 (0.002)	0.437 (0.009)	0.011 (0.001)
Fe pfu	$1.2 \cdot 10^{-03}$ ($3.6 \cdot 10^{-03}$)	$5.2 \cdot 10^{-03}$ ($4.0 \cdot 10^{-03}$)	$2.8 \cdot 10^{-04}$ ($4.7 \cdot 10^{-04}$)	$1.8 \cdot 10^{-03}$ ($6.2 \cdot 10^{-04}$)	$7.2 \cdot 10^{-05}$ ($2.7 \cdot 10^{-04}$)
Mn pfu	ND	$2.2 \cdot 10^{-04}$ ($2.7 \cdot 10^{-04}$)	ND	$2.5 \cdot 10^{-04}$ ($2.8 \cdot 10^{-04}$)	ND
Sr pfu	ND	$5.6 \cdot 10^{-05}$ ($1.7 \cdot 10^{-04}$)	ND	$8.4 \cdot 10^{-05}$ ($2.1 \cdot 10^{-04}$)	ND

Sample Mineral	L-8I dolomite	L-8L calcite	L-8L dolomite	L-8P calcite	L-8P dolomite
MgO	20.20 (0.80)	0.44 (0.10)	18.71 (0.56)	0.36 (0.06)	19.24 (0.48)
CaO	31.97 (0.91)	56.01 (0.27)	32.84 (1.14)	56.08 (0.27)	33.14 (0.53)
FeO	0.60 (0.37)	0.06 (0.18)	0.65 (0.52)	0.02 (0.02)	0.21 (0.19)
MnO	0.01 (0.01)	0.00 (0.00)	0.02 (0.03)	0.00 (0.01)	0.01 (0.02)
SrO	0.02 (0.01)	0.01 (0.01)	0.01 (0.01)	0.01 (0.01)	0.01 (0.01)
Sum	52.80	56.52	52.24	56.49	52.61
Ca pfu	0.528 (0.017)	0.989 (0.003)	0.553 (0.017)	0.991 (0.001)	0.552 (0.009)
Mg pfu	0.464 (0.015)	0.011 (0.003)	0.438 (0.013)	0.009 (0.002)	0.446 (0.009)
Fe pfu	$7.7 \cdot 10^{-03}$ ($4.7 \cdot 10^{-03}$)	$7.1 \cdot 10^{-04}$ ($2.4 \cdot 10^{-03}$)	$8.6 \cdot 10^{-03}$ ($6.8 \cdot 10^{-03}$)	$2.5 \cdot 10^{-04}$ ($4.4 \cdot 10^{-04}$)	$2.7 \cdot 10^{-03}$ ($2.6 \cdot 10^{-03}$)
Mn pfu	$1.4 \cdot 10^{-04}$ ($2.4 \cdot 10^{-04}$)	ND	$3.1 \cdot 10^{-04}$ ($4.2 \cdot 10^{-04}$)	ND	$1.3 \cdot 10^{-04}$ ($3.0 \cdot 10^{-04}$)
Sr pfu	ND	$7.1 \cdot 10^{-05}$ ($2.7 \cdot 10^{-04}$)	ND	ND	$3.3 \cdot 10^{-05}$ ($1.3 \cdot 10^{-04}$)

Appendix II . (cont.)

Sample	L-8Q	8T-1	8T-1	8T-2	8T-3
Mineral	dolomite	calcite	dolomite	dolomite	dolomite
MgO	19.30 (0.45)	0.60 (0.96)	19.03 (0.51)	19.48 (0.63)	19.64 (0.72)
CaO	32.67 (0.47)	55.92 (1.11)	33.25 (0.39)	32.92 (0.40)	32.87 (1.13)
FeO	0.53 (0.19)	0.02 (0.04)	0.45 (0.33)	0.40 (0.16)	0.32 (0.22)
MnO	0.02 (0.01)	0.01 (0.01)	0.03 (0.03)	0.02 (0.02)	0.01 (0.02)
SrO	0.01 (0.01)	0.02 (0.02)	0.02 (0.01)	0.01 (0.01)	0.01 (0.01)
Sum	52.52	56.57	52.77	52.83	52.86
Ca pfu	0.545 (0.008)	0.985 (0.024)	0.553 (0.010)	0.545 (0.010)	0.544 (0.017)
Mg pfu	0.448 (0.009)	0.014 (0.023)	0.441 (0.008)	0.449 (0.011)	0.452 (0.018)
Fe pfu	$6.9 \cdot 10^{-03}$ ($2.5 \cdot 10^{-03}$)	$1.5 \cdot 10^{-04}$ ($5.4 \cdot 10^{-04}$)	$5.8 \cdot 10^{-03}$ ($4.2 \cdot 10^{-03}$)	$5.2 \cdot 10^{-03}$ ($2.1 \cdot 10^{-03}$)	$4.1 \cdot 10^{-03}$ ($3.0 \cdot 10^{-03}$)
Mn pfu	$2.4 \cdot 10^{-04}$ ($2.6 \cdot 10^{-04}$)	$7.6 \cdot 10^{-05}$ ($2.7 \cdot 10^{-04}$)	$2.5 \cdot 10^{-04}$ ($2.8 \cdot 10^{-04}$)	$3.4 \cdot 10^{-04}$ ($2.5 \cdot 10^{-04}$)	$2.0 \cdot 10^{-04}$ ($2.7 \cdot 10^{-04}$)
Sr pfu	ND	$1.5 \cdot 10^{-04}$ ($3.7 \cdot 10^{-04}$)	$8.4 \cdot 10^{-05}$ ($2.1 \cdot 10^{-04}$)	$4.2 \cdot 10^{-05}$ ($1.4 \cdot 10^{-04}$)	$1.0 \cdot 10^{-04}$ ($2.2 \cdot 10^{-04}$)

Sample	8T-4	8T-4	8T-5	8T-5	8T-6
Mineral	calcite	dolomite	calcite	dolomite	dolomite
MgO	2.78 (4.71)	20.39 (0.58)	1.10 (0.33)	19.77 (0.49)	20.02 (0.83)
CaO	52.98 (5.27)	31.90 (0.53)	55.06 (0.53)	32.57 (0.55)	32.33 (0.80)
FeO	0.06 (0.10)	0.43 (0.20)	0.07 (0.03)	0.56 (0.18)	0.43 (0.30)
MnO	0.03 (0.02)	0.02 (0.02)	0.01 (0.01)	0.02 (0.02)	0.02 (0.03)
SrO	0.01 (0.02)	0.01 (0.02)	0.00 (0.00)	0.00 (0.01)	0.01 (0.02)
Sum	55.85	52.75	56.25	52.92	52.82
Ca pfu	0.933 (0.112)	0.526 (0.010)	0.972 (0.008)	0.538 (0.010)	0.534 (0.015)
Mg pfu	0.066 (0.110)	0.468 (0.011)	0.027 (0.008)	0.454 (0.010)	0.460 (0.017)
Fe pfu	$7.8 \cdot 10^{-04}$ ($1.3 \cdot 10^{-03}$)	$5.6 \cdot 10^{-03}$ ($2.6 \cdot 10^{-03}$)	$1.2 \cdot 10^{-03}$ ($4.5 \cdot 10^{-04}$)	$7.2 \cdot 10^{-03}$ ($2.4 \cdot 10^{-03}$)	$5.5 \cdot 10^{-03}$ ($3.9 \cdot 10^{-03}$)
Mn pfu	$3.9 \cdot 10^{-04}$ ($5.3 \cdot 10^{-04}$)	$2.1 \cdot 10^{-04}$ ($3.2 \cdot 10^{-04}$)	ND	$2.5 \cdot 10^{-04}$ ($2.6 \cdot 10^{-04}$)	$2.8 \cdot 10^{-04}$ ($3.7 \cdot 10^{-04}$)
Sr pfu	ND	$7.1 \cdot 10^{-05}$ ($1.8 \cdot 10^{-04}$)	ND	ND	$1.1 \cdot 10^{-04}$ ($2.2 \cdot 10^{-04}$)

Appendix II . (cont.)

Sample	8T-7	8T-9	8T-10	8T-11	8T-12
Mineral	dolomite	dolomite	dolomite	dolomite	dolomite
MgO	20.99 (0.32)	21.33 (0.16)	19.91 (0.60)	20.28 (0.57)	20.48 (0.71)
CaO	31.02 (0.32)	31.31 (0.28)	32.33 (0.68)	31.81 (0.85)	31.45 (0.58)
FeO	0.71 (0.23)	0.28 (0.08)	0.37 (0.30)	0.46 (0.28)	0.42 (0.14)
MnO	0.02 (0.01)	0.02 (0.02)	0.02 (0.02)	0.02 (0.03)	0.02 (0.01)
SrO	NA	NA	NA	NA	NA
Sum	52.74	52.94	52.63	52.57	52.37
Ca pfu	0.510 (0.005)	0.511 (0.004)	0.536 (0.012)	0.527 (0.013)	0.522 (0.012)
Mg pfu	0.480 (0.007)	0.485 (0.003)	0.459 (0.011)	0.467 (0.012)	0.473 (0.013)
Fe pfu	$9.2 \cdot 10^{-03}$ ($3.0 \cdot 10^{-03}$)	$3.7 \cdot 10^{-03}$ ($9.2 \cdot 10^{-04}$)	$4.8 \cdot 10^{-03}$ ($3.9 \cdot 10^{-03}$)	$6.0 \cdot 10^{-03}$ ($3.5 \cdot 10^{-03}$)	$5.4 \cdot 10^{-03}$ ($1.9 \cdot 10^{-03}$)
Mn pfu	$2.5 \cdot 10^{-04}$ ($2.6 \cdot 10^{-04}$)	$1.7 \cdot 10^{-04}$ ($2.6 \cdot 10^{-04}$)	$2.5 \cdot 10^{-04}$ ($2.6 \cdot 10^{-04}$)	$2.7 \cdot 10^{-04}$ ($4.2 \cdot 10^{-04}$)	$1.7 \cdot 10^{-04}$ ($2.5 \cdot 10^{-04}$)
Sr pfu	NA	NA	NA	NA	NA

Sample	8T-13	8T-14	L-9A	L-9F	L-9F
Mineral	dolomite	dolomite	calcite	calcite	dolomite
MgO	20.28 (0.49)	21.30 (0.17)	0.48 (0.14)	0.47 (0.06)	18.58 (1.19)
CaO	32.02 (0.54)	31.11 (0.35)	55.91 (0.28)	55.58 (0.29)	33.09 (1.13)
FeO	0.53 (0.23)	0.24 (0.14)	0.02 (0.01)	0.02 (0.02)	0.22 (0.13)
MnO	0.02 (0.01)	0.00 (0.01)	0.00 (0.00)	0.01 (0.01)	0.02 (0.02)
SrO	0.01 (0.01)	0.01 (0.01)	0.02 (0.01)	0.02 (0.01)	0.01 (0.01)
Sum	52.85	52.67	56.43	56.10	51.92
Ca pfu	0.528 (0.010)	0.511 (0.004)	0.988 (0.003)	0.988 (0.001)	0.560 (0.025)
Mg pfu	0.465 (0.010)	0.486 (0.003)	0.012 (0.003)	0.012 (0.001)	0.437 (0.024)
Fe pfu	$6.9 \cdot 10^{-03}$ ($3.0 \cdot 10^{-03}$)	$3.0 \cdot 10^{-03}$ ($1.8 \cdot 10^{-03}$)	ND	$1.9 \cdot 10^{-04}$ ($4.0 \cdot 10^{-04}$)	$3.0 \cdot 10^{-03}$ ($1.6 \cdot 10^{-03}$)
Mn pfu	$2.7 \cdot 10^{-04}$ ($2.6 \cdot 10^{-04}$)	$3.6 \cdot 10^{-05}$ ($1.3 \cdot 10^{-04}$)	ND	ND	$3.1 \cdot 10^{-04}$ ($2.6 \cdot 10^{-04}$)
Sr pfu	$7.7 \cdot 10^{-05}$ ($1.9 \cdot 10^{-04}$)	ND	ND	ND	ND

Appendix II . (cont.)

Sample Mineral	L-11A calcite	L-11A dolomite	L-11C dolomite	L-11E dolomite	L-11F calcite
MgO	0.35 (0.09)	19.07 (0.40)	20.81 (0.25)	19.78 (0.29)	0.31 (0.10)
CaO	55.50 (0.30)	32.52 (0.69)	30.92 (0.23)	32.74 (0.36)	55.57 (0.25)
FeO	0.04 (0.05)	0.75 (0.55)	0.73 (0.12)	0.28 (0.09)	0.03 (0.04)
MnO	0.01 (0.01)	0.03 (0.02)	0.02 (0.01)	0.01 (0.01)	0.01 (0.01)
SrO	0.01 (0.01)	0.01 (0.01)	0.01 (0.01)	0.01 (0.02)	0.01 (0.01)
Sum	55.91	52.39	52.48	52.83	55.93
Ca pfu	0.991 (0.002)	0.545 (0.010)	0.511 (0.004)	0.541 (0.006)	0.992 (0.002)
Mg pfu	0.009 (0.002)	0.445 (0.008)	0.479 (0.004)	0.455 (0.006)	0.008 (0.002)
Fe pfu	$5.3 \cdot 10^{-04}$ ($8.3 \cdot 10^{-04}$)	$9.8 \cdot 10^{-03}$ ($7.3 \cdot 10^{-03}$)	$9.4 \cdot 10^{-03}$ ($1.5 \cdot 10^{-03}$)	$3.6 \cdot 10^{-03}$ ($1.2 \cdot 10^{-03}$)	$4.4 \cdot 10^{-04}$ ($7.3 \cdot 10^{-04}$)
Mn pfu	$6.7 \cdot 10^{-05}$ ($2.6 \cdot 10^{-04}$)	$3.8 \cdot 10^{-04}$ ($2.9 \cdot 10^{-04}$)	$2.5 \cdot 10^{-04}$ ($2.6 \cdot 10^{-04}$)	$1.3 \cdot 10^{-04}$ ($2.3 \cdot 10^{-04}$)	$6.3 \cdot 10^{-05}$ ($2.5 \cdot 10^{-04}$)
Sr pfu	ND	$3.2 \cdot 10^{-05}$ ($1.3 \cdot 10^{-04}$)	ND	$8.4 \cdot 10^{-05}$ ($2.0 \cdot 10^{-04}$)	$6.2 \cdot 10^{-05}$ ($2.5 \cdot 10^{-04}$)

Sample Mineral	L-11F dolomite	L-11G dolomite	L-11H calcite	L-11H dolomite	L-12A dolomite
MgO	19.25 (0.77)	20.60 (0.20)	0.40 (0.12)	18.91 (0.31)	19.66 (0.62)
CaO	32.83 (0.83)	30.78 (0.28)	55.50 (0.33)	32.99 (0.24)	32.51 (0.56)
FeO	0.30 (0.23)	0.75 (0.07)	0.03 (0.03)	0.33 (0.18)	0.20 (0.11)
MnO	0.02 (0.02)	0.03 (0.01)	0.01 (0.01)	0.02 (0.02)	0.01 (0.01)
SrO	0.01 (0.01)	0.00 (0.01)	0.02 (0.02)	0.01 (0.01)	0.01 (0.01)
Sum	52.41	52.17	55.95	52.27	52.39
Ca pfu	0.548 (0.015)	0.513 (0.004)	0.990 (0.003)	0.554 (0.005)	0.542 (0.011)
Mg pfu	0.447 (0.016)	0.477 (0.004)	0.010 (0.003)	0.442 (0.005)	0.456 (0.011)
Fe pfu	$3.9 \cdot 10^{-03}$ ($3.1 \cdot 10^{-03}$)	$9.7 \cdot 10^{-03}$ ($9.9 \cdot 10^{-04}$)	$2.7 \cdot 10^{-04}$ ($5.9 \cdot 10^{-04}$)	$4.3 \cdot 10^{-03}$ ($2.4 \cdot 10^{-03}$)	$2.7 \cdot 10^{-03}$ ($1.4 \cdot 10^{-03}$)
Mn pfu	$2.5 \cdot 10^{-04}$ ($3.1 \cdot 10^{-04}$)	$3.8 \cdot 10^{-04}$ ($2.3 \cdot 10^{-04}$)	ND	$1.9 \cdot 10^{-04}$ ($2.6 \cdot 10^{-04}$)	$1.1 \cdot 10^{-04}$ ($2.1 \cdot 10^{-04}$)
Sr pfu	$1.0 \cdot 10^{-04}$ ($2.1 \cdot 10^{-04}$)	ND	$6.7 \cdot 10^{-05}$ ($2.6 \cdot 10^{-04}$)	$6.3 \cdot 10^{-05}$ ($1.8 \cdot 10^{-04}$)	$3.6 \cdot 10^{-05}$ ($1.4 \cdot 10^{-04}$)

Appendix II . (cont.)

Sample Mineral	L-12B dolomite	L-12D calcite	L-12D dolomite	L-12F calcite	L-12F dolomite
MgO	19.40 (0.56)	0.47 (0.11)	19.13 (0.35)	0.50 (0.08)	19.16 (0.41)
CaO	32.94 (0.74)	55.43 (0.30)	32.85 (0.62)	55.75 (0.34)	33.24 (0.70)
FeO	0.28 (0.20)	0.02 (0.02)	0.35 (0.38)	0.03 (0.02)	0.20 (0.13)
MnO	0.01 (0.01)	0.00 (0.01)	0.01 (0.02)	0.01 (0.01)	0.01 (0.01)
SrO	0.01 (0.01)	0.01 (0.02)	0.01 (0.01)	0.02 (0.02)	0.01 (0.01)
Sum	52.64	55.94	52.35	56.31	52.62
Ca pfu	0.548 (0.012)	0.988 (0.003)	0.550 (0.009)	0.987 (0.002)	0.553 (0.010)
Mg pfu	0.449 (0.012)	0.012 (0.003)	0.445 (0.007)	0.012 (0.002)	0.444 (0.010)
Fe pfu	$3.7 \cdot 10^{-03}$ ($2.6 \cdot 10^{-03}$)	$2.1 \cdot 10^{-04}$ ($4.3 \cdot 10^{-04}$)	$4.6 \cdot 10^{-03}$ ($5.0 \cdot 10^{-03}$)	$3.1 \cdot 10^{-04}$ ($4.8 \cdot 10^{-04}$)	$2.6 \cdot 10^{-03}$ ($1.7 \cdot 10^{-03}$)
Mn pfu	$1.7 \cdot 10^{-04}$ ($2.5 \cdot 10^{-04}$)	$7.1 \cdot 10^{-05}$ ($2.7 \cdot 10^{-04}$)	$1.7 \cdot 10^{-04}$ ($2.5 \cdot 10^{-04}$)	ND	$3.4 \cdot 10^{-05}$ ($1.3 \cdot 10^{-04}$)
Sr pfu	$3.4 \cdot 10^{-05}$ ($1.3 \cdot 10^{-04}$)	ND	$3.3 \cdot 10^{-05}$ ($1.3 \cdot 10^{-04}$)	$6.2 \cdot 10^{-05}$ ($2.5 \cdot 10^{-04}$)	$3.4 \cdot 10^{-05}$ ($1.3 \cdot 10^{-04}$)

Sample Mineral	L-12H dolomite	L-12J calcite	L-12J dolomite	L-13A calcite	L-13A dolomite
MgO	19.89 (0.49)	0.58 (0.06)	19.34 (0.63)	2.78 (2.86)	20.19 (0.69)
CaO	32.32 (0.75)	55.43 (0.20)	32.66 (0.98)	53.41 (2.94)	31.27 (0.62)
FeO	0.15 (0.11)	0.02 (0.02)	0.39 (0.18)	0.08 (0.06)	0.68 (0.34)
MnO	0.01 (0.01)	0.01 (0.01)	0.01 (0.01)	0.01 (0.01)	0.04 (0.03)
SrO	0.01 (0.01)	0.01 (0.01)	0.01 (0.01)	0.01 (0.01)	0.01 (0.01)
Sum	52.38	56.04	52.41	56.29	52.19
Ca pfu	0.537 (0.012)	0.986 (0.001)	0.545 (0.016)	0.932 (0.067)	0.522 (0.012)
Mg pfu	0.460 (0.011)	0.014 (0.001)	0.449 (0.014)	0.067 (0.066)	0.469 (0.013)
Fe pfu	$2.0 \cdot 10^{-03}$ ($1.4 \cdot 10^{-03}$)	$2.1 \cdot 10^{-04}$ ($4.2 \cdot 10^{-04}$)	$5.1 \cdot 10^{-03}$ ($2.4 \cdot 10^{-03}$)	$9.8 \cdot 10^{-04}$ ($8.7 \cdot 10^{-04}$)	$8.9 \cdot 10^{-03}$ ($4.5 \cdot 10^{-03}$)
Mn pfu	$1.3 \cdot 10^{-04}$ ($2.3 \cdot 10^{-04}$)	ND	$1.2 \cdot 10^{-04}$ ($2.2 \cdot 10^{-04}$)	ND	$5.7 \cdot 10^{-04}$ ($4.2 \cdot 10^{-04}$)
Sr pfu	$9.4 \cdot 10^{-05}$ ($2.0 \cdot 10^{-04}$)	ND	$7.8 \cdot 10^{-05}$ ($1.9 \cdot 10^{-04}$)	ND	ND

Appendix II . (cont.)

Sample Mineral	L-13B dolomite	L-13E calcite	L-13E dolomite	L-13F dolomite	LAS-1 calcite
MgO	20.79 (0.26)	0.75 (0.73)	19.55 (0.78)	20.13 (0.33)	0.43 (0.09)
CaO	30.72 (0.31)	55.58 (0.95)	32.21 (0.55)	31.00 (0.40)	55.99 (0.36)
FeO	0.47 (0.21)	0.03 (0.02)	0.32 (0.13)	1.14 (0.34)	0.02 (0.02)
MnO	0.03 (0.02)	0.02 (0.02)	0.03 (0.02)	0.03 (0.02)	0.01 (0.01)
SrO	0.00 (0.01)	0.02 (0.02)	0.01 (0.01)	0.01 (0.01)	0.02 (0.03)
Sum	52.01	56.40	52.12	52.31	56.47
Ca pfu	0.512 (0.004)	0.981 (0.018)	0.540 (0.013)	0.517 (0.005)	0.989 (0.003)
Mg pfu	0.482 (0.005)	0.018 (0.018)	0.456 (0.014)	0.467 (0.005)	0.011 (0.002)
Fe pfu	$6.1 \cdot 10^{-03}$ ($2.8 \cdot 10^{-03}$)	$3.3 \cdot 10^{-04}$ ($4.9 \cdot 10^{-04}$)	$4.2 \cdot 10^{-03}$ ($1.7 \cdot 10^{-03}$)	$1.5 \cdot 10^{-02}$ ($4.4 \cdot 10^{-03}$)	$1.5 \cdot 10^{-04}$ ($3.7 \cdot 10^{-04}$)
Mn pfu	$3.6 \cdot 10^{-04}$ ($3.7 \cdot 10^{-04}$)	$1.6 \cdot 10^{-04}$ ($3.8 \cdot 10^{-04}$)	$4.1 \cdot 10^{-04}$ ($3.9 \cdot 10^{-04}$)	$3.8 \cdot 10^{-04}$ ($2.9 \cdot 10^{-04}$)	ND
Sr pfu	ND	$8.3 \cdot 10^{-05}$ ($2.9 \cdot 10^{-04}$)	$3.3 \cdot 10^{-05}$ ($1.3 \cdot 10^{-04}$)	$6.3 \cdot 10^{-05}$ ($1.7 \cdot 10^{-04}$)	$1.5 \cdot 10^{-04}$ ($3.7 \cdot 10^{-04}$)

Sample Mineral	LAS-1 dolomite	LAS-5 dolomite	LAS-6 calcite	LAS-6 dolomite	LAS-7 calcite
MgO	19.34 (0.31)	21.02 (0.22)	0.54 (0.08)	19.42 (0.50)	0.26 (0.10)
CaO	32.86 (0.50)	30.92 (0.34)	56.09 (0.31)	32.54 (0.85)	56.31 (0.22)
FeO	0.61 (0.24)	0.36 (0.06)	0.01 (0.01)	0.48 (0.38)	0.03 (0.03)
MnO	0.04 (0.02)	0.02 (0.02)	0.01 (0.01)	0.01 (0.01)	0.01 (0.01)
SrO	0.01 (0.01)	0.01 (0.01)	0.03 (0.02)	0.01 (0.01)	0.01 (0.01)
Sum	52.86	52.32	56.67	52.46	56.62
Ca pfu	0.545 (0.007)	0.511 (0.005)	0.987 (0.002)	0.543 (0.013)	0.994 (0.002)
Mg pfu	0.446 (0.006)	0.484 (0.005)	0.013 (0.002)	0.451 (0.011)	0.006 (0.002)
Fe pfu	$8.0 \cdot 10^{-03}$ ($3.2 \cdot 10^{-03}$)	$4.7 \cdot 10^{-03}$ ($7.3 \cdot 10^{-04}$)	$8.2 \cdot 10^{-05}$ ($2.9 \cdot 10^{-04}$)	$6.2 \cdot 10^{-03}$ ($4.8 \cdot 10^{-03}$)	$1.1 \cdot 10^{-04}$ ($3.3 \cdot 10^{-04}$)
Mn pfu	$5.5 \cdot 10^{-04}$ ($1.6 \cdot 10^{-04}$)	$1.6 \cdot 10^{-04}$ ($2.4 \cdot 10^{-04}$)	ND	ND	ND
Sr pfu	$5.0 \cdot 10^{-05}$ ($1.6 \cdot 10^{-04}$)	ND	$8.3 \cdot 10^{-05}$ ($2.9 \cdot 10^{-04}$)	$6.3 \cdot 10^{-05}$ ($1.7 \cdot 10^{-04}$)	ND

Appendix II . (cont.)

Sample Mineral	LAS-7 dolomite	LAS-14 calcite	LAS-15 dolomite	LAS-17 calcite	LAS-24 dolomite
MgO	19.24 (0.45)	0.57 (0.16)	20.15 (0.63)	0.66 (0.18)	20.28 (0.66)
CaO	33.18 (0.64)	55.11 (0.43)	31.88 (0.72)	55.98 (0.35)	31.52 (0.81)
FeO	0.39 (0.38)	0.02 (0.01)	0.50 (0.35)	0.02 (0.01)	0.47 (0.11)
MnO	0.02 (0.03)	0.01 (0.01)	0.02 (0.02)	0.00 (0.01)	0.03 (0.02)
SrO	0.01 (0.01)	0.01 (0.02)	0.01 (0.01)	0.01 (0.01)	0.01 (0.01)
Sum	52.84	55.72	52.55	56.67	52.30
Ca pfu	0.551 (0.010)	0.986 (0.004)	0.528 (0.012)	0.984 (0.004)	0.524 (0.014)
Mg pfu	0.444 (0.009)	0.014 (0.004)	0.465 (0.013)	0.016 (0.004)	0.469 (0.014)
Fe pfu	$5.0 \cdot 10^{-03}$ ($5.0 \cdot 10^{-03}$)	$1.5 \cdot 10^{-04}$ ($3.8 \cdot 10^{-04}$)	$6.5 \cdot 10^{-03}$ ($4.6 \cdot 10^{-03}$)	ND	$6.1 \cdot 10^{-03}$ ($1.5 \cdot 10^{-03}$)
Mn pfu	$2.5 \cdot 10^{-04}$ ($3.7 \cdot 10^{-04}$)	ND	$2.5 \cdot 10^{-04}$ ($3.2 \cdot 10^{-04}$)	ND	$3.8 \cdot 10^{-04}$ ($2.9 \cdot 10^{-04}$)
Sr pfu	$6.3 \cdot 10^{-05}$ ($1.7 \cdot 10^{-04}$)	ND	$6.3 \cdot 10^{-05}$ ($1.7 \cdot 10^{-04}$)	ND	ND

Sample Mineral	LAS-26 calcite	LAS-27 dolomite	LAS-31 calcite	LAS-34 calcite	LAS-34 dolomite
MgO	0.73 (0.19)	21.70 (0.31)	0.76 (0.16)	2.38 (2.95)	20.18 (0.52)
CaO	55.46 (0.49)	30.65 (0.28)	55.67 (0.35)	53.28 (3.13)	32.20 (0.32)
FeO	0.05 (0.03)	0.48 (0.11)	0.02 (0.02)	0.05 (0.03)	0.56 (0.41)
MnO	0.00 (0.01)	0.03 (0.01)	0.00 (0.01)	0.01 (0.01)	0.04 (0.02)
SrO	0.03 (0.01)	0.01 (0.02)	0.02 (0.02)	0.02 (0.01)	0.01 (0.01)
Sum	56.28	52.87	56.47	55.75	52.99
Ca pfu	0.981 (0.004)	0.500 (0.005)	0.981 (0.004)	0.942 (0.070)	0.530 (0.007)
Mg pfu	0.018 (0.004)	0.493 (0.005)	0.019 (0.004)	0.057 (0.070)	0.462 (0.010)
Fe pfu	$7.2 \cdot 10^{-04}$ ($6.4 \cdot 10^{-04}$)	$6.1 \cdot 10^{-03}$ ($1.5 \cdot 10^{-03}$)	$1.9 \cdot 10^{-04}$ ($4.0 \cdot 10^{-04}$)	$6.6 \cdot 10^{-04}$ ($6.4 \cdot 10^{-04}$)	$7.2 \cdot 10^{-03}$ ($5.3 \cdot 10^{-03}$)
Mn pfu	ND	$5.0 \cdot 10^{-04}$ ($1.9 \cdot 10^{-06}$)	ND	ND	$5.0 \cdot 10^{-04}$ ($3.2 \cdot 10^{-04}$)
Sr pfu	ND	$4.6 \cdot 10^{-05}$ ($1.5 \cdot 10^{-04}$)	ND	ND	ND

Appendix II . (cont.)

Sample	LAS-35	LAS-37	LAS-39	LAS-41	LAS-43
Mineral	calcite	dolomite	calcite	dolomite	dolomite
MgO	0.68 (0.17)	19.65 (0.52)	0.47 (0.07)	19.86 (0.26)	21.20 (0.21)
CaO	55.79 (0.37)	32.45 (0.74)	55.27 (0.29)	32.52 (0.55)	30.56 (0.29)
FeO	0.02 (0.02)	0.64 (0.21)	0.03 (0.02)	0.32 (0.21)	1.13 (0.15)
MnO	0.01 (0.01)	0.02 (0.01)	0.01 (0.01)	0.02 (0.01)	0.03 (0.02)
SrO	0.02 (0.01)	0.01 (0.01)	0.02 (0.01)	0.01 (0.01)	0.00 (0.00)
Sum	56.52	52.77	55.80	52.72	52.92
Ca pfu	0.983 (0.004)	0.538 (0.013)	0.988 (0.002)	0.538 (0.007)	0.501 (0.004)
Mg pfu	0.017 (0.004)	0.453 (0.012)	0.012 (0.002)	0.457 (0.006)	0.484 (0.004)
Fe pfu	1.2·10 ⁻⁰⁴ (3.4·10 ⁻⁰⁴)	8.3·10 ⁻⁰³ (2.7·10 ⁻⁰³)	3.1·10 ⁻⁰⁴ (4.8·10 ⁻⁰⁴)	4.1·10 ⁻⁰³ (2.7·10 ⁻⁰³)	1.5·10 ⁻⁰² (2.0·10 ⁻⁰³)
Mn pfu	ND	3.4·10 ⁻⁰⁴ (2.5·10 ⁻⁰⁴)	ND	2.5·10 ⁻⁰⁴ (2.6·10 ⁻⁰⁴)	4.2·10 ⁻⁰⁴ (2.9·10 ⁻⁰⁴)
Sr pfu	ND	3.4·10 ⁻⁰⁵ (1.3·10 ⁻⁰⁴)	ND	7.2·10 ⁻⁰⁵ (1.8·10 ⁻⁰⁴)	ND

Sample	LAS-45	LAS-45	LAS-46	LAS-50	LAS-50
Mineral	calcite	dolomite	dolomite	calcite	dolomite
MgO	0.30 (0.11)	20.29 (0.90)	20.09 (0.24)	0.54 (0.22)	19.74 (0.38)
CaO	56.05 (0.35)	31.35 (0.86)	31.05 (0.22)	56.22 (0.28)	32.87 (0.73)
FeO	0.05 (0.03)	0.82 (0.35)	1.45 (0.18)	0.02 (0.02)	0.30 (0.28)
MnO	0.01 (0.02)	0.05 (0.03)	0.04 (0.02)	0.00 (0.01)	0.01 (0.01)
SrO	0.01 (0.02)	0.01 (0.01)	0.01 (0.01)	0.02 (0.02)	0.01 (0.01)
Sum	56.43	52.52	52.64	56.81	52.93
Ca pfu	0.992 (0.003)	0.520 (0.017)	0.516 (0.004)	0.987 (0.005)	0.543 (0.012)
Mg pfu	0.007 (0.003)	0.468 (0.017)	0.465 (0.004)	0.013 (0.005)	0.453 (0.009)
Fe pfu	8.6·10 ⁻⁰⁴ (6.4·10 ⁻⁰⁴)	1.1·10 ⁻⁰² (4.7·10 ⁻⁰³)	1.9·10 ⁻⁰² (2.4·10 ⁻⁰³)	1.4·10 ⁻⁰⁴ (3.6·10 ⁻⁰⁴)	3.9·10 ⁻⁰³ (3.6·10 ⁻⁰³)
Mn pfu	6.6·10 ⁻⁰⁵ (2.6·10 ⁻⁰⁴)	6.7·10 ⁻⁰⁴ (5.2·10 ⁻⁰⁴)	5.4·10 ⁻⁰⁴ (3.0·10 ⁻⁰⁴)	ND	9.1·10 ⁻⁰⁵ (2.0·10 ⁻⁰⁴)
Sr pfu	ND	ND	3.4·10 ⁻⁰⁵ (1.3·10 ⁻⁰⁴)	ND	ND

Appendix II . (cont.)

Sample	LAS-51	LAS-53	LAS-54	LAS-55	LAS-56
Mineral	dolomite	dolomite	dolomite	dolomite	dolomite
MgO	21.27 (0.28)	20.87 (0.42)	20.63 (0.65)	20.24 (0.24)	20.04 (0.18)
CaO	30.83 (0.17)	30.58 (0.60)	30.46 (0.49)	30.05 (0.39)	30.03 (0.28)
FeO	0.65 (0.16)	0.72 (0.17)	1.00 (0.58)	1.71 (0.15)	2.31 (0.23)
MnO	0.02 (0.01)	0.03 (0.02)	0.03 (0.02)	0.07 (0.02)	0.08 (0.02)
SrO	0.01 (0.01)	0.01 (0.02)	0.01 (0.01)	0.01 (0.01)	0.01 (0.01)
Sum	52.77	52.21	52.13	52.08	52.47
Ca pfu	0.506 (0.003)	0.508 (0.007)	0.503 (0.008)	0.504 (0.005)	0.502 (0.003)
Mg pfu	0.486 (0.004)	0.482 (0.008)	0.483 (0.013)	0.472 (0.005)	0.466 (0.004)
Fe pfu	$8.3 \cdot 10^{-03}$ ($2.2 \cdot 10^{-03}$)	$9.3 \cdot 10^{-03}$ ($2.2 \cdot 10^{-03}$)	$1.4 \cdot 10^{-02}$ ($8.3 \cdot 10^{-03}$)	$2.2 \cdot 10^{-02}$ ($1.9 \cdot 10^{-03}$)	$3.0 \cdot 10^{-02}$ ($3.0 \cdot 10^{-03}$)
Mn pfu	$2.8 \cdot 10^{-04}$ ($2.6 \cdot 10^{-04}$)	$4.1 \cdot 10^{-04}$ ($3.1 \cdot 10^{-04}$)	$3.9 \cdot 10^{-04}$ ($3.0 \cdot 10^{-04}$)	$9.4 \cdot 10^{-04}$ ($3.9 \cdot 10^{-04}$)	$9.4 \cdot 10^{-04}$ ($3.9 \cdot 10^{-04}$)
Sr pfu	$6.3 \cdot 10^{-05}$ ($1.7 \cdot 10^{-04}$)	$4.5 \cdot 10^{-05}$ ($1.5 \cdot 10^{-04}$)	$7.0 \cdot 10^{-05}$ ($1.8 \cdot 10^{-04}$)	$3.6 \cdot 10^{-05}$ ($1.4 \cdot 10^{-04}$)	$3.6 \cdot 10^{-05}$ ($1.4 \cdot 10^{-04}$)

Sample	LAS-57	LBS-1	LBS-4	LBS-4	LBS-5
Mineral	dolomite	dolomite	calcite	dolomite	dolomite
MgO	20.94 (0.54)	19.53 (0.33)	0.50 (0.15)	18.90 (0.66)	19.75 (0.67)
CaO	30.92 (0.48)	32.70 (0.44)	55.69 (0.29)	33.01 (0.20)	31.52 (0.64)
FeO	0.88 (0.92)	0.24 (0.15)	0.02 (0.02)	0.23 (0.25)	0.85 (0.57)
MnO	0.03 (0.03)	0.01 (0.01)	0.01 (0.01)	0.01 (0.01)	0.03 (0.02)
SrO	0.01 (0.01)	0.01 (0.01)	0.02 (0.01)	0.00 (0.01)	0.01 (0.01)
Sum	52.79	52.49	56.23	52.15	52.16
Ca pfu	0.509 (0.005)	0.544 (0.007)	0.987 (0.004)	0.555 (0.008)	0.528 (0.011)
Mg pfu	0.479 (0.009)	0.452 (0.007)	0.012 (0.004)	0.442 (0.010)	0.460 (0.014)
Fe pfu	$1.1 \cdot 10^{-02}$ ($1.2 \cdot 10^{-02}$)	$3.2 \cdot 10^{-03}$ ($2.0 \cdot 10^{-03}$)	$1.3 \cdot 10^{-04}$ ($3.5 \cdot 10^{-04}$)	$3.1 \cdot 10^{-03}$ ($3.4 \cdot 10^{-03}$)	$1.1 \cdot 10^{-02}$ ($7.6 \cdot 10^{-03}$)
Mn pfu	$4.4 \cdot 10^{-04}$ ($5.3 \cdot 10^{-04}$)	$1.6 \cdot 10^{-04}$ ($2.4 \cdot 10^{-04}$)	ND	$1.0 \cdot 10^{-04}$ ($2.3 \cdot 10^{-04}$)	$3.5 \cdot 10^{-04}$ ($3.6 \cdot 10^{-04}$)
Sr pfu	$3.4 \cdot 10^{-05}$ ($1.3 \cdot 10^{-04}$)	$6.3 \cdot 10^{-05}$ ($1.7 \cdot 10^{-04}$)	$6.7 \cdot 10^{-05}$ ($2.6 \cdot 10^{-04}$)	ND	$6.3 \cdot 10^{-05}$ ($1.7 \cdot 10^{-04}$)

Appendix II . (cont.)

Sample Mineral	LBS-9 calcite	LBS-9 dolomite	LBS-12 calcite	LBS-12 dolomite	LBS-15 calcite
MgO	0.66 (0.21)	20.15 (0.67)	0.60 (0.10)	19.37 (0.64)	0.63 (0.09)
CaO	55.39 (0.36)	31.68 (0.85)	55.72 (0.30)	33.03 (0.65)	55.37 (0.36)
FeO	0.06 (0.02)	0.46 (0.26)	0.02 (0.02)	0.50 (0.16)	0.02 (0.02)
MnO	0.01 (0.01)	0.03 (0.01)	0.00 (0.01)	0.01 (0.01)	0.00 (0.01)
SrO	0.06 (0.06)	0.03 (0.04)	0.01 (0.01)	0.01 (0.01)	0.04 (0.05)
Sum	56.17	52.35	56.36	52.92	56.06
Ca pfu	0.983 (0.005)	0.527 (0.014)	0.985 (0.002)	0.547 (0.013)	0.984 (0.002)
Mg pfu	0.016 (0.005)	0.466 (0.014)	0.015 (0.003)	0.446 (0.012)	0.016 (0.002)
Fe pfu	$8.0 \cdot 10^{-04}$ ($4.2 \cdot 10^{-04}$)	$6.0 \cdot 10^{-03}$ ($3.4 \cdot 10^{-03}$)	$1.9 \cdot 10^{-04}$ ($4.0 \cdot 10^{-04}$)	$6.5 \cdot 10^{-03}$ ($2.1 \cdot 10^{-03}$)	$1.2 \cdot 10^{-04}$ ($3.4 \cdot 10^{-04}$)
Mn pfu	ND	$3.5 \cdot 10^{-04}$ ($2.4 \cdot 10^{-04}$)	ND	$8.4 \cdot 10^{-05}$ ($2.1 \cdot 10^{-04}$)	ND
Sr pfu	$5.0 \cdot 10^{-04}$ ($7.0 \cdot 10^{-04}$)	$2.8 \cdot 10^{-04}$ ($4.1 \cdot 10^{-04}$)	ND	$8.4 \cdot 10^{-05}$ ($2.1 \cdot 10^{-04}$)	$3.1 \cdot 10^{-04}$ ($4.8 \cdot 10^{-04}$)

Sample Mineral	LBS-15 dolomite	LCS-1 calcite	LCS-6 calcite	LCS-8 calcite	LCS-8 dolomite
MgO	19.08 (0.41)	0.42 (0.04)	0.37 (0.09)	0.82 (0.70)	20.24 (0.80)
CaO	32.67 (0.72)	56.34 (0.19)	56.26 (0.29)	55.35 (1.10)	31.97 (1.03)
FeO	0.46 (0.37)	0.01 (0.01)	0.03 (0.02)	0.05 (0.02)	0.41 (0.21)
MnO	0.02 (0.01)	0.01 (0.01)	0.00 (0.01)	0.01 (0.01)	0.02 (0.01)
SrO	0.03 (0.03)	0.02 (0.01)	0.02 (0.02)	0.01 (0.01)	0.01 (0.01)
Sum	52.25	56.80	56.69	56.24	52.64
Ca pfu	0.548 (0.011)	0.990 (0.001)	0.990 (0.002)	0.979 (0.017)	0.529 (0.018)
Mg pfu	0.445 (0.009)	0.010 (0.001)	0.009 (0.002)	0.020 (0.017)	0.466 (0.017)
Fe pfu	$5.9 \cdot 10^{-03}$ ($4.8 \cdot 10^{-03}$)	ND	$3.8 \cdot 10^{-04}$ ($5.0 \cdot 10^{-04}$)	$7.9 \cdot 10^{-04}$ ($4.4 \cdot 10^{-04}$)	$5.3 \cdot 10^{-03}$ ($2.8 \cdot 10^{-03}$)
Mn pfu	$3.0 \cdot 10^{-04}$ ($2.6 \cdot 10^{-04}$)	ND	ND	ND	$2.0 \cdot 10^{-04}$ ($2.5 \cdot 10^{-04}$)
Sr pfu	$2.5 \cdot 10^{-04}$ ($2.7 \cdot 10^{-04}$)	ND	ND	ND	$3.3 \cdot 10^{-05}$ ($1.3 \cdot 10^{-04}$)

Appendix II . (cont.)

Sample Mineral	LCS-11 dolomite	LCS-12 calcite	LCS-13 calcite	LCS-15 calcite	LDS-1a calcite
MgO	19.81 (0.62)	0.39 (0.12)	0.41 (0.04)	0.47 (0.10)	0.49 (0.11)
CaO	32.98 (0.63)	56.23 (0.26)	55.95 (0.28)	55.60 (0.31)	56.13 (0.38)
FeO	0.11 (0.10)	0.01 (0.01)	0.03 (0.02)	0.08 (0.16)	0.02 (0.01)
MnO	0.01 (0.01)	0.01 (0.01)	0.01 (0.01)	0.01 (0.01)	0.00 (0.01)
SrO	0.00 (0.00)	0.01 (0.02)	0.01 (0.01)	0.02 (0.01)	0.01 (0.01)
Sum	52.92	56.66	56.41	56.18	56.66
Ca pfu	0.544 (0.012)	0.990 (0.003)	0.990 (0.001)	0.987 (0.002)	0.988 (0.003)
Mg pfu	0.455 (0.012)	0.010 (0.003)	0.010 (0.001)	0.012 (0.002)	0.012 (0.003)
Fe pfu	$1.4 \cdot 10^{-03}$ ($1.4 \cdot 10^{-03}$)	ND	$3.3 \cdot 10^{-04}$ ($4.8 \cdot 10^{-04}$)	$1.2 \cdot 10^{-03}$ ($2.1 \cdot 10^{-03}$)	ND
Mn pfu	$9.1 \cdot 10^{-05}$ ($2.0 \cdot 10^{-04}$)	$7.6 \cdot 10^{-05}$ ($2.7 \cdot 10^{-04}$)	ND	ND	ND
Sr pfu	ND	ND	ND	ND	ND

Sample Mineral	LDS-1a dolomite	LDS-2 dolomite	LDS-3 dolomite	LDS-5 dolomite	LDS-8 calcite
MgO	19.56 (0.76)	21.37 (0.33)	20.52 (0.52)	20.07 (0.65)	0.59 (0.07)
CaO	32.72 (0.82)	30.98 (0.36)	31.47 (0.45)	32.03 (0.77)	56.18 (0.11)
FeO	0.59 (0.39)	0.30 (0.09)	0.59 (0.34)	0.74 (0.31)	0.01 (0.01)
MnO	0.03 (0.02)	0.01 (0.01)	0.03 (0.02)	0.03 (0.02)	0.01 (0.02)
SrO	0.01 (0.01)	0.01 (0.01)	0.01 (0.01)	0.01 (0.01)	0.02 (0.01)
Sum	52.91	52.67	52.63	52.87	56.81
Ca pfu	0.542 (0.015)	0.508 (0.005)	0.520 (0.008)	0.529 (0.013)	0.985 (0.002)
Mg pfu	0.450 (0.016)	0.488 (0.006)	0.472 (0.010)	0.461 (0.014)	0.014 (0.002)
Fe pfu	$7.7 \cdot 10^{-03}$ ($5.0 \cdot 10^{-03}$)	$3.8 \cdot 10^{-03}$ ($1.2 \cdot 10^{-03}$)	$7.7 \cdot 10^{-03}$ ($4.4 \cdot 10^{-03}$)	$9.5 \cdot 10^{-03}$ ($4.1 \cdot 10^{-03}$)	ND
Mn pfu	$3.3 \cdot 10^{-04}$ ($3.3 \cdot 10^{-04}$)	$1.6 \cdot 10^{-04}$ ($2.4 \cdot 10^{-04}$)	$4.3 \cdot 10^{-04}$ ($2.6 \cdot 10^{-04}$)	$3.3 \cdot 10^{-04}$ ($3.1 \cdot 10^{-04}$)	$1.2 \cdot 10^{-04}$ ($3.5 \cdot 10^{-04}$)
Sr pfu	ND	$6.3 \cdot 10^{-05}$ ($1.7 \cdot 10^{-04}$)	ND	ND	ND

Appendix II . (cont.)

Sample	LDS-13	LDS-12	LDS-16	LDS-16	LDS-18
Mineral	calcite	dolomite	calcite	dolomite	calcite
MgO	0.69 (0.10)	19.48 (0.49)	1.42 (0.13)	19.96 (0.53)	0.67 (0.08)
CaO	56.00 (0.22)	31.94 (0.66)	54.79 (0.67)	32.29 (0.92)	56.03 (0.12)
FeO	0.03 (0.01)	1.06 (0.54)	0.03 (0.02)	0.42 (0.35)	0.03 (0.01)
MnO	0.00 (0.01)	0.06 (0.04)	0.00 (0.00)	0.03 (0.02)	0.01 (0.01)
SrO	0.01 (0.01)	0.01 (0.01)	0.00 (0.01)	0.00 (0.01)	0.02 (0.01)
Sum	56.74	52.55	56.24	52.69	56.75
Ca pfu	0.983 (0.002)	0.533 (0.010)	0.965 (0.003)	0.534 (0.014)	0.983 (0.002)
Mg pfu	0.017 (0.003)	0.452 (0.008)	0.035 (0.003)	0.460 (0.012)	0.016 (0.002)
Fe pfu	$5.3 \cdot 10^{-04}$ ($5.1 \cdot 10^{-04}$)	$1.4 \cdot 10^{-02}$ ($7.2 \cdot 10^{-03}$)	$3.3 \cdot 10^{-04}$ ($5.1 \cdot 10^{-04}$)	$5.4 \cdot 10^{-03}$ ($4.5 \cdot 10^{-03}$)	$3.0 \cdot 10^{-04}$ ($4.8 \cdot 10^{-04}$)
Mn pfu	ND	$7.8 \cdot 10^{-04}$ ($4.7 \cdot 10^{-04}$)	ND	$4.3 \cdot 10^{-04}$ ($3.3 \cdot 10^{-04}$)	ND
Sr pfu	ND	$3.4 \cdot 10^{-05}$ ($1.3 \cdot 10^{-04}$)	ND	ND	ND

Sample	LDS-18	LES-1	LES-3	LES-4	LES-8
Mineral	dolomite	calcite	dolomite	dolomite	calcite
MgO	18.86 (0.54)	0.55 (0.07)	19.62 (0.67)	20.11 (0.57)	0.55 (0.09)
CaO	33.09 (0.84)	55.94 (0.29)	32.76 (0.71)	32.19 (0.49)	55.93 (0.28)
FeO	0.69 (0.30)	0.03 (0.02)	0.47 (0.26)	0.58 (0.28)	0.03 (0.02)
MnO	0.03 (0.02)	0.01 (0.01)	0.03 (0.01)	0.03 (0.02)	0.01 (0.01)
SrO	0.01 (0.01)	0.02 (0.01)	0.01 (0.01)	0.01 (0.01)	0.02 (0.01)
Sum	52.69	56.55	52.89	52.91	56.54
Ca pfu	0.552 (0.014)	0.986 (0.002)	0.542 (0.013)	0.531 (0.009)	0.986 (0.002)
Mg pfu	0.438 (0.011)	0.014 (0.002)	0.452 (0.014)	0.461 (0.011)	0.014 (0.002)
Fe pfu	$9.1 \cdot 10^{-03}$ ($3.9 \cdot 10^{-03}$)	$4.2 \cdot 10^{-04}$ ($5.1 \cdot 10^{-04}$)	$6.1 \cdot 10^{-03}$ ($3.2 \cdot 10^{-03}$)	$7.4 \cdot 10^{-03}$ ($3.7 \cdot 10^{-03}$)	$4.6 \cdot 10^{-04}$ ($5.1 \cdot 10^{-04}$)
Mn pfu	$4.0 \cdot 10^{-04}$ ($3.9 \cdot 10^{-04}$)	$7.1 \cdot 10^{-05}$ ($2.7 \cdot 10^{-04}$)	$3.2 \cdot 10^{-04}$ ($2.5 \cdot 10^{-04}$)	$4.0 \cdot 10^{-04}$ ($3.4 \cdot 10^{-04}$)	ND
Sr pfu	$1.0 \cdot 10^{-04}$ ($2.1 \cdot 10^{-04}$)	ND	$9.1 \cdot 10^{-05}$ ($2.0 \cdot 10^{-04}$)	$3.4 \cdot 10^{-05}$ ($1.3 \cdot 10^{-04}$)	ND

Appendix II . (cont.)

Sample	LES-8	LES-11	LES-11	LES-13	LES-14
Mineral	dolomite	calcite	dolomite	dolomite	dolomite
MgO	19.06 (0.53)	0.40 (0.07)	19.47 (0.46)	19.74 (0.40)	21.07 (0.27)
CaO	32.43 (1.10)	56.27 (0.26)	32.46 (0.82)	32.71 (0.55)	31.32 (0.26)
FeO	1.47 (0.60)	0.02 (0.02)	0.78 (0.63)	0.31 (0.22)	0.43 (0.09)
MnO	0.06 (0.06)	0.01 (0.01)	0.02 (0.02)	0.02 (0.02)	0.02 (0.01)
SrO	0.01 (0.01)	0.02 (0.02)	0.01 (0.01)	0.01 (0.01)	0.01 (0.01)
Sum	53.02	56.72	52.74	52.79	52.84
Ca pfu	0.539 (0.019)	0.990 (0.002)	0.539 (0.013)	0.541 (0.009)	0.514 (0.004)
Mg pfu	0.441 (0.011)	0.010 (0.002)	0.450 (0.009)	0.454 (0.008)	0.481 (0.005)
Fe pfu	$1.9 \cdot 10^{-02}$ ($7.8 \cdot 10^{-03}$)	$2.8 \cdot 10^{-04}$ ($4.6 \cdot 10^{-04}$)	$1.0 \cdot 10^{-02}$ ($8.3 \cdot 10^{-03}$)	$4.1 \cdot 10^{-03}$ ($2.9 \cdot 10^{-03}$)	$5.4 \cdot 10^{-03}$ ($1.1 \cdot 10^{-03}$)
Mn pfu	$7.9 \cdot 10^{-04}$ ($7.0 \cdot 10^{-04}$)	ND	$2.3 \cdot 10^{-04}$ ($3.3 \cdot 10^{-04}$)	$2.3 \cdot 10^{-04}$ ($2.6 \cdot 10^{-04}$)	$3.2 \cdot 10^{-04}$ ($2.5 \cdot 10^{-04}$)
Sr pfu	ND	$7.1 \cdot 10^{-05}$ ($2.6 \cdot 10^{-04}$)	$2.1 \cdot 10^{-05}$ ($1.0 \cdot 10^{-04}$)	$6.7 \cdot 10^{-05}$ ($1.8 \cdot 10^{-04}$)	ND

Sample	LES-15	LES-15	LES-16a	LES-16a	LFS-1
Mineral	calcite	dolomite	calcite	dolomite	dolomite
MgO	0.62 (0.31)	20.05 (0.59)	0.51 (0.19)	19.57 (0.36)	20.14 (0.76)
CaO	55.75 (0.51)	32.67 (0.58)	56.00 (0.29)	32.83 (0.63)	32.21 (0.88)
FeO	0.16 (0.32)	0.23 (0.28)	0.02 (0.02)	0.41 (0.16)	0.34 (0.28)
MnO	0.02 (0.01)	0.01 (0.02)	0.01 (0.01)	0.02 (0.02)	0.01 (0.01)
SrO	0.01 (0.02)	0.01 (0.01)	0.02 (0.03)	0.01 (0.01)	0.00 (0.01)
Sum	56.56	52.97	56.56	52.84	52.71
Ca pfu	0.983 (0.010)	0.538 (0.011)	0.987 (0.005)	0.544 (0.010)	0.532 (0.015)
Mg pfu	0.015 (0.008)	0.459 (0.011)	0.013 (0.005)	0.451 (0.008)	0.463 (0.016)
Fe pfu	$2.0 \cdot 10^{-03}$ ($4.4 \cdot 10^{-03}$)	$3.0 \cdot 10^{-03}$ ($3.6 \cdot 10^{-03}$)	$7.1 \cdot 10^{-05}$ ($2.7 \cdot 10^{-04}$)	$5.3 \cdot 10^{-03}$ ($2.1 \cdot 10^{-03}$)	$4.3 \cdot 10^{-03}$ ($3.6 \cdot 10^{-03}$)
Mn pfu	$2.0 \cdot 10^{-04}$ ($4.4 \cdot 10^{-04}$)	$1.3 \cdot 10^{-04}$ ($2.3 \cdot 10^{-04}$)	ND	$2.5 \cdot 10^{-04}$ ($2.8 \cdot 10^{-04}$)	$1.8 \cdot 10^{-04}$ ($2.5 \cdot 10^{-04}$)
Sr pfu	ND	$6.3 \cdot 10^{-05}$ ($1.8 \cdot 10^{-04}$)	$7.1 \cdot 10^{-05}$ ($2.7 \cdot 10^{-04}$)	ND	ND

Appendix II . (cont.)

Sample	LFS-4	LFS-4
Mineral	calcite	dolomite
MgO	0.58 (0.09)	19.38 (0.28)
CaO	56.09 (0.20)	32.76 (0.57)
FeO	0.02 (0.01)	0.56 (0.38)
MnO	0.00 (0.01)	0.02 (0.02)
SrO	0.02 (0.01)	0.01 (0.01)
Sum	56.71	52.73
Ca pfu	0.986 (0.002)	0.544 (0.008)
Mg pfu	0.014 (0.002)	0.448 (0.005)
Fe pfu	$7.0 \cdot 10^{-05}$ ($2.6 \cdot 10^{-04}$)	$7.3 \cdot 10^{-03}$ ($5.1 \cdot 10^{-03}$)
Mn pfu	$7.0 \cdot 10^{-05}$ ($2.6 \cdot 10^{-04}$)	$3.2 \cdot 10^{-04}$ ($2.5 \cdot 10^{-04}$)
Sr pfu	ND	ND

Notes: ND not detected; NA not analyzed; standard deviation in parentheses

Appendix III. LA-ICPMS trace element data.

Sample	L-1A	L-1C	L-1D	L-4A	L-6B
	calcite	dolomite	dolomite	calcite	dolomite
Mn (ppm)	ND	344 (104)	268 (9)	11 (3)	251 (26)
Fe (ppm)	ND	12326 (3911)	12026 (494)	255 (48)	10251 (753)
Sr (ppm)	164.9 (24.4)	51.8 (11.0)	23.6 (4.1)	208.7 (24.3)	22.3 (1.8)
Cr (ppm)	ND	ND	2.02 (0.51)	4.57 (0.61)	2.11 (0.70)
Co (ppm)	1.84 (0.00)	0.21 (0.11)	0.25 (0.09)	0.27 (0.08)	0.70 (0.09)
Ni (ppm)	ND	ND	3.88 (0.00)	8.91 (4.37)	5.68 (2.73)
Cu (ppm)	ND	0.440 (0.212)	0.300 (0.097)	0.290 (0.000)	1.350 (1.400)
Zn (ppm)	ND	3.35 (1.96)	5.51 (0.82)	0.81 (0.15)	8.00 (1.05)
Ba (ppm)	0.660 (0.173)	1.460 (0.681)	0.900 (0.235)	0.830 (0.272)	0.680 (0.066)
Pb (ppm)	0.230 (0.031)	0.160 (0.094)	0.130 (0.063)	0.080 (0.019)	0.300 (0.069)
Mn pfu	ND	$5.8 \cdot 10^{-4}$ ($1.8 \cdot 10^{-4}$)	$4.6 \cdot 10^{-4}$ ($1.7 \cdot 10^{-5}$)	$1.7 \cdot 10^{-5}$ ($9.0 \cdot 10^{-6}$)	$4.3 \cdot 10^{-4}$ ($4.6 \cdot 10^{-5}$)
Fe pfu	ND	$2.1 \cdot 10^{-2}$ ($6.6 \cdot 10^{-3}$)	$2.0 \cdot 10^{-2}$ ($8.6 \cdot 10^{-4}$)	$3.9 \cdot 10^{-4}$ ($1.9 \cdot 10^{-4}$)	$1.7 \cdot 10^{-2}$ ($1.3 \cdot 10^{-3}$)
Sr pfu	$1.9 \cdot 10^{-4}$ ($2.9 \cdot 10^{-5}$)	$5.5 \cdot 10^{-5}$ ($1.2 \cdot 10^{-5}$)	$2.5 \cdot 10^{-5}$ ($4.6 \cdot 10^{-6}$)	$2.4 \cdot 10^{-4}$ ($3.0 \cdot 10^{-5}$)	$2.4 \cdot 10^{-5}$ ($2.0 \cdot 10^{-6}$)
Cr pfu	ND	ND	$3.6 \cdot 10^{-6}$ ($9.9 \cdot 10^{-7}$)	$3.5 \cdot 10^{-6}$ ($4.4 \cdot 10^{-6}$)	$3.3 \cdot 10^{-6}$ ($1.8 \cdot 10^{-6}$)
Co pfu	$4.3 \cdot 10^{-7}$ ($1.1 \cdot 10^{-6}$)	$8.2 \cdot 10^{-8}$ ($1.7 \cdot 10^{-7}$)	$3.9 \cdot 10^{-7}$ ($1.5 \cdot 10^{-7}$)	$3.8 \cdot 10^{-7}$ ($2.2 \cdot 10^{-7}$)	$1.1 \cdot 10^{-6}$ ($1.6 \cdot 10^{-7}$)
Ni pfu	ND	ND	$7.8 \cdot 10^{-7}$ ($2.2 \cdot 10^{-6}$)	$1.1 \cdot 10^{-5}$ ($1.0 \cdot 10^{-5}$)	$3.4 \cdot 10^{-6}$ ($5.5 \cdot 10^{-6}$)
Cu pfu	ND	$4.1 \cdot 10^{-7}$ ($4.1 \cdot 10^{-7}$)	$3.8 \cdot 10^{-7}$ ($2.1 \cdot 10^{-7}$)	$6.5 \cdot 10^{-8}$ ($1.7 \cdot 10^{-7}$)	$2.0 \cdot 10^{-6}$ ($2.2 \cdot 10^{-6}$)
Zn pfu	ND	$4.8 \cdot 10^{-6}$ ($2.9 \cdot 10^{-6}$)	$7.9 \cdot 10^{-6}$ ($1.3 \cdot 10^{-6}$)	$1.2 \cdot 10^{-6}$ ($2.2 \cdot 10^{-7}$)	$1.2 \cdot 10^{-5}$ ($1.6 \cdot 10^{-6}$)
Ba pfu	$4.8 \cdot 10^{-7}$ ($1.4 \cdot 10^{-7}$)	$1.0 \cdot 10^{-6}$ ($4.8 \cdot 10^{-7}$)	$6.1 \cdot 10^{-7}$ ($1.7 \cdot 10^{-7}$)	$6.4 \cdot 10^{-7}$ ($2.0 \cdot 10^{-7}$)	$4.1 \cdot 10^{-7}$ ($1.7 \cdot 10^{-7}$)
Pb pfu	$9.6 \cdot 10^{-8}$ ($4.4 \cdot 10^{-8}$)	$7.1 \cdot 10^{-8}$ ($4.3 \cdot 10^{-8}$)	$6.1 \cdot 10^{-8}$ ($3.0 \cdot 10^{-8}$)	$3.9 \cdot 10^{-8}$ ($1.0 \cdot 10^{-8}$)	$1.0 \cdot 10^{-7}$ ($7.0 \cdot 10^{-8}$)

Appendix III. (cont.)

Sample	L-7A	L-7D	L-7F	L-7K	7T-4
	calcite	calcite	dolomite	calcite	dolomite
Mn (ppm)	16 (8)	25 (4)	301 (41)	11 (4)	201 (115)
Fe (ppm)	ND	ND	12303 (1564)	287 (131)	ND
Sr (ppm)	159.3 (26.7)	58.6 (11.7)	29.5 (2.7)	160.5 (9.4)	65.0 (17.9)
Cr (ppm)	2.17 (0.77)	ND	2.94 (0.59)	4.64 (0.98)	3.42 (1.59)
Co (ppm)	ND	ND	0.40 (0.07)	0.40 (0.30)	ND
Ni (ppm)	ND	ND	ND	37.94 (23.61)	ND
Cu (ppm)	1.760 (0.000)	0.420 (0.000)	0.530 (0.250)	0.440 (0.293)	1.030 (0.676)
Zn (ppm)	0.60 (0.11)	1.55 (0.84)	5.71 (0.75)	0.81 (0.34)	2.67 (0.88)
Ba (ppm)	1.030 (0.263)	0.420 (0.454)	1.020 (0.256)	0.880 (0.247)	1.120 (0.482)
Pb (ppm)	0.410 (0.051)	0.140 (0.040)	0.210 (0.048)	0.290 (0.145)	0.180 (0.089)
Mn pfu	$2.9 \cdot 10^{-5}$ ($1.4 \cdot 10^{-5}$)	$4.5 \cdot 10^{-5}$ ($7.9 \cdot 10^{-6}$)	$5.1 \cdot 10^{-4}$ ($6.8 \cdot 10^{-5}$)	$1.9 \cdot 10^{-5}$ ($6.6 \cdot 10^{-6}$)	$3.4 \cdot 10^{-4}$ ($2.1 \cdot 10^{-4}$)
Fe pfu	ND	ND	$2.1 \cdot 10^{-2}$ ($2.6 \cdot 10^{-3}$)	$3.6 \cdot 10^{-4}$ ($3.1 \cdot 10^{-4}$)	ND
Sr pfu	$1.8 \cdot 10^{-4}$ ($3.0 \cdot 10^{-5}$)	$6.7 \cdot 10^{-5}$ ($1.3 \cdot 10^{-5}$)	$3.1 \cdot 10^{-5}$ ($3.0 \cdot 10^{-6}$)	$1.8 \cdot 10^{-4}$ ($1.1 \cdot 10^{-5}$)	$6.9 \cdot 10^{-5}$ ($2.0 \cdot 10^{-5}$)
Cr pfu	$2.6 \cdot 10^{-6}$ ($2.3 \cdot 10^{-6}$)	ND	$2.0 \cdot 10^{-6}$ ($2.7 \cdot 10^{-6}$)	$8.0 \cdot 10^{-6}$ ($3.2 \cdot 10^{-6}$)	$4.6 \cdot 10^{-6}$ ($3.9 \cdot 10^{-6}$)
Co pfu	ND	ND	$6.2 \cdot 10^{-7}$ ($1.1 \cdot 10^{-7}$)	$4.7 \cdot 10^{-7}$ ($5.2 \cdot 10^{-7}$)	ND
Ni pfu	ND	ND	ND	$6.4 \cdot 10^{-5}$ ($4.1 \cdot 10^{-5}$)	ND
Cu pfu	$3.4 \cdot 10^{-7}$ ($9.2 \cdot 10^{-7}$)	$8.3 \cdot 10^{-8}$ ($2.2 \cdot 10^{-7}$)	$6.8 \cdot 10^{-7}$ ($4.3 \cdot 10^{-7}$)	$6.9 \cdot 10^{-7}$ ($4.6 \cdot 10^{-7}$)	$1.3 \cdot 10^{-6}$ ($1.1 \cdot 10^{-6}$)
Zn pfu	$7.9 \cdot 10^{-7}$ ($3.4 \cdot 10^{-7}$)	$5.9 \cdot 10^{-7}$ ($1.2 \cdot 10^{-6}$)	$8.2 \cdot 10^{-6}$ ($1.1 \cdot 10^{-6}$)	$1.1 \cdot 10^{-6}$ ($6.3 \cdot 10^{-7}$)	$3.8 \cdot 10^{-6}$ ($1.3 \cdot 10^{-6}$)
Ba pfu	$3.7 \cdot 10^{-7}$ ($4.0 \cdot 10^{-7}$)	$2.7 \cdot 10^{-7}$ ($3.3 \cdot 10^{-7}$)	$7.0 \cdot 10^{-7}$ ($1.7 \cdot 10^{-7}$)	$6.4 \cdot 10^{-7}$ ($1.8 \cdot 10^{-7}$)	$7.7 \cdot 10^{-7}$ ($3.5 \cdot 10^{-7}$)
Pb pfu	$1.2 \cdot 10^{-7}$ ($9.7 \cdot 10^{-8}$)	$3.3 \cdot 10^{-8}$ ($3.6 \cdot 10^{-8}$)	$9.5 \cdot 10^{-8}$ ($2.2 \cdot 10^{-8}$)	$1.4 \cdot 10^{-7}$ ($7.0 \cdot 10^{-8}$)	$6.1 \cdot 10^{-8}$ ($5.3 \cdot 10^{-8}$)

Appendix III. (cont.)

Sample	7T-6	7T-7	7T-8	L-8I	8T-7
	dolomite	dolomite	dolomite	calcite	dolomite
Mn (ppm)	466 (16)	431 (12)	153 (86)	7 (1)	229 (55)
Fe (ppm)	18380 (546)	19004 (931)	2715 (2098)	ND	5360 (1254)
Sr (ppm)	30.2 (2.1)	26.3 (2.9)	57.5 (16.8)	160.1 (12.5)	32.3 (6.7)
Cr (ppm)	4.93 (1.92)	ND	ND	ND	ND
Co (ppm)	1.68 (0.16)	1.84 (0.12)	ND	ND	0.17 (0.06)
Ni (ppm)	19.49 (13.03)	8.39 (0.96)	ND	ND	ND
Cu (ppm)	0.370 (0.293)	0.210 (0.028)	2.080 (3.118)	ND	0.500 (0.266)
Zn (ppm)	14.04 (1.82)	10.51 (1.13)	2.09 (2.17)	1.95 (0.28)	4.20 (0.73)
Ba (ppm)	1.270 (0.611)	0.750 (0.125)	0.740 (0.609)	1.110 (0.448)	0.940 (0.351)
Pb (ppm)	0.550 (0.212)	0.230 (0.062)	0.130 (0.062)	0.280 (0.056)	0.410 (0.379)
Mn pfu	$8.1 \cdot 10^{-4}$ ($3.0 \cdot 10^{-5}$)	$7.4 \cdot 10^{-4}$ ($2.1 \cdot 10^{-5}$)	$2.6 \cdot 10^{-4}$ ($1.6 \cdot 10^{-4}$)	$4.6 \cdot 10^{-6}$ ($6.2 \cdot 10^{-6}$)	$3.8 \cdot 10^{-4}$ ($9.6 \cdot 10^{-5}$)
Fe pfu	$3.1 \cdot 10^{-2}$ ($9.7 \cdot 10^{-4}$)	$3.2 \cdot 10^{-2}$ ($1.6 \cdot 10^{-3}$)	$4.6 \cdot 10^{-3}$ ($3.7 \cdot 10^{-3}$)	ND	$8.8 \cdot 10^{-3}$ ($2.2 \cdot 10^{-3}$)
Sr pfu	$3.3 \cdot 10^{-5}$ ($2.4 \cdot 10^{-6}$)	$2.8 \cdot 10^{-5}$ ($3.3 \cdot 10^{-6}$)	$5.4 \cdot 10^{-5}$ ($2.8 \cdot 10^{-5}$)	$1.8 \cdot 10^{-4}$ ($1.5 \cdot 10^{-5}$)	$3.4 \cdot 10^{-5}$ ($7.4 \cdot 10^{-6}$)
Cr pfu	$4.5 \cdot 10^{-6}$ ($5.6 \cdot 10^{-6}$)	ND	ND	ND	ND
Co pfu	$2.7 \cdot 10^{-6}$ ($2.7 \cdot 10^{-7}$)	$2.9 \cdot 10^{-6}$ ($1.9 \cdot 10^{-7}$)	ND	ND	$1.7 \cdot 10^{-7}$ ($1.6 \cdot 10^{-7}$)
Ni pfu	$3.2 \cdot 10^{-5}$ ($2.3 \cdot 10^{-5}$)	$3.4 \cdot 10^{-6}$ ($6.3 \cdot 10^{-6}$)	ND	ND	ND
Cu pfu	$5.6 \cdot 10^{-7}$ ($4.7 \cdot 10^{-7}$)	$1.5 \cdot 10^{-7}$ ($1.7 \cdot 10^{-7}$)	$1.5 \cdot 10^{-6}$ ($3.8 \cdot 10^{-6}$)	ND	$5.4 \cdot 10^{-7}$ ($4.9 \cdot 10^{-7}$)
Zn pfu	$2.0 \cdot 10^{-5}$ ($2.9 \cdot 10^{-6}$)	$1.5 \cdot 10^{-5}$ ($1.7 \cdot 10^{-6}$)	$3.0 \cdot 10^{-6}$ ($3.3 \cdot 10^{-6}$)	$2.2 \cdot 10^{-6}$ ($1.4 \cdot 10^{-6}$)	$5.9 \cdot 10^{-6}$ ($1.1 \cdot 10^{-6}$)
Ba pfu	$8.8 \cdot 10^{-7}$ ($4.6 \cdot 10^{-7}$)	$5.2 \cdot 10^{-7}$ ($9.1 \cdot 10^{-8}$)	$5.1 \cdot 10^{-7}$ ($4.4 \cdot 10^{-7}$)	$7.1 \cdot 10^{-7}$ ($4.2 \cdot 10^{-7}$)	$6.3 \cdot 10^{-7}$ ($2.5 \cdot 10^{-7}$)
Pb pfu	$2.5 \cdot 10^{-7}$ ($1.1 \cdot 10^{-7}$)	$1.1 \cdot 10^{-7}$ ($3.0 \cdot 10^{-8}$)	$6.0 \cdot 10^{-8}$ ($3.0 \cdot 10^{-8}$)	$1.2 \cdot 10^{-7}$ ($5.2 \cdot 10^{-8}$)	$1.8 \cdot 10^{-7}$ ($1.8 \cdot 10^{-7}$)

Appendix III. (cont.)

Sample	8T-14	L-11C	L-11G	L-12B	L-12H
	dolomite	dolomite	dolomite	dolomite	dolomite
Mn (ppm)	79 (12)	180 (32)	245 (16)	66 (36)	80 (33)
Fe (ppm)	2041 (417)	5497 (958)	ND	1986 (1084)	1626 (687)
Sr (ppm)	23.4 (4.1)	23.4 (4.8)	24.7 (2.5)	63.1 (8.3)	44.4 (10.0)
Cr (ppm)	ND	2.96 (0.74)	6.12 (1.48)	4.81 (0.00)	ND
Co (ppm)	0.14 (0.03)	0.42 (0.13)	1.05 (0.23)	0.10 (0.02)	0.26 (0.33)
Ni (ppm)	ND	15.33 (5.45)	6.70 (2.02)	ND	5.14 (1.81)
Cu (ppm)	0.580 (0.307)	0.220 (0.094)	ND	0.430 (0.323)	1.230 (1.568)
Zn (ppm)	3.27 (1.28)	7.03 (1.17)	8.25 (0.87)	1.98 (0.53)	3.28 (2.00)
Ba (ppm)	0.740 (0.226)	1.010 (0.186)	0.960 (0.131)	1.900 (1.266)	2.460 (1.475)
Pb (ppm)	0.190 (0.099)	0.350 (0.388)	0.160 (0.096)	0.150 (0.046)	0.360 (0.268)
Mn pfu	$1.3 \cdot 10^{-4}$ ($2.0 \cdot 10^{-5}$)	$3.0 \cdot 10^{-4}$ ($5.7 \cdot 10^{-5}$)	$4.2 \cdot 10^{-4}$ ($3.0 \cdot 10^{-5}$)	$1.1 \cdot 10^{-4}$ ($6.4 \cdot 10^{-5}$)	$1.4 \cdot 10^{-4}$ ($6.4 \cdot 10^{-5}$)
Fe pfu	$3.2 \cdot 10^{-3}$ ($6.2 \cdot 10^{-4}$)	$9.1 \cdot 10^{-3}$ ($1.7 \cdot 10^{-3}$)	ND	$3.3 \cdot 10^{-3}$ ($1.9 \cdot 10^{-3}$)	$2.7 \cdot 10^{-3}$ ($1.3 \cdot 10^{-3}$)
Sr pfu	$2.3 \cdot 10^{-5}$ ($3.1 \cdot 10^{-6}$)	$2.5 \cdot 10^{-5}$ ($5.4 \cdot 10^{-6}$)	$2.3 \cdot 10^{-5}$ ($9.8 \cdot 10^{-6}$)	$6.7 \cdot 10^{-5}$ ($9.2 \cdot 10^{-6}$)	$4.8 \cdot 10^{-5}$ ($1.2 \cdot 10^{-5}$)
Cr pfu	ND	$2.6 \cdot 10^{-6}$ ($3.0 \cdot 10^{-6}$)	$1.1 \cdot 10^{-5}$ ($2.8 \cdot 10^{-6}$)	$1.1 \cdot 10^{-6}$ ($3.1 \cdot 10^{-6}$)	ND
Co pfu	$6.0 \cdot 10^{-8}$ ($1.0 \cdot 10^{-7}$)	$6.6 \cdot 10^{-7}$ ($2.2 \cdot 10^{-7}$)	$1.6 \cdot 10^{-6}$ ($3.8 \cdot 10^{-7}$)	$1.3 \cdot 10^{-7}$ ($6.0 \cdot 10^{-8}$)	$2.9 \cdot 10^{-7}$ ($5.0 \cdot 10^{-7}$)
Ni pfu	ND	$2.1 \cdot 10^{-5}$ ($1.2 \cdot 10^{-5}$)	$9.4 \cdot 10^{-6}$ ($5.0 \cdot 10^{-6}$)	ND	$2.3 \cdot 10^{-6}$ ($4.3 \cdot 10^{-6}$)
Cu pfu	$7.2 \cdot 10^{-7}$ ($5.2 \cdot 10^{-7}$)	$3.3 \cdot 10^{-7}$ ($1.5 \cdot 10^{-7}$)	ND	$4.0 \cdot 10^{-7}$ ($5.1 \cdot 10^{-7}$)	$1.6 \cdot 10^{-6}$ ($2.4 \cdot 10^{-6}$)
Zn pfu	$4.6 \cdot 10^{-6}$ ($1.8 \cdot 10^{-6}$)	$1.0 \cdot 10^{-5}$ ($1.8 \cdot 10^{-6}$)	$1.2 \cdot 10^{-5}$ ($1.3 \cdot 10^{-6}$)	$2.8 \cdot 10^{-6}$ ($8.1 \cdot 10^{-7}$)	$4.7 \cdot 10^{-6}$ ($3.1 \cdot 10^{-6}$)
Ba pfu	$5.0 \cdot 10^{-7}$ ($1.6 \cdot 10^{-7}$)	$6.9 \cdot 10^{-7}$ ($1.3 \cdot 10^{-7}$)	$6.6 \cdot 10^{-7}$ ($9.6 \cdot 10^{-8}$)	$1.3 \cdot 10^{-6}$ ($9.1 \cdot 10^{-7}$)	$1.7 \cdot 10^{-6}$ ($1.1 \cdot 10^{-6}$)
Pb pfu	$8.4 \cdot 10^{-8}$ ($4.5 \cdot 10^{-8}$)	$1.6 \cdot 10^{-7}$ ($1.8 \cdot 10^{-7}$)	$7.3 \cdot 10^{-8}$ ($4.6 \cdot 10^{-8}$)	$6.7 \cdot 10^{-8}$ ($2.2 \cdot 10^{-8}$)	$1.6 \cdot 10^{-7}$ ($1.3 \cdot 10^{-7}$)

Appendix III. (cont.)

Sample	L-13B	L-13E	L-13F	LAS-5	LAS-17
	dolomite	dolomite	dolomite	dolomite	calcite
Mn (ppm)	128 (13)	283 (74)	245 (89)	122 (11)	8 (5)
Fe (ppm)	2687 (206)	4749 (1512)	ND	3196 (230)	145 (14)
Sr (ppm)	20.6 (2.9)	54.7 (14.1)	39.8 (6.8)	24.6 (3.5)	127.5 (32.2)
Cr (ppm)	5.69 (2.39)	5.60 (0.00)	ND	ND	2.83 (0.14)
Co (ppm)	0.61 (0.26)	0.12 (0.02)	0.85 (0.28)	0.15 (0.02)	0.17 (0.05)
Ni (ppm)	10.07 (5.58)	2.65 (0.00)	ND	ND	13.65 (9.32)
Cu (ppm)	0.370 (0.057)	0.640 (0.320)	0.580 (0.127)	0.470 (0.203)	0.220 (0.077)
Zn (ppm)	2.77 (0.36)	2.11 (0.37)	5.13 (1.40)	4.63 (0.94)	0.81 (0.22)
Ba (ppm)	1.180 (0.361)	1.930 (0.726)	1.370 (0.414)	1.080 (0.394)	1.260 (0.298)
Pb (ppm)	0.250 (0.066)	0.540 (0.357)	0.160 (0.036)	0.140 (0.039)	0.200 (0.056)
Mn pfu	$2.2 \cdot 10^{-4}$ ($2.4 \cdot 10^{-5}$)	$4.8 \cdot 10^{-4}$ ($1.3 \cdot 10^{-4}$)	$4.2 \cdot 10^{-4}$ ($1.6 \cdot 10^{-4}$)	$2.1 \cdot 10^{-4}$ ($1.9 \cdot 10^{-5}$)	$1.2 \cdot 10^{-5}$ ($1.1 \cdot 10^{-5}$)
Fe pfu	$4.5 \cdot 10^{-3}$ ($3.6 \cdot 10^{-4}$)	$8.0 \cdot 10^{-3}$ ($2.7 \cdot 10^{-3}$)	ND	$5.3 \cdot 10^{-3}$ ($4.0 \cdot 10^{-4}$)	$6.4 \cdot 10^{-5}$ ($1.2 \cdot 10^{-4}$)
Sr pfu	$1.9 \cdot 10^{-5}$ ($8.4 \cdot 10^{-6}$)	$5.8 \cdot 10^{-5}$ ($1.6 \cdot 10^{-5}$)	$3.2 \cdot 10^{-5}$ ($2.1 \cdot 10^{-5}$)	$2.6 \cdot 10^{-5}$ ($4.0 \cdot 10^{-6}$)	$1.4 \cdot 10^{-4}$ ($3.8 \cdot 10^{-5}$)
Cr pfu	$6.4 \cdot 10^{-6}$ ($6.4 \cdot 10^{-6}$)	$1.4 \cdot 10^{-6}$ ($3.8 \cdot 10^{-6}$)	ND	ND	$1.3 \cdot 10^{-6}$ ($2.5 \cdot 10^{-6}$)
Co pfu	$9.5 \cdot 10^{-7}$ ($4.3 \cdot 10^{-7}$)	$1.4 \cdot 10^{-7}$ ($1.0 \cdot 10^{-7}$)	$5.0 \cdot 10^{-7}$ ($7.5 \cdot 10^{-7}$)	$1.7 \cdot 10^{-7}$ ($1.1 \cdot 10^{-7}$)	$1.8 \cdot 10^{-7}$ ($1.6 \cdot 10^{-7}$)
Ni pfu	$1.6 \cdot 10^{-5}$ ($9.4 \cdot 10^{-6}$)	$6.0 \cdot 10^{-7}$ ($1.6 \cdot 10^{-6}$)	ND	ND	$2.3 \cdot 10^{-5}$ ($1.7 \cdot 10^{-5}$)
Cu pfu	$5.4 \cdot 10^{-7}$ ($8.9 \cdot 10^{-8}$)	$1.0 \cdot 10^{-6}$ ($5.0 \cdot 10^{-7}$)	$2.2 \cdot 10^{-7}$ ($4.1 \cdot 10^{-7}$)	$5.1 \cdot 10^{-7}$ ($4.2 \cdot 10^{-7}$)	$2.6 \cdot 10^{-7}$ ($1.9 \cdot 10^{-7}$)
Zn pfu	$4.0 \cdot 10^{-6}$ ($5.5 \cdot 10^{-7}$)	$3.0 \cdot 10^{-6}$ ($6.1 \cdot 10^{-7}$)	$7.5 \cdot 10^{-6}$ ($2.2 \cdot 10^{-6}$)	$6.6 \cdot 10^{-6}$ ($1.4 \cdot 10^{-6}$)	$1.2 \cdot 10^{-6}$ ($3.4 \cdot 10^{-7}$)
Ba pfu	$8.0 \cdot 10^{-7}$ ($2.6 \cdot 10^{-7}$)	$1.4 \cdot 10^{-6}$ ($5.3 \cdot 10^{-7}$)	$9.5 \cdot 10^{-7}$ ($3.0 \cdot 10^{-7}$)	$7.3 \cdot 10^{-7}$ ($2.8 \cdot 10^{-7}$)	$7.9 \cdot 10^{-7}$ ($3.8 \cdot 10^{-7}$)
Pb pfu	$1.1 \cdot 10^{-7}$ ($3.1 \cdot 10^{-8}$)	$2.6 \cdot 10^{-7}$ ($1.8 \cdot 10^{-7}$)	$7.5 \cdot 10^{-8}$ ($1.8 \cdot 10^{-8}$)	$6.1 \cdot 10^{-8}$ ($1.8 \cdot 10^{-8}$)	$9.4 \cdot 10^{-8}$ ($2.8 \cdot 10^{-8}$)

Appendix III. (cont.)

Sample	LAS-26	LAS-34	LAS-35	LAS-41	LAS-46
	calcite	dolomite	calcite	dolomite	dolomite
Mn (ppm)	20 (9)	95 (39)	13 (8)	86 (18)	329 (17)
Fe (ppm)	ND	1388 (877)	252 (126)	1650 (431)	12122 (891)
Sr (ppm)	196.6 (47.2)	70.5 (7.8)	183.8 (13.6)	49.9 (5.3)	24.5 (2.1)
Cr (ppm)	ND	ND	3.64 (0.44)	ND	3.79 (0.00)
Co (ppm)	ND	ND	ND	0.29 (0.00)	ND
Ni (ppm)	ND	ND	ND	ND	3.99 (0.00)
Cu (ppm)	ND	ND	ND	0.140 (0.000)	0.710 (0.263)
Zn (ppm)	1.90 (0.42)	ND	ND	1.84 (0.40)	16.99 (0.73)
Ba (ppm)	0.990 (0.263)	0.700 (0.149)	1.060 (0.350)	0.890 (0.343)	1.140 (0.465)
Pb (ppm)	0.440 (0.086)	ND	ND	0.090 (0.032)	0.150 (0.054)
Mn pfu	$2.0 \cdot 10^{-5}$ ($2.3 \cdot 10^{-5}$)	$1.6 \cdot 10^{-4}$ ($6.7 \cdot 10^{-5}$)	$2.3 \cdot 10^{-5}$ ($1.6 \cdot 10^{-5}$)	$1.5 \cdot 10^{-4}$ ($3.1 \cdot 10^{-5}$)	$5.6 \cdot 10^{-4}$ ($3.0 \cdot 10^{-5}$)
Fe pfu	ND	$2.3 \cdot 10^{-3}$ ($1.5 \cdot 10^{-3}$)	$3.8 \cdot 10^{-4}$ ($2.8 \cdot 10^{-4}$)	$2.7 \cdot 10^{-3}$ ($7.3 \cdot 10^{-4}$)	$2.0 \cdot 10^{-2}$ ($1.5 \cdot 10^{-3}$)
Sr pfu	$2.2 \cdot 10^{-4}$ ($5.7 \cdot 10^{-5}$)	$7.5 \cdot 10^{-5}$ ($8.4 \cdot 10^{-6}$)	$2.1 \cdot 10^{-4}$ ($1.6 \cdot 10^{-5}$)	$5.3 \cdot 10^{-5}$ ($5.8 \cdot 10^{-6}$)	$2.6 \cdot 10^{-5}$ ($2.4 \cdot 10^{-6}$)
Cr pfu	ND	ND	$2.0 \cdot 10^{-6}$ ($3.4 \cdot 10^{-6}$)	ND	$8.5 \cdot 10^{-7}$ ($2.4 \cdot 10^{-6}$)
Co pfu	ND	ND	ND	$5.7 \cdot 10^{-8}$ ($1.6 \cdot 10^{-7}$)	ND
Ni pfu	ND	ND	ND	ND	$7.9 \cdot 10^{-7}$ ($2.2 \cdot 10^{-6}$)
Cu pfu	ND	ND	ND	$2.6 \cdot 10^{-8}$ ($7.0 \cdot 10^{-8}$)	$2.6 \cdot 10^{-7}$ ($5.2 \cdot 10^{-7}$)
Zn pfu	$5.0 \cdot 10^{-7}$ ($1.3 \cdot 10^{-6}$)	ND	ND	$2.6 \cdot 10^{-6}$ ($5.8 \cdot 10^{-7}$)	$2.4 \cdot 10^{-5}$ ($1.1 \cdot 10^{-6}$)
Ba pfu	$7.2 \cdot 10^{-7}$ ($2.0 \cdot 10^{-7}$)	$4.7 \cdot 10^{-7}$ ($1.0 \cdot 10^{-7}$)	$7.4 \cdot 10^{-7}$ ($2.8 \cdot 10^{-7}$)	$6.0 \cdot 10^{-7}$ ($2.4 \cdot 10^{-7}$)	$7.7 \cdot 10^{-7}$ ($3.3 \cdot 10^{-7}$)
Pb pfu	$2.1 \cdot 10^{-7}$ ($4.4 \cdot 10^{-8}$)	ND	ND	$4.3 \cdot 10^{-8}$ ($1.5 \cdot 10^{-8}$)	$6.9 \cdot 10^{-8}$ ($2.5 \cdot 10^{-8}$)

Appendix III. (cont.)

Sample	LAS-51	LCS-1	LCS-8	LCS-11	LCS-15
	dolomite	calcite	dolomite	dolomite	calcite
Mn (ppm)	219 (11)	12 (1)	403 (211)	72 (22)	20 (7)
Fe (ppm)	5657 (275)	442 (0)	12454 (10286)	ND	ND
Sr (ppm)	25.4 (4.0)	150.8 (29.2)	39.0 (14.3)	64.5 (6.6)	152.2 (13.9)
Cr (ppm)	ND	ND	ND	ND	12.68 (0.00)
Co (ppm)	0.34 (0.07)	1.61 (0.39)	0.29 (0.05)	0.38 (0.00)	ND
Ni (ppm)	ND	ND	ND	4.02 (0.66)	ND
Cu (ppm)	0.360 (0.189)	ND	0.360 (0.174)	ND	1.040 (0.000)
Zn (ppm)	5.04 (1.02)	ND	2.88 (0.53)	1.35 (0.47)	0.85 (0.14)
Ba (ppm)	0.710 (0.447)	0.490 (0.180)	1.280 (1.290)	2.030 (0.858)	1.010 (0.343)
Pb (ppm)	0.230 (0.060)	0.060 (0.000)	0.200 (0.097)	0.150 (0.133)	0.230 (0.072)
Mn pfu	$3.7 \cdot 10^{-4}$ ($2.0 \cdot 10^{-5}$)	$7.8 \cdot 10^{-6}$ ($1.1 \cdot 10^{-5}$)	$6.9 \cdot 10^{-4}$ ($3.7 \cdot 10^{-4}$)	$1.2 \cdot 10^{-4}$ ($3.9 \cdot 10^{-5}$)	$3.6 \cdot 10^{-5}$ ($1.4 \cdot 10^{-5}$)
Fe pfu	$9.3 \cdot 10^{-3}$ ($4.8 \cdot 10^{-4}$)	$9.7 \cdot 10^{-5}$ ($2.8 \cdot 10^{-4}$)	$2.2 \cdot 10^{-2}$ ($1.8 \cdot 10^{-2}$)	ND	ND
Sr pfu	$2.7 \cdot 10^{-5}$ ($4.5 \cdot 10^{-6}$)	$1.7 \cdot 10^{-4}$ ($3.5 \cdot 10^{-5}$)	$3.7 \cdot 10^{-5}$ ($1.4 \cdot 10^{-5}$)	$6.8 \cdot 10^{-5}$ ($7.4 \cdot 10^{-6}$)	$1.7 \cdot 10^{-4}$ ($1.7 \cdot 10^{-5}$)
Cr pfu	ND	ND	ND	ND	$3.5 \cdot 10^{-6}$ ($9.2 \cdot 10^{-6}$)
Co pfu	$5.2 \cdot 10^{-7}$ ($1.1 \cdot 10^{-7}$)	$1.7 \cdot 10^{-6}$ ($1.5 \cdot 10^{-6}$)	$2.5 \cdot 10^{-7}$ ($2.4 \cdot 10^{-7}$)	$7.2 \cdot 10^{-8}$ ($2.0 \cdot 10^{-7}$)	ND
Ni pfu	ND	ND	ND	$1.6 \cdot 10^{-6}$ ($3.0 \cdot 10^{-6}$)	ND
Cu pfu	$3.9 \cdot 10^{-7}$ ($3.5 \cdot 10^{-7}$)	ND	$3.7 \cdot 10^{-7}$ ($3.4 \cdot 10^{-7}$)	ND	$2.3 \cdot 10^{-7}$ ($6.2 \cdot 10^{-7}$)
Zn pfu	$7.1 \cdot 10^{-6}$ ($1.5 \cdot 10^{-6}$)	ND	$4.0 \cdot 10^{-6}$ ($8.3 \cdot 10^{-7}$)	$1.9 \cdot 10^{-6}$ ($7.0 \cdot 10^{-7}$)	$7.4 \cdot 10^{-7}$ ($7.2 \cdot 10^{-7}$)
Ba pfu	$4.7 \cdot 10^{-7}$ ($3.2 \cdot 10^{-7}$)	$3.5 \cdot 10^{-7}$ ($1.4 \cdot 10^{-7}$)	$8.6 \cdot 10^{-7}$ ($9.3 \cdot 10^{-7}$)	$1.4 \cdot 10^{-6}$ ($6.1 \cdot 10^{-7}$)	$7.0 \cdot 10^{-7}$ ($2.7 \cdot 10^{-7}$)
Pb pfu	$1.0 \cdot 10^{-7}$ ($2.8 \cdot 10^{-8}$)	$6.9 \cdot 10^{-9}$ ($1.3 \cdot 10^{-8}$)	$9.0 \cdot 10^{-8}$ ($4.7 \cdot 10^{-8}$)	$6.7 \cdot 10^{-8}$ ($6.3 \cdot 10^{-8}$)	$1.1 \cdot 10^{-7}$ ($3.7 \cdot 10^{-8}$)

Appendix III. (cont.)

Sample	LES-3 dolomite	LES-11 calcite	LES-14 dolomite
Mn (ppm)	155 (23)	24 (17)	162 (51)
Fe (ppm)	3269 (760)	ND	3883 (788)
Sr (ppm)	75.7 (12.2)	163.1 (26.7)	35.4 (5.0)
Cr (ppm)	ND	ND	ND
Co (ppm)	0.21 (0.07)	ND	0.20 (0.06)
Ni (ppm)	ND	ND	ND
Cu (ppm)	0.920 (0.490)	0.730 (0.206)	0.660 (0.439)
Zn (ppm)	3.08 (0.81)	0.48 (0.00)	3.58 (1.42)
Ba (ppm)	1.590 (0.476)	0.750 (0.222)	1.000 (0.316)
Pb (ppm)	0.260 (0.042)	0.220 (0.078)	0.240 (0.109)
Mn pfu	$2.7 \cdot 10^{-4}$ ($4.1 \cdot 10^{-5}$)	$3.8 \cdot 10^{-5}$ ($3.5 \cdot 10^{-5}$)	$2.7 \cdot 10^{-4}$ ($9.0 \cdot 10^{-5}$)
Fe pfu	$5.6 \cdot 10^{-3}$ ($1.3 \cdot 10^{-3}$)	ND	$6.4 \cdot 10^{-3}$ ($1.4 \cdot 10^{-3}$)
Sr pfu	$8.0 \cdot 10^{-5}$ ($1.4 \cdot 10^{-5}$)	$1.8 \cdot 10^{-4}$ ($3.2 \cdot 10^{-5}$)	$3.7 \cdot 10^{-5}$ ($5.5 \cdot 10^{-6}$)
Cr pfu	ND	ND	ND
Co pfu	$2.7 \cdot 10^{-7}$ ($1.5 \cdot 10^{-7}$)	ND	$3.0 \cdot 10^{-7}$ ($9.3 \cdot 10^{-8}$)
Ni pfu	ND	ND	ND
Cu pfu	$7.7 \cdot 10^{-7}$ ($8.9 \cdot 10^{-7}$)	$5.7 \cdot 10^{-7}$ ($6.5 \cdot 10^{-7}$)	$9.6 \cdot 10^{-7}$ ($6.7 \cdot 10^{-7}$)
Zn pfu	$4.4 \cdot 10^{-6}$ ($1.2 \cdot 10^{-6}$)	$9.0 \cdot 10^{-8}$ ($2.6 \cdot 10^{-7}$)	$5.0 \cdot 10^{-6}$ ($2.1 \cdot 10^{-6}$)
Ba pfu	$1.1 \cdot 10^{-6}$ ($3.3 \cdot 10^{-7}$)	$5.4 \cdot 10^{-7}$ ($1.7 \cdot 10^{-7}$)	$6.7 \cdot 10^{-7}$ ($2.2 \cdot 10^{-7}$)
Pb pfu	$1.2 \cdot 10^{-7}$ ($1.9 \cdot 10^{-8}$)	$3.9 \cdot 10^{-8}$ ($5.9 \cdot 10^{-8}$)	$1.0 \cdot 10^{-7}$ ($5.1 \cdot 10^{-8}$)

Notes: ND not detected; standard deviation in parentheses

Appendix IV. Oxygen and carbon isotopes.

Location	Sample Location	Mineral	$\delta^{13}\text{C}$ (‰ VPDB)	measured $\delta^{18}\text{O}$ (‰ VSMOW)	$\delta^{18}\text{O}_{\text{dol}}$ (‰ VSMOW) $\delta^{18}\text{O}_{\text{cal}} + \Delta_{\text{dol-cal}}$ (‰ VSMOW)	T (°C)
Location 1	L-1A	calcite	2.0	26.3	30.6	35.5
Location 1	L-1B	dolomite	2.1	25.5	25.5	61.7
Location 1	L-1C	dolomite	2.4	23.7	23.7	72.6
Location 1	L-1D	dolomite	3.4	25.8	25.8	60.3
Location 1	L-1E	calcite	1.8	23.8	27.7	49.5
Location 1	L-1G	calcite	2.2	24.7	28.7	44.5
Location 1	L-1H	calcite	2.2	25.4	29.5	40.3
Location 1	L-1I	dolomite	3.5	24.7	24.7	66.8
Location 1	L-1J	dolomite	2.2	26.3	26.3	57.2
Location 1	L-1K	dolomite	2.5	27.1	27.1	52.6
Location 1	L-1L	dolomite	2.2	25.9	25.9	59.7
Location 4	L-4A	calcite	2.0	26.1	30.3	36.6
Location 4	L-4B	calcite	1.9	26.6	30.9	34.1
Location 4	L-4C	calcite	1.8	26.1	30.3	36.8
Location 4	L-4D	calcite	2.2	27.5	32.0	29.1
Location 6	L-6A	dolomite	2.4	27.0	27.0	53.7
Location 6	L-6B	dolomite	4.2	26.3	26.3	57.0
Location 6	L-6C	dolomite	2.6	26.6	26.6	55.8
Location 6	L-6D	dolomite	2.6	26.5	26.5	56.0
Location 7	L-7A	calcite	2.1	25.5	29.7	39.5
Location 7	L-7B	calcite	2.1	25.9	30.1	37.6

Appendix IV. (cont.)

Location	Sample Location	Mineral	$\delta^{13}\text{C}$ (‰ VPDB)	measured $\delta^{18}\text{O}$ (‰ VSMOW)	$\delta^{18}\text{O}_{\text{dol}}$ (‰ VSMOW) $\delta^{18}\text{O}_{\text{cal}} + \Delta_{\text{dol-cal}}$ (‰ VSMOW)	T (°C)
Location 7	L-7C	dolomite	2.2	26.5	26.5	56.1
Location 7	L-7E	dolomite	2.3	27.3	27.3	52.1
Location 7	L-7F	dolomite	3.0	24.1	24.1	70.5
Location 7	L-7G	dolomite	2.0	27.1	27.1	53.1
Location 7	L-7H	dolomite	2.1	24.3	24.3	68.9
Location 7	L-7I	dolomite	2.3	27.0	27.0	53.6
Location 7	L-7J	calcite	2.0	26.0	30.2	37.1
Location 7	L-7K	calcite	2.1	25.3	29.4	41.1
Location 7	L-7L	dolomite	2.5	27.2	27.2	52.3
Location 7	L-7M	calcite	2.1	26.1	30.4	36.4
Location 7	L-7N	calcite	2.1	25.9	30.1	37.8
Location 7	L-7O	calcite	2.1	24.6	28.6	44.7
Location 7	L-7P	calcite	2.2	25.5	29.7	39.8
Location 7	7T-1	dolomite	2.5	26.3	26.3	57.5
Location 7	7T-2	dolomite	2.4	26.3	26.3	57.1
Location 7	7T-3	dolomite	2.2	26.1	26.1	58.2
Location 7	7T-4	dolomite	2.2	26.4	26.4	56.8
Location 7	7T-5	dolomite	4.5	24.7	24.7	66.5
Location 7	7T-6	dolomite	4.3	23.1	23.1	76.9
Location 7	7T-7	dolomite	4.3	22.7	22.7	79.2
Location 7	7T-8	dolomite	2.3	27.2	27.2	52.3

Appendix IV. (cont.)

Location	Sample Location	Mineral	$\delta^{13}\text{C}$ (‰ VPDB)	measured $\delta^{18}\text{O}$ (‰ VSMOW)	$\delta^{18}\text{O}_{\text{dol}}$ (‰ VSMOW) $\delta^{18}\text{O}_{\text{cal}} + \Delta_{\text{dol-cal}}$ (‰ VSMOW)	T (°C)
Location 7	7T-9	dolomite	2.2	27.1	27.1	52.9
Location 7	7T-10	dolomite	2.0	26.1	26.1	58.2
Location 7	7T-11	dolomite	2.0	26.4	26.4	56.8
Location 7	7T-12	dolomite	3.0	24.9	24.9	65.2
Location 7	7T-13	dolomite	3.8	23.8	23.8	72.2
Location 7	7T-14	dolomite	2.1	26.0	26.0	59.0
Location 7	7T-15	dolomite	2.4	25.7	25.7	60.6
Location 7	7T-16	dolomite	2.3	26.9	26.9	53.8
Location 8	L-8A	calcite	2.4	25.6	29.7	39.5
Location 8	L-8B	calcite	2.2	25.1	29.2	42.2
Location 8	L-8C	dolomite	2.6	27.1	27.1	53.0
Location 8	L-8D	dolomite	2.4	25.9	25.9	59.4
Location 8	L-8E	calcite	2.2	25.7	29.9	38.7
Location 8	L-8F	calcite	2.1	25.9	30.1	37.7
Location 8	L-8G	dolomite	2.4	27.3	27.3	51.8
Location 8	L-8H	calcite	2.4	25.5	29.6	39.9
Location 8	L-8I	calcite	2.2	25.1	29.2	41.9
Location 8	L-8J	calcite	2.2	28.0	32.5	27.0
Location 8	L-8K	dolomite	2.5	27.0	27.0	53.7
Location 8	L-8L	calcite	2.4	25.7	29.9	38.6
Location 8	L-8M	calcite	2.0	26.0	30.2	37.0

Appendix IV. (cont.)

Location	Sample Location	Mineral	$\delta^{13}\text{C}$ (‰ VPDB)	measured $\delta^{18}\text{O}$ (‰ VSMOW)	$\delta^{18}\text{O}_{\text{dol}}$ (‰ VSMOW) $\delta^{18}\text{O}_{\text{cal}} + \Delta_{\text{dol-cal}}$ (‰ VSMOW)	T (°C)
Location 8	L-8N	calcite	2.2	25.5	29.6	40.0
Location 8	L-8O	dolomite	2.5	23.6	23.6	73.2
Location 8	L-8P	calcite	2.1	25.5	29.7	39.6
Location 8	L-8Q	dolomite	2.6	26.7	26.7	54.8
Location 8	8T-1	calcite	2.1	25.5	29.7	39.7
Location 8	8T-1	dolomite	2.5	27.3	27.3	52.0
Location 8	8T-10	dolomite	2.4	25.9	25.9	59.5
Location 8	8T-11	dolomite	2.5	26.6	26.6	55.5
Location 8	8T-12	dolomite	2.7	25.6	25.6	61.1
Location 8	8T-13	dolomite	2.8	25.8	25.8	59.8
Location 8	8T-14	dolomite	2.2	23.1	23.1	76.8
Location 8	8T-2	dolomite	2.7	27.2	27.2	52.5
Location 8	8T-3	dolomite	2.5	26.8	26.8	54.4
Location 8	8T-4	dolomite	2.6	26.2	26.2	58.1
Location 8	8T-5	dolomite	2.3	26.4	26.4	56.8
Location 8	8T-6	dolomite	2.4	26.8	26.8	54.3
Location 8	8T-7	dolomite	2.5	23.0	23.0	77.4
Location 8	8T-8	dolomite	2.4	25.8	25.8	60.0
Location 8	8T-9	dolomite	2.3	23.4	23.4	74.5
Location 9	L-9A	calcite	2.6	26.3	30.6	35.4
Location 9	L-9B	calcite	2.6	25.7	29.8	39.0

Appendix IV. (cont.)

Location	Sample Location	Mineral	$\delta^{13}\text{C}$ (‰ VPDB)	measured $\delta^{18}\text{O}$ (‰ VSMOW)	$\delta^{18}\text{O}_{\text{dol}}$ (‰ VSMOW) $\delta^{18}\text{O}_{\text{cal}} + \Delta_{\text{dol-cal}}$ (‰ VSMOW)	T (°C)
Location 9	L-9C	calcite	2.0	27.5	32.0	29.2
Location 9	L-9D	calcite	2.6	26.2	30.4	36.1
Location 9	L-9E	calcite	2.6	25.1	29.2	42.0
Location 9	L-9F	calcite	2.2	26.8	31.1	32.9
Location 11	L-11A	calcite	3.9	26.3	30.5	35.6
Location 11	L-11B	dolomite	3.1	24.1	24.1	70.1
Location 11	L-11C	dolomite	4.0	23.9	23.9	71.4
Location 11	L-11D	calcite	3.0	24.9	29.0	43.2
Location 11	L-11E	dolomite	3.1	26.4	26.4	56.9
Location 11	L-11F	calcite	3.3	26.2	30.4	36.0
Location 11	L-11G	dolomite	4.0	24.9	24.9	65.5
Location 11	L-11H	calcite	3.8	25.3	29.4	40.8
Location 12	L-12A	dolomite	2.4	25.4	25.4	62.5
Location 12	L-12B	dolomite	2.3	26.6	26.6	55.5
Location 12	L-12C	dolomite	2.2	25.8	25.8	59.9
Location 12	L-12D	calcite	1.9	26.2	30.5	35.8
Location 12	L-12E	dolomite	2.1	25.9	25.9	59.6
Location 12	L-12F	calcite	2.0	25.3	29.4	41.0
Location 12	L-12G	calcite	1.6	24.0	27.9	48.6
Location 12	L-12H	dolomite	2.2	25.6	25.6	61.1
Location 12	L-12I	calcite	2.0	26.1	30.4	36.5

Appendix IV. (cont.)

Location	Sample Location	Mineral	$\delta^{13}\text{C}$ (‰ VPDB)	measured $\delta^{18}\text{O}$ (‰ VSMOW)	$\delta^{18}\text{O}_{\text{dol}}$ (‰ VSMOW) $\delta^{18}\text{O}_{\text{cal}} + \Delta_{\text{dol-cal}}$ (‰ VSMOW)	T (°C)
Location 12	L-12J	calcite	2.0	25.2	29.3	41.7
Location 13	L-13A	dolomite	2.5	24.6	24.6	67.1
Location 13	L-13B	dolomite	2.9	22.2	22.2	83.1
Location 13	L-13C	dolomite	2.3	23.1	23.1	77.0
Location 13	L-13D	dolomite	3.7	23.8	23.8	72.4
Location 13	L-13E	dolomite	2.4	25.8	25.8	60.3
Location 13	L-13F	dolomite	3.6	23.2	23.2	76.1
189 Traverse A	LAS-57	dolomite	4.2	25.4	25.4	62.5
Traverse A	LAS-56	dolomite	4.6	25.3	25.3	63.0
Traverse A	LAS-55	dolomite	4.2	23.6	23.6	73.4
Traverse A	LAS-54	dolomite	3.8	22.7	22.7	79.5
Traverse A	LAS-53	dolomite	3.1	23.3	23.3	75.6
Traverse A	LAS-52	calcite	3.0	25.2	25.2	63.8
Traverse A	LAS-51	dolomite	2.6	23.2	23.2	75.8
Traverse A	LAS-50	calcite	2.7	27.0	31.4	31.6
Traverse A	LAS-49	dolomite	2.4	23.6	23.6	73.6
Traverse A	LAS-48	dolomite	2.8	23.7	23.7	72.7
Traverse A	LAS-47	dolomite	2.5	25.1	25.1	64.2
Traverse A	LAS-46	dolomite	4.3	22.6	22.6	80.2
Traverse A	LAS-45	dolomite	3.4	22.6	22.6	80.4
Traverse A	LAS-44	calcite	3.8	25.6	29.7	39.5

Appendix IV. (cont.)

Location	Sample Location	Mineral	$\delta^{13}\text{C}$ (‰ VPDB)	measured $\delta^{18}\text{O}$ (‰ VSMOW)	$\delta^{18}\text{O}_{\text{dol}}$ (‰ VSMOW) $\delta^{18}\text{O}_{\text{cal}} + \Delta_{\text{dol-cal}}$ (‰ VSMOW)	T (°C)
Traverse A	LAS-42	calcite	2.8	27.6	32.1	28.7
Traverse A	LAS-43	dolomite	4.1	24.1	24.1	70.6
Traverse A	LAS-41	dolomite	2.8	25.6	25.6	61.0
Traverse A	LAS-40	calcite	3.4	26.2	30.4	36.1
Traverse A	LAS-1	calcite	4.0	26.1	30.3	36.8
Traverse A	LAS-2	calcite	3.5	26.3	30.6	35.3
Traverse A	LAS-3	calcite	2.8	27.3	31.7	30.3
Traverse A	LAS-4	calcite	2.7	28.1	32.6	26.5
Traverse A	LAS-5	dolomite	2.4	21.8	21.8	86.0
Traverse A	LAS-6	calcite	2.5	27.3	31.7	30.5
Traverse A	LAS-7	calcite	2.5	25.7	29.9	38.7
Traverse A	LAS-8	dolomite	2.7	26.1	26.1	58.3
Traverse A	LAS-9	dolomite	2.3	22.5	22.5	80.7
Traverse A	LAS-10	dolomite	2.7	25.6	25.6	61.3
Traverse A	LAS-11	calcite	2.4	26.3	30.6	35.5
Traverse A	LAS-12	dolomite	2.4	25.9	25.9	59.4
Traverse A	LAS-13	calcite	2.4	26.1	30.4	36.4
Traverse A	LAS-14	calcite	2.8	25.4	29.5	40.5
Traverse A	LAS-15	dolomite	3.1	25.1	25.1	63.9
Traverse A	LAS-16	calcite	2.6	26.8	31.1	33.0
Traverse A	LAS-17	calcite	2.3	26.8	31.2	32.7

Appendix IV. (cont.)

Location	Sample Location	Mineral	$\delta^{13}\text{C}$ (‰ VPDB)	measured $\delta^{18}\text{O}$ (‰ VSMOW)	$\delta^{18}\text{O}_{\text{dol}}$ (‰ VSMOW) $\delta^{18}\text{O}_{\text{cal}} + \Delta_{\text{dol-cal}}$ (‰ VSMOW)	T (°C)
Traverse A	LAS-18	calcite	2.3	27.4	31.8	29.8
Traverse A	LAS-19	calcite	2.4	26.1	30.3	36.7
Traverse A	LAS-20	calcite	2.5	24.0	27.9	48.3
Traverse A	LAS-21	dolomite	2.7	26.4	26.4	56.9
Traverse A	LAS-22	calcite	2.3	25.0	29.0	42.8
Traverse A	LAS-23	dolomite	2.3	26.7	26.7	55.2
Traverse A	LAS-24	dolomite	2.5	26.1	26.1	58.2
Traverse A	LAS-25	dolomite	2.5	25.8	25.8	59.9
Traverse A	LAS-26	calcite	2.0	24.6	28.6	45.2
Traverse A	LAS-27	dolomite	2.3	23.9	23.9	71.4
Traverse A	LAS-28	calcite	2.3	25.1	29.1	42.3
Traverse A	LAS-29	dolomite	2.5	26.7	26.7	55.0
Traverse A	LAS-30	calcite	2.0	27.4	31.8	30.0
Traverse A	LAS-31	calcite	2.1	27.3	31.7	30.5
Traverse A	LAS-32	calcite	2.0	26.9	31.3	32.4
Traverse A	LAS-34	dolomite	2.2	27.3	27.3	51.6
Traverse A	LAS-33	calcite	1.9	27.0	31.4	31.6
Traverse A	LAS-35	calcite	2.0	28.5	33.0	24.7
Traverse A	LAS-36	calcite	1.9	28.3	32.8	25.5
Traverse A	LAS-37	dolomite	2.6	25.9	25.9	59.5
Traverse A	LAS-38	calcite	1.9	25.6	29.8	39.0

Appendix IV. (cont.)

Location	Sample Location	Mineral	$\delta^{13}\text{C}$ (‰ VPDB)	measured $\delta^{18}\text{O}$ (‰ VSMOW)	$\delta^{18}\text{O}_{\text{dol}}$ (‰ VSMOW) $\delta^{18}\text{O}_{\text{cal}} + \Delta_{\text{dol-cal}}$ (‰ VSMOW)	T (°C)
Traverse A	LAS-39	calcite	2.0	25.9	30.2	37.4
Traverse B	LBS-1	dolomite	2.9	24.7	24.7	66.9
Traverse B	LBS-2	dolomite	2.4	24.8	24.8	65.9
Traverse B	LBS-3	calcite	2.6	27.1	31.5	31.2
Traverse B	LBS-4	calcite	2.3	26.9	31.2	32.6
Traverse B	LBS-5	dolomite	2.9	26.2	26.2	57.7
Traverse B	LBS-6	calcite	2.3	27.5	31.9	29.5
Traverse B	LBS-7	calcite	2.4	26.9	31.2	32.6
Traverse B	LBS-8	calcite	2.5	27.0	31.3	32.0
Traverse B	LBS-9	dolomite	2.6	25.2	25.2	63.9
Traverse B	LBS-10	calcite	2.8	26.9	31.2	32.6
Traverse B	LBS-11	calcite	2.4	26.5	30.7	34.7
Traverse B	LBS-12	calcite	1.1	23.4	27.2	52.3
Traverse B	LBS-13	calcite	2.2	26.3	30.6	35.5
Traverse B	LBS-14	calcite	1.9	26.1	30.3	36.5
Traverse B	LBS-15	calcite	2.1	25.6	29.8	39.1
Traverse C	LCS-1	calcite	1.8	26.5	30.8	34.6
Traverse C	LCS-2	calcite	2.3	25.0	29.1	42.6
Traverse C	LCS-3	calcite	2.3	25.1	29.1	42.2
Traverse C	LCS-4	calcite	2.1	26.3	30.6	35.2
Traverse C	LCS-5	calcite	2.4	25.0	29.1	42.6

Appendix IV. (cont.)

Location	Sample Location	Mineral	$\delta^{13}\text{C}$ (‰ VPDB)	measured $\delta^{18}\text{O}$ (‰ VSMOW)	$\delta^{18}\text{O}_{\text{dol}}$ (‰ VSMOW) $\delta^{18}\text{O}_{\text{cal}} + \Delta_{\text{dol-cal}}$ (‰ VSMOW)	T (°C)
Traverse C	LCS-6	calcite	2.6	24.5	28.5	45.5
Traverse C	LCS-7	calcite	2.4	25.2	29.3	41.4
Traverse C	LCS-8	dolomite	2.5	26.3	26.3	57.0
Traverse C	LCS-9	calcite	2.2	26.0	30.2	37.0
Traverse C	LCS-10	dolomite	2.6	26.5	26.5	56.4
Traverse C	LCS-11	dolomite	2.4	27.2	27.2	52.2
Traverse C	LCS-13	calcite	2.9	26.0	30.2	37.1
Traverse C	LCS-14	calcite	2.2	25.5	29.6	39.8
Traverse C	LCS-15	calcite	2.0	26.7	31.0	33.3
Traverse D	LDS-1a	calcite	2.1	27.3	31.7	30.5
Traverse D	LDS-1b	calcite	2.1	26.5	30.7	34.7
Traverse D	LDS-2	dolomite	3.4	25.0	25.0	65.0
Traverse D	LDS-3	dolomite	2.5	24.0	24.0	70.9
Traverse D	LDS-4	calcite	2.1	26.1	30.4	36.5
Traverse D	LDS-5	dolomite	2.3	25.0	25.0	65.1
Traverse D	LDS-6	calcite	2.4	26.9	31.2	32.4
Traverse D	LDS-7	calcite	2.5	28.0	32.6	26.6
Traverse D	LDS-8	calcite	2.5	25.7	29.9	38.6
Traverse D	LDS-9a	calcite	2.1	26.6	31.0	33.7
Traverse D	LDS-9b	calcite	2.3	25.5	29.6	40.1
Traverse D	LDS-10	calcite	2.2	26.0	30.2	37.3

Appendix IV. (cont.)

Location	Sample Location	Mineral	$\delta^{13}\text{C}$ (‰ VPDB)	measured $\delta^{18}\text{O}$ (‰ VSMOW)	$\delta^{18}\text{O}_{\text{dol}}$ (‰ VSMOW) $\delta^{18}\text{O}_{\text{cal}} + \Delta_{\text{dol-cal}}$ (‰ VSMOW)	T (°C)
Traverse D	LDS-11	dolomite	2.5	25.7	25.7	60.8
Traverse D	LDS-13	calcite	2.4	25.9	30.1	37.7
Traverse D	LDS-12	dolomite	2.5	27.1	27.1	53.0
Traverse D	LDS-14	dolomite	2.2	26.4	26.4	57.0
Traverse D	LDS-15	calcite	2.2	25.2	29.4	41.2
Traverse D	LDS-16	dolomite	2.6	25.8	25.8	60.3
Traverse D	LDS-17	calcite	2.0	24.6	28.6	44.9
Traverse D	LDS-18	calcite	1.9	25.6	29.8	39.2
Traverse E	LES-1	calcite	2.0	26.1	30.3	36.6
Traverse E	LES-2	calcite	2.8	24.3	28.3	46.5
Traverse E	LES-3	dolomite	2.5	27.2	27.2	52.6
Traverse E	LES-4	dolomite	2.7	27.1	27.1	53.0
Traverse E	LES-5	dolomite	2.9	26.0	26.0	59.1
Traverse E	LES-6	calcite	3.0	24.3	28.3	46.7
Traverse E	LES-7	dolomite	2.7	25.9	25.9	59.4
Traverse E	LES-8	calcite	2.0	23.5	27.3	51.6
Traverse E	LES-9	dolomite	2.5	27.7	27.7	49.9
Traverse E	LES-10	calcite	2.2	25.2	29.3	41.7
Traverse E	LES-11	calcite	1.9	26.3	30.5	35.6
Traverse E	LES-12	calcite	1.8	26.3	30.6	35.5
Traverse E	LES-13	dolomite	2.5	27.5	27.5	50.5

Appendix IV. (cont.)

Location	Sample Location	Mineral	$\delta^{13}\text{C}$ (‰ VPDB)	measured $\delta^{18}\text{O}$ (‰ VSMOW)	$\delta^{18}\text{O}_{\text{dol}}$ (‰ VSMOW) $\delta^{18}\text{O}_{\text{cal}} + \Delta_{\text{dol-cal}}$ (‰ VSMOW)	T (°C)
Traverse E	LES-14	dolomite	2.5	24.1	24.1	70.2
Traverse E	LES-15	dolomite	2.4	27.0	27.0	53.3
Traverse E	LES-16a	calcite	1.8	24.9	29.0	42.9
Traverse E	LES-16b	calcite	2.0	25.6	29.8	39.2
Traverse F	LFS-1	dolomite	2.4	25.5	25.5	62.0
Traverse F	LFS-2	calcite	2.1	23.9	27.8	49.0
Traverse F	LFS-3	dolomite	2.4	25.7	25.7	60.6
Traverse F	LFS-4	calcite	2.1	26.3	30.6	35.4

References

- Adams, J. E., and Rhodes, M. L., 1960, Dolomitization by seepage refluxion. American Association of Petroleum Geologists Bulletin, vol. 44, p. 1912-1920.
- Aharon P., Socki, R. A., and Chan, L., 1987, Dolomitization of atolls by sea water convection flow: Test of a hypothesis at Niue, South Pacific. Journal of Geology, vol. 95, p. 187-203.
- Antonelli, M., and Mollema, P.N., 2000, A natural analog for a fractured and faulted reservoir in dolomite: Triassic Sella Group, northern Italy. AAPG Bulletin, vol. 84, p. 314-344.
- Armstrong, J.T., 1988, Quantitative analysis of silicate and oxide minerals: Comparison of Monte Carlo, ZAF, and phi-rho-z procedures. In Newbury, D.E., ed., Microbeam Analysis - 1998: San Francisco, San Francisco Press, p. 239-246.
- Arvidson, R. S., and Mackenzie, F. T., 1999, The dolomite problem: control of precipitation kinetics by temperature and saturation state. American Journal of Science, vol. 299, p. 257-288.
- Badiozamani, K., 1973, The dorag dolomitization model – application to the Middle Ordovician of Wisconsin. Journal of Sedimentary Petrology, vol. 43, p. 965-984.
- Baker, P. A., and Kastner, M., 1981, Constraints on the formation of sedimentary dolomite. Science, vol. 213, p. 214-216.
- Bathurst, R. G. C., 1975, Carbonate sediments and their diagenesis. 2nd Edition, El Sevier, New York. 658 p.

- Baumgartner, L.P., and Valley, J.W., 2001, Stable isotope transport and contact metamorphic fluid flow. In: Valley, J.W. and Cole, D.R. (eds) Stable isotope geochemistry. *Reviews in Mineralogy*, vol. 43, p. 415-467.
- Blendinger, W., 1985, Middle Triassic strike-slip tectonics and igneous activity of the Dolomites (southern Alps). *Tectonophysics*, v. 113, p. 105-121.
- Bosellini, A., 1984, Progradation geometries of carbonate platforms: examples from the Triassic of the Dolomites, northern Italy. *Sedimentology*, v. 31, p. 1-24.
- Bosellini, A., and Hsü, K.J., 1973, Mediterranean plate tectonics and Triassic palaeogeography. *Nature*, vol. 244, p. 144-146.
- Bosellini, A., and Rossi, D., 1974a, Triassic carbonate buildups of northern Italy. In: Laporte, L, ed., *Reefs in Time and Space: Society of Economic Paleontologists and Mineralogists Special Publication 18*, p. 209-233.
- Bosellini, A., and Rossi, D., 1974b, Triassic carbonate buildups of northern Italy. *American Association of Petroleum Geologists Bulletin*, v. 54, p. 836-837.
- Bosellini, A, Gianolla, P., and Stefani, M., 2003, Geology of the Dolomites. *Episodes*, v. 26, no. 3, p. 181-185.
- Brack, P., Mundil, R., Oberli, F., Meier, M., and Rieber, H., 1996, Biostratigraphic and radiometric age data question the Milankovitch characteristics of the Latemar (southern Alps, Italy). *Geology*, v. 24, p. 371-375.
- Brady, J.B., 1988, The role of volatiles in the thermal history of metamorphic terranes, *Journal of Petrology*, vol. 29, part 6, p.1187-1213.
- Brady, P.V., Krumhansl, J.L., and Papenguth, H.W., 1996, Surface complexation clues to dolomite growth. *Geochimica et Cosmochimica Acta*, vol. 60, p. 727-731.

- Budd, D. A., 1984, Freshwater diagenesis of Holocene ooid sands, Schooner Cays, Bahamas, Ph.D. dissertation, University of Texas at Austin, Austin, TX, U.S.A.
- Budd, D. A., 1997, Cenozoic dolomites of carbonate islands: their attributes and origin. *Earth Science Reviews*, vol. 42, p. 1-47.
- Burke, W. H., Denison, R. E., Hetherington, E. A., Koepnick, R. B., Nelson, H. R., and Otto, J. B., 1982, Variation of seawater $^{87}\text{Sr}/^{86}\text{Sr}$ throughout Phanerozoic time. *Geology*, vol. 10, p. 516-519.
- Chacko T., Mayeda T.K., Clayton R.N., and Goldsmith J. R., 1991, Oxygen and carbon isotope fractionation between CO₂ and calcite. *Geochimica et Cosmochimica Acta*, vol. 55, p. 2867–2882
- Chai, L., Navrotsky, A., and Reeder, R. J., 1995, Energetics of calcium-rich dolomite. *Geochimica and Cosmochimica Acta*, vol. 59, p. 939-944.
- Cros, P., 1977, Donnée nouvelle sur la dolomitization des carbonates triassiques des Dolomites italiennes. *Sciences de la Terre*, vol. 21, p. 307-355.
- Curtis, R., Evans, G., Kinsman, D. J. J., and Shearman, D. J., 1963, Association of dolomite and anhydrite in the Recent sediments of the Persian Gulf. *Nature*, vol. 197, p. 679-680.
- De Dolomieu, D., 1791, Sur un genre de pierres calcaires très-peu effervescentes avec les acides, et phosphorescentes par la collision: *Journal de Physique, de Chimie, d'Historie Naturelle, et des Arts*, v. 39, p. 3-10.
- Deelman, J.C., 1999, Low-temperature nucleation of magnesite and dolomite. *Neues Jahrbuch für Mineralogie, Monatshefte*, vol. 7, p. 289-302.

- Deines, P., 2004, Carbon isotope effects in carbonate systems. *Geochimica et Cosmochimica Acta*, vol. 68, p. 2659–2679.
- Dipple, G.M., and Ferry, J.M., 1992, Metasomatism and fluid flow in ductile fault zones. *Contributions to Mineralogy and Petrology*, vol. 112, p. 149-164.
- Doglioni, C., 1987, Tectonics of the Dolomites (southern Alps, northern Italy). *Journal of Structural Geology*, vol. 9, no. 2, p. 181-193.
- Doglioni, C., 1990, The Venetian Alps thrust belt: in McClay, K.R., ed., *Thrust Tectonics*: London, Chapman, and Hall, p. 319-324.
- Doglioni, C., and Bosellini, A., 1987, Eoalpine and mesoalpine tectonics in the southern Alps. *Geologische Rundschau*, v. 76, no. 3, p. 735-754.
- Dunn, P. A., 1991, Cyclic stratigraphy and early diagenesis: an example from the Triassic Latemar platform, northern Italy. Ph.D. dissertation, Johns Hopkins University, Baltimore, MD, U.S.A.
- Edmond, J.M., Campbell, G.A., Palmer, M.R., Klinkhammer, G.P., German, C.R., Edmonds, H.N., Elderfield, H., Thompson, G., and Rona, P.A., 1995, Time series study of vent fluids from the TAG and MARK sites (1986, 1990) Mid-Atlantic Ridge: A new solution chemistry model and a mechanism for Cu/Zn zonation in massive sulphide orebodies. In *Hydrothermal Vents and Processes*, L.M. Parson, C.L. Walker, and D.R. Dixon, eds., Geological Society Special Paper 87, Longon, p. 77-86.
- Egenhoff, S. O., Peterhansel, A., Bechstaedt, T., Zuhlke, R., Grottsch, J., 1999, Facies architecture of an isolated carbonate platform; tracing the cycles of the Latemar (Middle Triassic, northern Italy). *Sedimentology*, vol. 46, no. 5, p. 893-912.

- Elder, J.W., 1977, Thermal convection: *Journal of the Geological Society of London*, vol. 133, p. 292-309.
- Elderfield, H., Wheat, C.G., Mottl, M.J., Monnin, C., and Spiro, B., 1999, Fluid and geochemical transport through oceanic crust: a transect across the eastern flank of the Juan de Fuca Ridge. *Earth and Planetary Science Letters*, vol. 172, p. 151-165.
- Emiliani, C., and Edwards, G., 1953, Tertiary ocean bottom temperatures. *Nature*, vol. 171, p. 887-888.
- Eugster, H. P., and Hardie, L. A., 1978, Saline lakes. In: Lerman, A. (Ed.), *Lakes: Chemistry, Geology, Physics*. Springer-Verlag, New York, p. 237-293.
- Fanning, K. A., Byrne, R. H., Breland, J. A., and Betzer, P. R., 1981, Geothermal springs of the west Florida continental shelf: evidence for dolomitization and radionuclide enrichment. *Earth and Planetary Science Letters*, vol. 52, p. 345-354.
- Ferry, J. M., and Gerdes, M. L., 1998, Chemically reactive fluid flow during metamorphism. *Annual Review in Earth and Planetary Sciences*, vol. 26, p. 255-287.
- Flood, P.G., Fagerstrom, J.A., and Rougerie, F., 1996, Interpretation of the origin of massive replacement dolomite within atolls and submerged carbonate platforms: strontium isotope signature ODP Hole 866°, Resolution Guyot, Mid-Pacific Mountains. *Sedimentary Geology*, vol. 101, p. 9-13.
- Folk, R. L., and Land, L. S., 1975, Mg/Ca ratio and salinity: two controls over crystallization of dolomite. *American Association of Petroleum Geologists Bulletin*, vol. 59, p. 60-68.

- Friedman, G. M., and Sanders, J. E., 1967, Origin and occurrence of dolostones. In Chilingar, G. V., Bissell, H. J., and Fairbridge, R. W., eds., Carbonate Rocks, Part A: Origin, Occurrence, and Classification. El Sevier, Amsterdam. p. 167-348.
- Friedman, I. and O'Neil, J.R., 1977 Compilation of stable isotope fractionation factors of geochemical interest. USGS Professional Paper 440-KK.
- Gaetani, M., Fois, E., Jadoul, F., and Nicora, A., 1981, Nature and evolution of Middle Triassic carbonate buildups in the Dolomites (Italy). *Marine Geology*, v. 44, p. 25-57.
- Gaines, A.M., 1980, Dolomitization kinetics: recent experimental studies. SEPM Special Publication No. 28, p. 81-86.
- Garrison, R. E., Kastner, M., and Zenger, D. H., Eds., 1984, Dolomites of the Monterey Formation and other organic-rich units. SEPM, Pacific Section, Los Angeles, CA, 215 p.
- Garven, G., 1985, The role of regional fluid flow in the genesis of the Pine Point deposit, western Canada sedimentary basin. *Economic Geology*, vol. 80, p. 307-324.
- Garven, G., and Freeze, R. A., 1984, Theoretical analysis of the role of groundwater flow in the genesis of stratabound ore deposits. *American Journal of Science*, vol. 284, Part 1, p. 1085-1124, Part 2, p. 1125-1174.
- Gebelein, C. D., Steinen, R. P., Garrett, P., Hoffman, E. J., Queen, J. M., and Plummer, L. N., 1980, Subsurface dolomitization beneath the tidal flats of central-west Andros Island, Bahamas. *Society of Economic Paleontologists and Mineralogists*, Special Publication 28, p. 31-49.

- Gianolla, P., De Zanche, V., and Mietto, P., 1998, Triassic sequence stratigraphy in the southern Alps. Definition of sequences and basin evolution. In: P.C. de Graciansky, J. Hardenbol, T. Jacquin, P.R. Vail, and D. Ulmer-Scholle (Eds.): Mesozoic-Cenozoic Sequence Stratigraphy of European basins. Society of Economic Paleontologists and Mineralogists Special Publication 60, p. 723-751.
- Goldhammer, R., 1987, Platform carbonate cycles, Middle Triassic of northern Italy: the interplay of local tectonics and global eustasy. Ph.D. dissertation, Johns Hopkins University, Baltimore, MD, U.S.A.
- Goldhammer, R. K., Dunn, P. A., and Hardie, L. A., 1987, High frequency glacio-eustatic sea level oscillations with Milankovitch characteristics recorded in Middle Triassic platform carbonates in N. Italy. *American Journal of Science*, v. 287, p. 853-892.
- Goldhammer, R. K., Dunn, P. A., and Hardie, L. A., 1990, Depositional cycles, composite sea-level changes, cycle stacking patterns, and the hierarchy of stratigraphic forcing: Examples from Alpine Triassic platform carbonates. *Geological Society of America Bulletin*, vol. 102, p. 535-562.
- Goldstein, R.H., 2001, Fluid inclusions in sedimentary and diagenetic systems. *Lithos*, vol. 55, p. 159-193.
- Graf, D. L., and Goldsmith, J. R., 1956, Some hydrothermal syntheses of dolomite and protodolomite. *Journal of Geology*, vol. 64, p.173-186.
- Gregg, J. M., 1985, Regional epigenetic dolomitization in the Bonneterre dolomite (Cambrian), southeastern Missouri. *Geology*, vol. 13, p. 503-506.

- Gregg, J.M, and Sibley, D.F., 1984, Epigenetic dolomitization and the origin of xenotopic dolomite texture. *Journal of Sedimentary Petrology*, vol. 54, p. 907-931.
- Halley, R. B., and Harris, P. M., 1979, Fresh-water cementation of 1000-year-old oolite. *Journal of Sedimentary Petrology*, vol. 49, p. 969-988.
- Hanshaw, B. B., and Back, W., 1980, Chemical mass-wasting of the northern Yucatán Peninsula by groundwater dissolution. *Geology*, vol. 8, p. 222-224.
- Hardie, L. A., 1987, Dolomitization: A critical view and some current views. *Journal of Sedimentary Petrology*, vol. 57, no. 1, p. 166-183.
- Hardie, L. A., 1996, Secular variations in seawater chemistry: An explanation for the coupled secular variation in the mineralogies of marine limestones and potash evaporites over the past 600 m.y. *Geology*, vol. 24, p. 279-283.
- Hardie, L. A., Bosellini, A., and Goldhammer, R. K., 1986, Repeated subaerial exposure of subtidal carbonate platforms, Triassic northern Italy: evidence for high frequency sea level oscillations on a 10^4 year scale. *Paleoceanography*, vol. 1, p. 447-457.
- Harris, M., 1988, Margin and foreslope deposits of the Latemar carbonate buildup (Middle Triassic), the Dolomites, northern Italy. Ph.D. dissertation, Johns Hopkins University, Baltimore, MD, U.S.A.
- Helgesen, H.C., Delaney, H.W., Nesbitt, H.W., and Bird, D.K., 1978, Summary and critique of the thermodynamic properties of rock-forming minerals. *American Journal of Science*, vol. 278-A, p. 1-229.

- Holland, T.J.B., and Powell, R., 1998, An internally consistent thermodynamic dataset for phases of petrological interest. *Journal of Metamorphic Geology*, vol.16, p. 309-343.
- Hyeong, K., and Capuano, R.M., 2001, Ca/Mg of brines in Miocene/Oligocene clastic sediments of the Texas Gulf Coast: Buffering by calcite/disordered dolomite equilibria. *Geochimica et Cosmochimica Acta*, vol. 65, p. 3065-3080.
- Illing, L. V., 1959, Deposition and diagenesis of some upper Paleozoic carbonate sediments in western Canada. *Fifth World Petroleum Congress Proceedings*, John Wiley and Sons, New York, p. 23-52.
- Jackson, S.E., 1997. LAMTRACE v 1.74, LAM-ICP-MS data reduction spreadsheet. Department of Earth Sciences, Memorial University of Newfoundland, St John's, Canada. Modified 2002 by Istvan Laszlo.
- James, R.H., and Elderfield, H., 1996, Chemistry of ore-forming fluids and mineral formation rates in an active hydrothermal sulfide deposit on the Mid-Atlantic Ridge. *Geology*, vol. 24, p. 1147-1150.
- Jodry, R. L., 1969, Growth and dolomitization of Silurian reefs, Saint Clair, Michigan. *The American Association of Petroleum Geologists Bulletin*, vol. 53, p. 957-981.
- Johnson, J.W., Oelkers, E.H., and Helgeson, H.C., 1992, SUPCRT92: A software package for calculating the standard molal thermodynamic properties of minerals, gases, aqueous species, and reactions from 1 to 5000 bar and 0° to 1000°C. *Computer Geoscience*, vol. 18, p. 899-947.
- Jones, B. F., 1965, The hydrology and mineralogy of Deep Springs Lake, California. U. S. Geological Survey Professional Paper No. 502-A, 56 p.

- Jones, G.D., and Rostron, B.J., 2000, Analysis of fluid flow constraints in regional-scale reflux dolomitization: constant versus variable-flux hydrogeological models. *Bulletin of Canadian Petroleum Geology*, vol. 48, p. 230-245.
- Jones, G.D., Whitaker, F., Smart, P., and Sanford, W.E., 2004, Numerical analysis of seawater circulation in carbonate platforms: II. The dynamic interaction between geothermal and brine reflux circulation. *American Journal of Science*, vol. 304, p. 250-284.
- Katz, A., and Matthews, A., 1976, The dolomitization of CaCO₃: an experimental study at 252-295°C. *Geochimica et Cosmochimica Acta*, vol. 41, p. 297-308.
- Kelleher, I.J., and Redfern, S.A.T., 2002, Hydrous calcium magnesium carbonate, a possible precursor to the formation of sedimentary dolomite. *Molecular Simulation*, vol. 28, p. 557-572.
- Kelley, D.S., Karson, J.A., Früh-Green, G.L., Yoerger, D.R., Shank, T.M., Butterfield, D.A., Hayes, J.M., Schrenk, M.O., Olson, E.J., Proskurowski, G., Jakuba, M., Bradley, A., Larson, B., Ludwig, K., Glickson, D., Buckman, K., Bradley, A., Brazelton, W.J., Roe, K., Elend, M.J., Delacour, A., Bernasconi, S.M., Lilley, M.D., Baross, J.A., Summons, R.A., and Sylva, S.P., 2005, A serpentine-hosted ecosystem: the Lost City Hydrothermal Field. *Science*, vol. 307, p. 1428-1434.
- Kelts, K., and McKenzie, J., 1982, Diagenetic dolomite formation in Quarternary anoxic diatomaceous muds of D.S.D.P. Leg 64, Gulf of California. *Initial Reports: D.S.D.P.*, vol. 64, Part 2, p. 553-569.

- Kim, S.T., and O'Neil, J.R., 1997, Equilibrium and nonequilibrium oxygen isotope effects in synthetic carbonates. *Geochimica et Cosmochimica Acta*, vol. 61, p. 3461-3475.
- Kohout, F. A., 1967, Groundwater flow and the geothermal regime of the Floridian plateau. *Transactions of the Gulf Coast Association of Geological Societies*, vol. 17, p. 339-354.
- Kohut, C., Muehlenbachs, K., and Dudas, M.J., 1995, Authigenic dolomite in a saline soil in Alberta, Canada. *Soil Science Society of America Journal*, vol. 59, p. 1499-1504.
- Land, L. S., 1980, The isotopic and trace element geochemistry of dolomite: the state of the art. *SEPM Special Publication No. 28*, p. 87-110.
- Land, L. S., 1985, The origin of massive dolomite. *Journal of Geological Education*, vol. 33, p. 125.
- Large, R.R., and McGoldrick, P.J., 1999, Carbonate alteration halos associated with Australian Proterozoic stratiform Zn-Pb-Ag deposits. In *Basins, fluids, and Zn-Pb ores*, O. Holm, J. Pongratz, P. McGoldrick, eds., *CODES Special Publication 2*, Second Edition, p. 29-40.
- Laurenzi, M.A., and Visona, D., 1996, $^{40}\text{Ar}/^{39}\text{Ar}$ chronology of Predazzo magmatic complex (southern Alps, Italy). *Geologia delle Dolomiti, 78^a Riunione Estiva*. Societa Geologica Italiana, Bologna.
- Leonardi, P., 1955, Breve sintesi geologica delle Dolomiti occidentali: *Bollettino della Società Geologica Italiana*, vol. 74, p. 1-140.

- Lumsden, D.N., Morrison, J.W., and Lloyd, R.V., 1995, The role of iron and Mg/Ca ratio in dolomite synthesis at 192°C. *Journal of Geology*, vol. 103, p. 51-61.
- Machel, H. G., and Mountjoy, E. W., 1986, Chemistry and Environments of Dolomitization – A reappraisal. *Earth Science Reviews*, vol. 23, p. 175-224.
- Masetti D., and Trombetta, G.L., 1998, L'eredità anisica nella nascita ed evoluzione delle piattaforme medio-trassiche delle Dolomiti occidentali. *Memorie di Scienze Geologiche*, vol. 50, p. 213-237.
- Massari, F., and Neri, C., 1997, The infill of a supradetachment (?) basin: the continental to shallow-marine Upper Permian succession of Dolomites and Carnia (Italy): *Sedimentary Geology*, v. 110, p. 181-221.
- Matthews, R.K. and Poore, R.Z., 1980, Tertiary $\delta^{18}\text{O}$ record and glacio-eustatic sea-level fluctuations. *Geology*, vol. 8, p. 501-504.
- Mojsisovics, E., 1879, Die Dolomitriffe von Südtirol und Venetien. *Beiträge zur Bildungsgeschichte der Alpen*: 552 pp., Hölder, Wien.
- Miller, K.G., and Katz, M.E., 1987, Oligocene to Miocene benthic foraminiferal and abyssal circulation changes in the North Atlantic. *Micropaleontology*, vol. 33, p. 97-149.
- Millero, F. J., and Sohn, M. L., 1992, *Chemical Oceanography*. CRC Press, Boca Raton, FL, 531 p.
- Milliken, K.L., Land, L.S., and Loucks, R.G., 1981, History of burial diagenesis determined from isotopic geochemistry, Frio Formation, Brazoria county, Texas. *AAPG Bulletin*, vol. 65, p.1397-1413.

- Morrow, D. W., 1982, Diagenesis 1. Dolomite - Part 1: The chemistry of dolomitization and dolomite precipitation. *Geoscience Canada*, vol. 9, no. 2, p. 5-13.
- Morrow, D., 1998, Regional subsurface dolomitization: models and constraints. *Geoscience Canada*, vol. 25, p. 57-70.
- Morrow, D.W., and Ricketts, B.D., 1988, Experimental investigation of sulfate inhibition of dolomite and its mineral analogues. *Society of Economic Paleontologists and Mineralogists*, vol. 43, p. 25-38.
- Mottl, M.J., Wheat, G., Baker, E., Becker, N., Davis, E., Feely, R., Grehan, A., Kadko, D., Lilley, M., Massoth, G., Moyer, C., and Sansone, F., 1998, Warm springs discovered on 3.5 Ma oceanic crust, eastern flank of the Juan de Fuca Ridge. *Geology*, vol. 26, p. 51-54.
- Mundil, R., Brack, P., Laurenzi, M.A., 1996, High resolution U-Pb single-zircon age determination: new constraints on the timing of Middle Triassic magmatism in the Southern Alps. *Geologia delle Dolomiti, 78^a Riunione Estiva*. Societa Geologica Italiana, Bologna.
- Nader, F.H., Swennen, R., and Ellam, R., 2004, Reflux stratabound dolostone and hydrothermal volcanism-associated dolostone: a two-stage dolomitization model (Jurassic, Lebanon). *Sedimentology*, vol. 51, p. 339-360.
- Nordeng, S.H., and Sibley, D.F., 1993, Dolomite stoichiometry and Ostwald's Step Rule. *Geochimica et Cosmochimica Acta*, vol. 58, p. 191-196.
- Northrop, D.A., and Clayton, R.N., 1966, Oxygen-isotope fractionations in systems containing dolomite. *Journal of Geology*, vol. 74, p.174-196.

- O'Neil, J.R., Clayton, R.N., and Mayeda, T.K., 1969, Oxygen isotope fractionation in divalent metal carbonates. *Journal of Chemistry and Physics*, vol. 51, p. 5547-5558.
- Oomori, T., and Kitano, Y., 1987, Synthesis of protodolomite from sea water containing dioxane. *Geochemical Journal*, vol. 17, p. 147-152.
- Pierret, M.C., Clauer, N., Bosch, D., Blanc, G., and France-Lanord, C., 2001, Chemical and isotopic ($^{87}\text{Sr}/^{86}\text{Sr}$, $\delta^{18}\text{O}$, δD) constraints to the formation processes of Red-Sea brines. *Geochimica et Cosmochimica Acta*, vol. 65, p. 1259–1275.
- Plummer, L. N., 1975, Mixing of seawater with calcium carbonate groundwater. In: E. H. T. Whitten (Ed.) *Quantitative Studies in Geological Sciences*, a memoir in honor of William C. Krumbein. *Geological Society of America Memoir*, vol. 142, p. 219-236.
- Plummer, L. N., Vacher, H. L., MacKenzie, F. T., Bricker, O. P., and Land, L. S., 1976, Hydrogeochemistry of Bermuda: a case history of ground-water diagenesis of biocalcarenites. *Geological Society of America Bulletin*, vol. 87, p. 1301-1316.
- Presbindowski, D.R., and Larese, R.E., 1987, Experimental stretching of fluid inclusions in calcite - implications for diagenetic studies. *Geology*, vol. 15, p. 333-336.
- Preto, N., Hinnov, L., Hardie, L., and De Zanche, V., 2001, Middle Triassic orbital signature recorded in the shallow-marine Latemar carbonate buildup (Dolomites, Italy). *Geology*, v. 29, n. 12, p. 1123-1126.
- Pursell, B.P., 1997, A record of changing seawater chemistry and diagenesis derived from $^{87}\text{Sr}/^{86}\text{Sr}$ variations through the Latemar carbonate platform, Dolomites, northern Italy. M.A. Thesis, University of Texas at Austin, Austin, TX, U.S.A.

- Radke, B.M., and Mathis, R.L., 1980, On the formation and occurrence of saddle dolomite. *Journal of Sedimentary Petrology*, vol. 50, p.1149-1168.
- Ravizza, G., Blusztajn, J., Von Damm, K.L., Bray, A.M., Bach, W., and Hart, S.R., 2001, Sr isotope variations in vent fluids from 9°46'-9°54'N East Pacific Rise: evidence of a non-zero-Mg fluid component. *Geochimica et Cosmochimica Acta*, vol. 65, p. 729-739.
- Richthofen von, F., 1860, *Geognostische Beschreibung der Umgebung von Predazzo, Sanct Cassian und der Seisseralpen in Südtirol*. Perthes Ed., 327 pp., Gotha.
- Riva A., and Stefani M., 2003, Synvolcanic deformation and intraplateform collapsing: The Latemar case history from the Middle Triassic of the Dolomites. *Memorie di Scienze Geologiche*, vol. 54, pp. 139-142
- Rodgers, K. A., Easton, A. J., and Downes, C. J., 1982, The chemistry of carbonate rocks of Niue island, South Pacific. *Journal of Geology*, vol. 90, p. 645-662.
- Rosen, M. R., Miser, D. E., Starcher, M. A., and Warren, J. K., 1989, Formation of dolomite in the Coorong region, South Australia. *Geochimica et Cosmochimica Acta*, vol. 53, p. 661-669.
- Rosenberg, P.E., and Holland, H.D., 1964, Calcite-dolomite-Magnesite stability relations in solutions at elevated temperatures. *Science*, vol. 145, p. 700-701.
- Rosenberg, P.E., Burt, D.M., and Holland, H.D., 1967, Calcite-dolomite-magnesite stability relation in solution: the effect of ionic strength. *Geochimica et Cosmochimica Acta*, vol. 31, p. 391-396.

- Rossi, D., 1967, Dolomitizzazione delle formazioni Anisiche e Ladino-Carniche delle Dolomiti. Memorie del Museo Tridentino di Scienze Naturali, Trento, Anno 29-30, vol. 16, p. 1-120.
- Saller, A. H., 1984, Petrologic and geochemical constraints on the origin of subsurface dolomite, Enewetak Atoll: An example of dolomitization by normal seawater. *Geology*, vol. 12, p. 217-220.
- Savin, S.M., Douglas, R.G., and Stehli, F.G., 1975, Tertiary marine paleotemperatures. *Geological Society of America Bulletin*, vol. 86, p. 1499-1510.
- Schmidt, M., Xeflide, S., Botz, R., and Mann, S., 2005, Oxygen isotope fractionation during synthesis of CaMg-carbonate and implications for sedimentary dolomite formation, *Geochimica et Cosmochimica Acta*, vol. 69, p. 4665–4674
- Schubel, K.A. (1997) Reaction mechanisms of dolomitization, an integrated TEM, SEM, geochemical, petrographic and field approach. Ph.D. Dissertation, Johns Hopkins University, Baltimore, MD, p. 352.
- Shannon, R.D. and Prewitt, C.T., 1969, Effective ionic radii in oxides and fluorides. *Acta Crystallographica*, vol. B25, p. 925-946.
- Sheppard, S. M. F., and Schwarcz, H. P., 1970, Fractionation of carbon and oxygen isotopes and magnesium between metamorphic calcite and dolomite. *Contributions to Mineralogy and Petrology*, vol. 26, p. 161-198.
- Sibley, D.F., Nordeng, S.H., and Borkowski, M.L., 1994, Dolomitization kinetics in hydrothermal bombs and natural settings. *Journal of Sedimentary Research*, vol. A64, p. 630-637.

- Siegel, F. R., 1961, Factors influencing the precipitation of dolomitic carbonates. State Geological Survey of Kansas Bulletin, vol. 152, p. 129-158.
- Simms, M., 1984, Dolomitization by groundwater flow systems in carbonate platforms. Gulf Coast Association of Geological Societies Transactions, vol. 34, p. 411-420.
- Skinner, B.J., 1997, Hydrothermal mineral deposits: what we do and don't know. In *Geochemistry of Hydrothermal Ore Deposits*, H.L. Barnes, ed., John Wiley and Sons, New York, p. 1-29.
- Slaughter, M., and Hill, R.J., 1991, The influence of organic matter in organogenic dolomitization. *Journal of Sedimentary Petrology*, vol. 61, p. 296-303.
- Spencer-Cervato, C., and Mullis, J., 1992, Chemical study of tectonically controlled hydrothermal dolomitization: an example from the Lessini Mountains, Italy. *Geologische Rundschau*, vol. 81, p. 247-370.
- Steinen, R. P., Matthews, R. K., and Sealy, H. A., 1978, Temporal variation in geometry and chemistry of the freshwater phreatic lens: the coastal aquifer of Christ Church, Barbados, West Indies. *Journal of Sedimentary Petrology*, vol. 48, p. 733-742.
- van Lith, Y., Vasconcelos, C., Warthmann, R., J.C.F., Martins, and McKenzie, J.A., 2002, Bacterial sulfate reduction and salinity: two control on dolomite precipitation in Lagoa Vermelha and Brejo do Espinho (Brazil). *Hydrobiologia*, vol. 485, p. 35-49.
- Vardebasso, S., 1930, Carta Geologica del Territorio Eruttivo di Predazzo e Monzoni nelle Dolomiti di Fiemme e Fasse. Scale 1:25000. Padova.

- Vasconcelos, C., McKenzie, J.A., Bernasconi, S., Grujic, D., and Tien, A.J., 1995, Microbial mediation as a possible mechanism for natural dolomite formation at low temperatures. *Nature*, vol. 377, p. 220-222.
- Vasconcelos, C., and McKenzie, J.A., 1997, Microbial mediation of modern dolomite precipitation and diagenesis under anoxic conditions (Lagoa Vermelha, Rio de Janeiro, Brazil). *Journal of Sedimentary Petrology*, vol. 67, p. 378-390.
- Vasconcelos, C., McKenzie, J.A., Warthmann, R., and Bernasconi, S.M., 2005, Calibration of the $\delta^{18}\text{O}$ paleothermometer for dolomite precipitated in microbial cultures and natural environments. *Geology*, vol. 33, 317–320.
- Visona, D., 1997, The Predazzo multipulse intrusive body (Western Dolomites, Italy). Field and mineralogical studies. *Memorie di scienze geologiche*, v. 49, p. 117-125.
- Von Damm, K.L., 1990, Seafloor hydrothermal activity: black smoker chemistry and chimneys. *Annual Reviews in Earth and Planetary Science*, vol. 18, p. 173-204.
- Von Damm, K.L., 1995, Controls on the chemistry and temporal variability of seafloor hydrothermal fluids, In *Seafloor Hydrothermal Systems: Physical, Chemical, Biological, and Geological interactions*, AGU Monograph 91, Humphris, S., Zierenberg, R., Mullineaux, L., and Thomson, R., eds., p. 222-247.
- Von Damm, K.L., 2004, Evolution of the hydrothermal system at East Pacific Rise 9°50'N: geochemical evidence for changes in the upper oceanic crust. In *The Thermal Structure of the Oceanic Crust and the Dynamics of Hydrothermal Circulation*, AGU Monograph 148, German, C., Lin, J., and Parson, L., eds., p. 285-304.

- Von Damm, K.L. & M.D. Lilley, 2004. Diffuse flow hydrothermal fluids from 9°50'N East Pacific Rise: Origin, evolution and biogeochemical controls. In *The Subsurface Biosphere at Mid-Ocean Ridges*, AGU Geophysical Monograph 144, W.S.D. Wilcock, E.F. DeLong, D.S. Kelley, J.A. Baross & S.C. Cary, eds., p. 243-266.
- Warren, J., 2000, Dolomite: occurrence, evolution and economically important associations. *Earth-Science Reviews*, vol. 52, p. 1–81.
- Warthmann, R., van Lith, Y., Vasconcelos, C., McKenzie, J.A., and Karpoff, A.M., 2000, Bacterially induced dolomite precipitation in anoxic culture experiments. *Geology*, vol. 28, p. 1091-1094.
- Wells, A. J., 1962, Recent dolomite in the Persian Gulf. *Nature*, vol. 194, p. 274-275.
- Wilson, A.M., Sanford, W., Whitaker, F., and Smart, P., 2001, Spatial patterns of diagenesis during geothermal circulation in carbonate platforms. *American Journal of Science*, vol. 301, p. 727-752.
- Wilson, E. N., 1989, Dolomitization of the Triassic Latemar buildup, Dolomites, northern Italy. Ph.D. dissertation, Johns Hopkins University, Baltimore, MD, U.S.A.
- Wilson, E. N., Hardie, L. A., and Phillips, O. M., 1990, Dolomitization front geochemistry, fluid flow patterns, and the origin of massive dolomite: the Triassic Latemar buildup, northern Italy. *American Journal of Science*, vol. 290, p. 741-796.

- Wilson, E. N., Hardie, L. A., and Phillips, O. M., 1990, Dolomitization front geochemistry, fluid flow patterns, and the origin of massive dolomite: the Triassic Latemar buildup, northern Italy. *American Journal of Science*, vol. 290, p. 741-796.
- Yao, Q., and Demicco, R.V., 1997, Dolomitization of the Cambrian carbonate platform, southern Canadian Rocky Mountains: dolomite front geometry, fluid inclusion geochemistry, isotopic signature, and hydrogeologic modeling studies. *American Journal of Science*, vol. 297, p. 892-938.
- Yardley, B. W. D., and Lloyd, G. E., 1995, Why metasomatic fronts are really metasomatic sides. *Geology*, vol. 23, p. 53-56.
- Yose, L., 1993, Stratal patterns and lithofacies in Triassic carbonate slope deposits of the Dolomites, Italy: implications for sequence stratigraphy and global sea level. Ph.D. dissertation, Johns Hopkins University, Baltimore, MD, U.S.A.
- Zempolich, W.G., 1995, Deposition, early diagenesis, and late dolomitization of deepwater resedimented oolite: the middle Jurassic Vajont limestone of the Venetian Alps, Italy. Ph.D. dissertation, Johns Hopkins University, Baltimore, MD, U.S.A.
- Zempolich, W.G., and Hardie, L.A., 1997, Geometry of dolomite bodies within deep-water resedimented oolite of the Middle Jurassic Vajont Limestone, Venetian Alps, Italy: analogs for hydrocarbon reservoirs created through fault-related burial dolomitization. In: *Reservoir quality prediction in sandstones and carbonates* (J.A. Kupecz, J. Gluyas, and S. Blochs, eds.), AAPG Memoir 69, p. 127-162.

Zenger, D. H., 1972, Significance of supratidal dolomitization in the geologic record.

Geological Society of America Bulletin, vol. 83, p. 1-11.

Zierenberg, R.A., 1990, Deposition of metalliferous sediment beneath a brine pool in the

Atlantis II deep, Red Sea. In *Gorda Ridge. A Seafloor Spreading Center in the*

United States' Exclusive Economic Zone, G.R. McMurray, ed., Springer-Verlag,

New York, p. 131-142.

**SARAH KATHERINE CARMICHAEL
VITA**

DATE AND PLACE OF BIRTH

September 24, 1976 in Newmarket, NH

EDUCATION

2000-2006: Johns Hopkins University

M.A. Earth and Planetary Sciences, 2002

Ph.D. Earth and Planetary Sciences, 2006

Dissertation: Dolomitization of a Triassic atoll by reaction of limestone
with diffuse effluent: Latemar carbonate buildup, Dolomites,
northern Italy

Advisor: John M. Ferry

Awards: Owen Fellowship, 2000-2003

1994-1998: Smith College

B.A. Geology with highest honors, 1998

Senior Thesis: Geothermobarometry of metamorphosed mafic dikes and
sills, Tobacco Root Mountains, southwestern Montana.

Advisor: John B. Brady

Awards: Highest Honors in Geology, 1998; Sigma Xi, 1998;

Mineralogical Society of America Undergraduate Award, 1997;

Dean's List, 1996-1998

PROFESSIONAL EXPERIENCE

2000-2006: Research Assistant, Johns Hopkins University, Department of Earth
and Planetary Sciences.

Supervisor: John M. Ferry

1998-2000: Project Hydrogeologist, GeoTrans, Inc., Harvard, Massachusetts.

Supervisor: John H. Guswa

TEACHING EXPERIENCE

Geochemical Thermodynamics, Teaching Assistant, Johns Hopkins University,
2004

Advanced Metamorphic Petrology, Teaching Assistant, Johns Hopkins
University, 2003

Dynamic Earth, Teaching Assistant, Johns Hopkins University, 2003

Earth Materials, Teaching Assistant, Johns Hopkins University, 2002

Geobiology, Teaching Assistant, Johns Hopkins University, 2001

Mineralogy, Teaching Assistant, Smith College, 1996, 1997

Petrology, Teaching Assistant, Smith College, 1997, 1998